RYANODINE RECEPTOR EXPRESSION IN TROPHOBLASTS

Limian Zheng, BSc, MRes

A thesis submitted to
The National University of Ireland, Cork
For the degree of
Doctor of Philosophy.

Department of Physiology
Heads of Department: Professor Edward Johns and Professor Ken O'Halloran
Supervisor of the Research: Dr. John Mackrill

April 2013

Contents

List of Figures

List of Tables

Declaration

The thesis submitted is the candidate's own work and has not been submitted for another degree, either at University College Cork or elsewhere.

Name of Candidate: Limian ZHENG

Signature:  L.Z.

Acknowledgements

The work presented in this thesis would not have been possible without the help of the following individuals:

First, I would like to express my greatest gratitude to my supervisor Dr. John Mackrill, for providing me with this excellent research opportunity. I would like to thank him for his continuous guidance, patience, inspiration and encouragement throughout my PhD experience. I would like to thank Prof. Edward Johns and Dr. Patrick Harrison for their full support in this study during their tenure as head of the Physiology Department; thank Prof. Ken O'Halloran for his support in this project as the successor of head of department. The brilliant technical staffs in the Department have been provided continuous support that made my lab work much more smoother and pleasant, so I would like to thank Ms. Miriam O'Sullivan, Mr. Tony Mulvihill, Mr. Kieran McDonnel, Mr. Stephen Dineen, and Dr. Marcella Burke; my gratitude is also extended to our excellent secretary staffs: Ms. Jackie Maguire, Ms. Nora O'Donovan, Ms. Maude Vernon and Ms. Verna Garret.

I would like to express a very special gratitude and appreciation to Prof. John Aplin, from the University of Manchester, UK, for the generosity of providing human placental samples and all pratical help. Thank to Dr. Karen Forbes, Dr. Sam Smith, Dr. Lynda Harris, Dr. Carolyn Jones and Dr. Sylvia Lui who from Prof. Aplin's group, thank for providing exceptional guidance, inspiring discussion and constructive suggestion during my work-visit in their lab in St. Mary's Hospital, Manchester.

I would also like to present my appreciation to the excellent scientists and researchers from the Department of Biochemistry, University College Cork: thank to Prof. Tommie McCarthy for the inspiration on molecular biology and for the gift of RyR primers; thank to Dr. Tom Moore and Dr. Melanie Ball for providing IHC protocols and consultation; thank to Dr. Cora O'Neill and her group members Aoife and Meghan who provided material and equipment sharing for my initial IHC experiments, and then provided instruction on the use of Leica fluorescence microscope and software.

Thank to Dr. Patrick Harrison and Dr. Farouk Hazim Markos for serving as my PhD committee. I truly appreciate all the feedback with honest opinion and helpful advice.

The experience of getting-on with everyone in the Department is much appreciated. Therefore, I would like to thank who I have worked with: Will, Ciaran, Belinda, Georgina, Ciara, Katrin, Jen, Kate, Eimear, Fiona, Julie, Niamh, Nurullah, Shane and Yzzam, wish them good luck in the future.

Finally, I would like to thank my parents for their understanding through the years. I could not thank them enough for their support. The love of my parents is the origin of my ambition and motivation that pursue this PhD project.

Abstract

Trophoblasts of the placenta are the frontline cells involved in communication and exchange of materials between the mother and fetus. Within trophoblasts, Ca^{2+}-signalling proteins, such as Ca^{2+} channels, Ca^{2+} pumps and Ca^{2+} binding proteins are richly expressed. Intracellular free calcium ions are a key second messenger, participating in regulation of various cellular activities. In the placenta, transcellular Ca^{2+} transport through trophoblasts is also essential in formation of the fetal skeleton. Ryanodine receptors (RyRs) are high conductance cation channels that mediate Ca^{2+} release from intracellular Ca^{2+} stores such as the sarcoplasmic and endoplasmic reticulum to the cytoplasm. To date, the roles of RyRs in trophoblasts have not been reported. By use of reverse transcription PCR and western blotting, the current study revealed that RyRs are expressed in both model trophoblast cell lines (BeWo and JEG-3) and in human tissue from first trimester and term placental villi. Immunohistochemistry of human tissue sections posed that both syncytiotrophoblast and cytotrophoblast cell layers were positively stained by antibodies recognising RyRs; likewise, expression of multiple RyR isoforms was also revealed in BeWo and JEG-3 cells by immunofluorescence microscopy. RyRs in BeWo and JEG-3 cells were further demonstrated to be actively involved in $[Ca^{2+}]_i$ regulation. Changes in $[Ca^{2+}]_i$ were observed in both BeWo and JEG-3 cells upon application of various RyR agonists and antagonists, using fura-2 fluorescent videomicroscopy. In addition, endogenous placental peptide hormones, namely angiotensin II, arginine vasopressin and endothelin 1, were demonstrated to increase $[Ca^{2+}]_i$ in BeWo cells, and such increases of $[Ca^{2+}]_i$ were suppressed by RyR antagonists, in addition to blockers of corresponding peptide hormone receptors. These findings indicate that human trophoblasts of the placenta express multiple RyR subtypes; BeWo and JEG-3 cells were functionally responsive to direct pharmacological activation of RyR agonists and antagonists; the suppression effect of RyR antagonists upon the rise in $[Ca^{2+}]_i$ that was evoked by hormones implies that RyRs mediate Ca^{2+} release from ER in response to the indirect stimulation by these endogenous peptides. These

observations suggest that RyR contributes to trophoblastic cellular Ca^{2+} homeostasis, and such RyR-mediated Ca^{2+} release is linked to endogenous placental peptide (e.g AGII, AVP and ET1) induced signalling pathways. The current study provides new insights on maternal-fetal Ca^{2+} mobilisation; characterisation of the involvement of RyRs and/or RyR accessory proteins in connection with signal transduction through external stimuli may provide better understanding of pregnancy-related pathological complications.

Abbreviations

$[Ca^{2+}]$	Calcium ion concentration
$[Ca^{2+}]_i$	Intracellular free calcium ion concentration
AC	Adenylyl cyclase
ADPR cyclase	ADP-ribosyl cyclase
APP	Atypical periodic paralyses
αAR	α-adrenergic recepor
ARVD2	Arrhythmogenic right ventricular dysplasia type 2
AT_1R	Angiotensin II type 1 receptor
βAR	β-adrenergic recepor
BBM	Brush border membrane
BPM	Basal plasma membrane
cADPR	Cyclic adenosine diphosphoribose ribose
cAMP	Cyclic adenosine monophosphate (cyclic AMP)
cGMP	Cyclic guanosine monophosphate (cyclic GMP)
CaBP	Ca^{2+}-binding protein
CaM	Calmodulin
CaT	Ca^{2+} transporter protein
CAT	Cationic amino acid transporter
CCD	Central core disease
CICR	Ca^{2+}-induced Ca^{2+} release
CmC	4-chloro-*meta*-cresol
CPVT	Catecholaminergic polymorphic ventricular tachycardia
CPVT1	Catecholaminergic polymorphic ventricular tachycardia type 1
CREB	cAMP-response element binding protein
CRT	Calreticulin
CSQ	Calsequestrin

CRH	Corticotrophin-releasing hormone
CT	Cytotrophoblasts
cTnI	Cardiac troponin I
DAG	1,2-diacylglycerol
DHPR	Dihydropyridine receptor
E-C	Excitation-contraction
EPAC	Exchange protein directly activated by cyclic adenosine monophosphate (cAMP); cAMP-regulated guanine-nucleotide-exchange factor
ER/SR	Endoplasmic and/or sarcoplasmic reticulum
ET1	Endothelin 1
ET_BR	Endothelin 1 type B receptor
EVT	Extravillous trophoblast
ERK1/2 (p42 MAPK, p44 MAPK)	Extracellular signal regulated protein kinases cascades
FBS	Fetal bovine serum
FKBPs	FK506-binding proteins
GC/sGC	Guanylate cyclase/soluble guanylate cyclase
GPCR	Guanine nucleotide-binding protein coupled receptor
hCG	Human chorionic gonadotropin
InsP	Inositol phosphates
IP_3	Inositol 1, 4, 5-trisphosphate
IP_3R	Inositol 1, 4, 5-trisphosphate receptor
IUGR	Intrauterine growth restriction
LTCC	L-type calcium channel
MAPK	Mitogen-activated protein kinases
MH	Malignant hyperthermia
MmD	Multi-minicore disease
NAADP	Nicotinic acid adenine dinucleotide phosphate
NCX	Na^+/Ca^{2+} exchanger
NO	Nitric oxide
NOS	Nitric oxide synthase/NO synthase

NSCC	Non-selective cation channels
PBS	Phosphate buffer saline
PKA	cAMP-dependent protein kinase
PKC	Ca^{2+}-dependent protein kinase
PKG	cGMP-dependent protein kinase
PLC	phospholipase C
PLD	phospholipase D
PLN	phsopholamban
PMCA	Plasma membrane Ca^{2+}-ATPase
PTHrP	Parathyroid hormone-related peptide
PI3K	Phosphoinositde-3-kinase
ROS	Reactive oxygen species
RyR	Ryanodine receptor
SCT	Syncytiotrophoblast
SERCA	Sarcoplasmic and endoplasmic reticulum calcium ATPase
SOCC	Store-operated Ca^{2+} channels
SOD	Superoxide dismutase
TPC	Two-pore channel
TRD	Triadin
TRPC	'Transient receptor potential canonical'; Transient receptor potential related Ca^{2+} channels
TRPV	'Transient receptor potential vanilloid'; Transient receptor potential related Ca^{2+} channels
V1	Arginine vasopressin receptor 1
V2	Arginine vasopressin receptor 2
VDCC	Voltage dependent Ca^{2+} channels

Chapter I.

Introduction

Chapter I. Introduction

The intracellular free calcium ion (Ca^{2+}) is a well-established second messenger that plays an important role in the regulation of cellular activity in all cell types (McPherson & Campbell,1993). Cellular events that rely on Ca^{2+} include muscle contraction, synaptic transmission, hormone secretion, fertilization, nuclear pore regulation, gene transcription, cell death and cell proliferation (Berridge *et al.*,2003). Under physiological conditions, the extracellular Ca^{2+} concentration ($[Ca^{2+}]$) is within millimolar range, whereas the internal $[Ca^{2+}]$ is in the micromolar range. However, the cytosolic/intracellular free Ca^{2+} concentration ($[Ca^{2+}]_i$) in most resting cells is approximately 100 nM (Fill & Copello,2002), which is far less than the $[Ca^{2+}]$ reported in the extracellular space and the internal Ca^{2+} store. The $[Ca^{2+}]$ difference between internal store, extracellular space and cytosolic space implicates that both internal and external Ca^{2+} sources can be involved in the generation of Ca^{2+} transients in response to extracellular cues, which trigger signalling pathways within the cell. Maintenance of such steep $[Ca^{2+}]$ gradients across the cell membranes involves a wide range of Ca^{2+}-regulating proteins, such as Ca^{2+} transporters and Ca^{2+} channels. The internal Ca^{2+} store of the endoplasmic and sarcoplasmic reticulum (ER/SR) in the cell provides a faster and more precise pathway for Ca^{2+} signalling generation relative to Ca^{2+} influx across the plasma membrane (Fill & Copello,2002). For instance, large global intracellular Ca^{2+} increase are required for muscle contraction, while localised Ca^{2+} sparks activate Ca^{2+}-dependent K^+ channels in plasma membrane that result in relaxation of smooth muscle cells (Nelson *et al.*,1995). The high ER/SR $[Ca^{2+}]$ is particularly maintained by the ER/SR Ca^{2+} ATPase (SERCA) pumps. One class of the Ca^{2+} channel that mediate Ca^{2+} release from the ER/SR is the ryanodine receptor (RyR) family. These ryanodine-sensitive Ca^{2+} channels can be activated by allosteric coupling to plasmalemmal voltage-dependent Ca^{2+} channels (VDCCs), or activated by sensing changes in cytosolic $[Ca^{2+}]_i$, as reviewed previously (Coronado *et al.*,1994; Mackrill,1999). The opening

of RyR channels mediates Ca^{2+} release from the internal stores; the generation of these intracellular Ca^{2+} spikes and Ca^{2+} waves subsequently triggers downstream cellular signalling pathways (Berridge,1997). Since changes in $[Ca^{2+}]_i$ are involved in the regulation of various cell functions, dysregulated cytosolic $[Ca^{2+}]$ can result in pathological conditions.

The placenta is a unique organ that provides an interface for communication and nutrient transport between the mother and the fetus. Trophoblasts in the placenta are the front line cells involved in such delivery and disposal activities, among which, Ca^{2+} transport through trophoblasts is essential in the process of skeletal development in fetus (Belkacemi *et al.*,2005). The abundance of Ca^{2+} channels, Ca^{2+} pumps and Ca^{2+} binding proteins expressed in trophoblasts is likely to fulfil the role of mineralisation (Moreau *et al.*,2003b). However, characterisation of these Ca^{2+} channels and relevant functional accessory proteins in trophoblasts has not been established completely; and the exact mechanism of Ca^{2+} delivery from the maternal circulation to the fetus is not fully understood. The current project examined the expression of RyRs in both human placental trophoblast and human model trophoblast cell lines (BeWo, JAR, JEG-3 and SGHPL-4); the functional properties of RyRs in cell lines were studied using fura-2 calcium imaging.

1.1 Overview of RyRs

RyRs are expressed widely in many tissues, including skeletal, cardiac and smooth muscles; neurons of both the central and peripheral nervous system; in organs of liver, lung, kidney, pancreas, testis and ovary; in osteocytes, neutrophils and macrophages; and in epithelial, endothelial and adrenal chromaffin cells (Sutko & Airey,1996; Franzini-Armstrong & Protasi,1997). RyRs are primarily expressed in the SR of muscle cells and the ER of non-muscle cells; the inner membrane of mitochondria was also reported to express RyRs (Beutner *et al.*,2001).

RyRs are large homotetrameric complexes with molecular weights of more than 2 million daltons (Takeshima *et al.*,1989). Each RyR protein complex consists of four identical subunits; of which, each subunit has molecular weight over 560 kDa (Jayaraman *et al.*,1992). Figure 1.1 illustrates the "triad foot" component of the cytoplasmic N-terminal region of the RyR subunit that represents over 80% of the monomer (McCarthy & Mackrill,2004). The 4-TM arrangement, indicated in Figure 1.1 as M1- M4 was adapted from the Takeshima model (Takeshima *et al.*,1989) for simplicity; a putative filter pore sequence of human RyRs (GVRAGGGIGD) is also indicated in the loop between M3 and M4 for later discussion. There are three genes (*RYR1*, *RYR2* and *RYR3*) in humans encoding three RyR isoforms. These three receptor isoforms share about 70% amino acid sequence identity (Sorrentino & Volpe,1993). In mammalian striated muscles, the expression of RyR isoforms is tissue-specific. RyR1 and RyR2 are the predominant receptor isoforms expressed in skeletal and cardiac muscle, respectively. RyR3 is also present in mammalian striated muscles, such as in diaphragm and smooth muscle, but at relatively low levels in comparison to RyR1 and RyR2. Although RyR3 was referred to as the brain RyR isoform, recent studies have shown that the neurons and brain tissue express all three RyR isoforms; in addition, low expression level of RyR3 is co-expressed with other RyR isoforms in a wide range of both excitable and non-excitable cells (Giannini *et al.*,1995).

Isoform-specific knock-out transgenic mice models were generated to investigate specific physiological roles of each RyR isoform. Mice with RyR1 gene

deficiency die perinatally with gross abnormalities of the skeletal muscle; the contractile response to electrical stimulation under physiological conditions is completely lost in RyR1-deficient muscle, which suggested the essential function of RyR1 in both muscular maturation and excitation-contraction coupling (E-C coupling) (Takeshima *et al.*,1994). Another study carried out by the same group reported mice lacking RyR2 developed large vacuolated SR, along with structurally abnormal mitochondria in the mutant cardiac myocytes; these animals died at around embryonic day 10 with morphological abnormalities in the heart tube; the authors proposed that RyR2 has a vital role in cellular Ca^{2+} homeostasis during the development of SR (Takeshima *et al.*,1998). These findings imply that RyR1 and RyR2 are essential for striated skeletal and cardiac muscle formation during embryo development. In contrast, RyR3-deficient mice were viable with no gross abnormalities (Takeshima *et al.*,1996). However, impairment in neonatal skeletal muscle contraction was observed at the first week after birth, suggesting RyR3 contributes to E-C coupling in neonatal skeletal muscle contraction (Bertocchini *et al.*,1997).. Another independent study also reported increased locomotion activity of RyR3 (-/-) mice in the open-field test (Balschun *et al.*,1999). Such deletion of RyR3 also resulted at specific changes in hippocampal synaptic plasticity without affecting hippocampal morphology, basal synaptic transmission or presynaptic function (Balschun *et al.*,1999). These findings reveal that RyR3 may be less important than RyR1 and RyR2 in striated muscle development but appears to be involved in spatial learning in the central nervous system, and the lack of RyR3-mediated Ca^{2+} signalling results in abnormalities of certain neurons in the central nervous system (Takeshima *et al.*,1996).

Figure 1.1 RyR membrane topology (4-TM model)

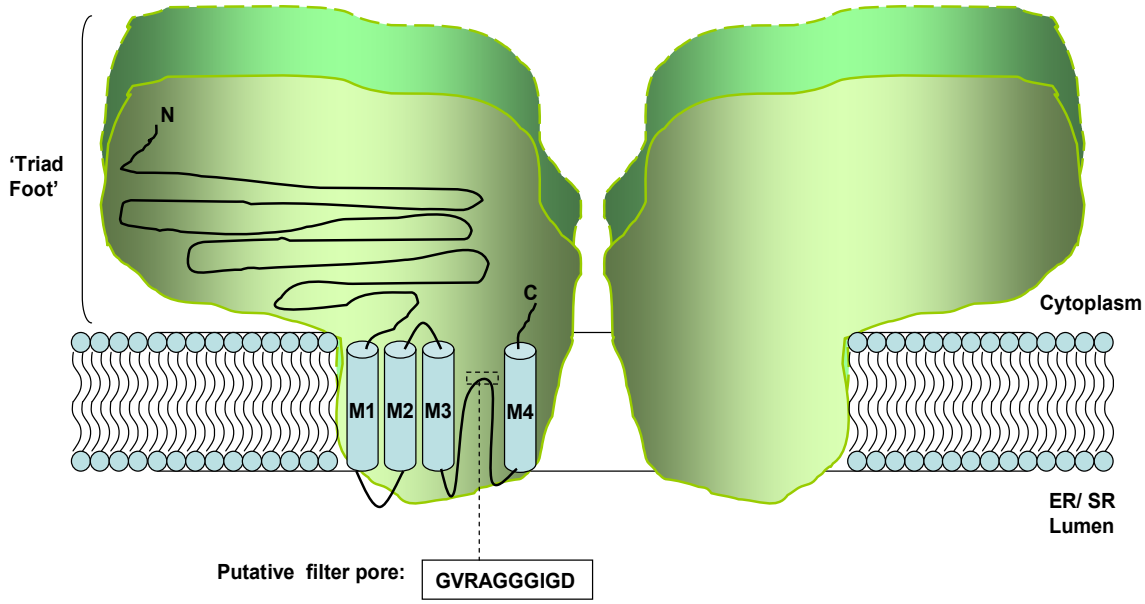

Figure 1.1. Schematic illustration of RyR homotetrametric structure: the 4-TM arrangement (M1- M4) was adapted from the Takeshima model (Takeshima *et al.*,1989) for simplicity. The bulky amino-terminal portion forms the 'triad foot' structure. The region between transmembrane domains M3 and M4 that dips inside the lipid bilayer forms the putative pore. The sequence of the human RyR pore (GVRAGGGIGD) is indicated within this loop region.

1.2 Molecular Structure Overview of RyRs

The human gene encoding RyR1 is located on chromosome 19q13.2 and contains 104 exons; the gene encoding RyR2 of human is located on chromosome 1q43 and contains 102 exons; and the human *RYR3* gene is found on chromosome 15q13.3-14, with 103 exons (Lanner *et al.*,2010). Both RyR1 and RyR2 are well studied subtypes of RyR, due to the relatively high expression level and ease of protein purification process from skeletal and cardiac muscle, respectively. The primary structures of RyRs were elucidated by cDNA cloning.

Although the protein sequences among mammalian RyRs (RyR1, RyR2 and RyR3) are well conserved, isoform specific functions are mainly governed by three divergent regions. Schematic diagram Figure 1.2A indicates the three divergent regions named D1, D2 and D3 within a subunit monomer. The D1 region (residues 4254-4631 and residues 4210-4562 of RyR1 and RyR2, respectively) is found at the proximal location of the putative four transmembrane segments (M1-M4) of Takeshima model (Takeshima,1993). Both D2 (residues 1342-1403 and residues 1353-1397 of RyR1 and RyR2, respectively), and D3 regions (residues 1872-1923 and residues 1852-1890 of RyR1 and RyR2, respectively) are found in the cytoplasmic domain of the N-terminus (Ma *et al.*,2004) where sites respond to ligand and regulatory protein binding (Rossi & Sorrentino,2002). Figure 1.2B shows a 3-dimensional reconstruction of human RyR2 protein with the views from the cytoplasm (left) and the ER/SR membrane (right). These 3D images were adapted from animation created by Dr. T. Wagenknecht (Jones *et al.*,2008), available for open-access (http://www.wadsworth.org/rvbc/animation.html). The corresponding D1, D2 and D3 regions are coloured in yellow, red and purple, respectively. The difference of D regions across RyR subtypes determines the isoform specificity. For example, the D3 region in RyR1 contains 38 net negative charges of 51 residues, but this D3 corresponding region in RyR2 only has 6 negative charges. In addition, the consecutive 17 glutamate residues of RyR1 D3 region are lacking in both RyR2 and RyR3 (Takeshima,1993). Furthermore, the corresponding D2 region is absent in RyR3 (Ma *et al.*,2004).

The membrane topology of RyR is not fully understood. However, it has been demonstrated by immunolocalisation studies that both N- and C- terminal domains of RyR1 are situated in the cytoplasm (Marty *et al.*,1994; Grunwald & Meissner,1995). This observation indicates an even number rather than an odd number of transmembrane (TM) domains in RyRs. Takeshima and colleagues first suggested the 4 TM model (M1-M4) of RyR1 (Takeshima *et al.*,1989). The amino acid sequence of these domains display high similarity to the pore region domains of IP_3R (Ma *et al.*,2004), another receptor channel that also mediates Ca^{2+} release. Another model proposed by Zorzato and colleagues suggested a 10 TM model (M1-M10) (Zorzato *et al.*,1990). Figure 1.2A shows the RyR monomer as a schematric based on this 10 TM model, adapted and modified from (Zissimopoulos & Lai,2007). For simplicity, only M5, M6, M8 and M10 are indicated. TMs between M6 and M8 are shown as a TM hairpin (Zissimopoulos & Lai,2007). The four TM domains: M5, M6, M8 and M10 of this 10 TM model correspond to the M1, M2, M3 and M4 of the Takeshima model. Subsequently, Tunwell and colleagues proposed a 6 TM model, based on competitive enzyme-linked immunosorbent assay experiments using domain specific antibodies on intact and permeabilized SR microsomes (Tunwell *et al.*,1996). This model suggests similarity with the consensus selectivity filter of K^+ channels, in which the channel pore contains 6 TM domains and a P-loop between M5 and M6 that functions as the ion selectivity filter. A similar P-loop between M3 and M4 of Takeshima model was also identified in RyR proteins, and the ion conducting pore has been revealed in the luminal-facing region of RyR (Zhao *et al.*,1999). Figure 1.2A indicates the putative Ca^{2+} filter domain sequence GVRAGGGIGD in the dashed rectangle in between M3 and M4 TM domains. This amino acid sequence of the pore structure is conserved in all RyR subtypes. For example, the protein sequence of human RyR1 that correspond to this putative filter segment is 4891-4900 (Zhao *et al.*,1999). The highly conserved motif GIG in RyR P-loop is structurally related to the K^+ channel filter GYG motif which contributes to this monovalent cation selective filter (Doyle *et al.*,1998). Mutations of the Ile to other hydrophobic amino acids such as Ala, Val and Leu, all resulted in a channel that lacked Ca^{2+} dependence, failed to bind ryanodine and displayed atypical Ca^{2+}

release in response to caffeine, an RyR agonist, in a cell-based assay (Gao *et al.*,2000).

Figure 1.2 Schematic illusion of RyR monomer (A) and 3-dimentional constructs of RyR2 (B)

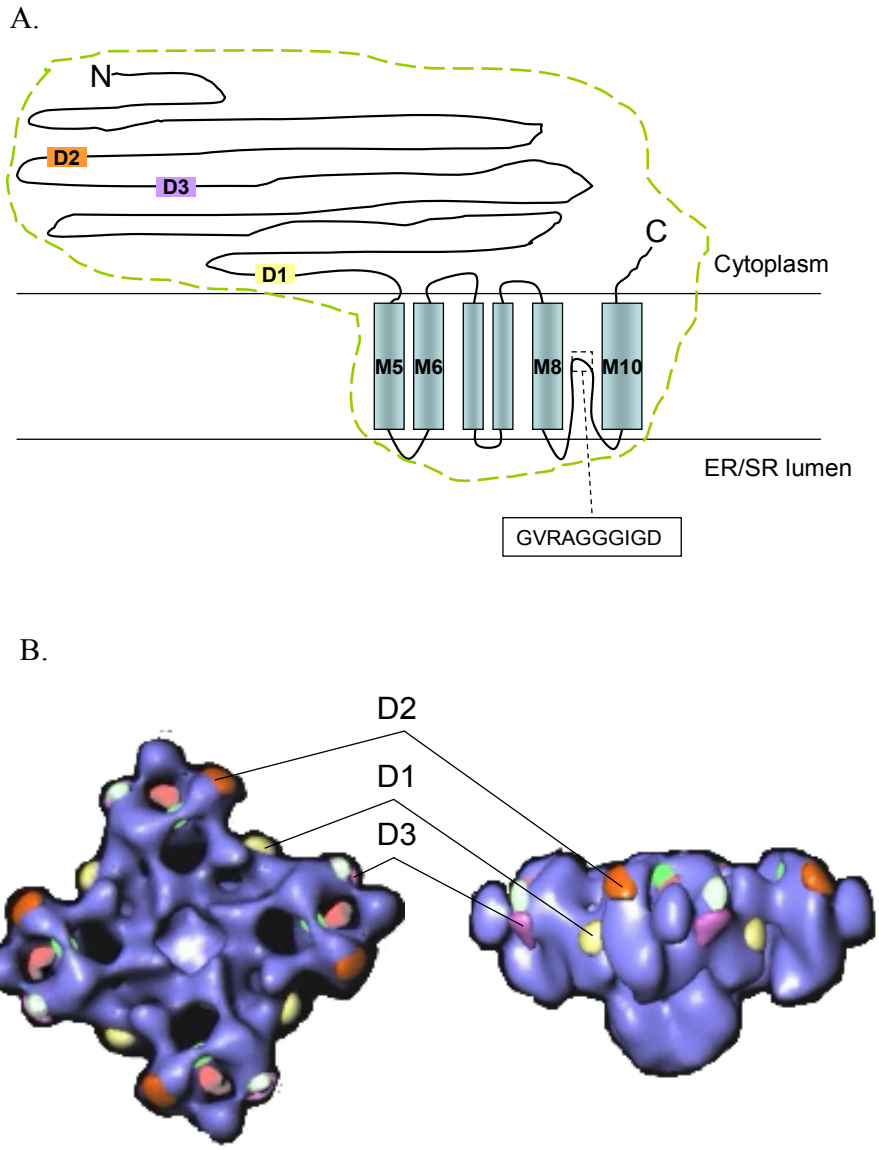

Figure 1.2A. A 6-TM model of RyR subunit (modified Takeshima model) adapted and modified from Zissimopoulos & Lai, 2007 (Zissimopoulos & Lai,2007). The isoform divergent regions are indicated as D1, D2, and D3 at the N-terminus. The amino acid sequence that involves pore formation is displayed in inset magnified from the dashed area between M8 and M10.

Figure 1.2B. Three-dimensional constructs of RyR2, adapted from Jones *et al*., 2008 (Jones *et al.*,2008). The three-dimensional constructs are shown in two views: *left*, top view from the cytoplasmic surface; *right*, side view at the level of the ER/SR membrane. The corresponding locations of the three divergent regions are indicated, in which, D1, D2 and D3 are coloured yellow, orange and purple, respectively.

1.3 Ryanodine Receptor and Excitation-contraction Coupling

RyRs were originally observed using transmission electron microscopy as electron-dense masses located within the SR terminal cisternae of skeletal muscle, the place where the SR is adjacent to the transverse-tubule (T-tubule) membranes (Franzini-Armstrong,1970). Based on their appearance, these proteins were initially named the "triad junctional foot proteins" (Franzini-Armstrong,1970) before they were characterised as ryanodine binding proteins (Pessah *et al.*,1985). The rectangular junctional feet fill up the gap between the SR and T-tubule; this architecture is crucial for subsequent excitation-contraction (E-C) coupling (Wagenknecht & Radermacher,1997). In skeletal muscle, RyRs in the SR membrane are in direct apposition to the dihydropyridine receptors (DHPRs) in the junctional T-tubule membrane. The propagation of an action potential that activates depolarisation at the neuromusclular junction leads to a conformational change of the DHPRs that are physically in contact with the adjacent RyR in the SR membrane through a protein-protein interaction mechanism (McPherson & Campbell,1993; Mackrill,1999) between DHPR and RyR: the RyR is activated and the opening of RyR channel subsequently mediates Ca^{2+} release from the SR.

Although the physical interaction between DHPRs and RyRs is one of the mechanisms for RyR activation, not all RyRs couple to DHPRs (Ikemoto & Yamamoto,2002). In skeletal muscle, only half of the RyR population are directly in contact with DHPRs; whereas the total number of RyRs are about 3 to 10 fold more abundant than the DHPR population in cardiac muscle, depending on species (Bers & Stiffel,1993). The remaining uncoupled RyRs in skeletal muscle are activated by the so-called Ca^{2+}-induced Ca^{2+} release (CICR) mechanism, which adds to the Ca^{2+} that is released from the nearby DHPR-coupled RyRs (Endo *et al.*,1970). In cardiac muscle tissue, the relative population of DHPRs is much lower than RyRs. The E-C coupling of cardiac RyRs relies more on the CICR mechanism than mechanical interaction with DHPRs. Therefore, cardiac muscle E-C coupling is initiated by membrane depolarisation which leads to activation and channel opening of the voltage-sensing DHPRs; a small amount of extracellular Ca^{2+} enters into the cell

through these DHPR channels and interacts with the Ca^{2+}-sensing domain of the SR RyR; this subsequently induces SR RyR activation, resulting in further release of Ca^{2+} from SR through the opened RyR channels. Eventually, the increase of $[Ca^{2+}]_i$ causes cardiac muscle contraction.

1.4 Gating Properties and Activation of RyRs

RyRs are the largest Ca^{2+} channels with Ca^{2+} conductance of about 100 pS, in comparison to about 20 pS for voltage-gated L-type Ca^{2+} channels ($Ca_v1.1$-1.4, i.e. DHPR) (Hess *et al.*,1989), as reviewed by (Zalk *et al.*,2007). Single channel electrophysiological studies on purified RyRs indicate that RyRs conduct both monovalent and divalent cations (Lindsay *et al.*,1991; Tinker & Williams,1992), as reviewed by (Fill & Copello,2002). The conductance of RyRs is over 500 pS in symmetrical monovalent cation containing solutions, containing about 200 mM K^+, Na^+, or Cs^+ as the main permeant species (Lindsay *et al.*,1991); whereas for a divalent cation in asymmetric solutions, containing about 50 mM Ca^{2+}, Ba^{2+}, or Sr^{2+} as the main permeant species, an RyR conductance of about 100 pS was measured (Tinker & Williams,1995). In addition, although RyRs show little selectivity for either monovalent or divalent cations as charge carrier, divalent cations are still more permeant than K^+ under bi-ionic conditions. RyRs are relatively more selective for divalent cations, as the permeability ratio (P_{Ca}/P_K: about 6) indicates that Ca^{2+} is six to seven times more permeable than K^+ (Fill & Copello,2002). This P_{Ca}/P_K value of RyRs is relatively low compared to DHPRs ($P_{Ca}/P_K > 20$), as the latter display a much higher selectivity to Ca^{2+} in the cell plasma membrane. The feature of RyRs with high conductance and little ion selectivity may be explained by their specific location and environment. As RyRs are located in the SR/ER membranes, Ca^{2+} is the predominent cation that is conducted by activated RyR channels. The Ca^{2+} flows passively from ER/SR to cytosol through the opened RyR channel, as cations are driven by the ionic concentration gradient across the SR/ER membrane ($[Ca^{2+}]$: 100 μM within SR/ER; 100 nM within cytosol). Discrimination between ions, therefore, is not an essential requirement for RyR channels. However, selectivity is crucial for

ion channels (e.g. L-type Ca^{2+} channels) expressed in the cell plasma membrane, as proteins in this location are important for the regulation of electrochemical concentration gradient among different ions across the barrier.

The neutral alkaloid ryanodine, a compound that was isolated from plant *Ryania speciosa*, binds to all RyR isoforms. It has been demonstrated that ryanodine binds to RyR via a negative allosteric mechanism, suggesting that each RyR channel protein contains one high-affinity ryanodine binding site per tetramer (Wang *et al.*,1993). The high-affinity binding site has been demonstrated to occur in association with the open state of the channel. This property governs ryanodine-binding as an index of RyR channel activation (Chu *et al.*,1990a). The first ryanodine molecule binds and locks the channel in a subconductance state with high affinity; the binding of this first ryanodine on the other hand inhibits ryanodine binding on the other sites (Pessah & Zimanyi,1991). Therefore, ryanodine at low concentration (about 10 nM) appears to activate the channel by increasing the channel opening frequency to the full conductance level. Intermediate ryanodine doses (about 1 μM) encourage binding to the low-affinity site and slows the dissociation of ryanodine from the high-affinity site, which subsequently induces a long-duration open events and simultaneously reduces ion conductance through the pore (Buck *et al.*,1992). High concentrations of ryanodine (about 100 μM) can cause RyR inactivation to a closed conformation (Zimányi *et al.*,1992).

Apart from ryanodine, 4-chloro-*meta*-cresol (CmC), caffeine and ruthenium red are also known as RyR pharmacological regulators (Endo *et al.*,1970; Ma,1993; Zorzato *et al.*,1993). In addition, ions such as Ca^{2+} and Mg^{2+}, and physiological molecules such as ATP, also regulate the RyR complex. The threshold activating concentration of Ca^{2+} for both RyR1 and RyR3 is about 1 μM (Smith *et al.*,1986; Sharma *et al.*,2000); whereas RyR2 is much more sensitive to Ca^{2+} as it can be activated in 0.1 μM [Ca^{2+}] (Ashley & Williams,1990). Evidence shows that the experimental Glu3987Ala mutation in RyR2 results in a mutant channel with decreased Ca^{2+} sensitivity (Li & Chen,2001); another study shows the mutant RyR1(Glu4032Ala) also presents reduced Ca^{2+} sensitivity (Fessenden *et al.*,2001). These findings suggest that the conserved residue Glu^{3987} forms part of the high-affinity Ca^{2+}-sensing device of both RyR1 and RyR2 (Ikemoto & Yamamoto,2002).

Additionally, an interesting study shows deletion of a highly acidic/negatively charged domain in the D3 region of RyR1 (Ile^{1641}-Ala^{2437}) caused about a 10-fold decrease in sensitivity to Ca^{2+} or Mg^{2+} inhibition (Bhat *et al.*,1997); this finding is consistent with the fact that RyR2 presents less inhibition sensitivity to Ca^{2+} or Mg^{2+}, and contains a less acidic D3 region domain. This finding suggests that the structural difference in the acidic residues of the D3 region might result in a difference in the receptor sensitivity to Ca^{2+} or Mg^{2+} inhibition (Ikemoto & Yamamoto,2002). Cytosolic Mg^{2+} is a potent RyR channel inhibitor, whereas cytosolic ATP is a RyR activator; the concentrations of both free Mg^{2+} and ATP within the resting cell are about 1 mM and 300 μM, respectively.

1.5 Endogenous Regulators of RyR

The regulation of RyR gating involves a wide variety of ions and molecules. Both cytoplasmic and luminal Ca^{2+} ions are involved in channel activation. In addition to Ca^{2+}, Mg^{2+} and ATP are also endogenous regulators of RyR.

It has been demonstrated that cytosolic Ca^{2+} regulates skeletal muscle RyR1 biphasically (Meissner *et al.*,1997). This RyR channel can be activated by Ca^{2+} as low as 100 nM and the peak channel activity activation can be observed at $[Ca^{2+}]_i$ between 10-100 μM. However, Ca^{2+} alone is not sufficient to fully activate these receptor channels. Moreover, $[Ca^{2+}]_i$ in the millimolar range almost completely inhibits the channel gating (Meissner *et al.*,1997). These results suggest that Ca^{2+} at low concentration favours binding at high affinity sites that activate the channel, while Ca^{2+} at high concentration also binds to low affinity inhibitory sites of the channel. In contrast, high $[Ca^{2+}]_i$ has less inhibitory effect on RyR2 and RyR3; both RyR2 and RyR3 can almost be fully activated by cytosolic Ca^{2+} alone at 100 μM (Schiefer *et al.*,1995; Jeyakumar *et al.*,1998; Murayama *et al.*,1999). Studies on single-channel activity of rabbit skeletal muscle RyR and dog cardiac RyR indicated that both tissues contain heterogenous channel populations (Copello *et al.*,1997). Sulfhydryl (SH) oxidation by SH-oxidising agents resulted in increased activity of different native RyR channels incoporated in lipid bilayers, while reduction of cardiac RyRs caused their decreased in channel activity (Marengo *et al.*,1998).

Luminal Ca^{2+} also modulates RyR activity allosterically (Györke & Györke,1998). The luminal Ca^{2+} sensor of the RyR had been demonstrated to sense the change of internal store [Ca^{2+}], and the receptor sensitivity to cytosolic Ca^{2+} is propotional to its luminal [Ca^{2+}] (Sitsapesan & Williams,1994; Sitsapesan & Williams,1995; Ching *et al.*,2000). On the other hand, increased luminal Ca^{2+} content also alleviates Mg^{2+} inhibition allosterically (Laver *et al.*,2004). Moreover, the channel inhibitory mechanism induced by high cytosolic Ca^{2+} can be reversed by luminal Ca^{2+} interaction (Györke *et al.*,1994; Györke & Györke,1998). Evidence shows that the luminal Ca^{2+} sensing ability of the receptor is granted by both an intrinsic Ca^{2+} binding domain and RyR accessory proteins, such as calsequestrin (CSQ), triadin and junctin that are expressed in the luminal region (Ching *et al.*,2000; Györke *et al.*,2004).

Another element that also modulates the RyR channel is Mg^{2+}. This divalent cation has a potent inhibitory effect on RyR channel. Experimental results provided by single channel recordings and ryanodine-binding assays have demonstrated that the Mg^{2+} inhihitory effect on RyR1 is concentration-dependent (Smith *et al.*,1986; Pessah *et al.*,1987). It has been demonstrated that Mg^{2+} is an RyR antagonist in the absence of Ca^{2+} (Laver *et al.*,2004). Mg^{2+} at a cytoplasmic concentraction of 1 mM was found to block the RyR1 (Copello *et al.*,2002), whereas RyR2 and RyR3 in contrast, are inhibited by Mg^{2+} at higher concentrations (Meissner & Henderson,1987; Chen *et al.*,1997). It has been suggested that Mg^{2+} inhibits the channel by competing with Ca^{2+} at its high-affinity activation site and also binding at the Ca^{2+} low-affinity inactivation site of the receptor (Laver *et al.*,2004).

Adenine nucleotides such as ATP, ADP, AMP, cyclic-AMP, adenosine and adenine are also RyR activators. Among these molecules, ATP is the most potent. Experimental results on SR flux measurements, single channel recordings and ryanodine-binding assays have shown that ATP at millimolar concentration activates RyR1 in the presence of Ca^{2+} at nanomolar concentration; whereas, millimolar ATP produces persistent channel activation in the presence of Ca^{2+} at micromolar concentration (Meissner,1984; Smith *et al.*,1986; Meissner & Henderson,1987; Pessah *et al.*,1987). ATP has been demonstrated to increase the frequency and duration of channel opening of RyR2 in the presence of cytosolic Ca^{2+} (Kermode *et*

al.,1998). RyR3 is also activated by 1 mM ATP at resting $[Ca^{2+}]_i$ levels; interestingly, RyR3 resembles RyR2 more than RyR1 concerning high $[Ca^{2+}]$ (millimolar) inactivation and this high $[Ca^{2+}]$ inhibition is overiden by ATP stimulation (Chen *et al.*,1997; Manunta *et al.*,2000). It has been suggested that ATP increases the channel sensitivity to Ca^{2+} activation, while decreasing channel sensitivity to Ca^{2+} inactivation (Meissner *et al.*,1997).

1.6 Modulatory Proteins of RyRs

The channel function of RyR macromolecular complexes is modulated by numerous proteins and molecules via direct or indirect interactions. Studies on skeletal muscle show that calmodulin and FKBP12 are accessory proteins that modulate RyR1 at the triad junction (Wagenknecht & Radermacher,1997). In addition, calreticulin and calsequestrins are high capacity, SR luminal Ca^{2+} storage proteins that help to maximise Ca^{2+} storage and to control cytosolic $[Ca^{2+}]$ at physiological levels; further studies proposed that the RyR, calsequestrin, and two SR/ER integral membrane proteins, triadin and junctin, form a quaternary complex that controls the accumulation and release of Ca^{2+} from SR (Zhang *et al.*,1997).

Calmodulin (CaM) is a 17 kDa Ca^{2+}-sensing protein that binds to and modulates gating of RyRs. The high affinity Ca^{2+}-binding property of CaM is governed by a pair of EF-hands: the helix-loop-helix structural motifs are situated on both N- and C-terminal globular domains; each EF-hand binds a Ca^{2+} ion (Moore *et al.*,1999). CaM binds to all types of mammalian RyRs with nanomolar affinity; each CaM molecule binds to an RyR subunit in a 1:1 stoichiometry, irrespective of whether CaM is Ca^{2+}-free or Ca^{2+}-bound. The primary binding site of both Ca^{2+}-free and Ca^{2+}-bound CaM is located at residues 3614-3643 of RyR1, 3583-3603 of RyR2 and 3469-3489 of RyR3 (Takeshima *et al.*,1989; Yamaguchi *et al.*,2003; Yamaguchi *et al.*,2005). CaM modulates both RyR1 and RyR3 biphasically with a similar Ca^{2+}-dependent mechanism. At $[Ca^{2+}]$ in the nanomolar range, Ca^{2+}-free CaM activates both RyR1 and RyR3, whereas under micromolar cytosolic $[Ca^{2+}]$, Ca^{2+}-bound CaM undergoes a conformational change and inhibits the channel (Rodney *et al.*,2000;

Yamaguchi *et al.*,2005). CaM has been demonstrated to increase the channel opening frequency without affecting other channel properties, suggesting that CaM is involved in initiation of SR Ca^{2+} release via skeletal muscle RyRs (Rodney & Schneider,2003). In contrast, CaM suppresses SR Ca^{2+} release via RyR2 at low micromolar to submicromolar [Ca^{2+}], and therefore, CaM facilitates the termination of SR Ca^{2+} release via cardiac muscle RyRs (Xu & Meissner,2004).

The FK506-binding proteins (FKBPs) are a family of binding proteins for the immunosuppressant drugs FK506 and rapamycin (Fruman *et al.*,1995), as reviewed previously (Mackrill,1999). Both FKBP12 (calstabin1) and FKBP12.6 (calstabin2) are known as Ca^{2+} channel-stablising proteins; both are enzymes with peptidyl-prolyl-*cis*-*trans* isomerase activity (Zalk *et al.*,2007). FKBP12 is the 12 kDa FKBP isoform that predominantly mediates the function of the immunosuppressant drugs. This small protein is mainly cytosolic, catalyses peptidylpropyl-*cis*-*trans*-isomerization, which subsequently shapes target proteins by modifying the tertiary structure of protein folding. However, the isomerase activity is not required for interaction with RyR1 (Timerman *et al.*,1995). Subsequent mutation studies revealed that residues Q3, R18 and M49 of FKBP12 are required for the interaction with RyR1 (Lee *et al.*,2004). A high affinity (K_d ~ 1nM) binding of FKBP12 to RyR1 requires channels to be in an open-state; such interaction was further enhanced by approximately 4 to 5 orders of magnitude in channels with a closed configuration (Jayaraman *et al.*,1992; Jones *et al.*,2005). Studies on isolated RyR1 or SR preparations with dissociated FKBP12 (by using FK506 or rapamycin) demonstrated that FKBP12-deficient channels display enhanced Ca^{2+} conductance and long-lasting subconductance states in their gating properties (Timerman *et al.*,1993; Ahern *et al.*,1997), in addition to increased sensitivity to Ca^{2+} or caffeine activation and reduced inhibition by millimolar Ca^{2+} or Mg^{2+} (Timerman *et al.*,1993; Mayrleitner *et al.*,1994). Restoration of FKBP12 to the FKBP12-deficient cells altered RyR channel gating from showing multiple subconductance states to predominantly fully open or closed state (Chen *et al.*,1994). This evidence suggests FKBP12 binding to RyR1 stabilises the channel conductance and subsequently enhances E-C coupling. *In vitro*, RyR1 interacts with both FKBP12 and FKBP12.6, a distinct FKBP isoform; but RyR2 selectively binds to FKBP12.6 (Timerman *et al.*,1996). In cardiac muscle,

FKBP12.6 has similar effects on RyR2 to those of FKBP12 on RyR1. Removal of FKBP12.6 from RyR2 results in long-lasting subconductance states. However, restoration of this protein did not reverse the abnormal gating of RyR2 (Barg *et al.*,1997). On the other hand, enhanced contractility and cardiac output were observed in transgenic mice over-expressing FKBP12.6 (Huang *et al.*,2006). This observation implies that FKBP12.6 binding to RyR2 inhibits the channel activity and also promotes channel closure (Huang *et al.*,2006). Other studies also demonstrated that dissociation of FKBP12.6 from cardiac muscle RyRs due to hyperphosphorylation of residue S2814 is connected with heart failure and cardiac arrhythmias that were primarily caused by RyR2-mediated Ca^{2+} leak (Marx *et al.*,2000; Yano *et al.*,2000). These studies suggest that FKBPs association with RyRs is essential for stablisation of the RyR macromolecular complex in both skeletal and cardiac muscle.

The roles of calreticulin (CRT) in Ca^{2+} storage and Ca^{2+} release channel modulation are controversial. However, both CRT and calsequestrin (CSQ) are structurally related high-capacity, moderate-affinity, non-EF-hand Ca^{2+} storage proteins (Mackrill,1999). Both CRT and CSQ are found in the lumen of ER/SR, of which CSQ is the major component and CRT is the minor component in skeletal and cardiac muscle SR (Michalak & Milner,1991). Both proteins bind up to 40 moles of Ca^{2+} per mole of protein. Evidence indicated that CRT may be expressed in parallel with inositol 1,4,5-trisphosphate receptor (IP_3R), whereas CSQ is found in close association with RyRs (Ikemoto *et al.*,1989; Camacho & Lechleiter,1995). CRT is present in a variety of non-muscle tissues (Michalak & Milner,1991). It has been demonstrated that CRT acts as an ER molecular chaperone; in addition, CRT is also a modulator of both integrin function and transcription factors within the plasmalemma and nucleus, respectively (Meldolesi *et al.*,1996).

The CSQs are rich in acidic residues, most of which are found in the C-terminal region. Net surface charges provided by these acidic residues enable Ca^{2+} binding to CSQ (Wang *et al.*,1998). CSQ buffers rises in SR Ca^{2+} by directly binding to the free cations and then undergoes conformational changes. At micromolar [Ca^{2+}] (up to 10 μM), compaction of CSQ monomers occurs; while from 10 to 100 μM [Ca^{2+}], dimerisation of CSQ begins; polymerisation of linear CSQ polymers occurs

at millimolar [Ca^{2+}], the luminal free [Ca^{2+}] under physiological conditions (Wang *et al.*,1998). Therefore, CSQs exist as stable polymers within ER/SR where the free [Ca^{2+}] is at about 1 mM (Fryer & Stephenson,1996). Polymers of CSQ have been observed as electron-dense material in electron micrographs of junctional muscle preparations, indicating polymerisation of CSQ on Ca^{2+} binding (Wang *et al.*,1998; Franzini-Armstrong,1999).

CSQ is highly abundant in the terminal cisternae, which suggests its role in Ca^{2+} recruitment for subsequent Ca^{2+} release. A transient increase in intraluminal free [Ca^{2+}] is observed prior to RyR activation and subsequent decrease in luminal Ca^{2+}; such transient increases in intraluminal free [Ca^{2+}] are abolished in the absence of CSQ in the SR, and this can be reversed when CSQ are restored (Ikemoto *et al.*,1989). These observations imply that there is a reciprocal coupling between RyRs and CSQ (Gilchrist *et al.*,1992). It has been demonstrated that CSQ is anchored to the junctional face of the SR membrane through interactions with other SR integral proteins. During these interactions, junctin and triadin bind to the aspartate-rich region of the C-terminus (amino acids 354-367) of CSQ, the region that also responds to Ca^{2+} binding (Shin *et al.*,2000). It has been suggested that Ca^{2+} and triadin/junctin compete at the same binding site, and CSQ dissociates from Ca^{2+} upon change of [Ca^{2+}] (Zhang *et al.*,1997). Therefore, by interacting with triadin/junctin, CSQ shuttles luminal Ca^{2+} to the Ca^{2+} release channel, RyR. Altered conformation and reduced affinity for Ca^{2+}, triadin and junctin had been demonstrated in mutation at D307H of CSQ (Houle *et al.*,2004), which consequently results in reduced SR Ca^{2+} content and dysfunctional RyR2, characterised by decreased E-C coupling and Ca^{2+} spark frequency (Viatchenko-Karpinski *et al.*,2004). In contrast, enhanced E-C coupling and Ca^{2+} spark frequency were observed with overexpression of CSQ with a R33Q mutation, despite normal SR Ca^{2+} content (Terentyev *et al.*,2006). In addition, R33Q mutant CSQ also enhanced RyR2 channel sensitivity to luminal Ca^{2+} activation in single channel recordings (Terentyev *et al.*,2006). Both CSQ mutations lead to cardiac arrhythmias in human subjects.

Triadin is a major integral membrane glycoprotein of the junctional SR of skeletal muscle triads (Mackrill,1999). All triadin isoforms contain a common N-terminal cytoplasmic segment, a single TM domain and a variable luminal domain

with unique sequences at the C-terminus (Zissimopoulos & Lai,2007). Triadins interact with both RyR and CSQ, except Trisk 49 and 32 which do not bind RyR (Vassilopoulos *et al.*,2005). Fusion protein affinity chromatography shows the C-terminal domain of triadin interacts with both CSQ and a luminal loop of RyR via the same KEKE motif (amino acids 210-224) (Guo *et al.*,1996; Kobayashi *et al.*,2000). The interaction between triadin C-terminus and CSQ is $[Ca^{2+}]$-dependent and this interaction activity can be inhibited by increased $[Ca^{2+}]$. In contrast, the binding of triadin to RyR is Ca^{2+}-independent. It was suggested that triadin brings Ca^{2+}-bound CSQ to the skeletal muscle Ca^{2+} release channel and such interaction between triadin and CSQ subsequently shuttles and concentrates the stored Ca^{2+} ions at positions closest to the Ca^{2+}-release sites, as mentioned in previous paragraph.

In heart junctional SR, the approximately 26 kDa junctin displays a high degree of sequence identity with triadin. Junctin from cardiac muscle interacts with calsequestrin, triadin and RyR. The interaction of junctin and calsequestrin is inhibited by Ca^{2+} at millimolar concentration. The binding between triadin and junctin is thought to be mediated by the 'polar zippers'. It has been suggested that triadin and junctin directly interact in the junctional SR membrane and stablise the quaternary complex of RyR, CSQ, triadin and junction; and such coordination within the complex may be required for normal operation of SR Ca^{2+} release (Zhang *et al.*,1997).

1.7 RyRs and Human Disease

Several human diseases are associated with mutations of *RYR1* and *RYR2*. Studies on malignant hyperthermia (MH), central core disease (CCD) multi-minicore disease (MmD), and atypical periodic paralyses (APP) have indicated that RyR1 mutations are one cause of these diseases (MacLennan *et al.*,1990; Zhang *et al.*,1993; Ferreiro *et al.*,2002; Zhou *et al.*,2010). Mutations in *RYR2* gene are linked to stress-induced heart diseases such as catecholaminergic polymorphic ventricular tachycardia type 1 (CPVT1) and arrhythmogenic right ventricular dysplasia type 2 (ARVD2). The pathophysiological consequences of these human diseases are due to the presence of abnormal RyR proteins that result in a dysregulated state of $[Ca^{2+}]_i$.

These disease-associated mutations in both RyR1 and RyR2 are found in three clusters: the N-terminus at position of amino acids 35 to 614 in RyR1 and 176-420 in RyR2; the central domain in the cytoplasmic region at position of amino acids 2162 to 2458 in RyR1 and 2246-2504 in RyR2; the last cluster is located at the adjacent C-terminal position of amino acids 4647–4914 in RyR1 and 3778-4950 in RyR2 (Hamilton,2005).

MH is an autosomal disease associated with a pharmacogenetic disorder of skeletal muscle. MH susceptible individuals are characterised by sustained muscle contactions, a rise in body temperature, skeletal muscle rigidity, and rhabdomyolysis. The trigger for these symptoms is the administration of certain inhalation anesthetics, such as halothane, and depolarising skeletal muscle relaxants, such as succinylcholine (Mickelson & Louis,1996), or when the patient is exposed to high ambient temperatures (above 37^{o}C) (Jurkat-Rott *et al.*,2000). These triggers subsequently result in uncontrolled release of Ca^{2+} from the SR via the mutant RyR1 that is hypersensitive to its agonists (such as Ca^{2+}, cADPr, caffeine and halogenated anaesthetics) (López *et al.*,2000; Kobayashi *et al.*,2005).

CCD is another RyR1-related disease that results at a loss of channel function (Zhang *et al.*,1993). CCD is a congenital myopathy inherited as an autosomal-dominant disease. CCD is characterised by hypotonia, muscle weakness of lower extremities at birth and delayed motor development. CCD diagonosis is determined histologically by the presence of large amorphous areas (cores), which lacks mitochondria and oxidative enzyme activities, as reviewed by Zissimopoulos and Lai (Zissimopoulos & Lai,2007).

The lack of oxidative enzyme activites is the common feature of both CCD and MmD, and clinically, patients with CCD and MmD share similar symptoms. MmD is an autosomal recessive congenital myopathy, in which multiple cores devoid of mitochondria and disorganised sarcomeric structure are present in skeletal muscles (Zissimopoulos & Lai,2007). Patients with MmD are chacterised by hypotonia and weakness in axial and proximal limb muscles (Lanner *et al.*,2010).

Disease states due to alteration of channel properties could be explained by the position of mutations within the receptor protein (Hamilton,2005). There are more than 150 MH-linked and 60 CCD-associated point mutations identified in

RYR1 (Vukcevic *et al.*,2010). These mutation spots have been found at three regions: the N-terminal, central and C-terminal domains, as reviewed by Hamilton (Hamilton,2005). The majority of MH mutations, however, are clustered in the RyR1 cytoplasmic domains that are responsible for the increased sensitivity to pharmacological agents (eg. caffeine and halothane) (Treves *et al.*,1994); whereas most of the CCD-linked mutations are located at the pore-forming region which contributes to the enhanced Ca^{2+} leak from the store (Tilgen *et al.*,2001). Interestingly, some mutations are suggested to be the cause of both MH and CCD (Zissimopoulos & Lai,2007). In addition, patients with CCD are at risk of MH when general anaesthesia is given (Quinlivan *et al.*,2003), and the RyR1 and RyR3 antagonist dantrolene is clinically used to reverse the symptoms of an MH episode.

Mutations in *RYR2* have been linked to two forms of stress-induced arrhythmogenic heart disease: CPVT1 and AVRD2. CPVT1 is an inherited disease, characterised by adrenergically mediated bidirectional or polymorphic ventricular tachycardia, which can cause heart failure and death (Francis *et al.*,2005; Kontula *et al.*,2005). Patients with CPVT are susceptible to ventricular tachycardia resulting from β–adrenergic receptor stimulation and can develop ventricular arrhythmias (Lanner *et al.*,2010). This complication is inducible during physical or emotional stress, and reproducible by catecholamine infusion (Zissimopoulos & Lai,2007). In contrast to the appearance of structurally normal hearts in patients with CPVT1, patients with ARVD2 are characterised by the replacement of myocytes with progressive fibro-fatty tissue in the right ventricular myocardium (Corrado *et al.*,2000). Despite the structural abnormality of ARVD2, both CPVT1 and ARVD2 display similar phenotypes as stress-induced polymorphic ventricular tachycardia. At least one 2-residue insertion and over 60 point mutations have been identified in RyR2 within the C-terminal pore-forming domains, and the cytoplasimic N-terminal and central domains (Zissimopoulos & Lai,2007). These mutation regions are analogous to the mutations in RyR1 linked to MH and CCD (Lanner *et al.*,2010). Any of these RyR2 mutations at either N-terminal or central regions are suggested to 'unzip' the stabilising domains and cause the diastolic Ca^{2+} leak from RyR2 channel (Oda *et al.*,2005). The SR Ca^{2+} leak probably triggers a net inward Na^{+} current that is generated by the activation of plasma membrane Na^{+}/Ca^{2+} exchanger. Subsequently,

the net inward Na^+ current causes membrane depolarisation of cardiomyocytes during diastole (Kannankeril *et al.*,2006), namely, delayed after-depolarisation, which triggers premature action potentials and initiation of arrhythmias (Zissimopoulos & Lai,2007).

RyR3 is the least characterised RyR, and the functional roles of RyR3 are not fully understood. Several studies have demonstrated the connection between alterations in RyR-mediated Ca^{2+} release and the pathology of Alzheimer's disease (Kelliher *et al.*,1999; Smith *et al.*,2005; Supnet *et al.*,2006; Stutzmann *et al.*,2007). One of these studies demonstrated upregulation of RyR3 in cultured cortical neurons from the TgCRND8 mouse model of Alzheimer's disease (Supnet *et al.*,2006). Neuronal death of TgCRND8 neurons was observed after RyR3 knockdown by siRNA; Supnet *et al*. subsequently suggested RyR3 upregulation contributes to the neuroprotective compensatory response (Supnet *et al.*,2010). Another independent study also found increase of RyR3 mRNA level in late stage animal models of Alzheimer's disease (Bruno *et al.*,2011). Although the exact mechanism of RyR3 participation in the progression of Alzheimer's disease is unclear; the discovery of an increase in RyR3 mRNA level at late stage of the disease may provide hints of finding novel therapeutic pathway (Bruno *et al.*,2011).

1.8 G-Protein-coupled Receptor Activated Ca^{2+} Release

The guanine nucleotide binding protein (G protein)-coupled receptors (GPCR) are seven α-helical transmembrane proteins that mediate cell signalling pathways via the activation of corresponding G proteins (Gether,2000). The activation of G proteins is triggered by a variety of extracellular stimuli that transmit through GPCRs and/or tyrosine kinase receptors (eg. epidermal growth factor receptors, insulin receptors, insulin-like growth factor receptors) (Kuemmerle & Murthy,2001; Kristiansen,2004). The activated GPCR acts on heterotrimeric G proteins via guanine-nucleotide exchange factors, inducing a conformational change in the associated G protein α-subunit; subsequently, the GDP is released from the α-subunit in exchange for GTP (Bourne *et al.*,1991). The resulting GTP-bound α-subunit

dissociates from the receptor complex and acts on proteins that the G protein subtype particularly targets. As reviewed by Kristiansen (Kristiansen,2004), the major G proteins are G_s, $G_{i/o}$, G_q, and $G_{12/13}$; each one binds directly to its specific effector that conducts the corresponding downstream pathway.

The G_s subfamily activates adenylyl cyclase (AC1 to AC9) through $G\alpha_s$ and results in cAMP augmentation that triggers various downstream siganalling pathways, as indicated in Figure 1.8 (*pink zone*). Examples of $G\alpha_s$-mediated GPCRs are cardiac subtype β-adrenergic recepor (βAR) and arginine vasopressin receptor 2 (V2). One of the well-established cAMP sensor proteins is cAMP-dependent protein kinase (PKA). In ventricular myocytes, it has been demonstrated that PKA signalling enhances contractility by phosphorylation of cardiac troponin I (cTnI), RyR, L-type calcium channel (LTCC) and phospholamban (PLN), as reviewed by Bers (Bers,2002). PKA also mediates phosphorylation of cAMP-response element binding protein (CREB) on Ser133, an essential step for the activation of gene transcription (Mayr & Montminy,2001). Another cAMP sensor that mediates downstream signalling pathways, independent of PKA, is the exchange protein directly activated by cAMP (EPAC). Increased EPAC activity has been shown to increase phosphorylation of cTnI, RyR, PLN and CaMKII in the heart (Pereira *et al.*,2007; Cazorla *et al.*,2009); EPAC has also been reported to activate phospholipase Cξ (PLC-ξ) which leads to Ca^{2+} release mediated via inositol 1,4,5-trisphosphate receptors (IP_3R) and subsequent CICR in cardiac myocytes (Oestreich *et al.*,2007). Therefore, as cAMP rises in response to extracellular stimulation that activates G_s-mediated GPCRs, PKA- and EPAC-mediated pathways can then be independently operated and lead to activation of their corresponding downstream effector proteins. The resulting Ca^{2+} mobilisation and/or activation of gene transcription can be the consequence of G_s-mediated GPCR activation, regardless whether the pathway is mediated by PKA or EPAC.

Stimulation of G_q subfamily activates phospholipase C (PLCβ1-4) through $G\alpha_q$ and results in production of 1,2-diacylglycerol (DAG) and inositol 1,4,5-trisphosphate (IP_3) (Berridge,1993; Lee & Severson,1994). Examples of $G\alpha_q$-mediated GPCR are α-adrenergic recepor (αAR), angiotensin II type 1 receptor (AT_1R), ET_A type endothelin receptor (ET_AR) and arginine vasopressin receoptor 1

(V1). As indicated in Figure 1.8 (*blue zone*), the production of DAG is essential for the activation of transient receptor potential (TRP) channel family TRPC1, TRPC3, TRPC6 and TRP7 channels, plasma membrane ion channels that mediate Ca^{2+} influx (Okada *et al.*,1999; Venkatachalam *et al.*,2001; Sydorenko *et al.*,2003). In addition, DAG production also results in activation of Ca^{2+}-dependent protein kinase (PKC); which initiates serval mitogen-activated potein kinases (MAPKs) signalling cascades, such as the extracellular signal-regulated kinases 1/2 (ERK1/2) signaling in the heart (Garrington & Johnson,1999; Dorn & Force,2005). The consequence of ERK1/2 signaling has been shown as gene expression in different cell types, as reviewed by Tohogo *et al*. and DeWire *et al*. (Tohgo *et al.*,2002; DeWire *et al.*,2008). The activation of IP_3R, by IP_3 is known to cause intracellular Ca^{2+} mobilisation (Berridge,1993). The formation of Ca^{2+}/CaM complexes upon increased $[Ca^{2+}]_i$ provides further opportunity for downstream protein interaction. In addition to PKC-ERK1/2 signaling, PKC activation also results in calmodulin-dependent protein kinase II (CaMKII) activation (Shobe,2002). Various CaMKII isoforms (e.g. α, γ and δ) have been demonstrated to alter expression of different genes independent of PKC activity (MacNicol *et al.*,1990; Wegner *et al.*,1992; Matthews *et al.*,1994; Misra *et al.*,1994; Ramirez *et al.*,1997).

RyR channel activity and the subsequent RyR-mediated Ca^{2+} current can be altered by phosphorylation on centain domains of the channel complex. Evidence from *in vitro* phosphorylation studies indicated that both skeletal and cardiac RyRs are substrates for serine (S)/threonine (T) protein kinases, such as PKA and CaMKII (Takasago *et al.*,1989; Chu *et al.*,1990b; Hohenegger & Suko,1993; Suko *et al.*,1993). CaMKII had been found tightly bound to the SR membranes and co-purifies with RyR through a direct association (Chu *et al.*,1990b). Subsequent studies using site-directed mutagenesis of recombinant RyR2 indicated that CaMKII specifically phosphorylates S2815 at RyR2 and results in more active RyR2 channels that are sensitized to cytosolic Ca^{2+} (Wehrens *et al.*,2004; Kushnir *et al.*,2010). The activation of CaMKII requires Ca^{2+} elevation and the interaction with Ca^{2+}/calmodulin. The elevated Ca^{2+} comes from either Ca^{2+} influx from extracellular space, or Ca^{2+} release from intracellular stores (such as the ER and lysosome-related acidic compartments). In contrast to CaMKII, PKA interacts with RyR through

indirect association via the A kinase anchoring protein (AKAP) (Marx *et al.*,2000), a protein that binds to the leucine/isoleucine zipper domains (3003-3039) of RyR2 (Marx *et al.*,2001). The condition of PKA phosphorylation on RyRs is complicated, as conflicting results have been yielded by studies on identification of specific PKA phosphorylation sites on RyR. Both PKA and CaMKII were initially proposed to phosphorylate human RyR2 S2809 (Rodriguez *et al.*,2003). However, site-directed mutagenesis of recombinant RyR2 demonstrated that S2809 of RyR2 and the corresponding S2843 at RyR1 are the phosphorylation sites specifically for PKA (Witcher *et al.*,1991; Wehrens *et al.*,2006). The PKA phosphorylation on RyR2 had been demonstrated to activate the channel at least in part by increasing the receptor sensitivity to cytosolic Ca^{2+} (Marx *et al.*,2000). Controversially, while FKBP12.6 dissociation and depletion in these PKA phosphorylated channels were reported (Marx *et al.*,2000; George *et al.*,2003), others presented the opposite case (Xiao *et al.*,2004); it has also been proposed that the enhanced channel activity of RyR2 due to PKA phosphorylation is independent of FKBP12.6 depletion (Wehrens *et al.*,2003). Moreover, although inhibition of channel activity by dephosphorylation of RyRs using protein phosphatase (PP) has been observed in the majority of studies, increased channel activity on PP-treated RyRs was also reported (Terentyev *et al.*,2003). Serval explanations have been given for these different observations. It has been suggested that the shift from a homeostatic phosphorylation level of RyR due to either further phosphorylation or dephosphorylation results in channel activation (Carter *et al.*,2006). In addition, nitrosylation and oxidation of RyR can affect FKBP12.6 binding to the channel (Aracena *et al.*,2005; Zissimopoulos *et al.*,2007). The molar ratio differences of RyR2 and FKBP12.6 also influence the available amount of FKBP12.6 bound to the PKA phosphorylated channels (Kushnir & Marks,2010).

Figure 1.8. Putative $G\alpha_s$- and $G\alpha_q$-mediated GPCR activation signalling pathways

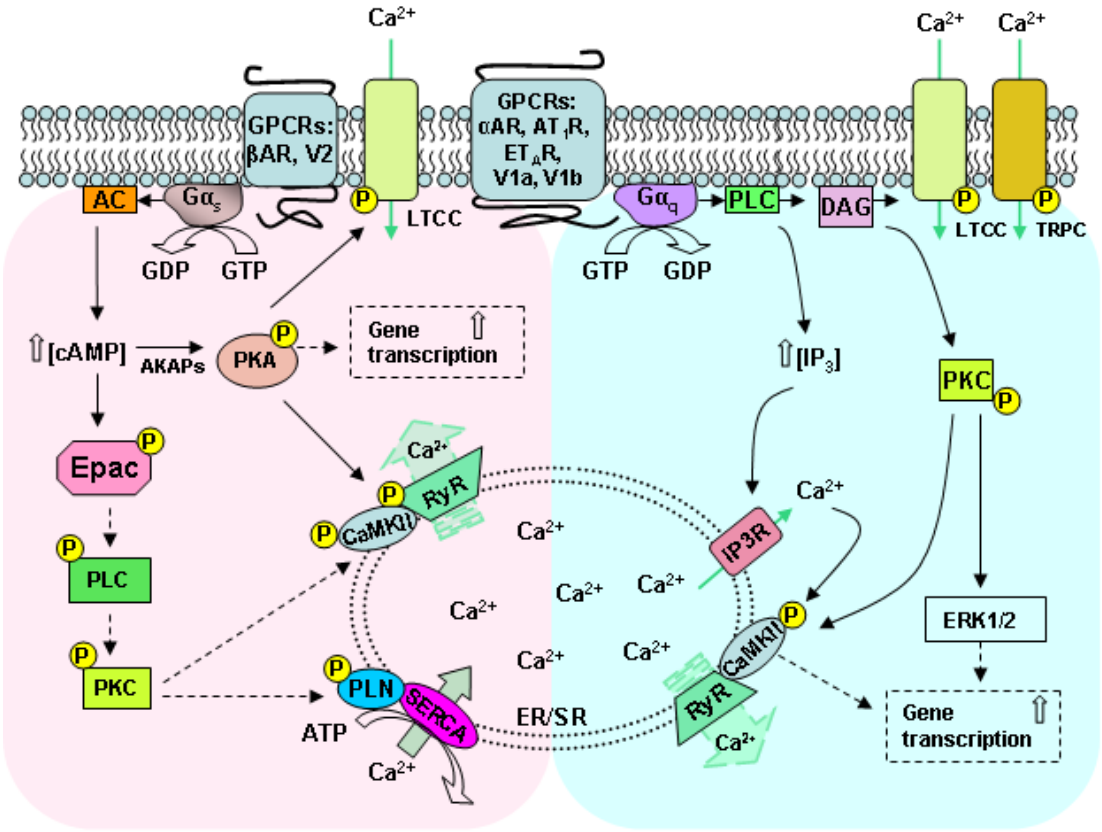

Figure 1.8. Putative GPCR-mediated Ca^{2+} release. Stimulation of $G\alpha_s$-coupled receptors, such as βAR and V2, leads to the activation of AC. The subsequent elevation of cAMP results in various cellular events via different signalling pathways (*left, pink zone*): 1). Augmentation of cAMP causes PKA phosphorylation; in the regulation of AKAPs, PKA phosphorylates RyRs and leads to Ca^{2+} mobilisation; PKA can phosphorylate LTCC to induce Ca^{2+} influx; the increase of PKA activity also leads to gene transcription. 2). Independent of PKA activation, cAMP also activates EPAC. Cardiac muscle EPAC mediates CICR from RyR via EPAC-PLCξ-PKCξ-CaMKII phosphorylation pathway; another downstream effector of EPAC is PLN; phosphorylated PLN promotes SERCA activation and Ca^{2+} re-uptake. Signalling pathways initiated by activation of $G\alpha_q$-coupled receptors, such as αAR, AT_1R, ET_AR and V1, are mediated through PLC activation (*right, blue zone*): the activation of PLC leads to the production of DAG and IP_3. 1). IP_3 activates IP_3R channel and mediates Ca^{2+} mobilisation; Ca^{2+} can stimulate RyR channel directly through the CICR mechanism; 2). DAG can phosphorylate TRPC causing Ca^{2+} influx; DAG can also activate PKC; leading to CaMKII activation, which subsequently phosphorylates RyR in the presence of Ca^{2+}; PKC also triggers ERK1/2 signalling cascade; the activation of both CaMKII and ERK1/2 leads to gene transcription.

1.9 Nitric Oxide-induced Ca^{2+} Mobilisation

Nitric oxide (NO) has been recognised as a regulator of multiple functions in the placenta. For example, the endogenous production of NO by placenta is essential for vascular tone maintainance during pregnancy (Poston,1997; Lopez-Jaramillo *et al.*,2008); in extravillous trophoblasts (EVT), NO has been shown to participate in decidual and myometrial invasion (Lyall *et al.*,1999); NO has been demonstrated to influence the release of corticotrophin-releasing hormone (CRH) and human chorionic gonadotropin hormone (hCG) (Ni *et al.*,1997; Rossmanith *et al.*,1999); moreover, NO also stimulates glucose uptake in the placenta via an insulin-independent mechanism (Acevedo *et al.*,2005). Decreased bioactivity and serum level of NO are thought to be associated with preeclampsia (PE), in which shallow trophoblast invasion of maternal spiral arteries in early gestation contributes to the development of a relatively hypoxic placenta in later gestation (Gilbert *et al.*,2008).

The NO molecule is synthesized by the NO synthase (NOS) from the amino acid L-arginine. The NOS substrate L-arginine can be transported into the placenta by cationic amino acid transportors CAT1 and CAT4 (Ayuk *et al.*,2000). On the other hand, NOS also catalyses the production of the reactive oxygen species (ROS) superoxide (O_2^-) when substrate and/or cofactor (tetrahydrobiopterin (BH_4)) levels are insufficient for NO synthesis. Superoxide can be metabolised by superoxide dismutase (SOD). However, the presence of NO results in the formation of a powerful oxidant peroxynitrite (ONO_2^-), as the two free radicals ($NO + O_2^- \rightarrow ONO_2^-$) react. The resulting product peroxynitrite competes with superoxide for SOD detoxification. The formation of superoxide, therefore, depletes the available NO in the placenta, as reviewed by Myatt (Myatt,2010). The elevated levels of superoxide and peroxynitrite, hence, contribute to the decrease in NO bioactivity which is generally associated with endothelial dysfunction, vasoconstriction and reduced trophoblast invasion in PE (Gilbert *et al.*,2008).

The activities of both endothelial (e) and inducible (i) NOS isoforms have been characterised in trophoblast populations (Eis *et al.*,1995; Lyall *et al.*,1998; Baylis *et al.*,1999; Schiessl *et al.*,2005). The Ca^{2+}/CaM-dependent isoform eNOS is expressed in the syncytiotrophoblast (SCT) throughout pregnancy; and also

expressed in endothelium within the primitive villous capillaries during human early and mid gestation (Rossmanith *et al.*,1999); both eNOS and iNOS (the Ca^{2+}/CaM-independent isoform), are expressed in intermediate and EVT of human first trimester placenta (Ariel *et al.*,1998; Rossmanith *et al.*,1999). In addition, the iNOS activity increases throughout pregnancy and peaks at mid gestation, as reviewed by Krause *et al*. (Krause *et al.*,2011). The precise mechanism of placental eNOS activation is not fully established yet. However, study in eNOS knockout mice suggests that signalling molecules of MAPK and phosphoinositide-3-kinase (PI3K)-Akt signaling system play a crucial role in the initial phosphorylation and activation of eNOS (Connelly *et al.*,2005). In addition, the eNOS trafficking inducer (NOSTRIN) which is involved in eNOS intracellular trafficking between cellular compartments, has been suggested to facilitate eNOS endocytosis in coordination with dynamin and neural Wiskott-Aldrich syndrome protein (N-WASP) (Icking *et al.*,2005). The N-WASP is involved in the formation of actin tails that propel pathogens and endogenous vesicles through the cytoplasm (Fehrenbacher *et al.*,2003).

One of the immediate downstream effectors of NO in the NO-induced signalling pathway is guanylate cyclase (GC). In human placenta, the cytoplasmic soluble form of GC (sGC) has been identified in SCT and villous trophoblast and umbilical blood vessels, sites of where NO is produced (Bamberger *et al.*,2001). As Figure 1.9 illustrates: the activation of GC initiates the elevation of intracellular cyclic guanosine monophosphate (cGMP) concentration (Murad,1994). Studies in sea urchin eggs demonstrated that NO stimulates cGMP production via GC activation, followed by the activation of cGMP-dependent kinase (PKG); the activated PKG is then phosphorylated and activates ADP-ribosyl cyclase (ADPR cyclase), which in turn produces cyclic ADP-ribose (cADPR) and/or nicotinic acid adenine dinucleotide phosphate (NAADP) (Lee *et al.*,1989). Both cADPR and NAADP are Ca^{2+} mobilising nucleotides that release Ca^{2+} from internal stores in a wide variety of cells from protist and plant to human, as reviewed by Lee (Lee,1997; Lee,2000b). The cyclic nucleotide cADPR is derived from nicotinamide adenine dinucleotide (NAD), while NAADP is a metabolite of nicotinamide adenine dinucleotide phosphate (NADP) (Lee,1997). Despite the structural and functional difference between cADPR and NAADP, both products are synthesised by the same

class of enzymes. Among these enzymes, ADPR cyclase and its homolog CD38 (cluster of differentiation 38) are the most well characterised. The CD38 is a mammalian antigen that can be found in a variety of tissues, present on membranes of both cell surfaces and intracellular organelles (Aarhus *et al.*,1995). The cyclisation of NAD by CD38 occurs optimally at physiological pH to produce cADPR, while the base-exchange reaction of the nicotinamide group in NADP with nicotinic acid by CD38 can only be achieved in acidic pH to produce NAADP, as reviewed by Lee (Lee,1997).

Both cADPR and NAADP are known as the second messengers for intracellular Ca^{2+} mobilisation. The NAADP targets the two-pore channels (TPCs), the members of the superfamily of voltage-gated channels expressed in the lysosomes, the acidic stores often found in close proximity to the ER/SR (Ishibashi *et al.*,2000; Churchill *et al.*,2002; Kinnear *et al.*,2004; Calcraft *et al.*,2009). Direct NAADP-dependent current measurements indicate that TPC in the lysosomes are permeable to Ca^{2+}; such Ca^{2+} permeability of TPC (TPC2) induced by NAADP is over 1000-fold more selective than K^+ under acidic intralysosomal pH (Pitt *et al.*,2010); the TPC single channel Ca^{2+} conductance is ~15 pS, which is about 4 and 8 times less than that measured in IP_3R and RyR, respectively (Schieder *et al.*,2010). In addition, immunopurified TPC1 and TPC2 from urchin eggs have been demonstrated to mediate NAADP-induced Ca^{2+} release in transfected HEK293 cells; of which, activation of TPC2 is more tightly coupled to subsequent IP_3R-mediated Ca^{2+} release; activation of TPC3, in contrast, suppresses NAADP-induced Ca^{2+} release; increased expression of either type of TPC affects endolysosmal strutures and dynamics (Ruas *et al.*,2010). The authors proposed that NAADP regulates the endolysosomal Ca^{2+} store via TPCs and subsequently affect ER Ca^{2+} release that may have impacts on Ca^{2+} signalling in health and disease (Lloyd-Evans *et al.*,2008; Ruas *et al.*,2010).

The ER Ca^{2+} channel RyR is generally accepted as the target for cADPR-induced Ca^{2+} release. It has been demonstrated that cADPR in nanomolar concentration enhances the RyR-mediated CICR mechanism in sea urchin eggs (Galione *et al.*,1991). As the RyR protein possesses binding sites for adenine nucleotide, such as ATP and ADP diadenosine compounds (Smith *et al.*,1985), these

compounds therefore, potentially compete the same binding sites with cADPR. In addition, experimentation has shown that cADPR pharmacologically behaves as a partial agonist of RyR (Sitsapesan *et al.*,1994). The exact mechanism by which cADPR induces RyR-mediated Ca^{2+} release is still unclear. However, evidence has shown that the action of cADPR on RyR requires associate proteins such as FKBPs, CaM and CaMII, as reviewed by Lee (Lee,2011) and Venturi (Venturi *et al.*,2012). Apart from RyR, cADPR can also paradoxically induce Ca^{2+} influx via the plasma membrane channel TRPM2 in certain cells such as neutrophils and pancreatic β-cells (Partida-Sánchez *et al.*,2001; Togashi *et al.*,2006). This TRPM2 channel belongs to the M-family of TRPCs. In addition, the physiological consequence of cADPR-dependent Ca^{2+} influx via TRPM2 has been revealed in several studies. For instance, cADPR-induced Ca^{2+} influx has been demonstrated to stimulate secretion of insulin and oxytocin from pancreatic islets and neuronal cells, respectively (Togashi *et al.*,2006; Jin *et al.*,2007); in human bone marrow mesenchymal stem cells, such cADPR-TRPM2 signals increase the frequency of Ca^{2+} oscillations and result in enhanced cell proliferation (Scarfì *et al.*,2008; Tao *et al.*,2011).

Figure 1.9 Putative NO-induced Ca^{2+} signalling pathways

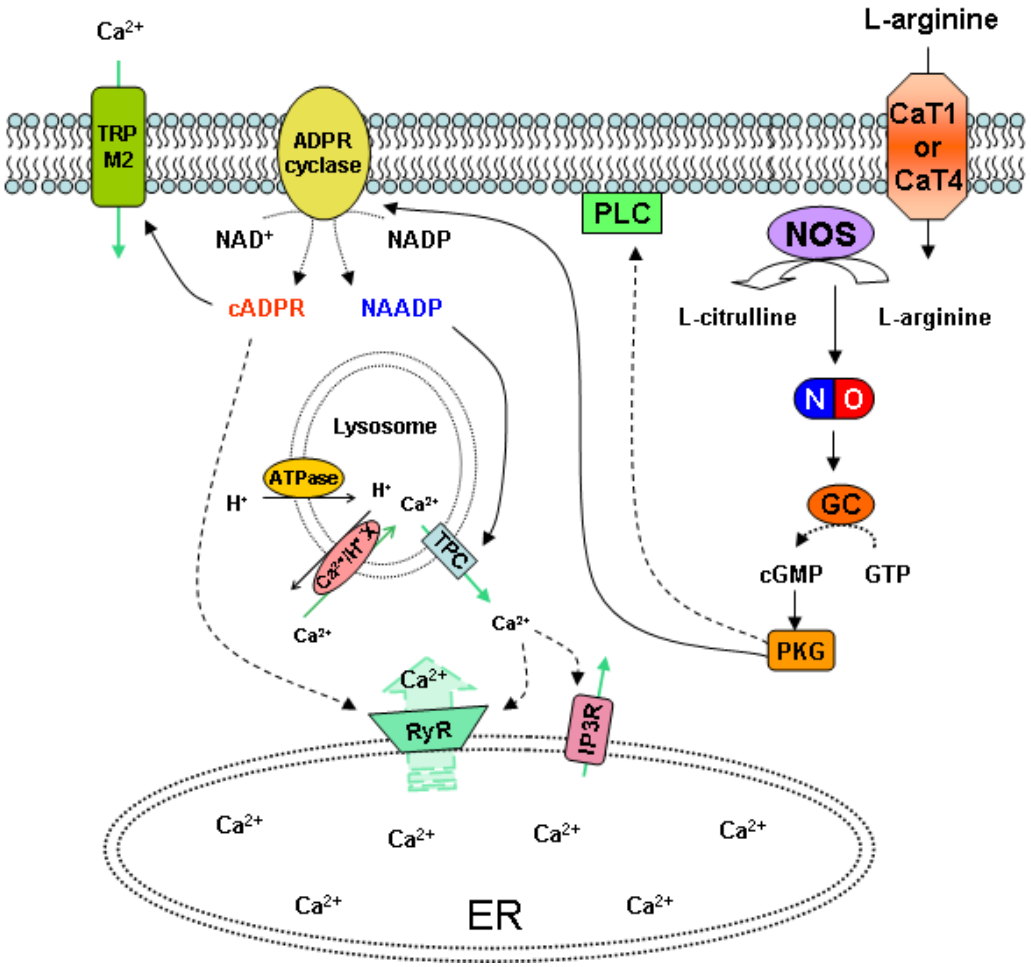

Figure 1.9. Possible signalling pathways trigger Ca^{2+} mobilisation initiated by nitric oxide synthesis. The substrate L-arginine enters the cell via cationic transporter CaT1 or CaT4. L-arginine is then converted to nitric oxide (NO) by nitric oxide synthase (NOS); NO activates soluble guanylate cyclase (GC) and produces intracellular cyclic guanosine monophosphate (cGMP) (Murad,1994). Elevated cGMP activates cGMP-dependent kinase (PKG) and phosphorylates ADP-ribosyl cyclase (ADPR cyclase); activated ADPR cyclase in turn produces cyclic ADP-ribose (cADPR) and/or nicotinic acid adenine dinucleotide phosphate (NAADP) (Lee *et al.*,1989). NAADP binds to the lysosmal two-pore channel (TPC) to release Ca^{2+}, which subsequently results in CICR possibly via endoplasmic RyR and/or IP_3R (Lee,1997). The cADPR activates on ER Ca^{2+} releasing channel RyR and M2 TRP (TRPM2) in certain cell types to induce Ca^{2+} release and Ca^{2+} influx, respectively, as reviewed by Lee (Lee,2011).

1.10 Ca^{2+} in Human Placenta

Ionised intracellular free calcium is a universal signalling ion. Free $[Ca^{2+}]_i$ in resting cells is about 100 nM; elevated cytosolic Ca^{2+} is a known trigger of various cellular events, such as gene transcription, cell proliferation, differentiation, apoptosis and necrosis (Berridge *et al.*,2000). The versatility of Ca^{2+} signalling is highly regulated; the control of $[Ca^{2+}]_i$ is governed by a sophisticated functional coordination among a wide range of Ca^{2+}-related proteins, which include Ca^{2+} pumps, Ca^{2+} channels, Ca^{2+} transporters/exchangers and Ca^{2+} binding proteins.

The elevated cytosolic Ca^{2+} level as a cellular signal is derived either from internal stores or from the external medium. The release of Ca^{2+} from the ER/SR via RyRs or IP_3Rs is regulated by various endogenous factors, such as cADPR and IP_3, respectively (Furuichi *et al.*,1989; Lee *et al.*,1989; Berridge,1993). In addition, Ca^{2+} mobilisation has also been demonstrated from lysosome-related acidic compartments by NAADP (Churchill *et al.*,2002; Yamasaki *et al.*,2004), and such Ca^{2+} release is mediated by the TPCs that comprise a family of the NAADP receptors (Calcraft *et al.*,2009). Both RyR and IP_3R respond to cellular signalling molecules that transduce extracellular stimuli via activation of different plasma membrane receptors/channels (Berridge *et al.*,2003). In the placenta, these Ca^{2+} signalling processes usually involve activation of different protein kinases and G-protein-coupled receptors (GPCR) (Baczyk *et al.*,2011). Figure 1.10.1 summarises the putative signalling pathways initiated by GPCR activation, indicating the possible movement of calcium ions. It has been demonstrated that elevated $[Ca^{2+}]_i$ is a trigger of extravillous trophoblast (EVT) migration as a result of external stimulation by endothelin 1 (ET1) or prostaglandin E2 (PGE2) (Chakraborty *et al.*,2003; Nicola *et al.*,2005a). Both the prostaglandin E receptor 1 (EP1) and endothelin receptors (ET_A and ET_B) are GPCRs for PGE2 and ET1, respectively. The EP1 receptor is a G_q-coupled GPCR that is known to activate the phospholipase C (PLC) that causes accumulation of IP_3 which subsequently activates IP_3-sensitive receptors (IP_3R) in the ER membrane. Opening of IP_3 receptor channels leads to rise of $[Ca^{2+}]_i$. It has been demonstrated that such rise in intracellular Ca^{2+} has a crucial role in the migration of first trimester human

EVT (Nicola *et al.*,2005a). In the EVT cell line HTR8/svneo, stimulation of ET_A and ET_B by ET1 results in the activation of G_q-dependent but G_i-independent mitogen-activated protein kinase (MAPK) cascades, also known as extracellular signal regulated protein kinases cascades (ERK1/2). These signalling events involve activation of PLC and the subsequent production of IP_3 and DAG (Chakraborty *et al.*,2003). Both IP_3 and DAG are important second messenger molecules. The former activates IP_3R in the ER and causes the initial rise of $[Ca^{2+}]_i$; while the following sustained plateau is gained from the external entry via non-selective cation channels (NSCC) and store-operated Ca^{2+} channels (SOCC) (Chakraborty *et al.*,2003). On the other hand, DAG is involved in the activation of Ca^{2+}-dependent protein kinase (PKC) activated MAPK signaling pathways (Gill *et al.*,1989). In BeWo cells, activation of MAPK signaling pathway (ERK1/2 and p38 MAPK) by forskolin stimulation is involved in cell fusion (Delidaki *et al.*,2011). In cultured primary human cytotrophoblasts (CT), spontaneous differentiation and fusion occurs; and the formation of syncytiotrophoblast (SCT) displays a positive correlation with Ca^{2+} uptake and up-regulation of Ca^{2+} channel expression (Niger *et al.*,2004). In addition to cell migration and cell differentiation, intracellular Ca^{2+} signaling in trophoblasts also participates in cell proliferation, as reviewed by Baczyk *et al*. (Baczyk *et al.*,2011).

Figure 1.10.1 Putative signaling pathways in placental trophoblast initiated by GPCR activation

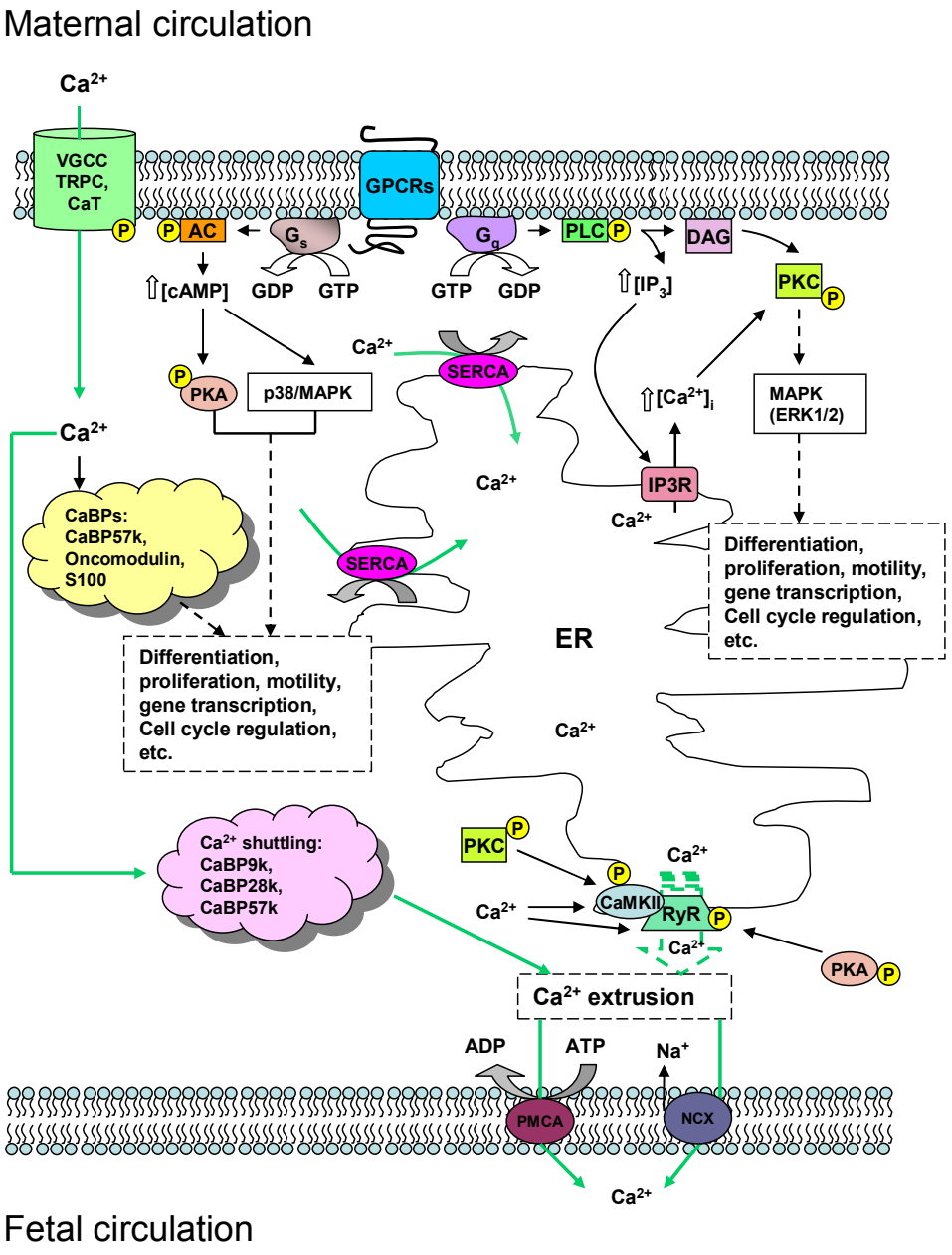

Figure 1.10.1. Two putative GPCR-initiated signalling pathways within placental trophoblast. As illustrated: (1) the cAMP-dependent G_s-mediated pathway; and (2) the Ca^{2+}-dependent G_q-mediated pathway. Green bold arrows indicate the movement of Ca^{2+}: free Ca^{2+} from maternal circulation enters the brush border membrane (BBM) via various apical membrane receptor/channel proteins of placental trophoblastic cell, e.g. Ca^{2+} transporter proteins (CaT), voltage gated Ca^{2+} channels (VGCC) and transient receptor potential (TRP)-related /'transient receptor potential vanilloid' (TRPV) Ca^{2+} channels. Free Ca^{2+} entering the cytoplasm is speedily and actively compartmentalised and stored in organelles such as the ER by sarcoendoplasmic reticulum Ca^{2+}-ATPase pumps (SERCA); meanwhile, Ca^{2+} can also be buffered immediately by a variety of Ca^{2+} binding proteins (CaBPs). Protein bound Ca^{2+} is divided in two groups depending on which CaBPs are bound. For example, CaBP67k, oncomodulin, and S100 bound Ca^{2+} leads to cell differentiation, proliferation and cell cycle regulation; while CaBP9k, CaBP28k and CaBP57k bound Ca^{2+} is shuttled for Ca^{2+} extrusion at the basal plasma membrane (BPM). Compartmentalised Ca^{2+} can also be released from the ER mediated by activation of IP_3Rs or RyRs, which can be phosphorylated by CaMKII, PKC and/or PKA; internally released Ca^{2+} along with protein bound Ca^{2+} at positions close to the plasma membrane Ca^{2+}-ATPase (PMCA) and/or Na^+/Ca^{2+} exchanger (NCX) at the BPM can be extruded and transferred to the fetal circulation.

A functional placenta is crucial to successful pregnancy. During the formation of placenta, Ca^{2+} signalling plays a key role throughout blastocyst implantation and trophoblast cell differentiation (Baczyk *et al.*,2011). More importantly, Ca^{2+} and Ca^{2+} maternal-fetal transport are vital for fetal development (Lafond *et al.*,2001). The human placenta transfers up to 30 g of Ca^{2+} during pregnancy; particularly, from week 28 of pregnancy: the third trimester, the weight of the fetus triples and the Ca^{2+} transport quadruples to about 140 mg/kg/d for mineralization of the fetal skeleton (Salle *et al.*,1987). In the plasma, about 40% calcium is protein-bound (mainly albumin) form; approximately 10% forms complexes with other negatively charged molecules such as bicarbonate; the remaining calcium population is regarded as ionised free Ca^{2+} (Husain & Mughal,1992). Calcium in both ionised and ion complex forms are ultrafilterable: the forms of calcium that can be utilised by the body. The concentration of ultrafilterable calcium in the fetal circulation (2.65 ± 0.19 mM, ionised free Ca^{2+} 1.41 ± 0.09 mM) is higher than in the maternal circulation (2.13 ± 0.15 mM, ionised free Ca^{2+} 1.12 ± 0.06 mM) (Schauberger & Pitkin,1979). Such hypercalcemic status of fetal calcium homeostasis is maintained by the parathyroid hormone-related peptide (PTHrP), an oncofetal hormone produced from early gestation until term (Senior *et al.*,1991). In contrast to plasma [Ca^{2+}], cytosolic free [Ca^{2+}] of SCT is maintained as low as 40 nM (Husain & Mughal,1992). These observations suggest the passive Ca^{2+} entry from maternal circulation via microvillous membrane of SCT is speedily buffered and compartmentalised without causing unwanted $[Ca^{2+}]_i$ fluctuations in placental trophoblast.

The delivery of Ca^{2+} ions from maternal circulation into the fetal circulation is initially facilitated by a variety of active Ca^{2+} transporters expressed in the brush border membrane (BBM) of trophoblasts. Figure 1.10.2 summarises the putative transepithelial Ca^{2+} transport through trophoblast. As reviewed by Belkacemi *et al*., Ca^{2+} entry through the BBM of SCT involves activation of Ca^{2+} transporter proteins (CaT); voltage dependent Ca^{2+} channels (VDCC) eg. L-type, T-type VDCC, and transient receptor potential (TRP)-related Ca^{2+} channels/'transient receptor potential vanilloid' (TRPV), such as TRPV5 and TRPV6; Ca^{2+} entering via these protein

channels can be actively transported into the ER by sarcoendoplasmic reticulum Ca^{2+}-ATPase pumps (SERCA), or can bind to Ca^{2+}-binding proteins such as calbindins (CaBPs) CaBP9k, CaBP28k and CaBP57k (Belkacemi *et al.*,2002); Ca^{2+} extrusion at the basal plasma membrane (BPM) is carried out by plasma membrane Ca^{2+}-ATPase (PMCA) and likely in parallel with Na^{+}/Ca^{2+} exchanger (NCX) (Kamath & Smith,1994; Belkacemi *et al.*,2005). At these extrusion venues, free Ca^{2+} ions are delivered trans-trophoblasticaly into the fetal circulation.

It has been demonstrated that SERCA in the ER functions together with NCX and PMCA in series for the removal of cytosolic free Ca^{2+} in isolated rabbit aortic endothelial cells (Wang *et al.*,2002). The same research group has also suggested that endothelial Ca^{2+} removal/transport is through serial actions of Ca^{2+} active uptake by SERCA, then release by RyR, and finally extrusion by NCX and PMCA (Liang *et al.*,2004). This study indicates close functional proximity of RyR and both NCX and PMCA; the authors also emphasised that only RyRs but not IP_3Rs are involved in Ca^{2+} extrusion in these cells (Liang *et al.*,2004). These observations suggesting RyR plays a potential role in Ca^{2+} transcellular transport in trophosphoblasts. A more recent study by Haché and collegues reported that Ca^{2+} transport by SCT is disturbed in preeclampsia (PE), a condition in which high blood pressure and high level of protein in urine develop after week 20 of pregnancy (Haché *et al.*,2011). This study demonstated the expression of BPM plasma membrane PMCAs were downregulated together with both TRPV5 and TRPV6 Ca^{2+} channels in the BBM and cytosolic CaBPs CaBP9k and CaBP28k. These results suggest low efficiency of Ca^{2+} transport at both BBM and BPM. In contrast mRNA levels of SERCA were upregulated, while of RyRs and IP_3Rs mRNAs were downregulated in this pathlogical condition (Haché *et al.*,2011). The authors proposed this alteration is an adaptation of avoiding Ca^{2+} overload from internal stores. The entry of Ca^{2+} may be partially compartmentalised into the ER in addition to Ca^{2+} transport by CaBP buffering. As indicated in Figure 1.10.2, it is possible that Ca^{2+} can be actively transported into the ER by SERCA and released via Ca^{2+} release channels, the RyRs or IP_3Rs, in addition to Ca^{2+} transport by CaBP shuttling.

Figure 1.10.2 Putative Ca^{2+} trans-trophoblast transport pathways

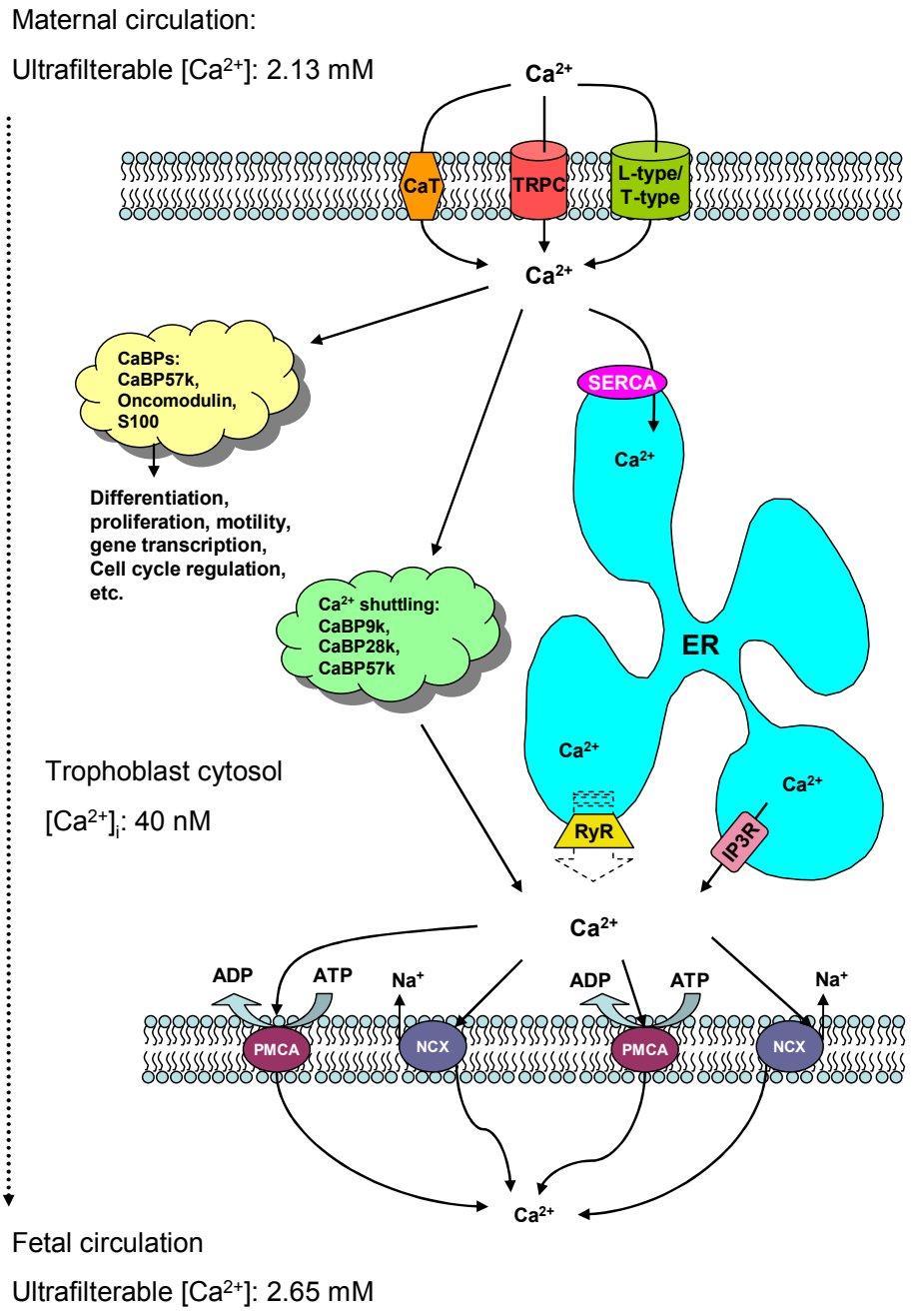

Figure 1.10.2. Putative Ca^{2+} trans-trophoblast transport. Bold arrows indicate the possible pathways of Ca^{2+} movement in placental trophoblast, while the dotted arrow indicates the overall Ca^{2+} movement from maternal circulation to fetal circulation is against its concentration gradient. Free Ca^{2+} enters the brush border membrane (BBM) via various apical membrane receptor/channel proteins of placental trophoblastic cell, eg. transient receptor potential (TRP)-related Ca^{2+} channels/'transient receptor potential vanilloid' (TRPV) and the voltage gated Ca^{2+} channels (VGCC: eg. L-type, T-type). Free Ca^{2+} is speedily and actively compartmentalised and stored in organelles such as the ER by sarcoendoplasmic reticulum Ca^{2+}-ATPase pumps (SERCA); Ca^{2+} can also be buffered immediately by a variety of Ca^{2+} binding proteins (CaBPs). CaBP67k, oncomodulin, and S100 bound Ca^{2+} is involved in cell differentiation, proliferation and cell cycle regulation; while CaBP9k, CaBP28k and CaBP57k bound Ca^{2+} is shuttled for Ca^{2+} extrusion at the basal plasma membrane (BPM). Compartmentalised Ca^{2+} could also be released from ER via RyRs or IP_3Rs that are in close apposition to plasma membrane Ca^{2+}-ATPase (PMCA) and/or Na^{+}/Ca^{2+} exchanger (NCX) at the BPM, where protein bound Ca^{2+} is released and extruded. Therefore, the transfer of Ca^{2+} is completed actively from the maternal to the fetal circulation.

1.11 Formation of Placenta

Trophoblasts are epithelial cells forming the peripheral part of the human conceptus. These cells are derived from the blastocyst cytotrophoblast layer of the embryo and regarded as the precursor cells of the human placenta. Trophoblasts initially present as an outer layer of cells of the blastocyst, which can be found as early as from the third day of fertilization. The formation of a functional human placenta relies on trophoblast proliferation and differentiation. The sequential regulation of placental trophoblast development is crucial for successful pregnancy. A fully developed human placenta is an haemochorial villous organ (Gude *et al.*,2004), in which maternal blood is intimately in contact with the placental trophoblast, delivering nutrients and essential elements from the maternal side, meanwhile removing waste products from the blood circulation of fetus. The placenta is also a barrier that protects the fetus from immune attack from the maternal side. Apart from these protection and transportation functions, the placenta also generates hormones that are essential for the fetal development (Knobil & Neill,1998).

The ovum is fertilized within the fallopian tube. After three days development, the germ cell forms a blastocyst that arrives at the uterus cavity (Figure 1.11.1.A). The blastocyst is composed of two groups of cells: the inner cell mass which will develop into the fetus, and the outer trophoblasts which are a determinant for the process of blastocyst implantation and the subsequent development of the human placenta (Knobil & Neill,1998), as Figure 1.11.1.B illustrates trophoblast invasion starts by pentrating the uterine epithelium. Trophoblasts start generating human chorionic gonadotropin (hCG) after fertilization. The release of this signalling hormone increases the receptivity of uterus to the implanting embryo. Blastocyst implantation is a complicated process relying on communication between embryo and uterus. The trophoblasts are naturally invasive; but the uterine wall is usually covered by a thick layer of mucin and transmembrane glycoproteins which prevent blastocyst attachment and trophoblast invasion. However, the receptivity of endometrial surface to trophoblast invasion can be altered in a restricted period

termed the “window of receptivity” (Lunghi *et al.*,2007). In this particular period of the menstrual cycle (usually days 20-24) (Salamonsen *et al.*,2003), the endometrial surface is modified by estrogen and progesterone to prepare for blastocyst implantation (Gude *et al.*,2004). These hormones regulate the secretion of locally acting factors such as growth factors, chemokines, cytokines and adhesion molecules of the endometrium (Hoover,2004). These locally acting factors provide a docking site for the embryo attachment, and also limit the trophoblast invasion to a specific area rather than to anywhere over the uterus. Secretion of hCG together with the endometrial surface modification therefore, facilitate the docking of the floating blastocyst into the uterus.

The zona pellucida, as illustrated in Figure 1.11.1.A, the ‘red coat’ surrounding the cell complex, disappears before the blastocyst attaches to the endometrial epithelium (Gude *et al.*,2004; Sadler,2006a). Once the embryo successfully docks into the endometrium, the trophoblasts of the blastocyst proliferate rapidly and differentiate into an inner mononuclear cytotrophoblast and an outer multinucleated syncytiotrophoblastic mass which continuously invades into the endometrial epithelium and connective tissues. Twelve days after fertilization, as illustrated in Figure 1.11.2.A, these invasive trophoblasts penetrate the maternal blood vessels and start forming new branches of vessels in terms of ‘intertrophoblastic maternal blood filled sinuses’(maternal sinusoids, Figure 1.11.2.A) to support the growth of fetus and placenta (Knobil & Neill,1998; Sadler,2006b). Therefore, a primitive uteroplacental circulation is formed by the end of second week of fertilization. Meanwhile, cytotrophoblastic cell columns are formed as the non-vascular primary chorionic villi that penetrate into the syncytium (Sadler,2006b). Three weeks after fertilization, the embryo starts generating its own circulatory system. This process begins with migration of mesodermal cells to the primary villi core towards the decidua. Mesodermal cells in the core of the villus are then differentiated into hematopoietic cells and small blood vessels to form the villous carpillary system, the intraembryonic circulatory system that connecting the placenta and embryo (Doetschman *et al.*,1985). The longitudinal villus section in Figure 1.11.2.B shows the formation of capillaries within the mesoderm core of chorionic villi, the tertiary villus. There vessels are part of the intraembryonic circulatory

system that connecting the placenta and the fetus; the development of these villous capillary system is essential for future delivery of nutrients and gas exchange in the placenta (Sadler,2006c). The embryonic tissue and maternal blood are separated by a layer of cytotrophoblasts and syncytiotrophoblasts. At week 4, the basic structure of the placenta is formed; the chorionic villi adjacent to the maternal blood supply continuously expanding into a mass of chorionic tissue as the placenta matures; the villi gradually degenerating to form the chorionic layer of the external membranes (Knobil & Neill,1998). At about week 20, the amnion-chorion membrane reaches the opposite side of the uterus and fuses with the decidualized maternal endometrium, and the full external membrane (consisting of amnion, chorion and decidua layers) is formed.

Figure 1.11.1 Development of germ cell and implantation of blastocyst.

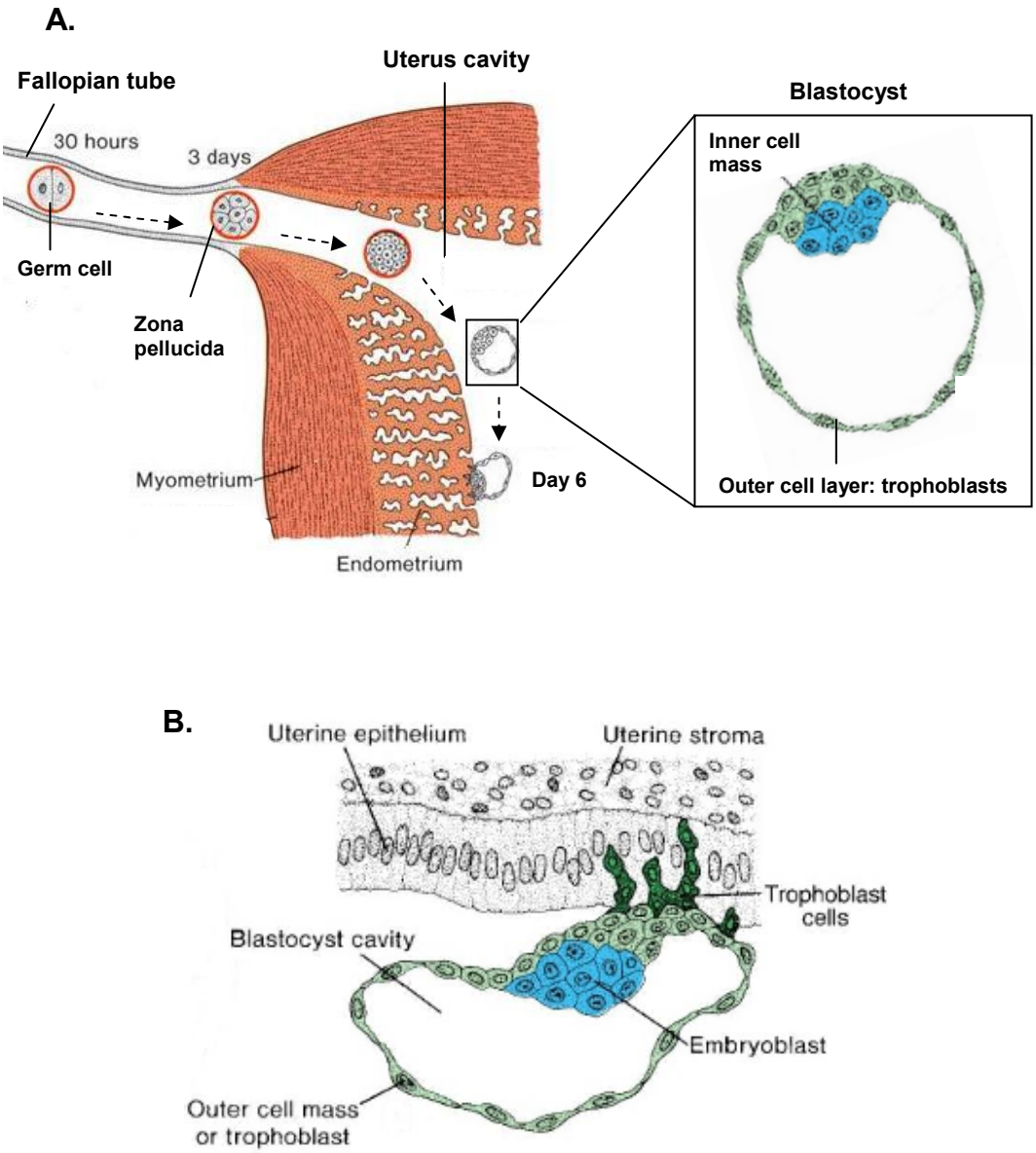

Figure 1.11.1. Schematic representation of the development of germ cell and implantation of blastocyst. These figures are adapted from Sadler (Sadler,2006a). **A.** The fertilized ovum (germ cell) travels from the fallopian tube to the uterus cavity; meanwhile it has gone through a series of cleavages. As from Day 4, the germ cell develops into the morula stage and undergoes compaction to form a blastocyst. The blastocyst is composed of inner cell mass and outer trophoblast cell layer. The zona pellucida (the 'red coat') surrounding the blastocyst disappears at about Day 5. On about Day 6, the blastocyst docks into the uterine endometrium and starts implantation (Sadler,2006a). **B.** Schematic illustration of trophoblast invasion. Ourter trophoblast cells of blastocyst are penetrating the uterine epithelium. This marks the initiation of blastocyst implantation.

Figure 1.11.2 Post-implantation development of blastocyst and formation of chorionic villi.

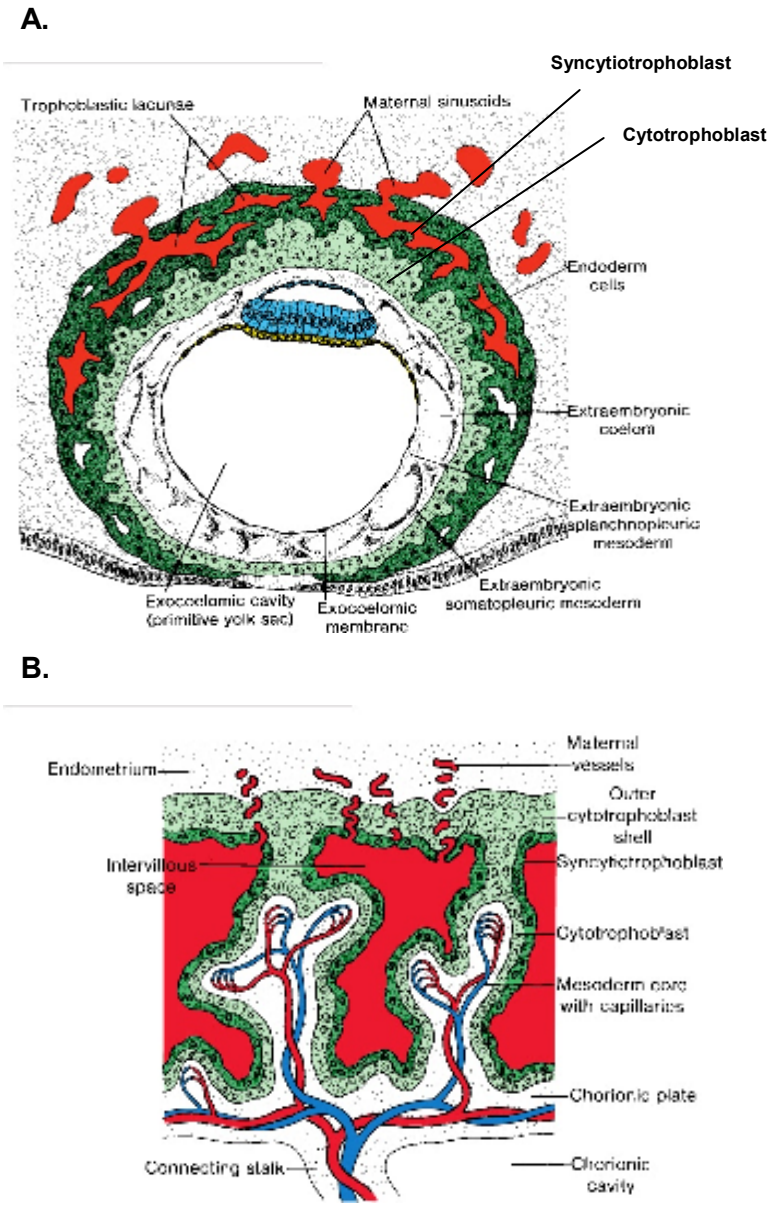

Figure 1.11.2. Post-implantation development of blastocyst. These figures are adapted from Sadler. A (Sadler,2006b; Sadler,2006c). A. Illustration of human blastocyst on about Day 12. Invading trophoblasts penetrate the maternal blood vessels and form maternal sinusoids; this marks the formation of uteroplacental circulation that maternal blood is delivered for placenta development and fetus growth (Sadler,2006b). B. Illustration of longitudinal section of villus at the end of the third week development. Villous capillary system is surrounded by maternal vessels that penetrate the cytotrophoblastic shell and fill in the intervillous spaces. These capillary vessels are connecting to the connecting stalk in the chorionic plate, which in turn are connected to intraembryonic vessels (Sadler,2006c).

1.12 Differentiation of Trophoblasts

Once implantation is successful and placentation is initiated, trophoblasts undergo rapid proliferation and differentiation (Gude *et al.*,2004). Primary blastocyst trophoblasts sequentially differentiate into the villous and extravillous trophoblasts during blastocyst implantation (Lunghi *et al.*,2007). Around day 13 of pregnancy, the cytotrophoblast cells form columns of extravillous cytrophoblast cells by penetrating the syncytiotrophoblast layer that surrounding the conceptus. The extravillous trophoblast column shell forms the interface of the feto-maternal compartments (Boyd & Hamilton,1970; Aplin,1991). These extravillous trophoblast cells can invade into the decidua and modify the uterine arteries. Uterine artery modification results in dilated and compliant uterine arterioles, which subsequently lead to increased placental blood supply from the maternal blood (Gude *et al.*,2004). On the other hand, extravillous cytotrophoblast cells also invade interstitially. These interstitial trophoblasts facilitate the placental expansion in size and also promote recruitment of maternal arterioles. By week 8 of pregnancy, the interstitial trophoblasts form a multinucleated placental bed of giant cells and invade deeper into the decidua (Boyd & Hamilton,1970; Aplin,1991). This morphology of the interstitial trophoblasts is thought to be the differentiation end-point of the extravillous cytotrophoblasts (Gude *et al.*,2004).

Another differentiation pathway of cytotrophoblasts is towards to the formation of syncytiotrophoblasts. The non-migratory cytotrophoblasts proliferate, differentiate and fuse to form villous syncytiotrophoblasts, the barrier of cells that function as sites for material transport between fetus and maternal sides, which also act as endocrine secretion sites of the placenta. Villous syncytiotrophoblast cells generate most placental hormones. The best characterised of these is the hCG, the hormone that crucial to successful pregnancy. In addition, hCG is the diagnostic marker of pregnancy, as it is secreted and can be detected from the early conceptus (Knobil & Neill,1998).

1.13 Aims of Study

The crucial roles of Ca^{2+} and Ca^{2+} signalling during placenta formation in process of blastocyst implantation and trophoblast differentiation, and during pregnancy in terms of fetal skeleton mineralisation have been reviewed (Husain & Mughal,1992; Baczyk *et al.*,2011). The association of Ca^{2+} transport disturbance has been proposed as a pathological condition of pregnancy-related disease such as PE (Haché *et al.*,2011). The discovery of channels for Ca^{2+} entry (L-type and CaT) and proteins for Ca^{2+} extrusion (PMCAs and NCXs) in human trophoblasts (Moreau *et al.*,2003b), in addition to the finding of multiple CaBPs in the placenta as reviewed by Belkacemi *et al*. (Belkacemi *et al.*,2002), lead to the proposal that placental Ca^{2+} transepthelial transport can be achieved by the effect of trophoblastic CaBPs on Ca^{2+} buffering and Ca^{2+} shuttling. However, placental Ca^{2+} signalling is not fully understood and the mechanism of Ca^{2+} trans-trophoblastic transport is still unclear. Particularly, the pathway of passive Ca^{2+} entry that undergoes compartmentalisation into ER or mitochondria before delivery to fetal circulation has not been investigated. Although the expression of Ca^{2+} ATPase (Belkacemi *et al.*,2005), and only recently mRNA of Ca^{2+} release channels (RyRs and IP_3Rs) of ER had been confirmed in human placenta (Haché *et al.*,2011), there is no direct information concerning how these Ca^{2+}-related proteins of the ER membrane might be involved in placental Ca^{2+} signalling and Ca^{2+} trans-trophoblastic transport.

It is clear that the *in vivo* examination of human placental trophoblast is not a viable approach. Different trophoblastic cells have been isolated from placental tissue for *in vitro* studies. However, limits in cell mass and passages are often associated with these materials, especially when first trimester placentae are used (Huch *et al.*,1998). Choriocarcinomas are the malignant counterpart of the trophoblast which share a number of characteristics of early placental trophoblasts in terms of placental hormone production and the ability to differentiate into syncytiotrophoblast-like cells *in vitro* (Pattillo *et al.*,1971; Friedman & Skehan,1979). Since human choriocarcinoma cell lines possess many similarities to normal human trophoblasts, these cell lines are considered as models for research of early stages of

implantation in humans. For instance, BeWo cells originate from a malignant gestational choriocarcinoma of the foetal placenta; this cell line was also the first human trophoblastic endocrine cell type to be maintained in continuous culture. BeWo cells have been demonstrated to be heterogeneous, consisting of predominant (96 to 99%) proliferative mononucleate cytotrophoblast-like cells, and the non-proliferative syncytiotrophoblast-like multinucleate giant cells as the remaining cell population (Friedman & Skehan,1979; Grümmer *et al.*,1990; Aplin,1991). JEG-3 choriocarcinoma was derived from a cerebral metastasis of BeWo cells transplanted into the cheek pouch of the hamster (Pattillo & Gey,1968). JEG-3 cells form multinucleated syncytia in culture, similar to the syncytiotrophoblast *in vivo* (Babalola *et al.*,1990). Moreover, JEG-3 has the same DNA profile as BeWo; the former was established by serial cloning of the latter. Both BeWo and JEG-3 cells produce 17-β-estradiol and β-hCG; while JAR cells, another choriocarcinoma cell line, produces progesterone and β-hCG (Grümmer *et al.*,1994). In addition, JAR cells were also demonstrated to differentiate into syncytiotrophoblast-like cells (Grümmer *et al.*,1994).

In human model trophoblast cell line BeWo, the presence of specific binding sites for fluorescent BODIPY-FLX-ryanodine was discovered, and the rise of $[Ca^{2+}]_i$ in response to ryanodine in these cells was also observed (Mackrill, *unpublished observations*). These two novel findings lead to the proposal of the possible involvement of RyRs in Ca^{2+} trans-trophoblast transport, based on the demonstration of RyR involvement in vectorial Ca^{2+} transcellular transport in another epithelial cell type. As Liang and colleagues proposed, RyR in series mediates Ca^{2+} efflux from ER in close proximity to where NCX is located in the plasma membrane of isolated rabbit aortic endothelial cells; PMCA in addition, likely in parallel with NCX, could facilitate Ca^{2+} removal (Liang *et al.*,2004). As mentioned in Section 1.8, Ca^{2+} 'removal' from placental trophoblasts is crucial for both maternal-fetal Ca^{2+} delivery and placental function during pregnancy. Dysregulated Ca^{2+} signalling and/or disturbed Ca^{2+} homeostasis of trophoblastic cells is associated with pathological conditions such as intrauterine growth restriction (IUGR), maternal diabetes and fetal hypocalcaemia (Regnault *et al.*,2002; Strid *et al.*,2003). Therefore, investigation of trophoblastic Ca^{2+} signalling and Ca^{2+} transport has direct impacts in maternal and

fetal health research, leading to dentification of potential targets for therapeutic interventions for certain pregnancy-related diseases (Moreau *et al.*,2003b; Belkacemi *et al.*,2005). In this aspect, the roles of RyRs in Ca^{2+} homeostasis are drawn into attention; understanding how these Ca^{2+} channel proteins function in trophoblast could lead to the discovery of alternative therapeutic strategies in Ca^{2+}-related pregnancy pathologies. Thereby, the objectives of this present study were to: (i) establish the expression of RyRs in human placental trophoblast and in model trophoblast cell lines; (ii) examine the expression of accessory proteins of RyR in both human cell lines and human tissues; (iii) investigate trophoblast RyR function by pharmacological stimulation and inhibition.

Chapter II.

Materials and Methods

Chapter II. Materials and Methods

2.1 Materials

Cell culture media and antibodies were obtained from Sigma-Aldrich, Poole, UK, unless stated elsewhere; animal sera were from Biowest Ltd., Ringmer, UK. General laboratory chemicals of analaytical reagent grade or better were obtained from Sigma or Calbiochem-Novabiochem Ltd., Nottingham, UK. The BeWo, JAR, and JEG-3 cell lines were obtained from European Collection of Animal Cell Cultures (ECACC) Salisbury, UK. SGHPL-4 cells were originally derived from primary extravillous trophoblasts, formerly known as MC4 (Choy & Manyonda,1998).

All immunohistochemistry involving human placental tissues was performed at Maternal and Fetal Health Research Lab, St. Mary's Hospital, Manchester under approval of the Central Manchester Local Ethics Committee. RNA and cDNA extracted from human term placental villous tissue of healthy individuals, cDNA from human first trimester villous tissue, and villous tissue homogenates of both human first and term placenta of healthy individuals were received as gifts from Prof. Aplin, Maternal and Fetal Health Research Group, University of Manchester, under approval of the Central Manchester Local Ethics Committee. Samples of small scale frozen human term placental villous tissues were obtained from Dr. Ball, Department of Biochemistry, University College Cork, as approved by the Clinical Research Ethics Committee of the Cork Teaching Hospitals.

2.2 Cell Culture

Human BeWo trophoblast cells were maintained in Nutrient Mixture F12 Ham medium, supplemented with 2 mM L-glutamate, 50 IU/ml of penicillin, 50 μg/ml of streptomycin, and 10% (v/v) heat-inactivated fetal bovine serum (FBS). Human JAR and JEG-3 trophoblast cells were maintained in Dulbecco's modified Eagles's Medium (DMEM) containing 10% (v/v) heat-inactivated fetal bovine serum (FBS), 50 IU/ml of penicillin and 50 μg/ml of streptomycin. Human SGHPL-4 trophoblast cells were grown in Nutrient Mixture F10 Ham medium containing 10% (v/v) heat-inactivated fetal bovine serum (FBS), 50 IU/ml of penicillin and 50 μg/ml of streptomycin. All cells were maintained in a humidified atmosphere of 95% air and 5% CO_2 at 37 ^{o}C.

2.3 Differentiation of C2C12 Cells

C2C12 is a mouse myoblast cell line. The purpose of C2C12 differentiation in this study was to serve as a positive control, to compare and contrast with human trophoblast cell lines and human placental tissue examined for the expression of calsequestrins and RyR proteins. Differentiated C2C12 myotubes were used for both immunoblotting and immunofluorescence staining.

C2C12 cells were grown in normal growth medium (10% FBS (v/v), 50 IU/ml penicillin and 50 μg/ml streptomycin, DMEM) to confluency in both 175 cm^2 and on cover slips that were placed in 12-well plates. To differentiate myoblasts, normal growth medium was removed and replaced by differentiation medium (0.5% FBS (v/v), 50 IU/ml penicillin and 50 μg/ml streptomycin, DMEM). During the differentiation period, differentiation medium was changed in every two days; and complete differentiation of cells from myoblasts to myotubes was observed within 6 – 8 days of switching medium.

2.4 Preparation of Microsomes and Membrane Subfractionation

All steps were performed at 0 to 4 ^{o}C, as described previously by Mackrill *et al*. (Mackrill *et al.*,1997). All buffers (wash buffer, Buffer I, Buffer II and Buffer A) contained freshly added protease inhibitors (2 mM benzamidine, 2 μg/ml aprotinin, 2 μg/ml leupeptin, 2 μg/ml pepstatin A, and 0.5 mM PMSF). Crude microsomal membranes were prepared from 175 cm^2 cell monolayers. Culture medium was removed from flasks and cell monolayers were briefly washed twice with wash buffer (0.02% EDTA, 0.9% NaCl, 10 mM Tris, pH7.4). After the second wash, same buffer was added to detach cells by 5 minutes incubation followed by gentle tapping of the flasks. Cells were harvested with 10 ml per 175 cm^2 monolayer of wash buffer. Cell pellets were obtained by centrifugation at 500 x *g* for 5 minutes at 4^{o}C (Rotor F34-6-38, Eppendorf Centrifuge 5810R; Eppendorf UK Ltd.). Resultant cell pellets were homogenized with 500 μl buffer I (0.5 mM $MgCl_2$, 25 mM Tris pH 7.4) by 50 strokes of a hand-held glass-Teflon homogeniser. An equal volume of buffer II (0.3 M KCl, 0.5 M sucrose, 25 mM Tris, pH 7.4) was added, followed by another 25 strokes with the homogenizer. The homogenate was centrifuged at 500 x *g* for 5 minutes at 4^{o}C (Rotor F34-6-38, Eppendorf Centrifuge 5810R; Eppendorf UK Ltd.), and the supernatant was centrifuged at 30,000 x *g* for 60 minutes at 4 ^{o}C (Beckman JA-25.50 rotor, Beckman Avanti^{TM} J-25 centrifuge, Beckman Coulter, Inc. U.S.A). The resultant microsomal pellets were resuspended in 50-100 μl buffer II by 10 passes through a 21-gauge needle. Protein concentrations of microsomes were determined by Bradford protein assay using bovine serum albumin as a standard (Bradford, 1976). Microsomes were immediately flash-frozen in liquid nitrogen and stored at -80^{o}C. Alternatively, microsomes were prepared and used immediately for SDS-PAGE and western blotting.

Crude microsomal membranes from various rabbit or rat tissues (including rabbit skeletal muscle, rat brain, rat heart and rat skeletal muscle) were prepared by a differential centrifugation method. Frozen tissues were thawed in 10 volumes of (ie. 1 g/10 ml) ice-cold buffer A (0.25 M sucrose, 10 mM Tris, pH 7.4), and cut into pieces of approximately 1 cm^3. For fresh tissues, excess fat, major nerves and blood vessels were removed before diced and immersed into ice-cold buffer A. Tissues

were then homogenized with buffer A for three 30 second bursts by using Ultra-Turrax homogenizer (T-25 probe, maximum speed). Crude homogenates were centrifuged at 1,100 x *g* for 10 minutes at 4°C (Rotor F34-6-38, Eppendorf Centrifuge 5810R; Eppendorf UK Ltd.); supernatants were centrifuged at 7,700 x *g* for 20 minutes at 4°C (Rotor F34-6-38, Eppendorf Centrifuge 5810R; Eppendorf UK Ltd.); crude microsomal membranes were obtained by further 60 minutes centrifugation at 4°C (Beckman JA-25.50 rotor, Beckman Avanti™ J-25 centrifuge, Beckman Coulter, Inc. U.S.A) at maximum speed (75,600 x *g*). Resultant membrane pellets were resuspended in buffer A to a protein concentration of 10-20 µg/µl by 10 strokes of a loose-fitting glass-Teflon homogenizer. After the protein concentration was determined using the Bradford protein assay, membranes were immediately flash-frozen in liquid nitrogen and stored at -80°C until further use.

Small scale frozen human term placental villous tissue homogenates were prepared in 1.5 ml Eppendorf tubes. Ice-cold buffer A (500 µl) was added and tissues were homogenised directly by using pellet pestles. Crude homogenates were centrifuged at 1,100 x *g* for 10 minutes at 4°C (Rotor F45-30-11, Eppendorf Centrifuge 5810R; Eppendorf UK Ltd.). Post-nuclear supernatants were obtained by further 20 minutes centrifugation of these supernatants at 7,700 x *g* at 4°C (Rotor F45-30-11, Eppendorf Centrifuge 5810R; Eppendorf UK Ltd.). Protein concentrations of homogenates were determined using the Bradford protein assay and samples were stored as described previously at the first paragraph of this section.

2.5 SDS/PAGE and Western Blotting

To denature proteins for SDS-PAGE, membrane extracts containing 80 to 100 µg of protein were made up with 5x SDS-PAGE sample buffer (0.1% (w/v) bromophenol blue, 4% (w/v) SDS, 20% (v/v) glycerol, 125 mM Tris pH6.8) in addition to 50 mM dithiothreitol (DTT) in a total volume of 20 µl. Samples were incubated at 100°C for 5 minutes and briefly centrifuged at 12,000 x *g* before loading onto 7% SDS-PAGE gels, then electrophoresed at 20 mA constant current per mini gel for about 90 minutes. The components of resolving and stacking gels are shown

in Table 2.5.1 During electrophoresis, gel cassettes were immersed in running buffer containing 24.8 mM Tris Base, 191.8 mM glycine and 0.1% (w/v) SDS.

Table 2.5. 1 Formulation of SDS-PAGE gels

7% Resolving gel Formulation (10 ml)			5% Stacking gel Formulation (10 ml)	
30% acrylaminde	2.3 ml		30% acrylaminde	1.67 ml
deionised H_2O	5.1 ml		deionised H_2O	5 ml
Resolving Gel Buffer (1.5 M Tris-Base, pH 8.8)	3 ml		Stacking Gel Buffer (1 M Tris-HCl, pH 6.8)	2.5 ml
10% w/v SDS	100 µl		10% w/v SDS	100 µl
Glycerol	-		Glycerol	625 µl
10% APS	100 µl		10% APS	100 µl
TEMED	10 µl		TEMED	10 µl

Separated membrane proteins were transferred from SDS-PAGE gels to polyvinylidene difluoride (PVDF) membranes that were pre-wetted with 100% methanol and equilibrated with 1 x transfer buffer. Transfer was performed at 70 V constant voltage for 2 hours for ryanodine receptor proteins, or for 1 hour for all other lower molecular weight proteins. The transfer cassette was immersed in transfer buffer containing 20 mM Tris Base, 150 mM glycine and 0.037% (w/v) SDS. At the end of protein transfer, membranes were incubated with blocking buffer containing 5% Marvel dried skimmed milk powder in phosphate buffered saline (PBS, 0.8% (w/v) NaCl, 0.02% (w/v) KCl, 0.144% (w/v) Na_2HPO_4, 0.024% (w/v) KH_2PO_4, pH 7.4) for 45 minutes, prior to overnight 4^oC incubation on a shaker at ~60 rpm, with the same blocking buffer containing primary antibodies at desired concentrations (Table 2.5.2). At the end of incubation with the primary antibody, PVDF membranes were washed with PBS three times at 5 minutes intervals prior to incubation with secondary antibody. Membranes were incubated for 1 hour at room

temperature on the shaker with blocking buffer containing secondary antibodies at working dilution (Table 2.5.3).

At the end of the secondary antibody incubation, membranes were washed with PBS for 20, 15, 10 and 10 minutes (a total of four washes). Immunoreactive protein bands were visualized using an enhanced chemiluminescence (ECL) kit (Pierce ECL Western Blotting Substrate (Product # 32106), Thermo Scientific, Fisher Scientific Ireland). ECL detection reagents 1 and 2 were freshly mixed at a 1:1 ratio and were applied to the membrane. Chemiluminescence was detected using Kodak X-Omat LS film (Sigma, F1274-50 EA) using AGFA CP1000 developer in a dark room.

Table 2.5. 2 Primary antibodies for western blotting

Primary Antibodies	Source and Catalogue Number	Working Dilution
Polyclonal Rabbit Anti-RyRs (RS4) with amino acid sequence: SFPNNYWDKFVKRKV	Rabbit polyclonal antiserum supplied by Dr. Richard Tunwell, University College London	1:500
Polyclonal Rabbit Anti-RyR1	Millipore, AB9078	1:1000
Polyclonal Rabbit Anti-RyR2	Sigma, HPA016697	1:250
Polyclonal Rabbit Anti-RyR3	Millipore, AB9082	1:1000
Polyclonal Rabbit Anti-Calsequestrin (CSQ)	Pierce, PA1-913	1:250
Monoclonal Mouse Anti-Triadin (TRD)	Pierce, MA3-927 (clone 10: GE 4.90)	1:100

Table 2.5. 3 Secondary antibodies for western blotting

Secondary Antibodies (horseradish peroxidase (HRP))	Source and Catalogue Number	Working Dilution
Goat Anti-Mouse IgG-Peroxidase Antibody	Sigma, A9917	1:1000
Goat Anti-Rabbit IgG-Peroxidase Antibody	Sigma, A6154	1:2000

2.6 RNA Isolation

The Absolutely RNA® miniprep kit (Stratagene, Catalog #400800) was used for RNA isolation from human trophoblast cell lines, according to the manufacturer's protocol. β-Mercaptoethanol (β-ME, 0.7% (v/v)) was added to the desired volume of lysis buffer before use. Cells were grown to approximately 90% confluence on 6-well plates. β-ME-lysis buffer (400 µl per well) was added and cells were lysed by repeated pipetting. The lysate was transferred into microcentrifuge tubes and the tubes were vortexed to further homogenize the cells.

Cell lysates were then transferred into the prefilter spin cups which were placed on the 2 ml receptacle tube, and centrifuged at 16,300 x *g* for 5 minutes using the Labnet Spectrafuge 24D (Labnet, Labnet International inc.). Filtrates were mixed thoroughly with equal volume of 70% ethanol and the mixture was transferred into the RNA binding Spin Cups which were placed in the new 2 ml receptacle tubes. The filtrate of the mixture was discarded after 60 seconds centrifugation at 16,300 x *g*. The spin cup was then washed with 600 µl of 1 x Low-Salt Wash Buffer. Following a 60 second maximum speed centrifugation and an additional 2 minute centrifugation, the filtrate was discarded.

DNase treatment of samples was done within the fiber matrix of the filter spin cup using a 15 minute incubation with the DNase solution in a 37^{o}C air incubator. The DNase solution was made up freshly by gently mixing 50 µl of DNase Digestion Buffer with 5 µl of reconstituted RNase-Free DNase I, and the 55 µl of DNase solution was directly loaded onto the fiber matrix of spin cup. At the end of the incubation, 600 µl of 1 x High-Salt Wash Buffer was added and tubes were centrifuged at 16,300 x *g* for 60 seconds in the Spectrafuge. Spin cups were washed twice with Low-Salt Wash Buffer using volumes of 600 µl and 300 µl. The fiber matrix was dried by 2 minute 16,300 x *g* centrifugation after the second wash.

RNA elution was achieved by 10 minute room temperature incubation with Elution Buffer, followed by centrifugation at 16,300 x *g* for 1 minute. The Elution Buffer was pre-warmed to 60 ^{o}C and 50 µl of this buffer was loaded directly onto the fiber matrix of the spin cup which was placed on a fresh 1.5 ml microcentrifuge tube.

The quality and concentration of eluted RNA was determined by an Eppendorf BioPhotometer (Eppendorf UK Ltd.), according to the manufacturer's instruction.

RNA from flash-frozen term placental villous tissue was isolated by using TRIzol®-Reagent (Invitrogen Cat.No. 15596-018, Bio Sciences, Dublin, Ireland). Tissue samples were directly homogenised with 1 ml TRIzol reagent using pellet pestles. The crude homogenates were obtained by centrifugation for 10 minutes at 12,000 x *g* at 4°C (Rotor F45-30-11, Eppendorf Centrifuge 5810R; Eppendorf UK Ltd.). The supernatant was transferred into a fresh microcentrifuge and incubated at room temperature (RT, 18-22°C) for 5 minutes to allow the complete dissociation of nucleoprotein complexes. At the end of this incubation, 200 µl of chloroform was added and the tube was vortexed vigorously for 1 minute. The mixture was incubated at RT for 3 minutes before phase separation by centrifugation for 15 minutes at 12,000 x *g* at 4°C. The resultant colourless upper aqueous phase was transferred into a fresh microtube, and the RNA was precipitated by mixing with 0.5 ml isopropyl alcohol, followed by 10 minute room temperature incubation. The RNA precipitate was obtained by centrifugation at 12,000 x *g* 4°C for 10 minute, and the gel-like pellet on the side and the bottom of tube was washed with 1 ml 75% ethanol by vortexing. The ethanol was removed using a 5 minute 7,500 x *g* centrifugation at 4°C. The RNA pellet was allowed to air-dry for 5 to 10 minutes. The resultant RNA pellet was redissolved in DNase/RNase-free H_2O. The quality and concentration of RNA were determined by Eppendorf BioPhotometer as previously stated. All RNA samples were stored at -80°C until further use.

2.7 Reverse Transcription-Polymerase Chain Reaction (RT-PCR)

cDNA was synthesized in a 20 µl reaction using the ImProm-II™ Reverse Transcription System (Promega, Catalog #A3800). Total RNA (1–5 µg in a volume of 10 µl) was used as template, mixed with 0.5 µg (1 µl) Oligo $(dT)_{15}$ primer and denatured at 70°C for 5 minutes. The template and primer mix (11 µl) was chilled on ice for at least 5 minutes before proceeding to reverse transcription. The reaction mixture (9 µl) containing ImProm-II™ 5x Reaction Buffer, 2.5 mM $MgCl_2$, 0.5 mM

each dNTP, 20 units of Recombinant RNasin Ribonuclease Inhibitor, and 1 unit of ImProm-II™ Reverse Transcriptase, was subsequently combined and equilibrated with the pre-treated RNA/ Oligo $(dT)_{15}$ mix to the final reverse transcription reaction mix (20 µl). The cDNA synthesis was performed on an Eppendorf Mastercycler Thermal Cycler for one hour at 42°C, and the Reverse Transcriptase was inactivated using 15 minute incubation at 70°C. The resultant cDNA was either stored on ice for immediate amplification, or stored at -20°C for future use.

To determine whether the ryanodine receptor transcripts present in human trophoblast cell lines and human placental trophoblast villous tissues, cDNA synthesized from total RNA of cell lines and tissues was amplified using the PCR (GoTaq® PCR Core System I, Catalog # M7650, Promega), using primers that selectively amplify specific region of RyR isoforms. The same downstream primer (5′-dCAGATGAAGCATTTGGTCTCCAT-3′) pairs to the upstream primers JBR1 (5′-dGACATGGAAGGCTCAGCTGCT-3′), JBR2 (5′-dAAGGAGCTCCCCACGAGAAGT-3′), and JBR3 (5′-dGAGGAAGAAGCGATGGTGTT-3′) amplified products from *RYR1*, *RYR2*, and *RYR3* at approximate sizes of 1112 bp, 1082 bp and 1013 bp, respectively (Sei *et al.*,1999). The 50 µl PCR reaction volume contained 5x Colourless GoTaq® Flexi Buffer, 3 mM $MgCl_2$, 300 µM of each PCR Nucleotides, 5 µg of each primer, 1.25 units of GoTaq® DNA Polymerase, and 5 µl of cDNA.

Amplification was performed in a Eppendorf Mastercycler Thermal Cycler by 'touchdown' PCR method (Don *et al.*,1991). This protocol was modified from method of Sei *et al*. (Sei *et al.*,1999), optimised according to manufacturer's instruction from Promega. Of which, the reaction was started with a 4 minute initial denaturation at 95°C of target DNA templates, followed by 19 cycles of 1 minute denaturation at 95°C, 1 minute annealing from 65°C to a 'touchdown' at 55°C (0.5°C decrease every cycle), and 1 minute extension at 72°C. At cycle 20, the annealing temperature was expected to reach 55°C. The next 19 cycles were performed at this annealing temperature (55°C) under the same conditions. After the final 5 minute extension at 72°C, the entire PCR (total 40 cycles) was terminated. The quality and concentration of resultant products were determined by the Eppendorf BioPhotometer, according to the manufacturer's instructions. PCR products (5 µl)

were then mixed with 1 µl 6x DNA loading dye (#R0611, supplied with GeneRuler 100bp DNA Ladder (#SM0243), Fermentas Life Sciences, Germany), prepared for electrophoresis in agarose gel. The 1% agarose gel was made up with 1 g of agarose per 100 ml 1 x Tris-acetate-EDTA (TAE) buffer (40 mM Tris, 20 mM acetic acid and 1 mM EDTA) in a conical flask. The agarose was dissolved in the buffer by heating in a microwave oven for approximately 2 minute. The gel solution was swirled for mixing and kept inside the fume hood at room temperature for approximately 5 minutes; ethidium bromide was then added into the solution by gentle mixing to a final concentration of 0.8 µg/ml. This gel solution was then slowly poured into the gel tank. After the gel was set, the whole gel-tank assembly was immersed with 1 x TAE buffer; PCR product mixed with DNA loading dye was loaded into the wells of the gel and resolved by electrophoresis at constant voltage of 180 V for approximately 45 minutes. DNA fragments were then visualised on a UV transilluminator.

Examination of house-keeping gene (human *β-ACTIN*) as a loading control was performed using the same Thermal Cycler. Human *β-ACTIN* primers were from Stratagene (#302010). The sequences of sense and antisense primers were 5'-TGACGGGGTCACCCACACTGTGCCCATCTA-3' and 5'-CTAGAAGCATTTGCGGTGGACGATGGAGGG-3', respectively. Lyophilised primers were reconstituted in low-TE buffer (5 mM Tris-HCl and 0.1 mM EDTA). The 20 µl PCR reaction volume contained 5x Colourless GoTaq® Flexi Buffer, 2 mM $MgCl_2$, 300 µM of each PCR Nucleotides, 1 µM of primer mix, 1 unit of GoTaq® DNA Polymerase, and 2 µl of cDNA. The PCR cycles were setup according to manufacturer's instruction: starting with a 5 minute initial denaturation at 94°C, 5 minute annealing at 60°C and 1.5 minute extension at 72°C; the next 35 cycles were performed at 94°C for 45 seconds denaturation, followed by 45 seconds annealing at 60°C, then 1.5 minute extension at 72°C; the duration for the final extension at 72°C was 10 minutes. The expected size of product is 661 bp. These PCR products were then examined by electrophoresis in agarose gels and visualised on a UV transilluminator.

2.8 DNA Purification from PCR Products

To optimize the PCR product purity for sequencing, DNA of the expected size was isolated and extracted from agarose gels after electrophoresis using a StrataPrep DNA Gel Extraction Kit (Catalog # 400768, Agilent Technologies, Agilent Technologies Ireland Ltd, Ireland). The DNA was isolated from the gel by single-use sterile surgical blade and dissolved in 3 volumes of DNA extraction buffer (ie. 300 µl of buffer per 100 mg isolated agarose gel containing DNA). The mixtures were heated at 50^{o}C for 10 minutes with occasional gentle flicking for mixing. When DNA gels were completely dissolved, mixtures were transferred into microspin cups which were placed in 2 ml receptacle tubes and centrifuged at 16,300 x *g* for 30 seconds using the Labnet Spectrafuge 24D. The filtrates were discarded and the microspin cups were washed with 1 x wash buffer which was made up with equal volumes of 2 x wash buffer and 100% ethanol. The wash buffer was removed from the microspin cups by centrifugation twice for 30 seconds at 16,300 x *g*. DNA elution from the matrix of the microspin cups was achieved by a 10 minute room temperature incubation with 50 µl of DNase/RNase-free H_2O, followed by centrifugation for 1 minute at 16,300 x *g*. The quality and concentration of DNA were determined using an Eppendorf BioPhotometer. The purified DNA was then analysed by electrophoresis on a 1% agarose gel containing 0.8 µg/ml ethidium bromide.

In cases where the recovered product concentration was too low, the purified DNA was used as a template (1 µl in 50 µl reaction) for re-amplification using a 10 cycle PCR with constant annealing temperature at 55^{o}C at the same conditions as previously stated in Section 2.7. The resulting PCR products were examined by electrophoresis and purified by gel extraction, as described in the first paragraph of the current section, prior to sequencing.

DNA samples for sequencing were prepared at a concentration of 10 ng/µl in duplicate, premixed with 15 pmol of either forward or reverse primer in a total volume of 20 µl DNase/RNase-free H_2O. Samples were commercially sequenced by Eurofins MWG Operon Sequencing lab (Germany).

2.9 Indirect Immunofluorescence (IIF) Microscopy

RT-PCR and western blotting experiments indicated (Chapter III, 3.1-2), there were a detectable levels of RyR transcripts and proteins in BeWo and JEG-3 trophoblast cell lines. To visualize the subcellular distribution of RyRs and their accessory proteins, cultures of BeWo and JEG-3 cells were selected for analyses using indirect immunofluorescence microscopy.

Cells were grown to approximately 80% confluency on 10 mm glass cover slips in 12-well plates. Cells were briefly washed twice with sterile-filtered PBS before 15 minute fixation with 100% methanol at -20^{o}C. At the end of fixation, cells were washed twice with PBS, and then incubated with 50 mM ammonium chloride at room temperature for 15 minutes to quench autofluorescence. After two washes with PBS, cells were incubated with 10% v/v fetal bovine serum/phosphate buffer saline (FBS/PBS) at room temperature for one hour to block non-specific protein binding. At the end of this blocking step, cells were incubated with both mouse monoclonal and rabbit polyclonal primary antibodies in the same blocking solution (10% v/v FBS/PBS) at desired concentrations (Table 4.8.1) for one hour.

Table 2.9. Primary antibodies for indirect immunofluorescence microscopy

Primary Antibodies	Catalogue Number	Working Dilution
Polyclonal Rabbit Anti-RyR1	Millipore, AB9078	1:400
Polyclonal Rabbit Anti-RyR2	Millipore, AB9080	1:400
Polyclonal Rabbit Anti-RyR3	Millipore, AB9082	1:400
Monoclonal Mouse Anti-RyRs	Pierce, MA3-916 (clone: C3-33)	1:500
Polyclonal Rabbit Anti-CSQ	Pierce, PA1-913	1:200
Monoclonal Mouse Anti-TRD	Pierce, MA3-927 (clone: GE 4.90)	1:200
Monoclonal Mouse Anti-E Cadherin	Abcam, ab1416 (clone: HECD-1)	1:50
Monoclonal Mouse Anti-Pan Cadherin	Sigma, C1821 (clone: CH-19)	1:400

At the end of incubation with primary antibodies, cells were washed twice with PBS and then were incubated for 40 minutes at room temperature with secondary antibodies in the same blocking solution. The secondary antibodies blocking solution cocktails contained Cy2-conjugated anti-rabbit IgG (Jackson ImmunoResearch, 711-225-152) 7.5 μg/ml, Cy3-conjugated anti-mouse IgG (Jackson ImmunoResearch, 715-165-150) 7 μg/ml, and 4, 6-diamidino-2-phenylindole (DAPI, 1 ng/ml) (Catalog # D9542, Sigma) for staining of nuclei. From the secondary antibody addition on, all incubations and washes were performed in dark to avoid unnecessary photobleaching.

Cells were washed twice with PBS at the end of secondary antibody incubation. Cover slips were briefly rinsed with dH_2O to remove the salt. Excessive water was absorbed in tissue before cover slips were mounted on microscopy slides with mowiol mounting medium (10.3% (w/v) Mowiol (575904, Mowiol 4-88, Calbiochem, Germany), 22.8% (v/v) glycerol, 0.1 M TrisHCl pH8.5). Slides were allowed to air dry in dark before further examination.

Fluorescence microscopy was performed using a Leica DMI3000 B inverted microscope; cells were observed using HCX PL FLUOTAR 40x/0.75 numerical aperture (NA) PH2 objective lens. Immunostaining within the same observation area was visualized by switching fluorescent filter cubes to produce UV light (excitation filter BP340-380), blue light (excitation filter BP470/40) and green light (excitation filter BP545/30) that excited DAPI (blue), Cy2 (green) and Cy3 (red) emission, respectively. Images of each fluorochrome within the same observation area were captured using a Leica DFC340 FX digital camera fitted to the microscope. Images were managed and processed using Leica AF6000 E Fluorescence software, and then exported as jpeg files into a PC for further analysis. Contrast and intensity of images were adjusted to the same degree by Microsoft Office Picture Manager 2003 or Photoshop CS2; the images of DAPI (blue), Cy2 (green), and Cy3 (red) that were captured within the same observation area were superimposed to produce merged images.

2.10 Immunohistochemistry (IHC)

Immunohistochemistry involving use of human placental tissue was performed in the Maternal and Fetal Health Research Group, University of Manchester, under supervision of Prof. Aplin and members of his research group. All tissue samples used were obtained with the approval of the Local Ethics Committee, Manchester. Three representative samples of both first trimester and term placental villous tissue from healthy individuals were randomly selected for IHC analysis.

Human placental villous tissue from healthy individuals was isolated and dissected before it underwent dehydration and embedding with paraffin by members

of Prof. Aplin's research group (Forbes *et al.*,2008). Paraffin embedded samples were sectioned by Leica disposable blades using semi-automatic rotary microtome Leica RM2245 at a thickness of 5 μm. Tissue sections were mounted on the microscopy slides pre-coated with poly-L-lysine, allowed to dry overnight in the oven at 37^{o}C and stored at room temperature until use. Slides mounted with tissue sections were arranged in slide racks and warmed to 60^{o}C for 10 minutes before dewaxing and rehydration was performed in the fume hood. Sections were dewaxed in Histoclear series (i.e. Histoclear A, Histoclear B and Histoclear C) for 10 minutes each with agitation. Racks of slides were then transferred and rehydrated through an ethanol series (100% ethanol (A), 100% ethanol (B), 70% ethanol (A), 70% ethanol (B)) for 2 minutes at each step, with agitation. At the end of the last step with alcohol rehydration, sections were equilibrated with tap water for 10 minutes.

Antigen retrieval was then performed by boiling the sections in 10 mM sodium citrate (pH 6.0) for 2 x 5 minutes. Buffer was allowed to cool at RT for 20 minutes before sections were further cooled using running tap water. At the end of cooling, water was drained off from slides and sections were circled with hydrophobic pen. Tissue sections were equilibrated with TBS (5 mM Tris Base, 0.3 M NaCl, pH 7.6) for 5 minutes before the 10 minute endogenous peroxidase quenching at room temperature with 3% hydrogen peroxide in H_2O (v/v). At the end quenching, sections were washed with TBS (2 x 5 minutes) before 30 minute non-immune block at room temperature with 2% human serum/10% normal goat serum in 0.1% Tween TBS (v/v). Sections were incubated with primary antibodies (Table 2.9.1) diluted into the same blocking solution for at least 1 hour at room temperature.

Table 2.10. Primary antibodies for IHC

Primary Antibodies	Catalogue Number	Working Dilution
Polyclonal Rabbit Anti-RyR1	Millipore, AB9078	1:500
Polyclonal Rabbit Anti-RyR2	Sigma, HPA016697	1:25
Polyclonal Rabbit Anti-RyR3	Millipore, AB9082	1:500
Monoclonal Mouse Anti-TRD	Pierce, MA3-927 (clone: GE 4.90)	1:100
Monoclonal Mouse Anti-Human Cytokeratin 7	Dako, M7018 (Clone OV-TL 12/30)	1:500

At the end of primary antibody incubation, sections were washed with TBS for 5 minutes, followed by two 5 minute TBS-Tween (0.6% v/v) washes, and a further 5 minute TBS wash. Biotinylated goat anti-mouse IgG (E0433, DakoCytomation Ltd., Cambridgeshire, UK) and biotinylated swine anti-rabbit IgG (E0413, DakoCytomation Ltd., Cambridgeshire, UK) were applied as secondary antibodies diluted into TBS (1:200). Tissue sections were incubated with the corresponding biotinylated secondary antibodies for 30 minutes at RT and washed in the same way as before (5 minute TBS, 2 x 5 minute TBS-Tween (0.6%), 5 minute TBS).

The tertiary step was applied by 30 minute RT incubation with 5 µg/ml avidin-peroxidase (Sigma, A3151) in TBS. Sections were then washed with TBS-Tween (0.6%) for 2 x 5 minute and TBS for 5 minutes. Peroxidase activity was detected using 3, 3'-diaminobenzidine (DAB) peroxidase substrate (Sigma, D4168). One tablet of each DAB and urea hydrogen peroxide were dissolved together into 1 ml ultrapure water. The DAB solution was then applied onto tissue sections; colour development was monitored using a light microscope with a 10x objective. Reactions

were terminated by rinsing off DAB solution on sections with ultrapure water. Sections were allowed to equilibrate with water for 5 minutes. Nuclei were counterstained with filtered Harris's hematoxylin for 1 minute and rinsed with cold tap water. The differentiation of section stains was achieved using acid alcohol (1% HCl in 70% methanol, v/v) to wash off overstaining of hemotoxylin on sections and to define the nuclei staining with hematoxylin. Section slides were dipped into acid alcohol for 3 seconds to remove undesired overstaining, and then washed with running tap water.

Sections were dehydrated through a fresh alcohol series (2 minutes in each of 70% ethanol (A), 70% ethanol (B), 100% ethanol (A), and 100% ethanol (B)) with agitation in the fume hood. Excess ethanol was drained off before transfer into a fresh Histoclear series (2 minutes in Histoclear (A), 5 minutes in Histoclear (B), and 30 minute Histoclear (C), with agitation at each step). Sections were then directly mounted with DPX mounting medium (Fluka, 44581) and allowed to dry overnight in the fume hood. Stained tissue sections were visualized by Leitz Dialux 22 microscope, using Phaco 100x/1.20 NA water objective; images were captured using a QI Cam Fast 1394 camera and analyzed by Image Proplus 6.0 imaging system. Images were subsequently exported to a PC as .jpeg files; contrast and intensity were adjusted using Microsoft Office Picture Manager 2003.

2.11 MTT Assay

To determine whether direct pharmacological stimulation of RyRs by agonists affected the viability of human trophoblast cell lines, BeWo and JEG-3 cells were selected for MTT assay according to manufacturer's instruction (Cat. # 1465007, Roche, Roche Applied Science, Germany). MTT assay is a colourimetric assay that reveals metabolic activity of viable cells. In this method, the tetrazolium salt MTT is used; and MTT can only be converted to a coloured, water-insoluble formazan salt by viable cells; the formazan salt can be solubilised in a solubilisation solution and can be quantitated in a conventional ELISA plate reader. Therefore, MTT assay is used to quantitate cell proliferation and cytotoxicity (Mosmann,1983).

Cells (~3000 per well) were seeded and grown with normal growth medium overnight in the 96-well plates in the 37°C incubator before stimulation. The next day, normal growth medium was replaced by assay medium with addition of drugs: ryanodine (final concentrations: 0.1 μM, 0.2 μM, 0.5 μM, 1 μM, 2 μM, and 5 μM), 4-CmC (final concentrations: 5 μM, 10 μM, 50 μM, 100 μM, 200 μM, and 500 μM), and etoposide (final concentrations: 10 μM, 25 μM, 50 μM, and 100 μM). Etoposide served as a positive control for cytotoxicity. Quadruplets of wells were assigned for each concentration. In addition, quadruplet blank wells without cells were used to determine the background absorbance of solutions; while quadruplet wells of cells without addition of drugs were used as viability controls. Cells were stimulated for 24 hours at 37°C before labelling with 10 μl (0.5 mg/ml) MTT reagent. At the end of the 4 hour labeling period, medium was removed and replaced by 100 μl per well of solubilisation solution. After overnight solubilisation at 37°C in the cell-culture incubator, the absorbance of solution in each well was measured by a spectrophotometer at 595 nm.

Values of absorbance in each well were normalised by subtracting the averaged background reading from blank wells. Percentages reflecting relative formazan production from MTT reduction in each reaction were deduced from the averaged normalised absorbance of control and stimulated wells. The percentage of relative formazan salt formation in control wells was regarded as 100% at their averaged normalized absorbance. This value was then divided by the averaged normalized absorbance from each experiment and expressed as percentage. The percentages of relative formazan formation were also regarded as an indicator of the percentage of viable cells in relation to controls. These values were plotted against drug concentration for analysis.

2.12 Fura-2 Fluorescence Microscopy

To determine the changes in intracellular [Ca^{2+}] upon direct and indirect pharmacological stimulation of ryanodine receptors, BeWo and JEG-3 cells were loaded with fura-2 (Grynkiewicz *et al.*,1985), using a protocol modified from the

method of Ratto *et al*. (Ratto *et al.*,1988). Cells were grown on 35 mm γ–irradiated glass bottom dishes (MatTek) to approximately 80% confluency. Cells were washed twice with sterile-filtered modified Krebs-Henseleit bicarbonate (KHB) buffer (NaCl 120 mM, KCl 4.8 mM, $MgSO_4$ 1.2 mM, KH_2PO_4 1.2 mM, $NaHCO_3$ 25 mM, $CaCl_2$ 2 mM, glucose 10 mM, HEPES 5 mM, pH 7.2) before incubation with the ratiometric fluorophore. The fluorophore-loading solution was freshly prepared by making up 5 μM fura-2 AM (F-1221, Invitrogen, Ireland) and 5 μM Pluronic F-127 (P3000MP, Invitrogen, Ireland) in KHB. Cells were incubated with the fluorescent dye for 30 to 45 minutes in a 37^{o}C incubator. At the end of the incubation, cells were washed twice with KHB and allowed to equilibrate with the buffer for 10 to 20 minutes before pharmacological stimulation. During experiments, cell dishes were placed on the microscope stage. The fluorescence of cells was monitored using an Olympus IX51 inverted fluorescent microscope (Olympus Optical Co. (UK) Ltd.) with Olympus UPlanFI100XOI3 oil-immersion 100x/1.3NA objective, using Andor iQ acquisition software (Andor Technology Ltd. Belfast, N. Ireland) which synchronized with a Hamamatsu ORCA-ER Digital Camera C4742-80. Non-stimulated cell images were recorded for at least 1 minute to obtain a basal value, prior to addition of drugs. Pharmacological agents (5 μl) at 200x the desired concentration were added directly into the cell dish containing 995 μl KHB using a micropipette. Experiments were terminated when there was no further change observed. The duration of stimulation was between 5 to 15 minutes. All experiments were performed on the microscope stage within a humidified encapsulating incubator at 37^{o}C.

Microscope-equipped IX2-RFAC Reflected Fluorescence System (Olympus Optical Co. (UK) Ltd.) was used during experiment. The excitation light was generated by a 75W xenon lamp; the wavelengths of 340 nm and 380 nm lights were selected by the Cairn Optoscan monochromator. The combination of U-MWU2 mirror unit and BP330-385 excitation filter controlled the wavelengths of emitted light reaching the camera. During experiments, cells were illuminated alternately with two wavelengths of 340 nm and 380 nm that specifically excited Ca^{2+}-bound and Ca^{2+}-free fura-2 within dye-loaded cell (Thomas & Delaville,1991). The light emitted at both excitation wavelengths (peak emission ~510 nm) was collected by the

Hamamatsu ORCA-ER Digital Camera (Hamamatsu Photonics (UK) Ltd.); the camera-synchronized widefield emission paired images of the fura2 (excited by 340 nm and 380 nm wavelengths) was produced and processed by Andor iQ software. The acquisition control and data analysis of images (including generation of ratio images) were also achieved by using Andor iQ program.

Images were collected and the intensity was recorded in the pixels of each frame. The paired images were presented in red and blue images represented light emitted at 340 nm and 380 nm excitation wavelengths, respectively. The exposure time of each excitation wavelength was set at 800 ms, and the interval in between was set at the fastest possible value. The image recording was initiated by clicking the 'run' button in the software control panel. At the end of experiment, recording was terminated by clicking the 'stop' button at the same place. The duration of pharmacological stimulation was various between 5 to 15 minutes. All original data images were saved as multi-dimensional .TIFF files.

To process the fura-2 data, a stack of ratio images was created per stack of original paired fura-2 images. The background fluorescence of individual raw image was masked based on the Ca^{2+}-sensitive 340 nm excited images; a stack of intermediate threshold paired images was then generated to remove 'background' fluorescence. The ratio images were generated from the original and threshold paired images.

Cells of interest (at least four cells) were outlined by polygons, defining regions of interest. The mean fura-2 intensity ratios within the outlined regions were averaged in every ratio image for analysis. The average value of at least 30 frames of non-stimulated ratio images (~ 60 seconds) at the beginning of each experiment was taken as basal fluorescence ratio, and this value was then subtracted from values obtained during pharmacological stimulation to obtain the mathematical value of change in fura-2 ratio. Mean ratios of fura-2 intensity were plotted against time in seconds to display the changes of fura-2 ratio during experiment, using Microsoft Excel 2003.

2.13 Statistics

Statistical analyses of numerical data were made by unpaired t test (two groups) or one-way ANOVA followed by Tukey's Multiple Comparison Test (more than two groups), using GraphPad Prism software version 4. All quantitative data represent mean values from at least four independent experiments. Significance of differences between these mean values was taken at $P < 0.05$.

Chapter III.

Expression of Ryanodine Receptors

Chapter III. Expression of Ryanodine Receptors

To establish the expression of RyRs in both human first trimester and term placental tissues, RNA/cDNA and protein extracts were used for RT-PCR and western blotting, respectively. The expression of RyR proteins was also investigated using indirect immunofluorescent microscopy in cell lines and immunohistochemistry in human tissue sections from first and term placenta of healthy individuals.

3.1 Ryanodine Receptor Transcripts are Expressed in Human Trophoblast Cell Lines and Human Placental Villous Tissues.

The expression of ryanodine receptors was examined in both human first trimester and term placental tissues, and in the human trophoblast cell lines BeWo, JAR, JEG-3 and SGHPL-4. The total RNA was extracted from cells and tissues, followed by RT-PCR as described in Chapter II 2.6 and 2.7. Figure 3.1.1 shows representative agarose gel images indicating the presence of RyR transcripts in samples, in which 5 μl of the original 50 μl reaction PCR products from each sample were loaded into the gel. Figure 3.1.1.A shows products amplified using *RYR1* primers. A549 cells are a human lung carcinoma cell line which served as a positive control, as they have been reported to express RyR1 (Xue *et al.*,2000), whereas Jurkat T cells were reported as RyR1/2-negative (Hosoi *et al.*,2001). Results show that the ~1112 bp PCR products amplified from *RYR1* mRNA (Figure 3.1.1.A (n = 3)) were found in the trophoblast cell lines BeWo and JAR; a weaker *RYR1* PCR product was also present in human first trimester placental villous sample. Sequencing of PCR products confirmed the presence of RyR1 transcripts. The nucleotide sequences of *RYR1* PCR products from both BeWo and first trimester villous samples displayed 99% mRNA identity to *Homo sapiens RYR1* on both plus and minus strands; whereas JAR *RYR1* PCR products were showed 100%/99% mRNA identity to *Homo sapiens RYR1* on plus/minus strands (see Appendix I, III and VII). A single nucleotide polymorphism (SNP) exists in sequence of products in BeWo, JAR and human first

trimester samples. However, protein sequences of conceptual translation from these PCR products showed 100% identity to *Homo sapiens* RyR1 in these samples, i.e SNPs do not affect protein sequence in cells and tissue samples were examined.

In Figure 3.1.1.B (n = 3), PCR product from an RNA extract of SH-SY5Y (Lane 3), a cell line which has been reported to express RyR2 protein (Mackrill *et al.*,1997), were used as an *RYR2* positive control. Along with SH-SY5Y, the *RYR2* PCR product of ~ 1082 bp was also detected in BeWo, JAR and first trimester tissue samples. PCR product sequencing indicated 99% identity to *Homo sapiens RYR2* on plus /minus strands of BeWo and JAR; 100%/99% mRNA identity to *Homo sapiens RYR2* on plus/minus strands of first trimester villous sample. Sequences derived from conceptual protein translations based on these *RYR2* PCR products showed 100% identity to *Homo sapiens* RyR2 protein in samples of both BeWo cells and first trimester tissues.

Jurkat cells were used as an *RYR3* positive control (Hakamata *et al.*,1994). However, no *RYR3* products from Jurkat cells were amplified in current study (Figure 3.1.1.C.I. (n = 3)). A rabbit skeletal muscle cDNA library (Stratagene) was also used for *RYR3* PCR control. As Figure 3.1.1.C.II shows, *RYR3* PCR products of expected size (~1013 bp) were detected in BeWo, JAR, JEG-3 and SGHPL-4 cells, along with rabbit skeletal muscle cDNA. In addition, a weak signal at expected size found in human term placental samples indicates presence of *RYR3* (Figure 3.1.1.C.I). Amplification of housekeeping gene *β-ACTIN* in both trophoblast cell lines and positive control samples indicated there was sufficient RNA of suitable quality in each sample, and that the amount of cDNA did not vary much between these samples (Figure 3.1.1.C.III). The PCR products of the expected size for *RYR3* were isolated and purified for sequencing. The sequencing results indicated 92% mRNA identity to *Homo sapiens RYR3* on plus/minus strands in PCR products from JEG-3 and SGHPL-4 cells. In addition, small amount of *RYR3* PCR product were also produced from a term placental villous tissue sample. Sequencing results indicated 94% mRNA identity to *Homo sapiens RYR3*.

Figure 3.1.1 Selective RT-PCR products of *RYR1*, *RYR2* and *RYR3* from human cell lines and human placental villous tissues

Figure 3.1.1.A Selective RT-PCR products of *RYR1* from human cell lines and human placental villous tissues

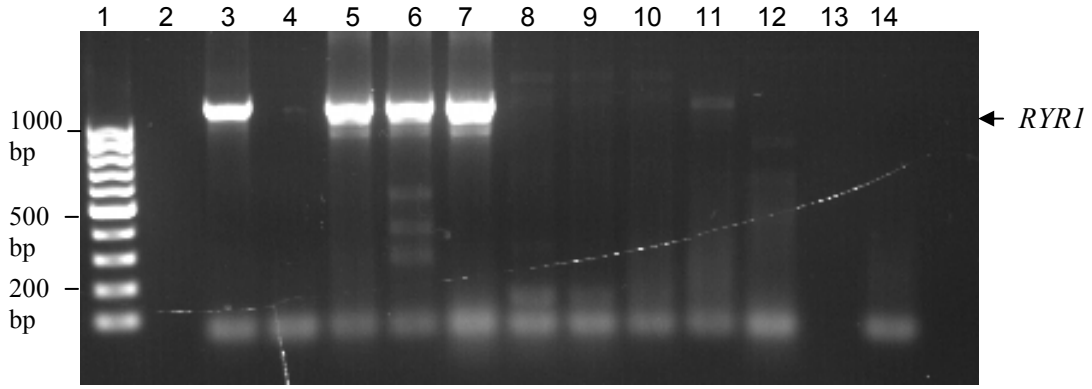

Figure 3.1.1.A. Reverse-transcription PCR of *RYR1*. PCR products were amplified from total cell RNA extracts of A549, BeWo and JAR, using selective *RYR1* selective primers. A weaker product of *RYR1* segment was also amplifed from human first trimester placental villous cDNA (sample Ep63). Lane 1. GeneRuler (0.5 μg/ lane, ~8 cm length gel); Lane 2. blank lane; Lane 3. A549; Lane 4. Jurkat; Lane 5. BeWo (1 of 2); Lane 6. BeWo (2 of 2); Lane 7. JAR; Lane 8. JEG-3 (1 of 2); Lane 9. JEG-3 (2 of 2); Lane 10. SGHPL-4; Lane 11. human first trimester placental villous tissue (Ep63); Lane 12. human term placental villous tissue (T1); Lane 13. blank lane; Lane 14. template-free control (PCR without template).

Figure 3.1.1.B Selective RT-PCR products of *RYR2* from human cell lines and human placental villous tissues

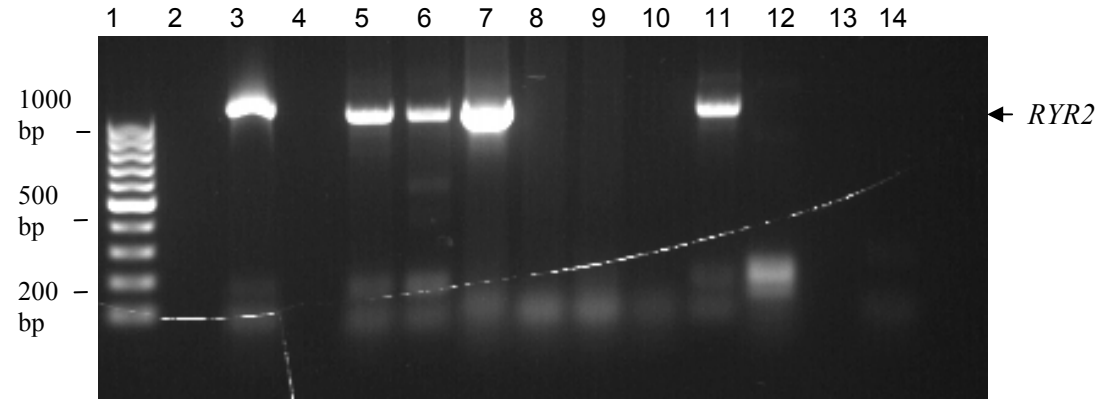

Figure 3.1.1.B. Reverse-transcription PCR of *RYR2*. Sequence of *RYR2* was amplified from total cell RNA extract of SH-SY5Y, BeWo and JAR; sequence of *RYR2* was also amplified from human first trimester placental villous cDNA (sample E63). Lane 1. GeneRuler (0.5 µg/ lane, ~8 cm length gel); Lane 2. blank lane; Lane 3. SHSY-5Y; Lane 4. blank lane; Lane 5. BeWo (1 of 2); Lane 6. BeWo (2 of 2); Lane 7. JAR; Lane 8. JEG-3 (1 of 2); Lane 9. JEG-3 (2 of 2); Lane 10. SGHPL-4; Lane 11. human first trimester placental villous tissue (Ep63); Lane 12. human term placental villous tissue (T1); Lane 13. blank lane; Lane 14. template-free control (PCR without template).

Figure 3.1.1.C. Selective RT-PCR products of *RYR3* from human cell lines and human placental villous tissues

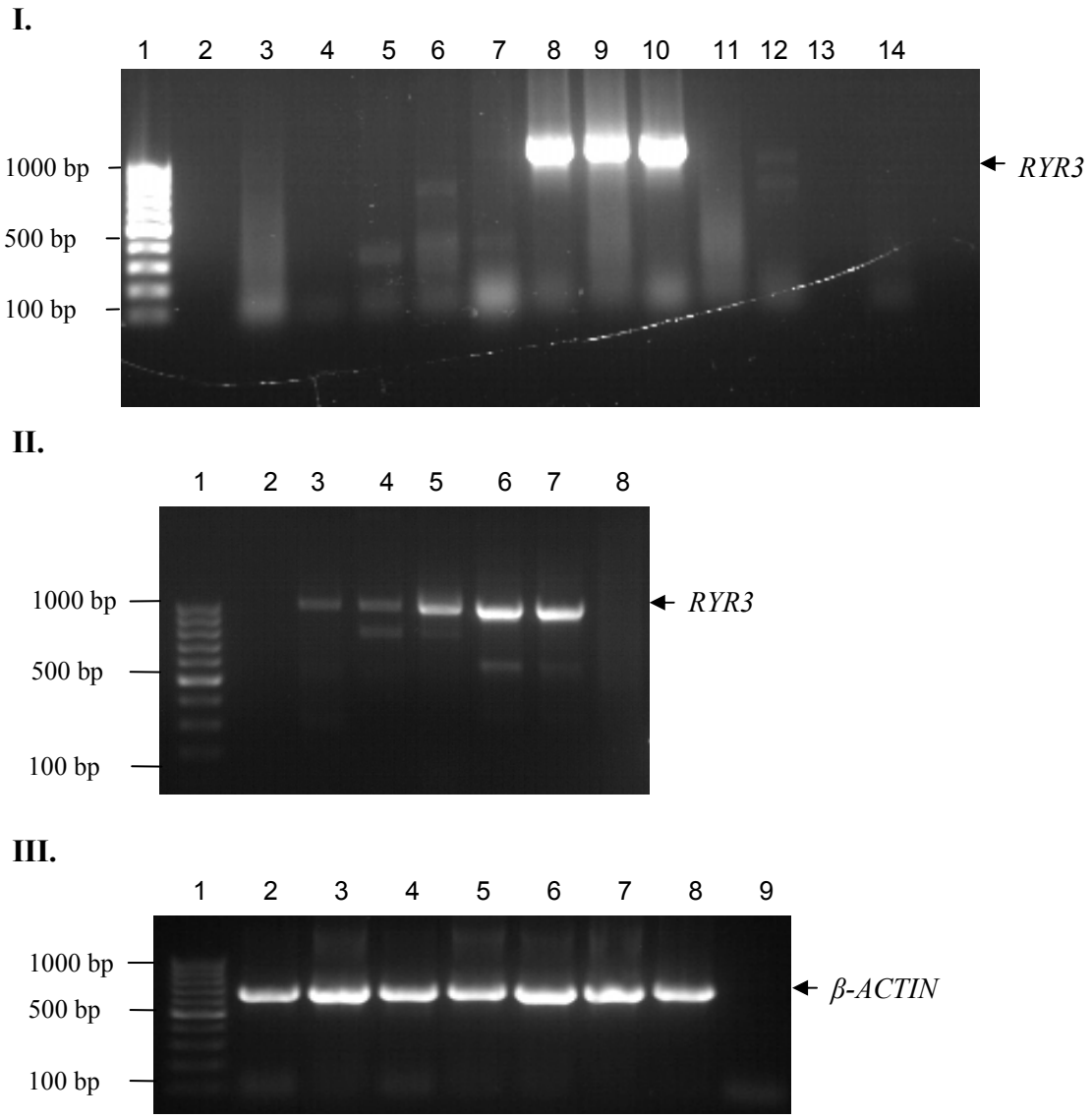

Figure 3.1.1.C. Reverse-transcription PCR of *RYR3* (~1013 bp). Panel **I**. Product of *RYR3* was amplified from cell total RNA extract of JEG-3 and SGHPL-4; smaller amount of *RYR3* product was also amplified from RNA extract of human term placental tissue (T1). Lane 1. GeneRuler (0.5 µg/ lane, ~8 cm length gel); Lane 2. blank; Lane 3. A549; Lane 4. Jurkat; Lane 5. BeWo (1 of 2); Lane 6. BeWo (2 of 2); Lane 7. JAR; Lane 8. JEG-3 (1 of 2); Lane 9. JEG-3 (2 of 2); Lane 10. SGHPL-4; Lane 11. human first trimester placental villous tissue (Ep63); Lane 12. human term placental villous tissue (T1); Lane 13. blank lane; Lane 14. template-free control (PCR without template). Panel **II**. PCR Products of *RYR3* from cells. Lane 1. GeneRuler (0.5 µg/ lane, ~8 cm length gel); Lane 2. blank; Lane 3. rabbit skeletal muscle (cDNA); Lane 4. BeWo; Lane 5. JAR; Lane 6. JEG-3; Lane 7. SGHPL-4; Lane 8. template-free control (PCR without template). Panel III. PCR product of *β-ACTIN* (~661 bp) from cells. Lane 1. GeneRuler (0.5 µg/ lane, ~8 cm length gel); Lane 2. rabbit skeletal muscle (cDNA); Lane 3. A549; Lane 4. Jurkat; Lane 5. BeWo; Lane 6. JAR; Lane 7. JEG-3; Lane 8. SGHPL-4; Lane 9. template-free control (PCR without template).

To determine whether RyR transcripts are present commonly in placental villous tissues, three more independent samples of human first trimester villous tissue were examined using RT-PCR. Products were visualized by UV illumination following agarose gel electrophoresis. As shown in Figure 3.1.2, products of the expected size of both *RYR1* (Figure 3.1.2.A) and *RYR2* (Figure 3.1.2.B) were found in samples of Ep64, Ep65, and Ep66, in addition to Ep63 which is presented in Figure 3.1.1.

In contrast, no PCR products of *RYR3* transcript were produced by selective primers in placental samples examined, while products of *RYR1* and *RYR2* were found in several samples. Amplification of housekeeping gene *β-ACTIN* in all samples indicated the presence of sufficient RNA of suitable quality in each sample, and that the amount of cDNA did not vary much between these samples (Figure 3.1.4). These results indicated the *RYR1* and *RYR2* mRNA is commonly expressed in human first trimester villous placental tissue.

Figure 3.1.2 Selective RT-PCR products of *RYR1*, *RYR2* and *RYR3* from human first trimester placental villous tissue.

Figure 3.1.2.A Selective RT-PCR products of *RYR1* from human first trimester placental villous tissues

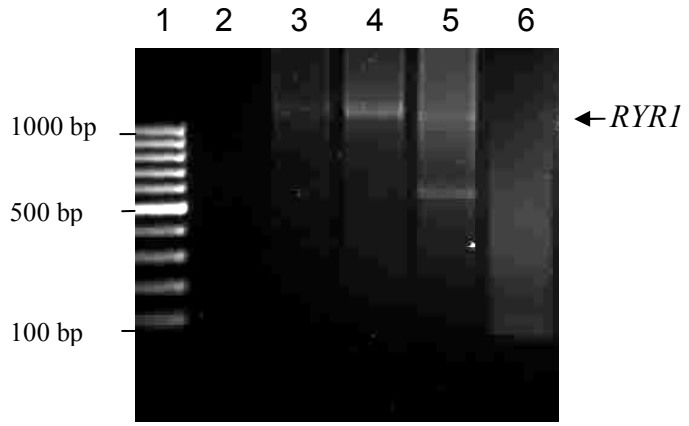

Figure 3.1.2.A. Reverse-transcription PCR of *RYR1*. Sequence of *RYR1* was amplifed from cDNA from human first trimester placental villous samples (Ep64, Ep65 and Ep66). Lane 1. GeneRuler (0.1 µg/ lane, ~8 cm length gel); Lane 2. blank lane; Lane 3. Ep64; Lane 4. Ep65; Lane 5. Ep66; Lane 6. template-free control (PCR without template).

Figure 3.1.2.B Selective RT-PCR products of *RYR2* from human first trimester placental villous tissues

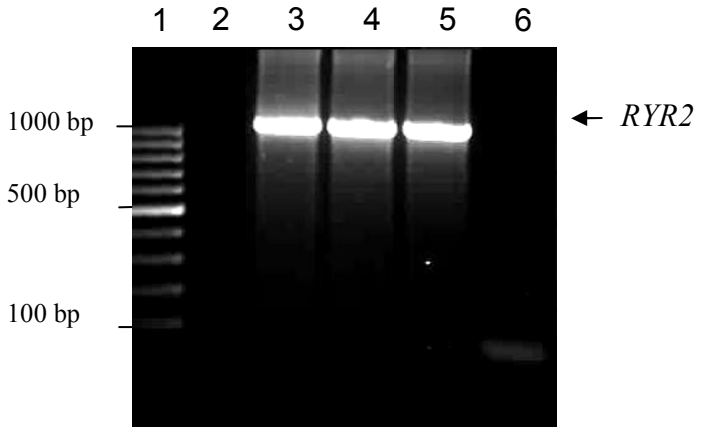

Figure 3.1.2.B. Reverse-transcription PCR of *RYR2*. Sequence of *RYR2* was amplified from cDNA of human first trimester placental villous samples (E64, Ep65 and Ep66). Lane 1. GeneRuler (0.1 μg/ lane, ~8 cm length gel); Lane 2. blank lane; Lane 3. Ep64; Lane 4. Ep65; Lane 5. Ep66; Lane 6. template-free control (PCR without template).

Figure 3.1.2.C Selective RT-PCR products of *RYR3* from human first trimester placental villous tissues

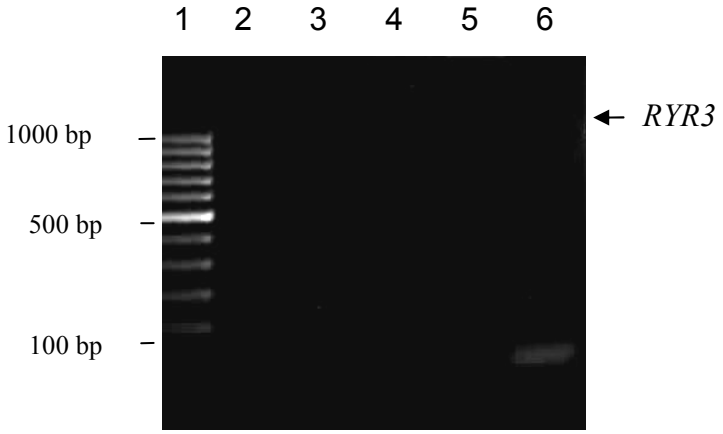

Figure 3.1.2.C. Reverse-transcription PCR of *RYR3*. Sequence of *RYR*3 was not amplified from available human first trimester placental villous samples. Lane 1. GeneRuler (0.5 µg/ lane, ~8 cm length gel); Lane 2. blank lane; Lane 3. Ep64; Lane 4. Ep65; Lane 5. Ep66; Lane 6. template-free control (PCR without template).

Similarly, three more independent samples of human term placental villous tissue were also examined by RT-PCR. Products were visualized using UV illumination following agarose gel electrophoresis. Figure 3.1.3. shows that *RYR1* (Figure 3.1.3. A) and *RYR2* (Figure 3.1.3.B) PCR products were amplified from samples T3 and T410, respectively. However, no *RYR1* and *RYR2* PCR products were amplified from the other term samples examined. In contrast, *RYR3* PCR products were detected in 4 out of 5 term placental tissue villous samples, together with observation presented in Figure 3.1.1.C. showing that, with the exception of sample T4, *RYR3* DNA nucleotides were amplified from samples T2, T3 and T410. These results indicated that the *RYR*3 mRNA is detectable in some human term placental villous tissue.

The presence of house-keeping gene human *β-ACTIN* was examined in samples from both human first trimester and term placental villi. Figure 3.1.4 shows the expected 661 bp products were detected in first trimester samples (Ep64, Ep65 and Ep66) and term samples (T2, T3, T4 and T410). These results indicate each sample contains a substantial amount of cDNA required for amplification. Therefore, the relatively low yield of *RYR* PCR products was unlikely due to lack of templates.

Figure 3.1.3 Selective RT-PCR of *RYR1*, *RYR2* and *RYR3* from RNA extracts of human term placental villous tissue.

Figure 3.1.3.A Selective RT-PCR of *RYR1* from human term placental villous tissue

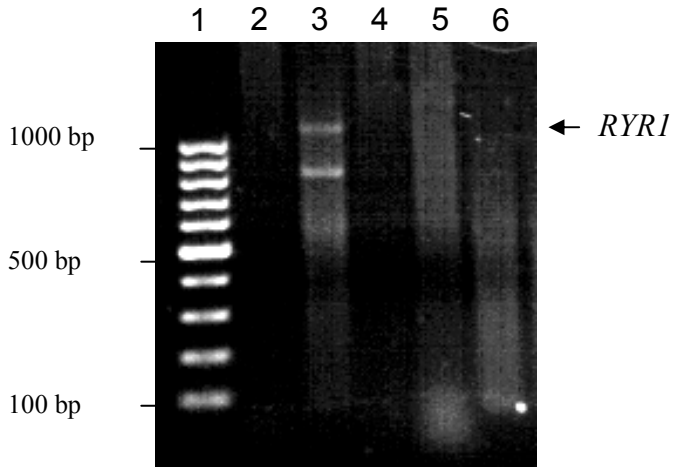

Figure 3.1.3.A. Reverse-transcription PCR of *RYR1*. Sequence of *RYR1* was amplifed from RNA extract of human term placental villous sample T3. Lane 1. GeneRuler (0.1 µg/ lane, ~8 cm length gel); Lane 2. T2; Lane 3. T3; Lane 4. T4; Lane 5. T410; Lane 6. template-free control (PCR without template).

Figure 3.1.3.B Selective RT-PCR of *RYR2* from human term placental villous tissue

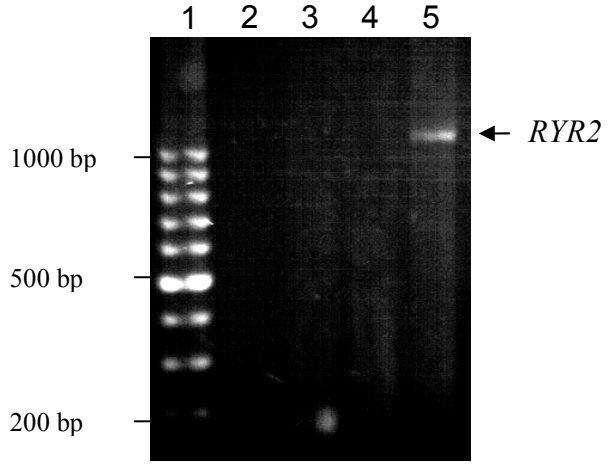

Figure 3.1.3.B. Reverse-transcription PCR of *RYR2*. Sequence of *RYR2* was amplified from RNA extract of human term placental villous sample T410. Lane 1. GeneRuler (0.1 µg/ lane, ~8 cm length gel); Lane 2. T2; Lane 3. T3; Lane 4. T4; Lane 5. T410.

Figure 3.1.3.C Selective RT-PCR of *RYR3* from human term placental villous tissue

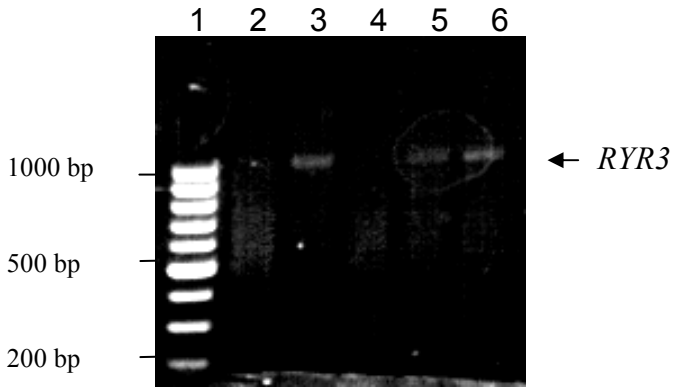

Figure 3.1.3.C. Reverse-transcription PCR of *RYR3*. Sequence of *RYR*3 was amplified from RNA extracts from human term placental villous samples (T2, T3 and T410). Lane 1. GeneRuler (0.1 µg/ lane, ~8 cm length gel); Lane 2. template-free control (PCR without template); Lane 3. T410; Lane 4. T4; Lane 5. T3; Lane 6. T2.

Figure 3.1.4. PCR of *β-ACTIN* in samples of human first trimester and term placental villous tissue.

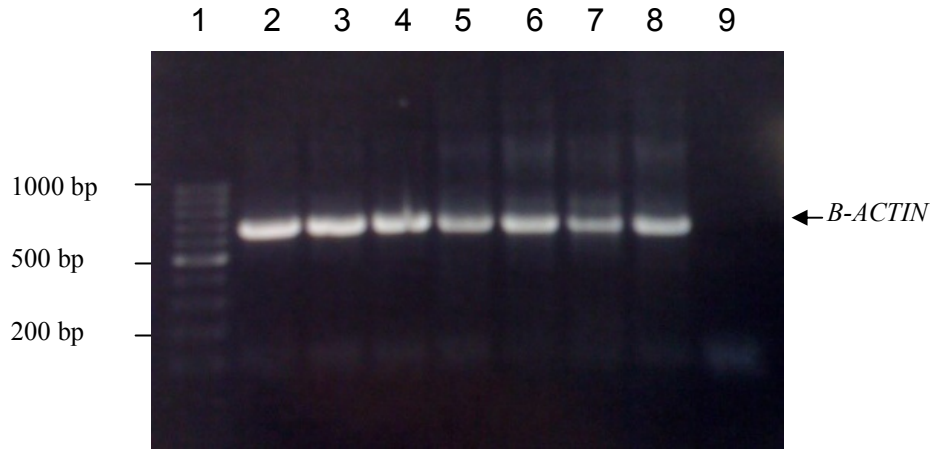

Figure 3.1.4. PCR products of human *β-ACTIN*. Sequence of *β-ACTIN* (~661 bp) was amplified from samples of both human first and term placental villous samples Lane 1. GeneRuler (0.1 μg/ lane, ~8 cm length gel); Lane 2. Ep64; Lane 3. Ep65; Lane 4. Ep66; Lane 5. T2; Lane 6. T3; Lane 7, T4; Lane 8, T410; Lane 9. template-free control (PCR without template).

3.2 RyR Proteins are Expressed in Human Trophoblast Cell Lines and Tissues: Western Blotting

The expression of RyR proteins was also examined by western blotting. Figure 3.2.1 shows representative blots probed with various antibodies that recognize RyRs. Proteins of approximately 560 kDa apparent molecular weight were detected by RS4, an antiserum that recognizes all RyR isoforms, in BeWo, JAR and JEG-3 membrane fraction preparations, as indicated in Figure 3.2.1.A (n = 4).

In other independent experiments under the same conditions, antibodies specifically recognizing RyR subtypes were used. Figure 3.2.1.B, C and D are the representative blots (all n = 4) that were probed with antisera against RyR1, RyR2, and RyR3, respectively, at working dilutions shown in Table 2.5.2. Expression of RyR1 was detected in JEG-3 and in BeWo cell membrane fraction preparations. The expression of RyR2 and RyR3 proteins was not detectable in these western blotting experiments.

Although the expression of RyR subtypes was not detectable using RyR isoform seletective antibodies, the expression of RyR1, RyR2 and RyR3 was detected in rat skeletal muscle, heart muscle and brain tissue microsomes, respectively. Among these positive control samples, both RyR1 and RyR3 were detected in rat brain microsomal preparations.

The expression of RyRs was also determined in human placental tissues homogenates. Figure 3.2.2 showed the representative blot (n = 3) incubated with pan-RyR antiserum (RS4), which indicated both first trimester and term placental villous tissue expressing RyRs, along with samples of rat skeletal muscle, SH-SY5Y cells and BeWo cells.

Figure 3.2.1 Expression of RyRs in human trophoblast cell lines detected by western blotting.

Figure 3.2.1.A RyR proteins in human trophoblast cell lines: western blot

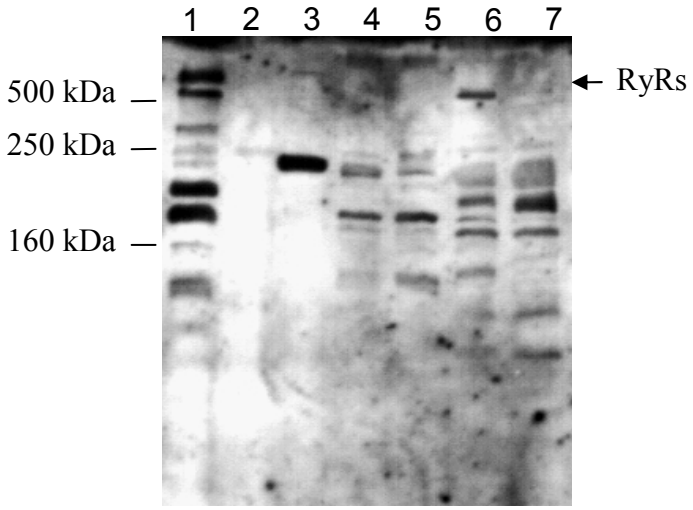

Figure 3.2.1.A. Representative blot (n = 4) using antiserum RS4 that recognizes all RyR isoforms: expression of RyRs was detected in microsomes from both rat brain and skeletal muscle, and membrane fraction preparation of BeWo, JAR and JEG-3. Higher molecular weight protein bands of RyR were recognized by this pan RyR antisera in BeWo and JAR samples. Samples were loaded with 80 μg of protein per well. Lane 1. rat brain microsomes; Lane 2. rat heart microsomes; Lane 3. rat skeletal muscle microsomes; Lane 4. BeWo membrane fraction; Lane 5. JAR membrane fraction; Lane 6. JEG-3 membrane fraction; Lane 7. SGHPL-4 membrane fraction.

Figure 3.2.1.B RyR1 in human trophoblast cell lines: western blot

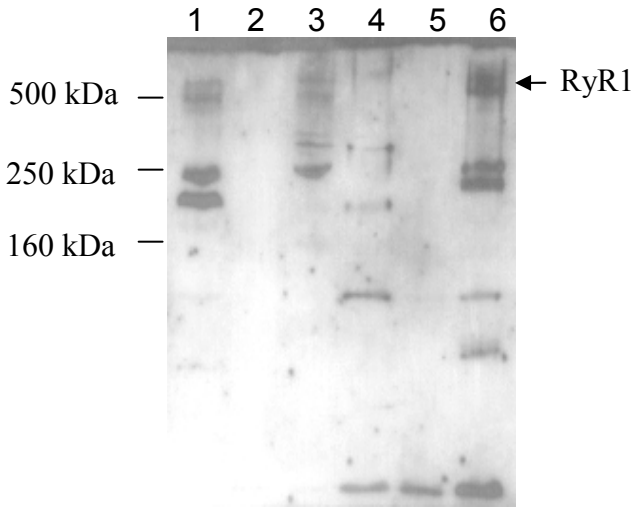

Figure 3.2.1.B. Representative blot (n = 4) probed with an antiserum recognizes RyR1: expression of RyR1 was detected in microsomes of both rat brain and skeletal muscle, and membrane fraction preparations of BeWo and JEG-3. Samples were loaded with 80 μg of protein per well. Lane 1. rat brain microsomes; Lane 2. rat heart microsomes; Lane 3. rat skeletal muscle microsomes; Lane 4. BeWo membrane fraction; Lane 5. JAR membrane fraction; Lane 6. JEG-3 membrane fraction.

Figure 3.2.1.C RyR2 in human trophoblast cell lines: western blot

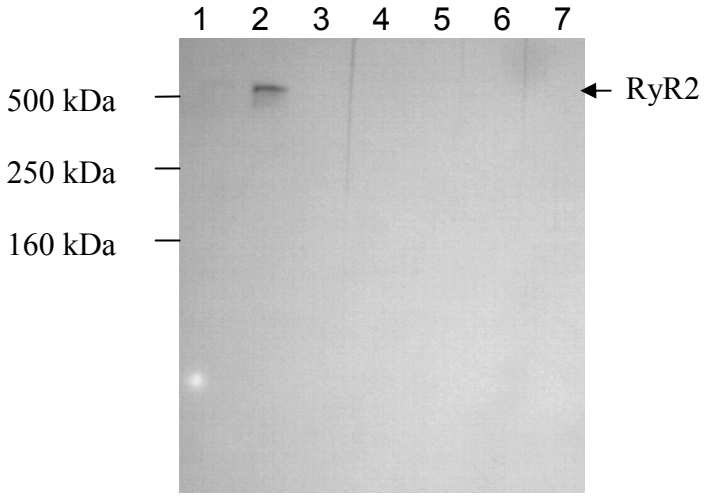

Figure 3.2.1.C. Representative blot (n = 4) probed with an antiserum recognizes RyR2: expression of RyR2 was not detected in any human trophoblast cell lines (BeWo, JAR, JEG-3 and SGHPL-4). Samples were loaded with 80 μg of protein per well. Lane 1. rat brain microsomes; Lane 2. rat heart microsomes; Lane 3. rat skeletal muscle microsomes; Lane 4. BeWo membrane fraction; Lane 5. JAR membrane fraction; Lane 6. JEG-3 membrane fraction; Lane 7. SGHPL-4 membrane fraction.

Figure 3.2.1.D RyR3 in human trophoblast cell lines: western blot

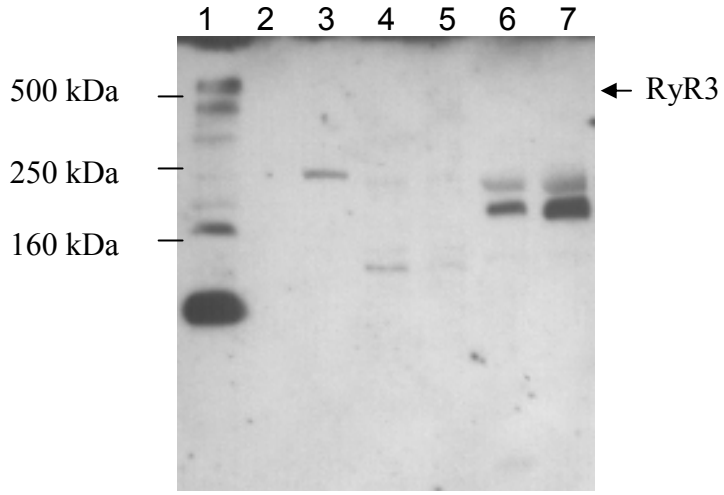

Figure 3.2.1.D. Representative blot (n = 4) probed with an antiserum recognizes RyR3: expression of RyR3 was not detected in human trophoblast cell lines (BeWo, JAR, JEG-3 and SGHPL-4). Samples were loaded approximately 80 μg of protein per well. Lane 1. rat brain microsomes; Lane 2. rat heart microsomes; Lane 3. rat skeletal muscle microsomes; Lane 4. BeWo membrane fraction; Lane 5. JAR membrane fraction; Lane 6. JEG-3 membrane fraction; Lane 7. SGHPL-4 membrane fraction.

Figure 3.2.2 RyRs in human placental tissues: western blot

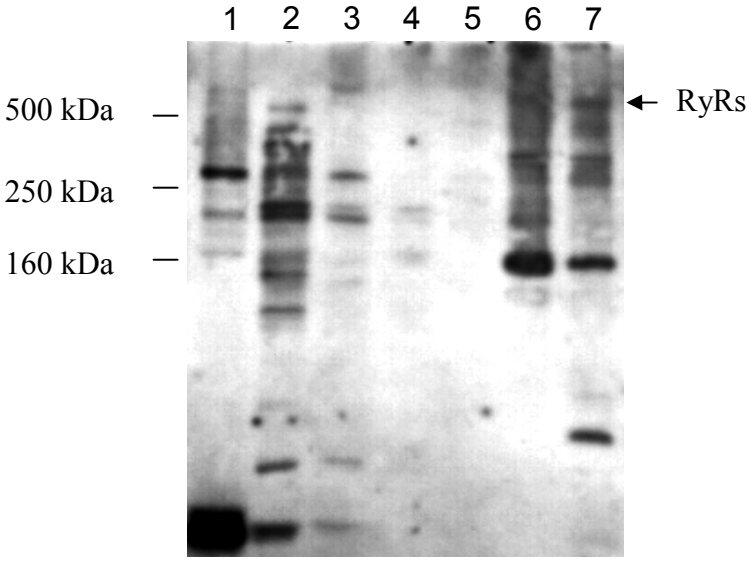

Figure 3.2.2. Representative blot (n = 3) using antiserum RS4 that recognizes all RyR isoforms: expression of RyRs was detected in microsomes of rat skeletal muscle, membrane fraction preparations of SH-SY5Y and BeWo cell-lines, and in homogenates of both human first trimester and term placental tissue. Samples were loaded approximately 80 µg of protein per well. Lane 1. rat skeletal muscle microsomes; Lane 2. SH-SY5Y membrane fraction; Lane 3. BeWo membrane fraction; Lane 4. JAR membrane fraction; Lane 5. JEG-3 membrane fraction; Lane 6. human first trimester placental homogenate; Lane 7. human term placental homogenate.

3.3 RyR Accessory Proteins, CSQ and TRD, are Expressed in Human Trophoblast Cell Lines and Tissues: Western Blotting.

To determine whether RyR accessory proteins are expressed along with RyRs, the expression of CSQ and TRD was examined in both human trophoblast cell lines and human term placental villous tissues. High levels of CSQs were detected in rat heart and skeletal muscle microsomes (Lane 1 and Lane 2, respectively, Figure 3.3.1 (n = 3)); along with these two positive control samples, CSQ was detected in the trophoblast cell lines BeWo and JEG-3. The 55 kDa RyR accessory proteins were also detected in five independent human term placental villous tissue homogenates, as indicated in Figure 3.3.1. In addition to CSQ, the 97 kDa CSQ-like proteins (Zhang *et al.*,1997) were also found in BeWo, JEG-3 and differentiated C2C12 myotubes.

Expression of another accessory protein TRD was also determined. The trophoblast cell lines of BeWo, JAR, JEG-3 and SGHPL-4 were found to express TRD as indicated in blot image, Figure 3.3.2.A. In human samples, TRD was detected in sample Ep1 and Ep4 of first trimester villous homogenates, and sample T1 term placental villous homogenates (Figure 3.3.2.B (n = 3)).

Figure 3.3.1 CSQ in trophoblast cells and human tissues: western blot

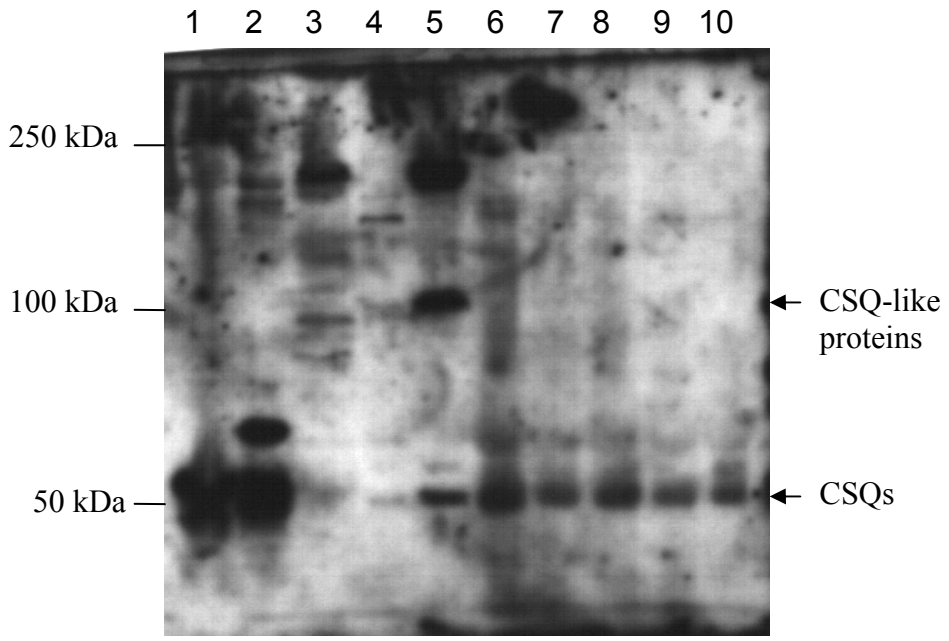

Figure 3.3.1. Representative blot (n = 3) using an antiserum recognizes all CSQ isoforms: expression of CSQs was detected in all samples examined from both cell lines and tissue. The 97 kDa CSQ-like proteins were also detected in human trophoblast cell lines (BeWo and JEG-3) and in differentiated C2C12 myoblasts. Samples were loaded with 80 μg of protein per well. Lane 1. rat heart microsomes; Lane 2. rat skeletal muscle microsomes; Lane 3. cell lysate of differentiated C2C12 myotubes; Lane 4. BeWo membrane fraction; Lane 5. JEG-3 membrane fraction; Lane 6 to Lane 10. Samples (359, 364, 374, 387, 393) of human term placental homogenate.

Figure 3.3.2 Determination of TRD expression by western blotting.

Figure 3.3.2.A TRD in trophoblast cells: western blot

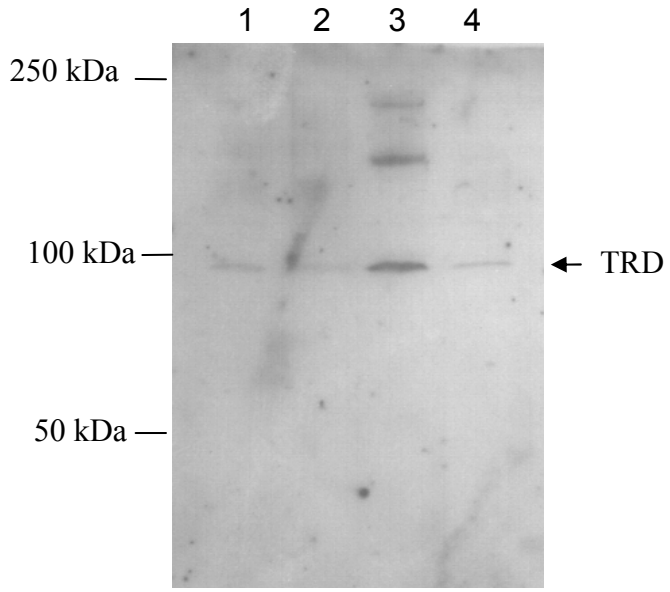

Figure 3.3.2.A. Determination of triadin (TRD) expression in human trophoblast cell lines by western blotting (n = 3). Each well was loaded with 60 μg of protein. The antiserum used recognizes all TRD isoforms. Expression of TRDs was detected in all samples examined (human trophoblast cell lines: BeWo, JAR, JEG-3 and SGHPL-4). Lane 1. BeWo membrane fraction; Lane 2. JAR memebrane fraction; Lane 3. JEG-3 membrane fraction; Lane 4. SGHPL-4 cell lysate.

Figure 3.3.2.B TRD in human placental tissues: western blot

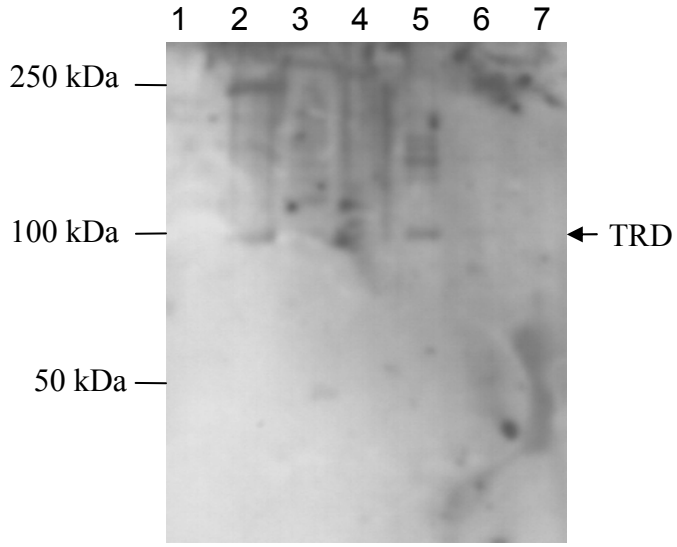

Figure 3.3.2.B. Determination of triadin (TRD) expression in human placental tissue by western blotting (n = 3). The antiserum used recognizes all TRD isoforms. Expression of TRDs was detected in human first trimester villous homogenate samples (first trimester sample Ep1 and Ep4, and human term placental villous sample T1). Lane 1. rat heart microsomes (70 μg protein); Lane 2. human first trimester villous homogenate (Ep1, 70 μg protein); Lane 3. human first trimester villous homogenate (Ep3, 50 μg protein); Lane 4. human first trimester villous homogenate (Ep4, 70 μg protein); Lane 5. human term placental villous homogenate (T1, 70 μg protein); Lane 6. human term placental villous homogenate (T2, 50 μg protein); Lane 7, human term placental villous homogenate (T3, 40 μg protein).

3.4 Expression of RyRs and TRD Revealed in Human Placental Villous Tissue Sections

To determine whether RyRs and their accessory proteins are primarily expressed in human placental tissues rather than just being present in choriocarcinoma cell lines that originated from the trophoblasts of human placenta, paraffin embedded human trophoblast tissue sections were examined by IHC as described in Chapter II 2.10. Results of sections from both first trimester and term tissues supported the protein expression of RyR1, RyR3, and TRD in human trophoblast tissues.

3.4.1 RyRs and TRD are expressed in human first trimester villous trophoblast

Figure 3.4.1 shows representative IHC images of human first trimester villous sections (n = 3). The brown staining represents the DAB detection of peroxidase activity; the blue stain represents counterstaining with Harris's haematoxylin. Both syncytiotrophoblasts (outer monolayer of the villi) and cytotrophoblasts (cell layer underneath the syncytiotrophoblasts) were stained positively as shown in panel A, C and D of Figure 3.4.1. This brown colour development in sections implies that RyR1 (A), RyR3 (C) and TRD (D) are present in both syncytio- (* SCT) and cyto- (▲CT) trophoblast of human first trimester placental villous tissue. In contrast, panel B shows no detectable staining for RyR2. Panel E shows a positive control IHC image, stained using anti-cytokeratin 7, which outlined cells of interest including both syncytio- and cyto- trophoblast cell layers. Panel F presented the primary antibody-free control IHC image, in which, these sections were stained in parallel with other sections but without adding primary antibody.

Figure 3.4.1 RyRs and TRD in human first trimester villous tissues: IHC

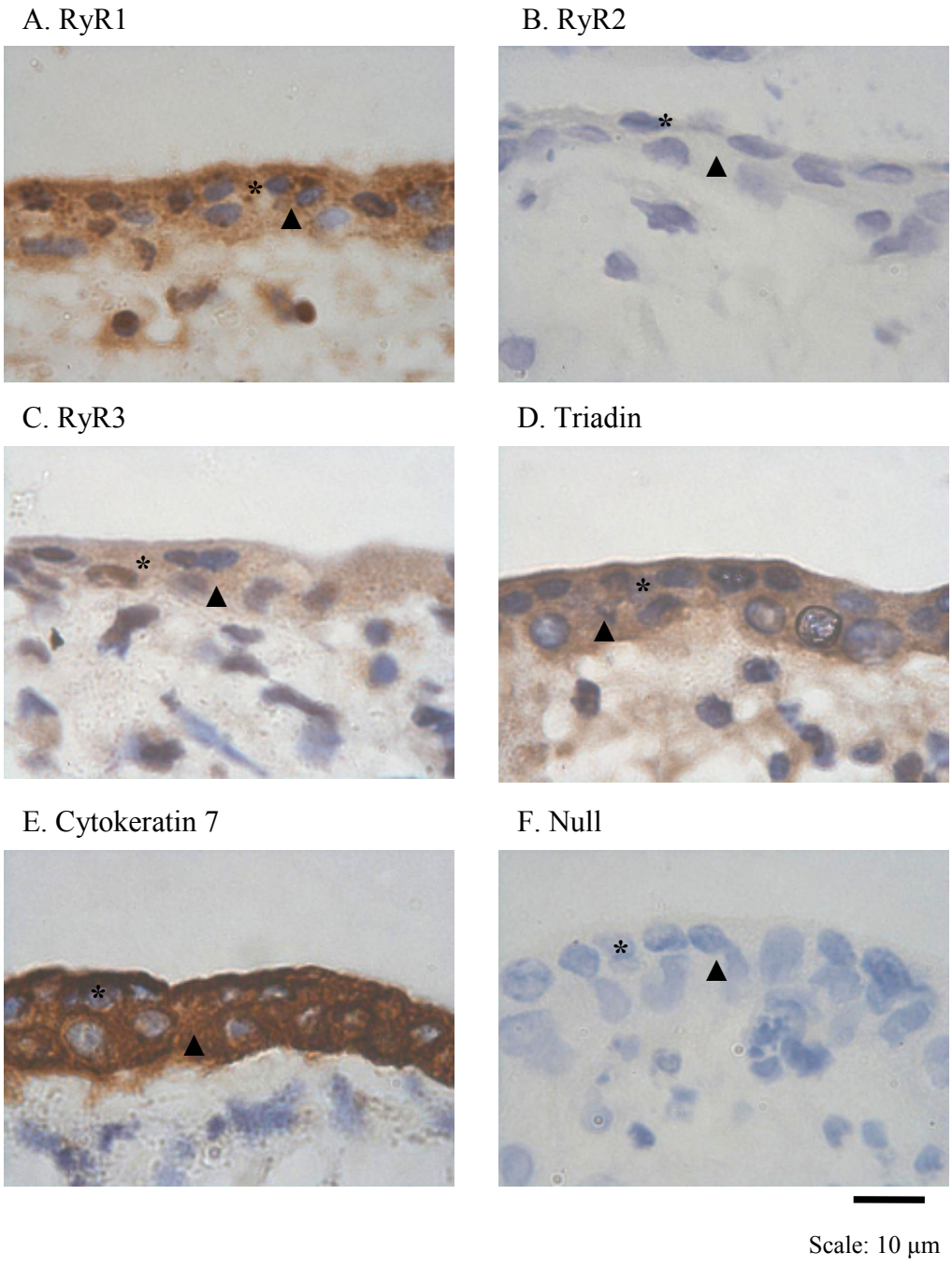

Figure 3.4.1. Determination of RyRs and TRD expression in human first trimester placental villous tissue section by IHC (n = 3). * SCT: Syncytiotrophoblast; ▲CT: cytotrophoblast. Panel A. Antiserum used recognizes RyR1; Panel B. Antiserum used recognizes RyR2; Panel C. Antiserum used recognizes RyR3; Panel D. Antiserum used recognizes all TRD isoforms; Panel E. Antiserum used recognizes cytokeatin 7; Panel F. no primary antiserum was applied.

3.4.2 RyRs and TRD are expressed in human term placental villous trophoblast

Figure 3.4.2 shows representative IHC images of human term placental villous sections (n = 3). Similar to IHC results in first trimester sections, both syncytio- (* SCT) and cyto- (▲CT) trophoblast of term placental villous sections were stained positively with primary antibodies recognising RyR1, RyR3 and TRD, as indicated by brown colour development in panel A, C and D of Figure 3.4.2, respectively; while sections stained with anti-RyR2 antibody showed no positive staining, as the corresponding representative IHC image in Panel B displayed no detectable difference in sections performed as primary antibody-free controls in Panel F.

Figure 3.4.2 RyRs and TRD in human term placental villous tissues: IHC

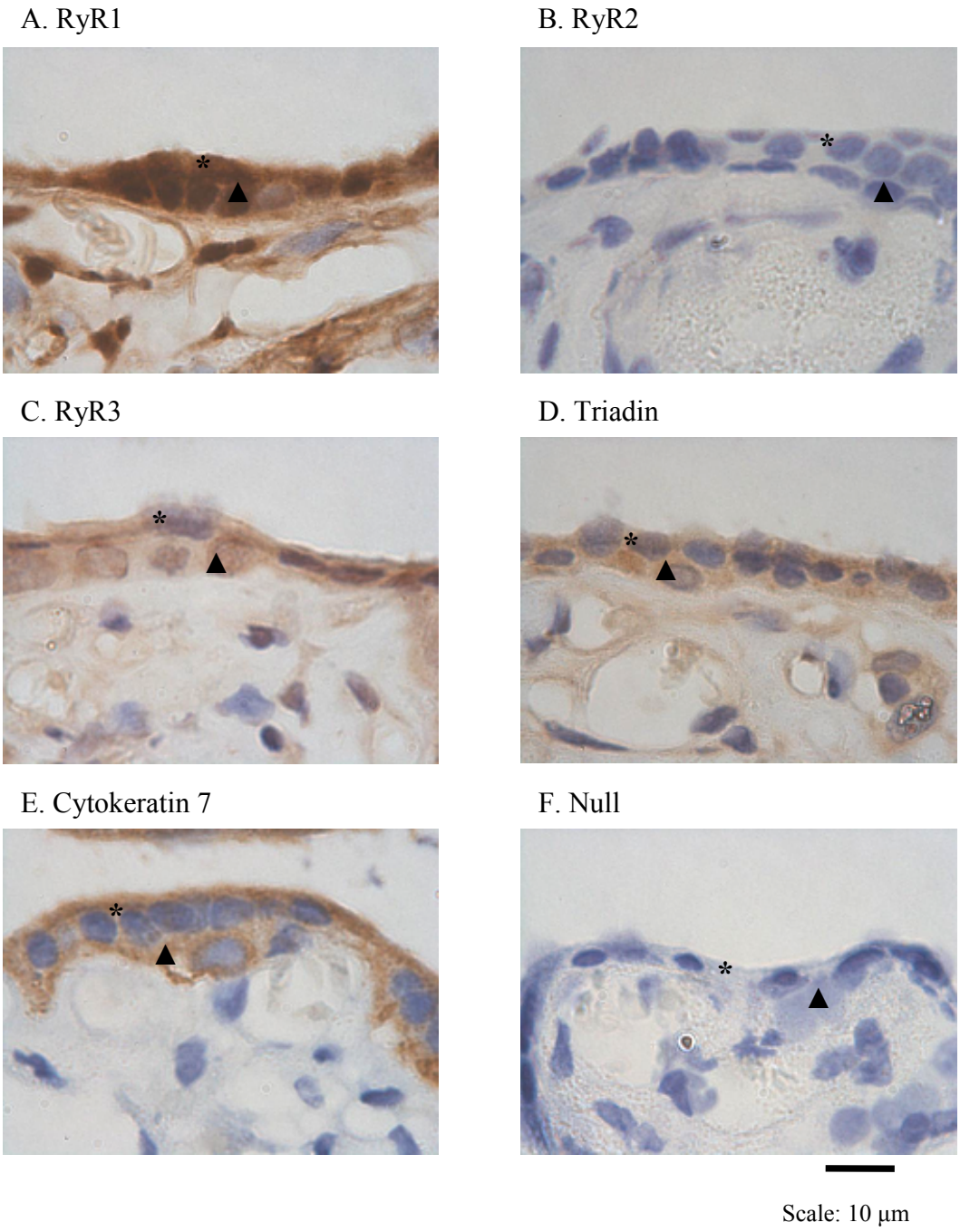

Figure 3.4.2. Determination of RyRs and TRD expression in human term placental villous tissue section by IHC (n = 3). * SCT: Syncytiotrophoblast; ▲CT: cytotrophoblast. Panel A. Antiserum used recognizes RyR1; Panel B. Antiserum used recognizes RyR2; Panel C. Antiserum used recognizes RyR3; Panel D. Antiserum used recognizes all TRD isoforms; Panel E. Antiserum used recognizes cytokeratin 7; Panel F. no primary antiserum was applied.

3.4.3 RyR2 is expressed in trophoblast of human first trimester decidua

Representative IHC images from both human first trimester and term placental villous sections displayed negative staining for RyR2, as shown in Figure 3.4.1.B and Figure 3.4.2.B shown. However, a preliminary result shows RyR2 staining was positive in one sample from sections of human first trimester decidua (EP98DC). These sections contained invasive forms of trophoblast, the extravillous trophoblast. Cytokeratin 7 is a known specific marker for human trophoblast (Haighn *et al.*,1999); this protein marker is also expressed in extravillous trophoblast (Hallikas *et al.*,2006). In current study, cytokeratin 7 was used as marker of all types of trophoblast. Figure 3.4.3.C shows trophoblastic cells that were identified by antibodies recognising cytokeratin 7 (▲) localised as outer layer of cells in this tissue section. Another section from the same sample was treated with primary antibodies recognising RyR2. In this experiment, positive staining of cells morphologically remembling trophoblasts (▲) was obtained as shown in Figure 3.4.3.A. This result indicates the anti-serum used to label RyR2 (HPA016697, Sigma) was workable in current IHC method; RyR2-positve section found in samples of placental decidua but not in villi, suggesting differential expression of RyR2 in different trophoblast populations.

Figure 3.4.3 RyR2 in human first trimester decidua bed (IHC)

A. RyR2

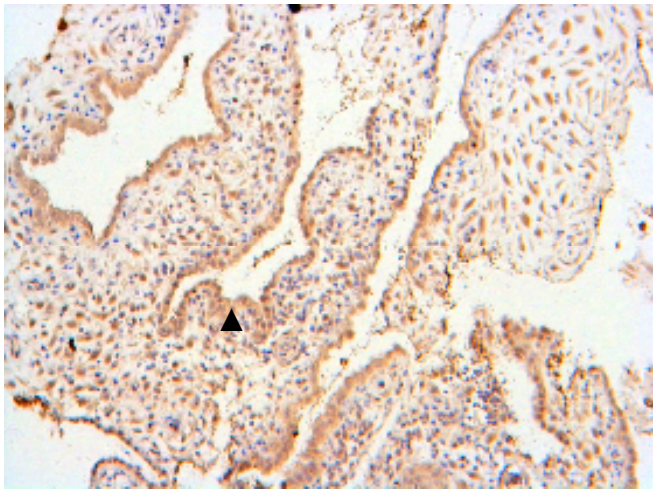

B. -ve

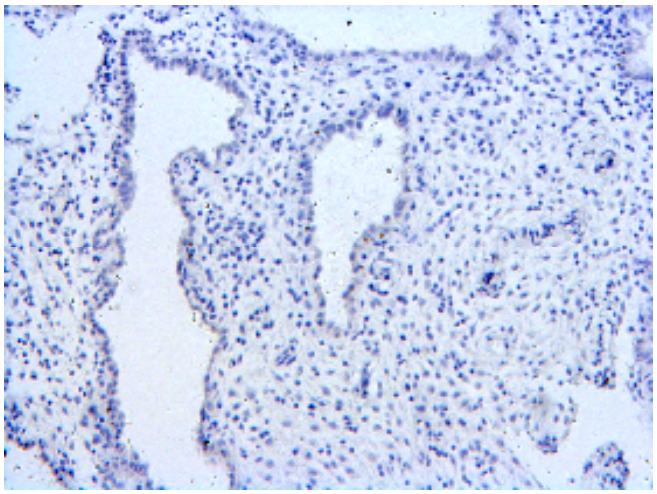

C. Cytokeratin 7

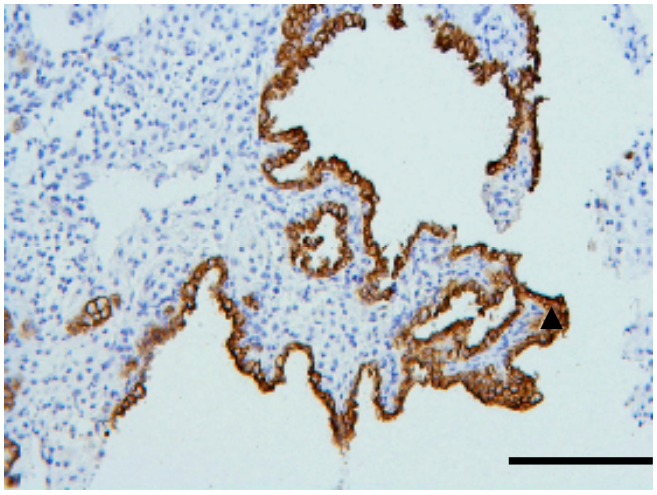

Scale: 100 μm

Figure 3.4.3 RyR2 expression detected using IHC in decidua bed of first trimester tissue sections (Sample: EP98DC). Panel **A.** The antiserum used recognizes RyR2 (HPA016697, Sigma).▲: trophoblast. Panel **B**. Negative control (no primary antibody used); Panel **C**. Cytokeratin 7 stain indicating trophoblastic cells within tissue section.

3.5 Determination of RyRs, CSQs and TRDs in BeWo and JEG-3: immunofluorescence microscopy

RT-PCR and western blotting data indicated that both RyR transcripts and proteins were detectable in BeWo and JEG-3 cell lines. Transcripts encoding RyR1 and RyR2 and protein expression of RyR1 were detectable in BeWo, whereas mRNA transcripts of RyR3 and protein expression of RyR1 were found in JEG-3. In addition, RyR proteins in both BeWo and JEG-3 were recognising by RS4 anti-panRyR serum. In other words, of all cell lines examined, BeWo and JEG-3 had the most extensive evidence of RyR expression. Therefore, both BeWo and JEG-3 were chosen for indirect immunofluorescence (IF) microscopy and Ca^{2+}-imaging studies as described in the following sections.

3.5.1 RyRs are distributed intracellularly in BeWo and JEG-3 cells

Apart from ER/SR membrane-expressing RyRs, expression of RyRs has been revealed in other areas of cells, such as plasma membranes and mitochondira (Zaidi *et al.*,1995; Beutner *et al.*,2001). To determine whether RyRs are expressed on the ER membrane of trophoblastic cell lines, BeWo and JEG-3 cells were treated with rabbit anti-RyR isoform specific antisera together with either mouse anti-E-cadherin or mouse anti-pan-cadherin primary antibodies. Cells were then incubated with Cy2-conjugated anti-rabbit and Cy3-conjugated anti-mouse secondary antibodies that recognized the corresponding primary antibodies. Cadherin is regarded as a plasma membrane marker that outlines cell membrane. E-cadherin is reported to be expressed in both BeWo and JEG-3 trophoblast (Coutifaris *et al.*,1991; Al-Nasiry *et al.*,2006; Pospechova *et al.*,2009).

The IF images in Figure 3.5.1.A indicate the presence of RyR1, RyR2 and RyR3 by Cy2-conjugated IgG as green fluorescence (Figure 3.5.1.A, left column), with a recticular intracellular distribution in BeWo cells (n = 4). Detection of E-cadherin by Cy3-conjugated IgG that presented in red fluorescence (Figure 3.5.1.A,

middle column), which was limited within cell plasma membrane. Merged images shown limited overlap of green and red fluorescence (Figure 3.5.1.A, right column), indicating that RyR1, RyR2 and RyR3 were localized within ER/ cytoplasm rather than being juxtaposed to the plasma membrane of BeWo cells.

Similarly, detection of RyR1, RyR2 and RyR3 by IF in JEG-3 cells also revealed the reticular, intracellular distribution of all three RyR isoforms (Figure 3.5.1.B). The green fluorescence was more intense in perinuclear regions (Figure 3.5.1.B, left column), consistent with an ER localization of RyR expression. The primary antibodies of plasma membrane marker used in JEG-3 cells for IF detection recognized all types of cadherin protein, which resulted in a stronger intensity of red fluorescence (Figure 3.5.1.B, middle column) when coupled to Cy3-conjugated secondary antibodies. Although overlaps of green and red fluorescence appeared in intracellular space of JEG-3 cells in merged images (Figure 3.5.1.B, right column), areas of cell-cell contact still presented strong red fluorescence without extensive overlap with green fluorescence.

In both BeWo and JEG-3 cells, there was no non-specific fluorescence detected in either green or red channels when cells were treated under the same experimental conditions but without adding primary antibodies (BeWo cells: Figure 3.5.1.A, bottom row; JEG-3 cells: Figure 3.5.1.B, bottom row). These results indicated that the fluorescence that produced by secondary antibodies (Cy2-/Cy3-conjugated) was dependent on the recognition of antigens by their primary antibodies.

Figure 3.5.1.A RyRs in BeWo cells: immunofluorescence microscopy

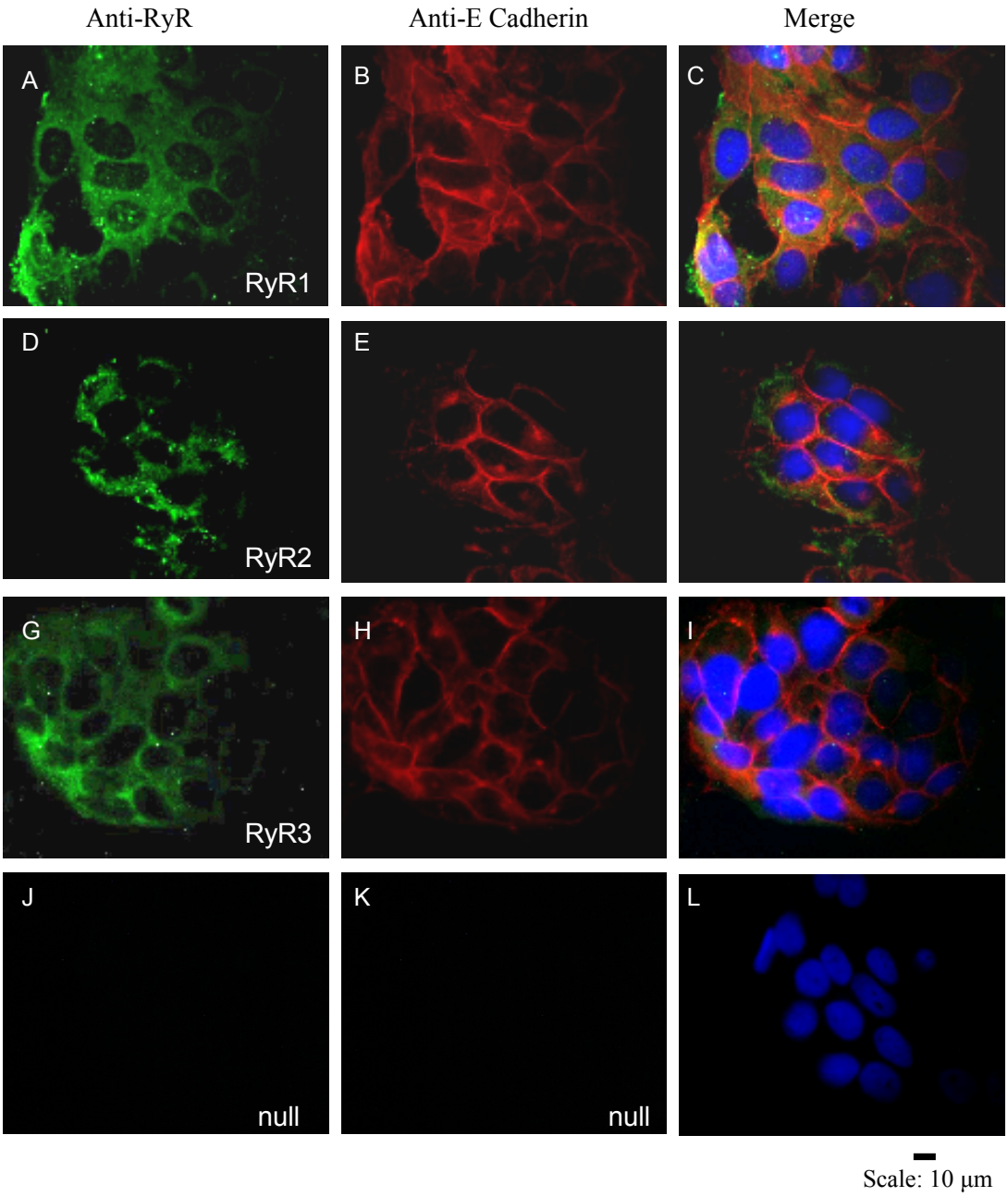

Figure 3.5.1.A. **Immunofluorescence microscopy of BeWo cells.** 'Green fluorescence' images at the left column (panels A, D, G and J): Cy2-conjugated anti-rabbit secondary antibodies are used; 'Red fluorescence' images at the middle column (panels B, E, H and K): Cy3-conjugated anti-mouse secondary antibodies are used; Merged images at the right column (panels C, F, I and L): Cy2- (green) and Cy3- (red) stained images merge with DAPI- (blue) stained images. Panels A, D and G: Cy2-conjugated anti-rabbit secondary antibodies (green fluorescence) recognize primary antiserum of RyR1, RyR2 and RyR3, respectively; Panels B, E and H: Cy3-conjugated anti-mouse secondary antibodies (red fluorescence) recognize primary antiserum of E cadherin. Bottom images (Panels C, F and I): no primary antiserum was applied.

Figure 3.5.1.B RyRs in JEG-3 cells: immunofluorescence microscopy

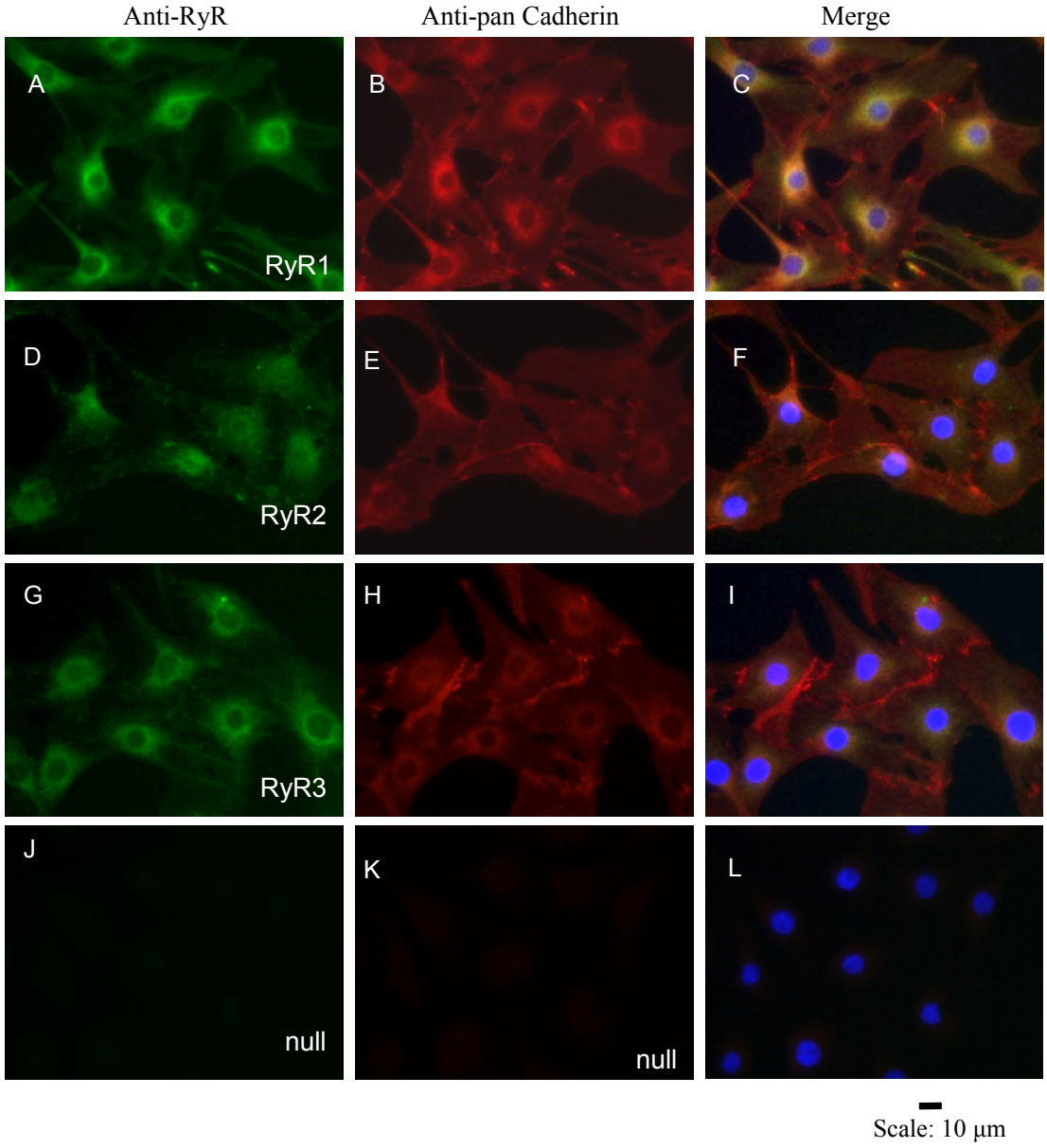

Figure 3.5.1.B. Immunofluorescence microscopy of JEG-3 cells. 'Green fluorescence' images at the left column (panels A, D, G and J): Cy2-conjugated anti-rabbit secondary antibodies are used; 'Red fluorescence' images at the middle column (panels B, E, H and K): Cy3-conjugated anti-mouse secondary antibodies are used; Merge images at the right column (panels C, F, I and L): Cy2- (green) and Cy3- (red) stained images merge with DAPI- (blue) stained images. Panels A, D and G: Cy2-conjugated anti-rabbit secondary antibodies (green fluorescence) recognize primary antiserum of RyR1, RyR2 and RyR3, respectively; Panels B, E and H: Cy3-conjugated anti-mouse secondary antibodies (red fluorescence) recognize primary antiserum of pan cadherin. Bottom images (Panels C, F and I): no primary antiserum was applied.

3.5.2 CSQs are Co-distributed with RyRs in BeWo and JEG-3 Cells

Western blot analyses in the current study have shown that RyRs, CSQs and TRDs are detected in BeWo and JEG-3 cells. To find out whether these RyR accessory proteins are co-distributed with RyRs, BeWo and JEG-3 cells were stained with anti pan-CSQ (Cy2: green) and anti pan-RyR (Cy3: red) antibodies, respectively. Figure 3.5.2 shows that overlaps of green (Cy2) and red (Cy3) occurred in the intracellular structures surrounding the nucleus in both BeWo (Figure 3.5.2.J) and JEG-3 (Figure 3.5.2.K) cells. This observation indicated that CSQ and RyRs were co-distributed in a perinuclear domain in BeWo and JEG-3 cells.

The Cy2-conjugated green fluorescence stain was also visualized in a perinuclear region in BeWo cells (Figure 3.5.2.G), which suggests that CSQ is present within the ER membrane that surrounds the nucleus. In contrast, the distribution of anti-RyR (Cy3: red) in JEG-3 cells (Figure 3.5.2.H) extended from nuclear membrane to the plasma membrane.

Differentiated C2C12 mouse myotubes (Figure 3.5.2.C, F, I, and L) served as positive controls for expression of RyRs (Lorenzon *et al.*,2000) and CSQs (Shin *et al.*,2003). The extensively overlap of green and red fluorescence suggests that RyRs and CSQ were co-distributed in C2C12 mouse myotubes.

Figure 3.5.2 CSQs and RyRs in BeWo and JEG-3 Cells: immunofluorescence microscopy

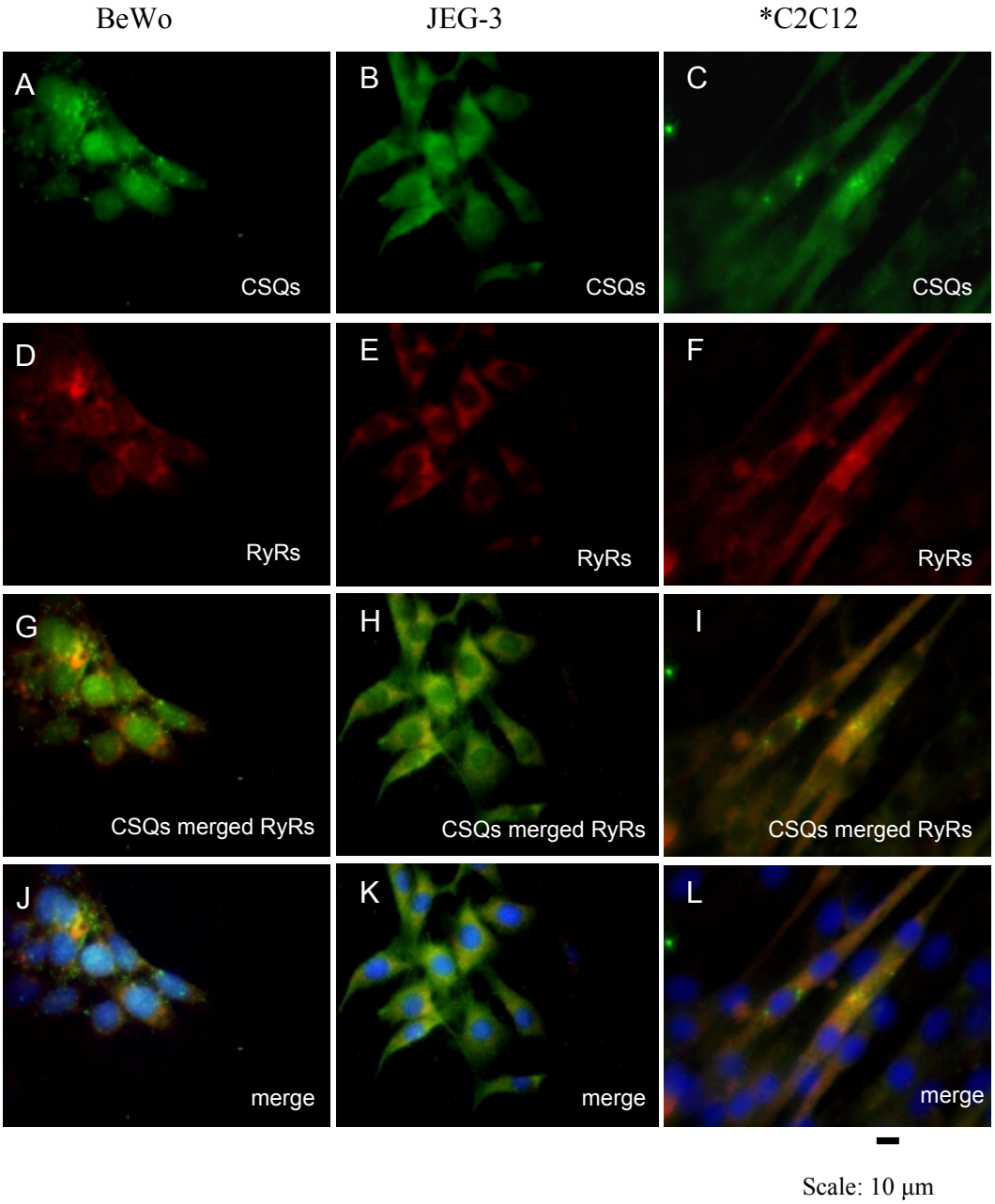

Figure 3.5.2. Immunofluorescence microscopy of BeWo (left column), JEG-3 (middle column) and differentiated C2C12 (right column) cells. 'Green fluorescence' images (panels A, B and C): Cy2-conjugated anti-rabbit secondary antibodies are used, of which recognize primary antiserum of all types of CSQ; 'Red fluorescence' images (panels D, E and F): Cy3-conjugated anti-mouse secondary antibodies are used, of which recognize primary antiserum of all types of RyR. Merged images (panels G, H and I): Cy2- (green) merged with Cy3- (red) stained images. Merged images (panels J, K and L): Cy2- (green) and Cy3- (red) stained images merged with DAPI- (blue) stained images.

3.5.3 CSQs co-distribute with TRD in BeWo and JEG-3 cells

Both CSQ (Figure 3.3.1) and TRD (3.3.2.A) were detected in BeWo and JEG-3 cells by western blotting. In order to determine whether CSQs and TRDs are co-distribute within the same region of cells, BeWo and JEG-3 cells were stained with anti-pan-CSQ and anti-TRD antibodies and visualized using IF microscopy. Figure 3.5.3 shows overlaps of CSQ and red TRD occurred in a perinuclear intracellular region in both BeWo (Figure 3.5.3.J) and JEG-3 (Figure 3.5.3.K) cells. This observation indicated that CSQ and TRD were co-distributed in the perinuclear region of BeWo and JEG-3 cells. In addition, the red fluorescence staining that represents TRD cellular distribution found in BeWo (Figure 3.5.3.D) and JEG-3 (Figure 3.5.3.E) cells was similar to that observed in IF stain of RyRs (Figure 3.5.2.D, and E, for BeWo and JEG-3, respectively). Therefore, TRD was expected to also co-distribute with RyRs.

Differentiated C2C12 mouse myotubes (Figure 3.5.3.C, F, I, and L) served as positive controls for expression of both CSQ (Shin *et al.*,2003) and TRD (Fodor *et al.*,2008; Wang *et al.*,2009). The overlap of green and red fluorescence implies that CSQ and TRD were co-expressed, along with RyRs, in C2C12 mouse myotubes.

.

Figure 3.5.3 CSQs and TRDs in BeWo and JEG-3 cells: immunofluorescence microscopy

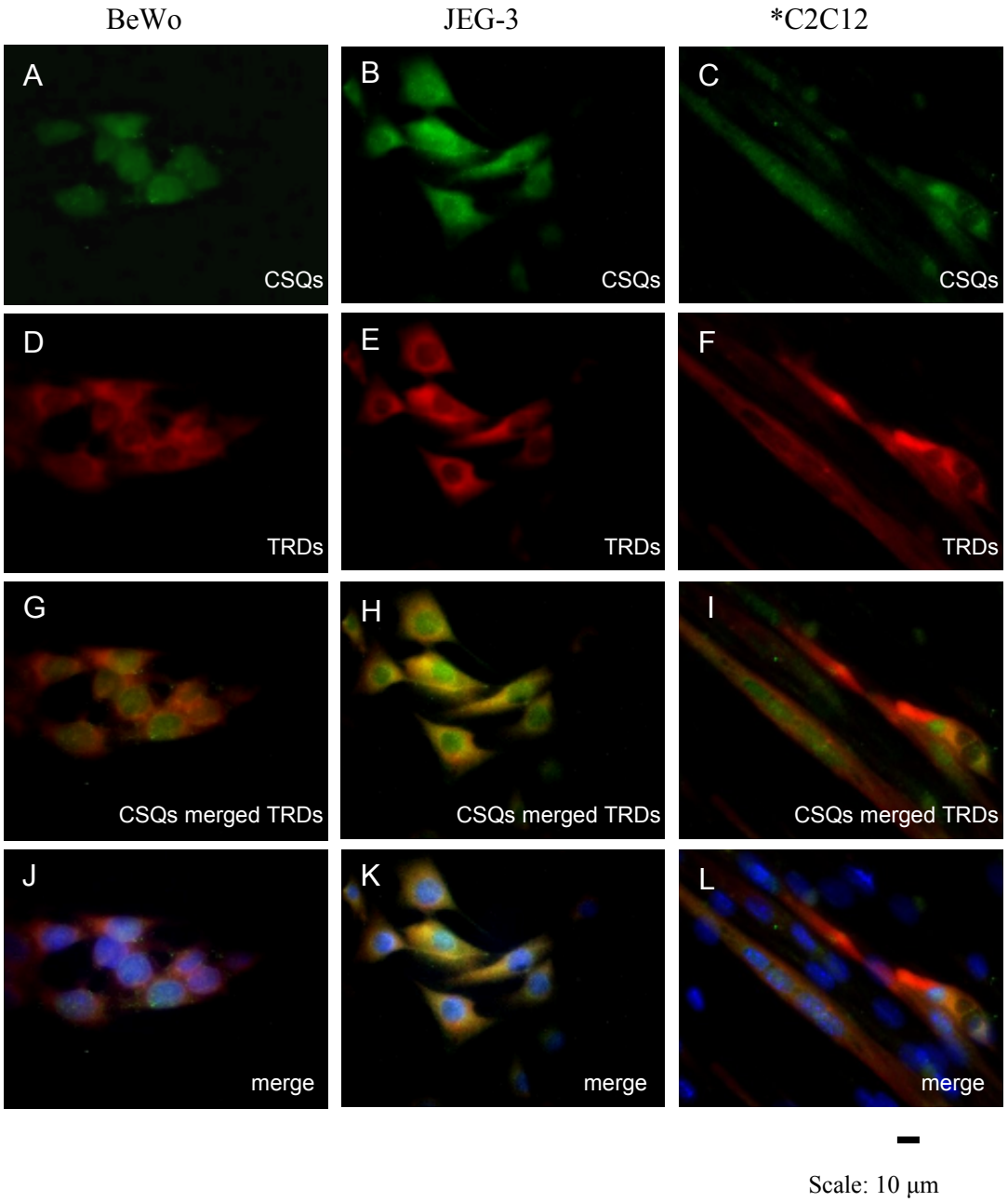

Figure 3.5.3. Immunofluorescence microscopy of BeWo (left column), JEG-3 (middle column) and differentiated C2C12 (right column) cells. 'Green fluorescence' images (panels A, B and C): Cy2-conjugated anti-rabbit secondary antibodies are used, which recognize primary antiserum of all types of CSQ; 'Red fluorescence' images (panels D, E and F): Cy3-conjugated anti-mouse secondary antibodies are used, which recognize primary antiserum of TRDs. Merged images (panels G, H and I): Cy2- (green) merge with Cy3- (red) stained images. Merged images (panels J, K and L): Cy2- (green) and Cy3- (red) stained images merged with DAPI- (blue) stained images.

Chapter IV.

Functional Analysis of Ryanodine Receptors in Human Trophoblast Cell Lines

Chapter IV. Functional Analysis of Ryanodine Receptors in Human Trophoblast Cell Lines

By use of RT-PCR, immunoblotting and immunofluorescence microscopy, the previous results chapter indicated the expression of more than one isoform of RyR in both BeWo and JEG-3 cells. To find out whether the RyR proteins in trophoblasts are actively involved in $[Ca^{2+}]_i$ homeostasis, BeWo and JEG-3 were treated with various agents, including RyR agonists and antagonists. Changes of $[Ca^{2+}]_i$ were monitored by using ratiometric fluorescence dye fura-2, as described in Chapter II, 2.12. Data are expressed as mean ± S.E.M. and were analysed using GraphPad Prism version 4.0. Unpaired t tests were used to compare differences in changes in mean fura-2 ratio between two groups, while one-way ANOVA followed by Tukey's test was used to analyse between more than two groups. A *P*-value < 0.05 was considered statistically significant.

4.1 CmC induces rapid increases in fura-2 ratio in BeWo and JEG-3 cells

To examine whether the RyRs expressed in BeWo and JEG-3 trophoblast cell lines are functionally involved in $[Ca^{2+}]_i$ regulation, RyR agonists were applied to cells and changes of $[Ca^{2+}]_i$ were indicated by changes in fura-2 ratios. Figure 4.1.1 shows a representative trace of mean fura-2 ratio over time during stimulation with 500 μM CmC in BeWo cells. CmC is a RyR activator that has higher selectivity for RyR1 and RyR2 rather than for RyR3 (Zorzato *et al.*,1993; Herrmann-Frank *et al.*,1996; Matyash *et al.*,2002). As Figure 4.1.1.A shows, an increase in fura-2 ratio was observed in BeWo cells, with the maximal rise in mean fura-2 ratio of 0.41 ± 0.06 (n = 7) over basal level (0.55 ± 0.06); the rise of fura-2 ratio was equivalent to increase over the basal as a percentage of 69 ± 19 %. A fast drop of mean fura-2 ratio followed the peak increase, and the fura-2 fluorescence at both 340 nm and 380 nm wavelength was completely lost within 3 minutes of the addition of CmC. The pseudocolour ratio images in Figure 4.1.1.B display high colour constrast between peak response to CmC (~175 s) and pre-stimulation ratios, indicating a large change

in fura-2 ratio and $[Ca^{2+}]_i$. The loss of fluorescence in cells might indicate that the fura-2 dye leaked out into the extracellular space. This unexpected outcome from CmC stimulation suggests that this molecule had effects on memebrane permeability that might not be dependent on RyR activation.

Increases in mean fura-2 ratio were also observed in JEG-3 cells upon addition of 500 μM CmC. Two types of response were observed. Figure 4.1.2.A is representative of one type of response in JEG-3 cells, observed in 6 out of 16 independent experiments, as representative trace shown in Figure 4.1.2.A. A plateau-like rise in mean fura-2 ratio was detected after the initially rapid increase within 200 seconds, as indicated in the pseudocolour images in Figure 4.1.2.B. Meanwhile, in the other 10 out of 16 experiments, a rapid rise of fura-2 ratio was followed by a slow decline, as shown in Figure 4.1.3. During the recording period, a less rapid decrease in ratio than in observed BeWo cells was detected after maximum increase was reached, as represented in Figure 4.1.3.A. Pseudocolour images shown in Figure 4.1.3.B displayed a smaller change between peak response and resting ratios in JEG-3 cells. Despite these were two different types of response following the peak, similar maximal increases in ratio were measured. The average peak change of mean fura-2 ratio was 0.23 ± 0.02 (n = 16) over basal ratio (0.49 ± 0.04), equivalent to 37 ± 4 % increase above the resting value.

Addition of ryanodine to BeWo and JEG-3 cells triggered distinct Ca^{2+} responses from those caused by CmC. A representative trace in Figure 4.1.4.A indicates a gradual increase in fura-2 ratio in BeWo cells when 1 μM ryanodine was applied, and the elevated fura-2 ratio did not decrease with time; the change of mean fura-2 ratio was measured as 0.24 ± 0.03 (n = 11) over basal ratio (0.54 ± 0.02), equivalent to 44 ± 6 % increase of the basal. Addition of 1 μM ryanodine to JEG-3 cells caused an initial rise in mean fura-2 ratio of 0.18 ± 0.02 (n = 9) over basal level (0.58 ± 0.03), equivalent to 25 ± 4 % increase of the resting value. This change fully recovered within approximately 4 minutes after addition of ryanodine. The representative trace in Figure 4.1.4.B displayed the mean fura-2 ratio against time during pharmacological stimulation with ryanodine in JEG-3 cells. As shown in the trace, the mean fura-2 ratio at the end of stimulation had returned to a steady level.

Figure 4.1.1 Changes in fura-2 ratio in BeWo cells in response to CmC.

A.

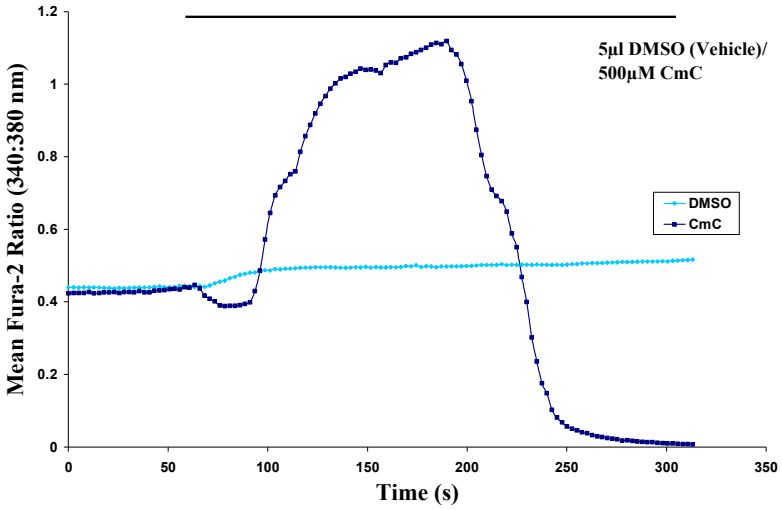

B.

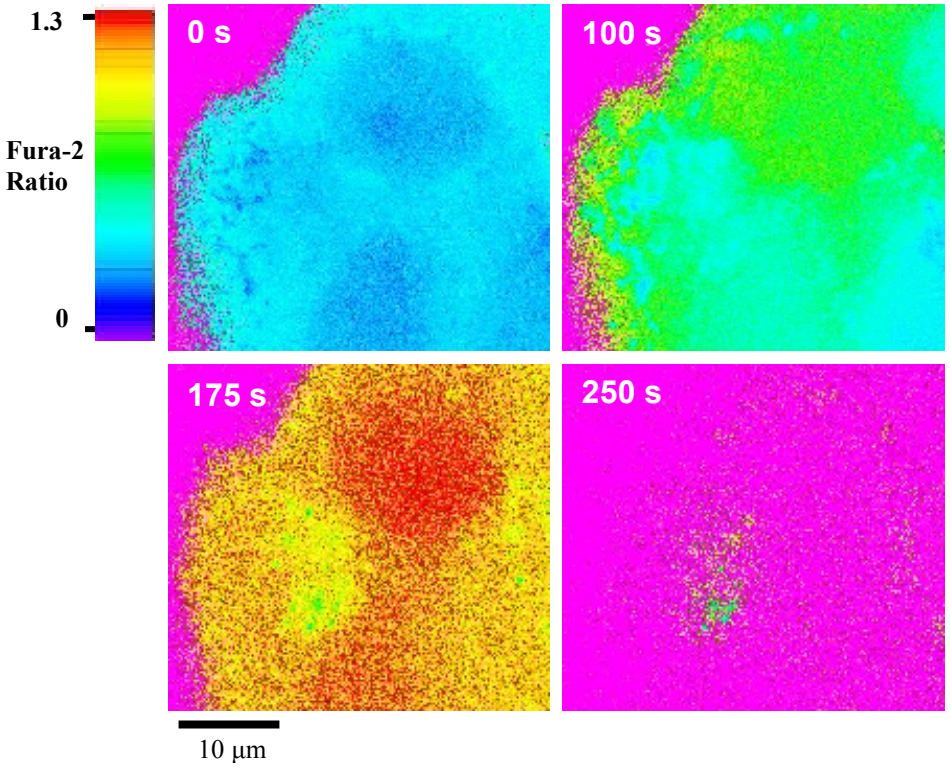

Figure 4.1.1. BeWo cell calcium response to CmC. Panel **A**. Representative trace of mean fura-2 ratio in BeWo (n = 7) cells in response to CmC. The *black bar* at the top represents the stimulation period; *light blue trace* represents mean fura-2 ratio during addition of vehicle; *dark blue trace* represents mean fura-2 ratio during addition of 500 µM CmC. Panel **B**. Pseudocolour images of change in fura-2 ratio during CmC stimulation in BeWo cells at about 0, 100, 175, and 250 seconds. The look up table in the upper left indicates the fura-2 ratio from 0 to 1.2, as a pseudocolour scale.

Figure 4.1.2 Changes in fura-2 ratio in JEG-3 cells in response to CmC (type 1).

A.

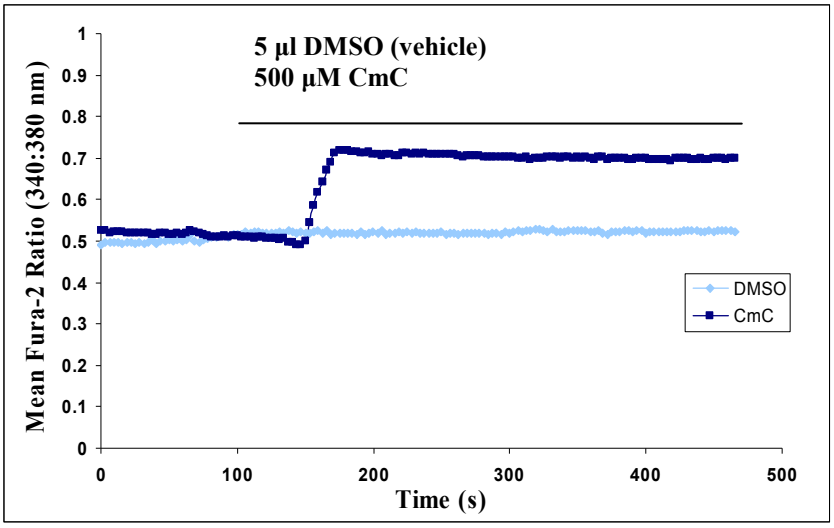

B.

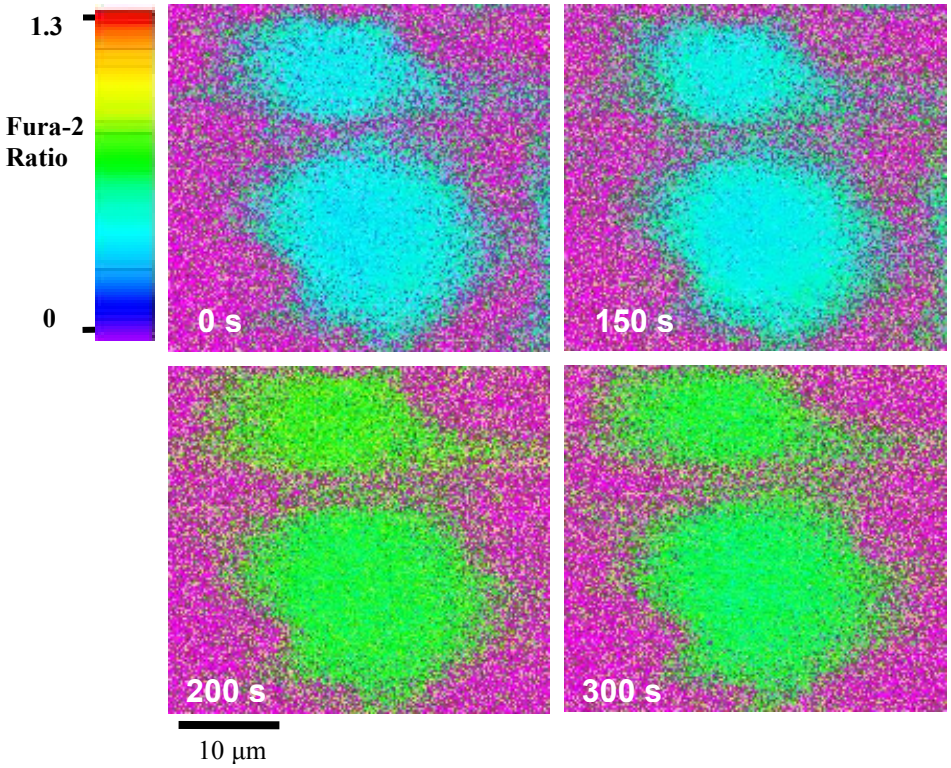

Figure 4.1.2. JEG-3 cell calcium response to CmC (type 1). Panel **A**. Representative trace of mean fura-2 ratio in JEG-3 (n = 6) cells in response to CmC. The *black bar* at the top represents the stimulation period; *light blue* trace represents mean fura-2 ratio during addition of vehicle; *dark blue* trace represents mean fura-2 ratio during addition of 500 µM CmC. Panel **B**. Pseudocolour images of change in fura-2 ratio during CmC stimulation in JEG-3 cells at about 0, 150, 200, and 300 seconds. The look up table on the upper left indicates the fura-2 ratio from 0 to 1.2, as a pseudocolour scale.

Figure 4.1.3 Changes in fura-2 ratio in JEG-3 cells in response to CmC (type 2).

A.

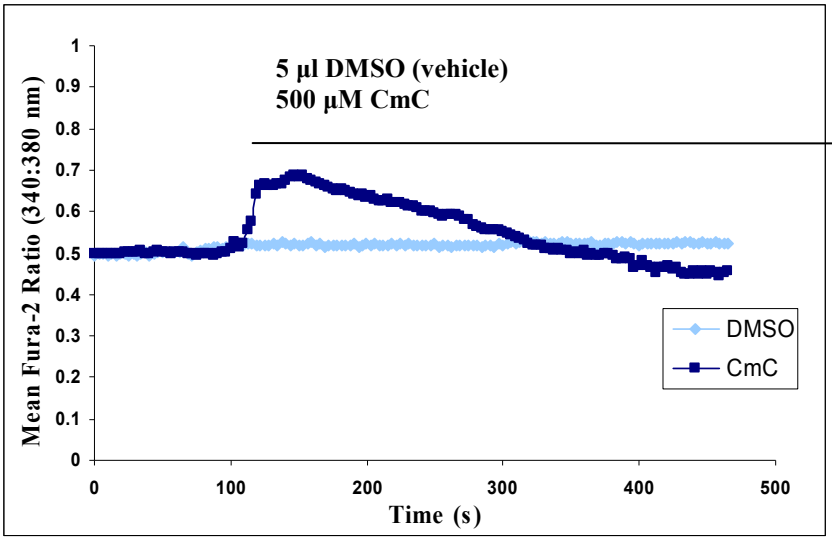

B.

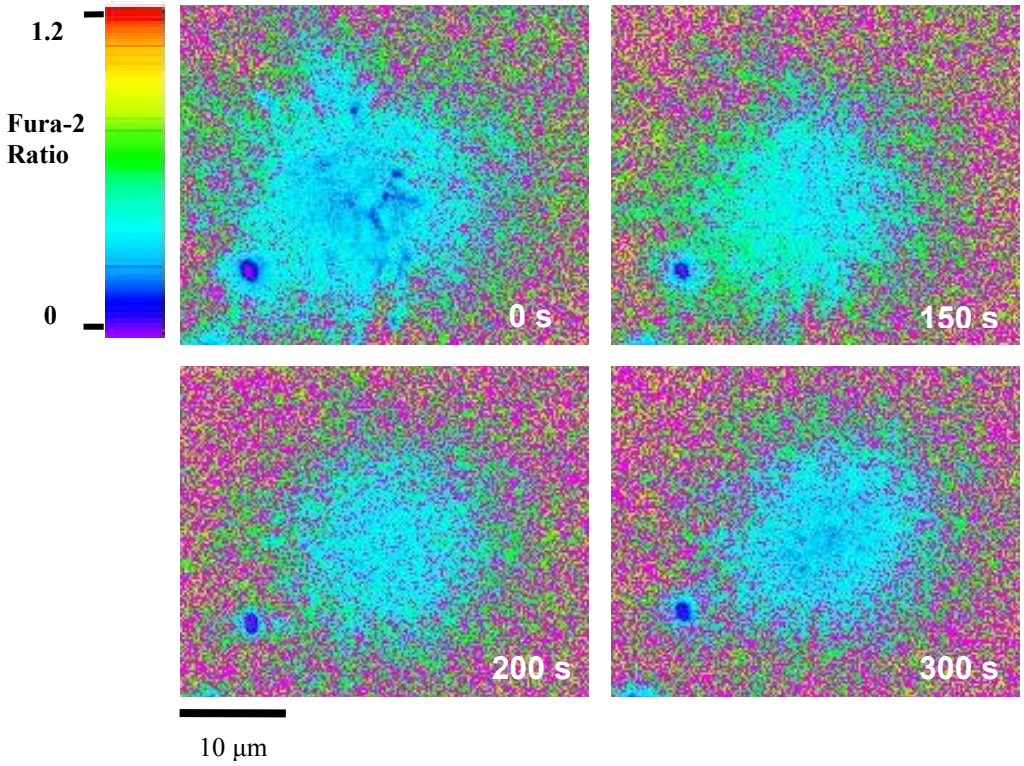

Figure 4.1.3. JEG-3 cell calcium response to CmC (type 2). Panel **A**. Representative trace of mean fura-2 ratio in JEG-3 (n = 10) cells in response to CmC. The *black bar* at the top represents the stimulation period; *light blue* trace represents mean fura-2 ratio during addition of vehicle; *dark blue* trace represents mean fura-2 ratio during addition of 500 µM CmC. Panel **B**. Pseudocolour images of change in fura-2 ratio during CmC stimulation in JEG-3 cells at about 0, 150, 200, and 300 seconds. The look up table on upper left indicates the fura-2 ratio from 0 to 1.2, as a pseudocolour scale.

Figure 4.1.4 Changes in fura-2 ratio in BeWo and JEG-3 cells in response to ryanodine.

A. BeWo

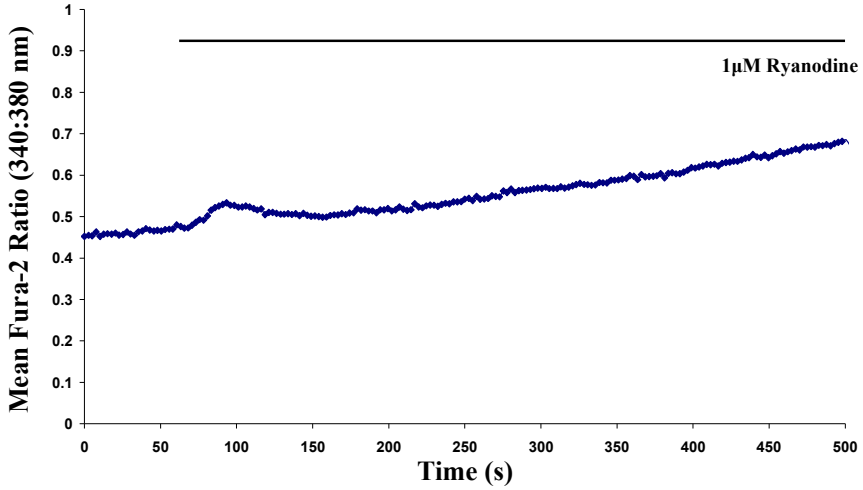

B. JEG-3

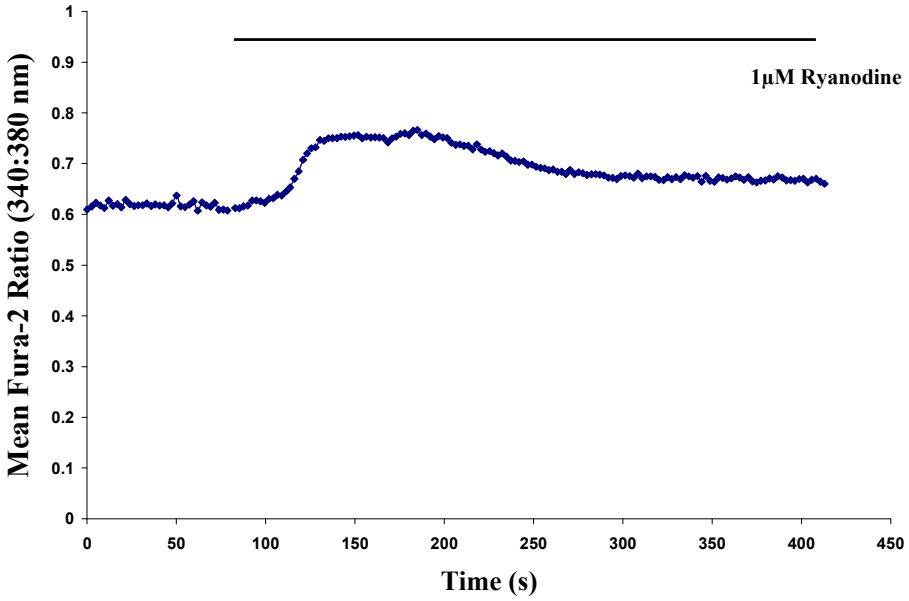

Figure 4.1.4. Representative traces of changes in fura-2 ratio in BeWo (panel A, n = 11) and JEG-3 (panel B, n = 9) cells in response to ryanodine. In both Panel A and B: the *black bar* at the top represents stimulation period; *dark blue* trace represents change in fura-2 ratio during addition of 1 µM ryanodine.

4.2 Dantrolene decreases fura-2 ratio in BeWo and JEG-3 cells.

To further examine the involvement of RyRs in the elevation of $[Ca^{2+}]_i$ stimulated by CmC or ryanodine in BeWo and JEG-3 cells, the RyR subtype selective antagonist dantrolene was pre-incubated with cells before the application of these agonists. Dantrolene is a muscle relaxant that is clinically used for the treatment of malignant hyperthermia. The inhibitory effect of dantrolene on RyRs is by directly targeting RyR1 and RyR3 to reduce the Ca^{2+}-sensitivity of the channel activation (Fruen *et al.*,1997), but not that of RyR2 (Zhao *et al.*,2001). Therefore, incompleted suppression or partial inhibition of $[Ca^{2+}]_i$ elevation is expected on the co-application of dantrolene with CmC or ryanodine on cells that co-express RyR2 with other RyR subtypes.

Figure 4.2.1 panel A, shows a representative trace of mean fura-2 ratio against time during the co-application of dantrolene and CmC in BeWo cells. Dantrolene (50 μM) was added and cells were incubated with this drug for 3 to 4 minutes before the addition of CmC. A decline followed by a slow incline of fura-2 ratio was observed during dantrolene pre-incubation in BeWo cells. Subsequent addition CmC resulted in a smaller increase of mean fura-2 ratio than when CmC was added alone. This observation indicates that the increase of fura-2 ratio induced by CmC was partially suppressed by dantrolene. The maximum change in mean fura-2 ratio was 0.24 ± 0.04 (n = 17) over basal level (0.46 ± 0.02), which was equivalent to 45 ± 7 % increase of the basal value. Despite the pre-incubation with dantrolene, the fura-2 signal was completely lost within 5 minutes after addition of CmC to BeWo cells. Similar partial inhibition in BeWo cells was also observed when dantrolene was co-applied with ryanodine. The application of ryanodine after dantrolene pre-incubation resulted in a smaller increase in mean fura-2 ratio than that induced by ryanodine alone. Figure 4.2.2 panel A shows a representative trace of mean fura-2 ratio during co-application of dantrolene and ryanodine; the change of mean fura-2 ratio was 0.09 ± 0.03 (n = 7), which was equivalent to 20 ± 4 % increase above the basal value (0.53 ± 0.02).

Pre-incubation with dantrolene in JEG-3 cells, however, resulted in complete suppression in both CmC and ryanodine-induced $[Ca^{2+}]_i$ elevation. Panels B of

Figure 4.2.1 and Figure 4.2.2 show representative traces of mean fura-2 ratio upon addition of CmC and ryanodine after dantrolene pre-treatment, respectively. Neither CmC nor ryanodine were able to induce rises in fura-2 ratio in JEG-3 cells pre-incubated with dantrolene. In addition, the post-dantrolene fura-2 ratios were lower than that pre-dantrolene ratio in these cells, regardless of the addition of either CmC or ryanodine.

Decreases in fura-2 ratios were observed in both BeWo and JEG-3 cells during the application of dantrolene, suggesting that this drug may interfere with intracellular Ca^{2+} homeostasis by blocking channels participating in either Ca^{2+} release, Ca^{2+} influx, or both. There is also a possibility that dantrolene induces change in fura-2 ratios by a photochemical rather than a physiological mechanism. Published data indicates that dantrolene can enhance cellular autofluorescence at UV wavelengths, particularly at the 380 nm wavelength used to excite the calcium-free form of fura-2 (Nohmi *et al.*,1991). Therefore, it was essential to examine the effect of dantrolene on the fluorescence emitted at either 340 nm or 380 nm in the cells used in this study. Such examination was necessary to determine whether dantrolene can be used in combination with fura-2 AM in current study.

Responses during dantrolene stimulation of BeWo and JEG-3 cells are shown in Figure 4.2.3. Traces of mean fura-2 ratio, along with mean fluorescence intensity (AU, arbitrary unit) at either 340 nm (F_{340}) and 380 nm (F_{380}) excitation wavelength are shown in the same graph. In both BeWo and JEG-3 cells, the appearance of steady *red* traces (F_{340}) indicated little changes in $[Ca^{2+}]_i$. The ranges of these Ca^{2+}-sensitive traces were seemingly from 180 to 190 AU in BeWo cells, and from 160 to 165 AU in JEG-3 cells, respectively, as shown in Figure 4.2.3. This result indicated that dantrolene has little effect on the intracellular Ca^{2+} balance in both BeWo (Figure 4.2.3.A) and JEG-3 cells (Figure 4.2.3.B). However, despite the presence of a stable Ca^{2+}-sensitive F_{340} intensity, increased F_{380} was observed upon addition of dantrolene, as *blue* traces in Figure 4.2.3.A and B indicate. These *blue* traces (F_{380}) represent the change in fluorescence intensity that is independent of $[Ca^{2+}]_i$. In these representative experiments, F_{380} in BeWo cells increased from 356 AU to 508 AU; whereas, in JEG-3 cells raised from 259 AU to 349 AU. As a result, increase in F_{380} with little change in F_{340} caused declines in fura-2 ratios, as indicated by *purple*

traces. In BeWo cells, dantrolene induced a decrease (from 0.50 down to 0.37) followed by a slow increase in fura-2 ratio (up to 0.63); whereas, the recovery of decline in fura-2 ratio stimulated by dantrolene in JEG-3 cells was not seen, as ratios dropped from 0.49 to 0.39, and only increased to 0.41 by the end of the experiment. These values are similar to those observed when RyR-agonists (CmC and ryanodine) were added after dantrolene pre-incubation. Therefore, suppression of fura-2 ratios recorded during co-application of RyR-agonists and dantrolene, was due to rises in F_{380} unaccompanied by changes in F_{340} induced by dantrolene, rather than being due to genuine decreases in intracellular Ca^{2+} content of cells.

To further examine whether dantrolene could enhance the autofluorescence of cells during excitation at 380 nm in the absence of fura-2, cells not loaded with the fluorescent calcium indicator were used to repeat these dantrolene experiments. The mean ratio and mean fluorescence intensity were plotted against time in seconds, as shown in Figure 4.2.4 (BeWo: Figure 4.2.4.A; JEG-3: Figure 4.2.4.B). A rise in F_{380} was observed in both cell types, while F_{340} remained steady. For example, in one experiment following addition of dantrolene, a maximum F_{380} of 397 AU was recorded in BeWo cells from the initial value of 150 AU; whereas, in an experiment with JEG-3 cells a maximum F_{380} of 363 AU was increased from an initial F_{380} of 140 AU. Although increases in F_{380} were observed, the ratios of fluorescence were relatively stable in comparison to fura-2-loaded experiments in both BeWo and JEG-3 cells. These obervations suggest that the cellular free Ca^{2+} indicator fura-2 and dantrolene co-ordinately enhance the F_{380} fluorescence and suppress the F_{340}/F_{380} ratio in BeWo and JEG-3 cells. Hence, the RyR antagonist property of dantrolene would be hard to monitor in these fura-2 loaded cells, as unaccompanied rises in F_{380} fluorescence were induced. Therefore, dantrolene is not a suitable antagonist for assessment of RyR function in BeWo and JEG-3 cells when fura-2 is used as the cellular free Ca^{2+} indicator.

Figure 4.2.1 Traces of changes in fura-2 ratio in BeWo and JEG-3 cells in response to dantrolene and CmC.

A. BeWo

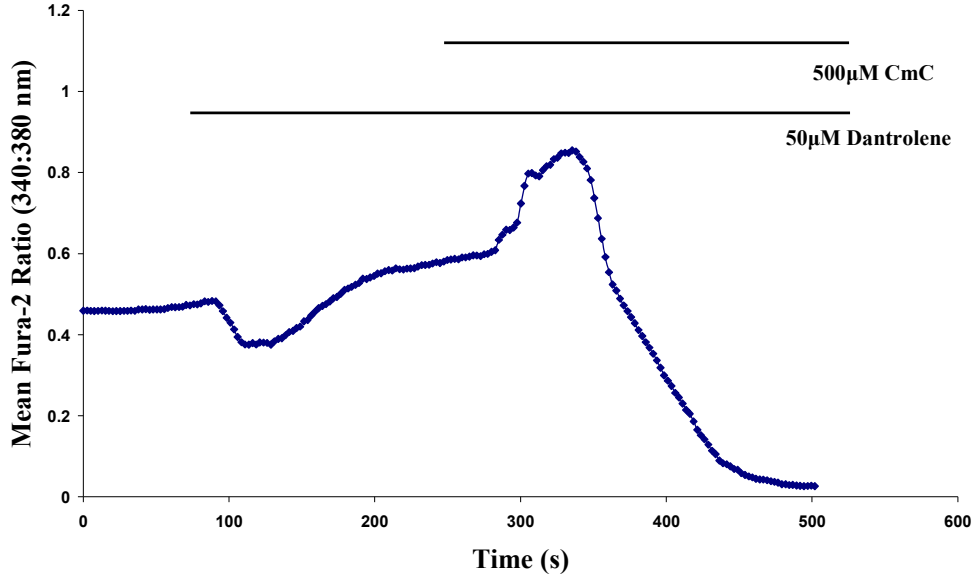

B. JEG-3

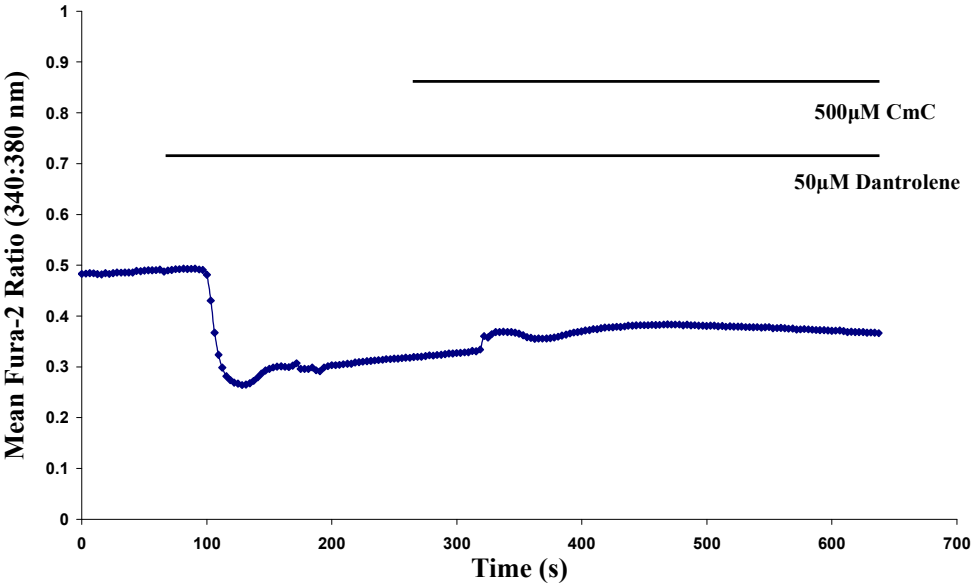

Figure 4.2.1. Representative traces of changes in fura-2 ratio in BeWo (panel A, n = 17) and JEG-3 (pancel B, n = 9) cells upon 500 µM CmC stimulation in presence of 50 µM dantrolene. On both Panel A and B: *black bars* at the top represent stimulation periods of dantrolene and CmC in cells; *dark blue trace* represents changes in fura-2 ratio during stimulation.

Figure 4.2.2 Traces of changes in fura-2 ratio in BeWo and JEG-3 cells in response to dantrolene and ryanodine.

A. BeWo

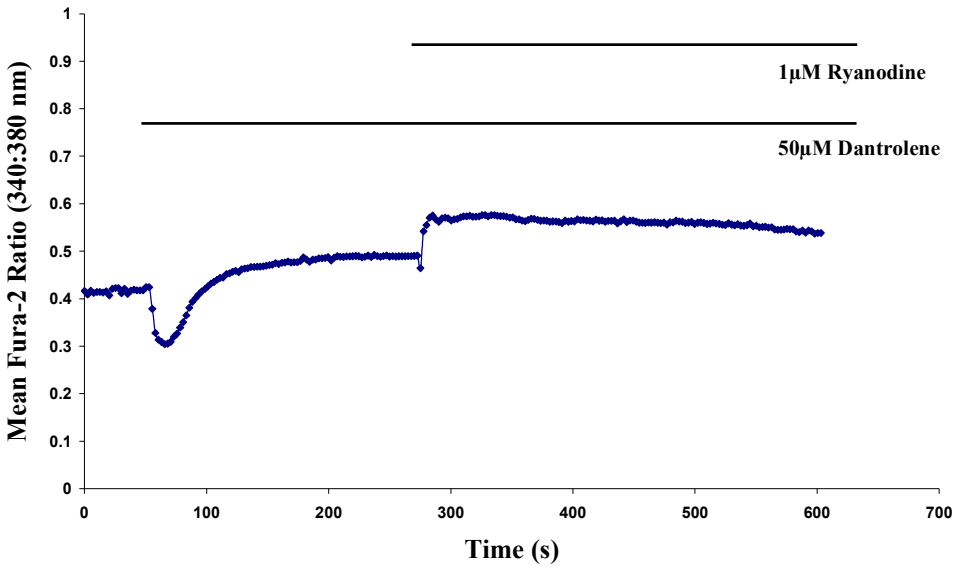

B. JEG-3

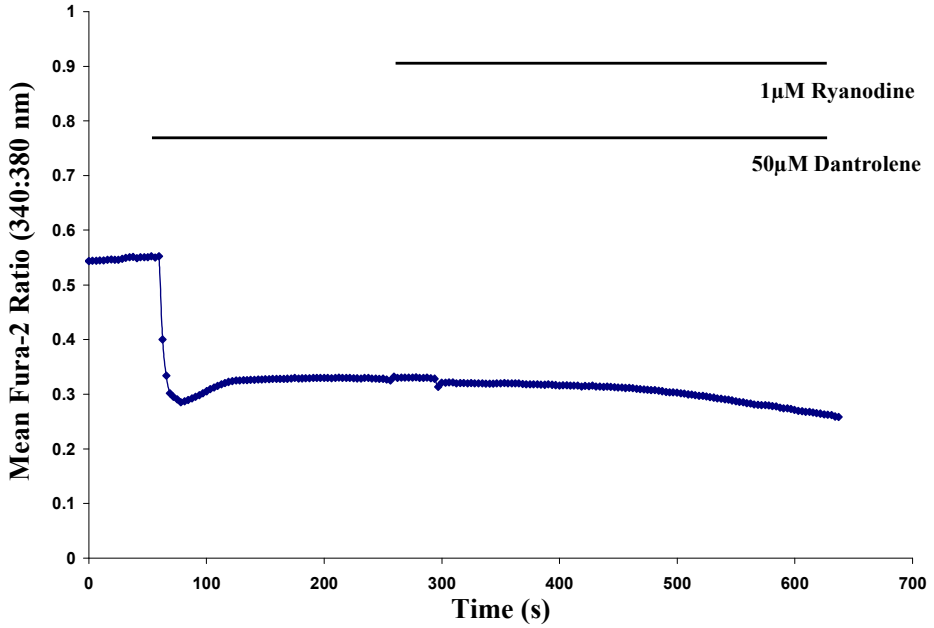

Figure 4.2.2. Representative traces of changes in fura-2 ratio in BeWo (panel A, n = 7) and JEG-3 (pancel B, n = 7) cells upon 1 µM ryanodine stimulation in presence of 50 µM dantrolene. On both Panel A and B: *black bars* at the top represent stimulation periods of dantrolene and ryanodine in cells; *dark blue trace* represents changes in fura-2 ratio during stimulation.

Figure 4.2.3 Changes in fluorescence intensity and fura-2 ratio in response to dantrolene in fura-2-loaded BeWo (A) and JEG-3 (B) cells.

A. BeWo

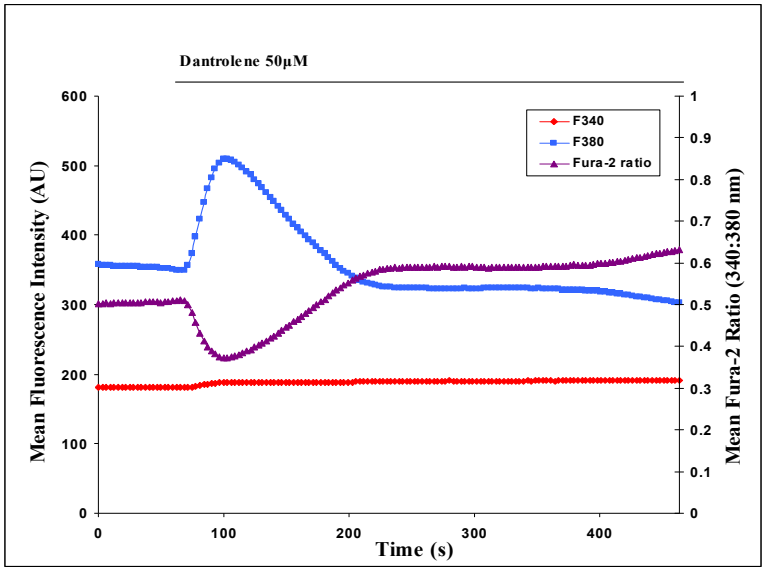

B. JEG-3

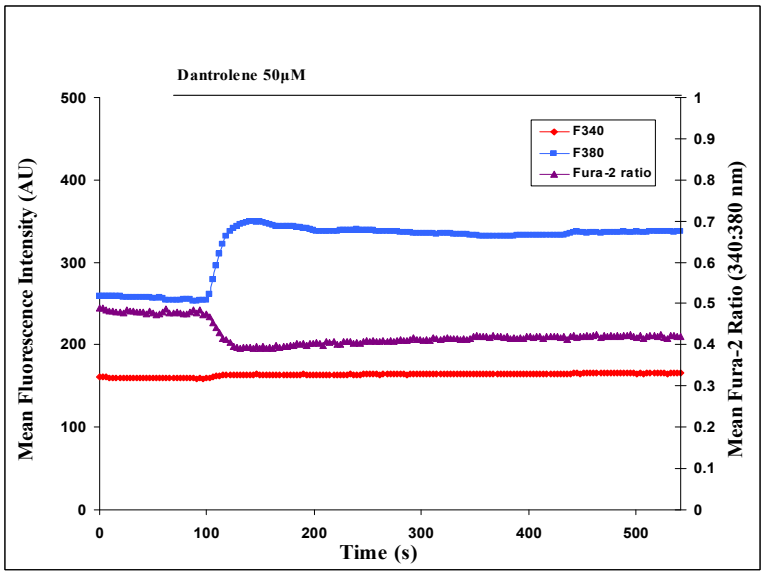

Figure 4.2.3. Representative traces showing fluorescence intensity and ratio alterations in fura-2-loaded BeWo (**A**) and JEG-3 (**B**) cells during dantrolene stimulation. Values shown on the *left Y axis* are mean fluorescence intensity (AU), and the values displayed on the *right Y axis* are mean fura-2 ratios. The *red* (F340: excited by 340 nm light) and *blue* (F_{380}: excited by 380 nm light) traces representing the fluorescence intensities during the experiment. The *purple* trace represents changes in mean fura-2 ratios during stimulation. The *black bars* at the top on both Panel A and Panel B represent periods of stimulation with dantrolene.

Figure 4.2.4 Changes in fluorescence intensity and ratio in response to dantrolene in fura-2-free BeWo (A) and JEG-3 (B) cells.

A. BeWo

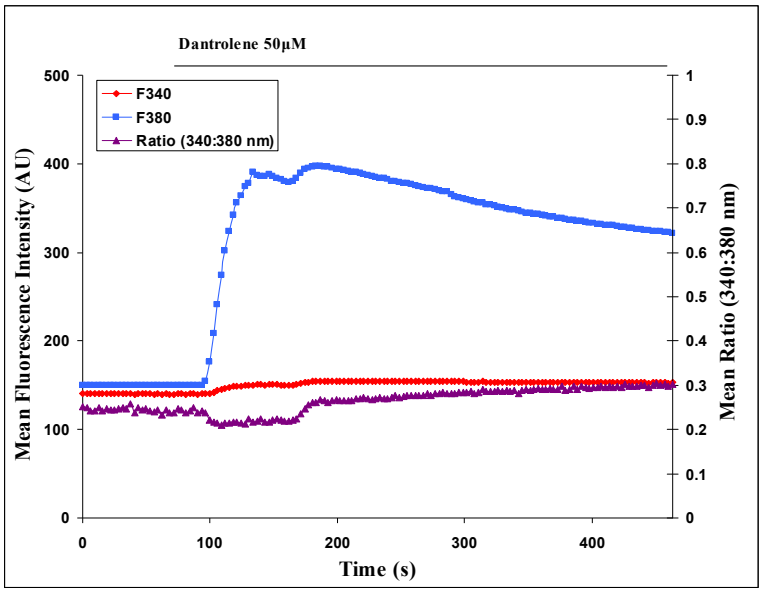

B. JEG-3

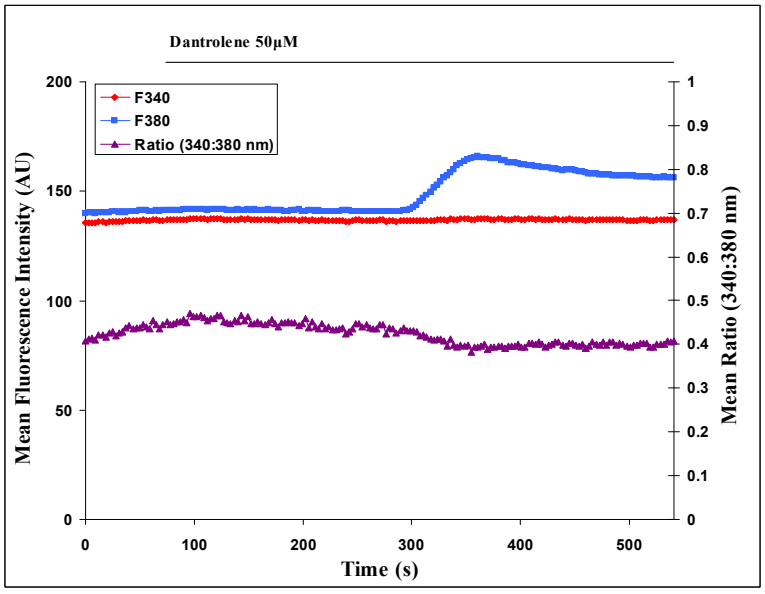

Figure 4.2.4. Representative traces showing fluorescence intensity and ratio alternations in fura-2-free BeWo (**A**) and JEG-3 (**B**) cells during dantrolene stimulation. Values shown on the *left Y axis* are mean fluorescence intensity (AU), and the values displayed at the *right Y axis* are mean fura-2 ratio. The *red* (F340: excited by 340 nm light) and *blue* (F380: excited by 380 nm light) traces representing the fluorescence intensity alterations during experiment. The *purple* trace represents changes in mean ratios during stimulation. The *black bars* at the top on both Panel A and Panel B represent periods of stimulation with dantrolene.

4.3 Tetracaine blocks the ryanodine-induced rise in fura-2 ratio in BeWo and JEG-3 cells

Since dantrolene caused an artefactual increase in F_{380} autofluorescence in BeWo and JEG-3 cells, thereby affecting fura-2 ratios, an alternative RyR inhibitor was considered. Tetracaine is a local anaesthetic, which is reported to inhibit RyR-mediated Ca^{2+} release in mammalian skeletal and cardiac muscles (Lukyanenko *et al.*,1996; Csernoch *et al.*,1999). Figure 4.3.1.A shows the effect of tetracaine (TET: 100 μM) on the change in fura-2 ratio caused by ryanodine (RYD: 1 μM) in BeWo cells. A significant suppression of the ryanodine-induced fura-2 rise was observed in the presence of tetracaine (Panel B, Figure 4.3.1). The change in mean fura-2 ratio was 0.15 ± 0.03 (n = 8) over basal level (0.57 ± 0.03), which was equivalent to 30 ± 7 % increase above the resting value. Despite the significant inhibitory effect of tetracaine on RyR-mediated Ca^{2+} release, an increase in fura-2 ratio was still measured in the presence of tetracaine. Figure 4.3.1.B indicated that, even though tetracaine was present during ryanodine stimulation, the rise in fura-2 ratio was still significantly higher than those vehicle-alone responses. This result suggests, when RyR-mediated Ca^{2+} release was blocked by tetracaine, an alternative mechanism was still functional to sustain the rise in $[Ca^{2+}]_i$ in BeWo cells.

In JEG-3 cells, tetracaine appeared to completely abolish ryanodine-induced rise in $[Ca^{2+}]_i$ (Panel A, Figure 4.3.2). The rise in fura-2 ratio measured in the presence of tetracaine during ryanodine stimulation was 0.03 ± 0.006 (n = 6). This value was significantly smaller than that measured in response to ryanodine alone (0.18 ± 0.02, n = 9). This result was also similar to the response to vehicle alone (Figure 4.3.2.B), suggesting that tetracaine completed inhibited ryanodine-induced Ca^{2+} release in JEG-3 cells.

Figure 4.3.1 Changes in fura-2 ratio in BeWo cells in response to tetracaine and ryanodine.

A.

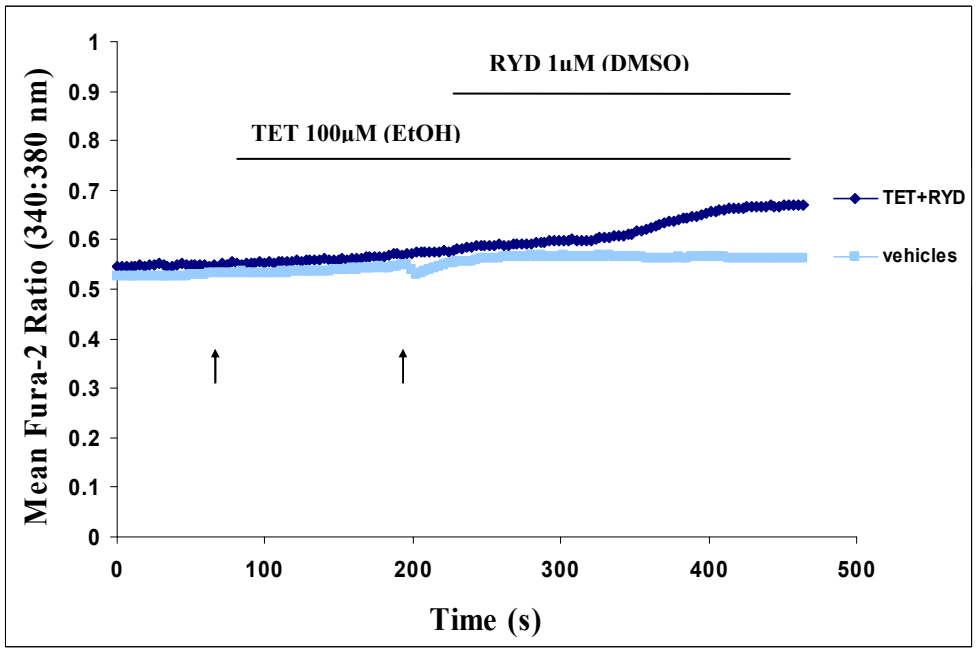

B.

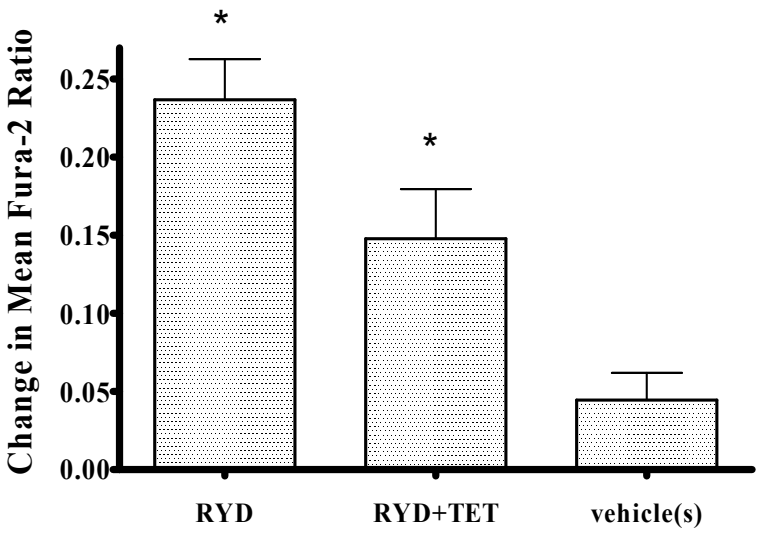

Figure 4.3. Panel **A**. Representative traces (n = 8) of changes in fura-2 ratio in BeWo cells upon stimulation with 1 µM ryanodine (RYD) in the presence or absence of 100 µM tetracaine (TET). *Black bars* at the top represent stimulation periods of tetracaine and ryanodine; arrows below traces represent time points when drugs or vehicle were added; *dark blue* trace represents changes in fura-2 ratio during stimulation; *light blue* trace represents changes in fura-2 ratio during application of vehicle that delivered TET and RYD. Panel **B**. Change in fura-2 ratio in BeWo cells in response to RyR agonist and antagonist. $P = 0.04$, RYD vs RYD plus TET (n = 11 vs 8); $P = 0.02$, RYD plus TET vs vehicles (n = 8 vs 3); * = $P < 0.05$, two-tailed unpaired t test.

Figure 4.3.2 Changes in fura-2 ratio in JEG-3 cells in response to tetracaine and ryanodine.

A.

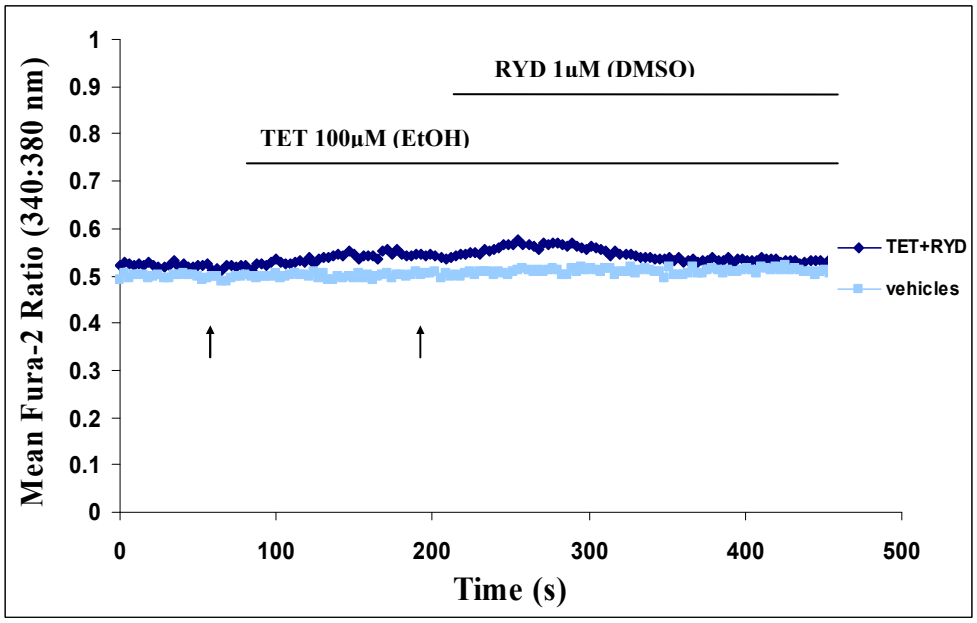

B.

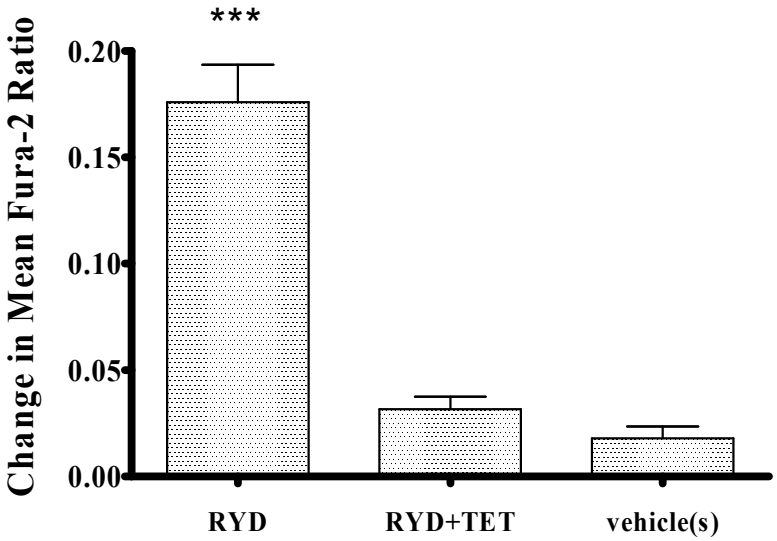

Figure 4.3.2 Panel **A**. Representative traces (n = 6) of changes in fura-2 ratio in JEG-3 cells upon 1 µM ryanodine (RYD) stimulation in presence or absence of 100 µM tetracaine (TET). *Black bars* at the top represent stimulation periods of tetracaine and ryanodine; arrows below traces represent time points when drugs/vehicles were added; *dark blue* trace represents changes in fura-2 ratio during stimulation; *light blue* trace represents changes in fura-2 ratio during application of vehicle that delivered TET and RYD. Panel **B**. Change in fura-2 ratio in JEG-3 cells in response to RyR agonist and antagonist. $P < 0.0001$, RYD vs RYD plus TET (n = 9 vs 6); *** = $P < 0.0001$, two-tailed unpaired t test.

4.4 CmC-induced $[Ca^{2+}]_i$ rise in BeWo and JEG-3 cells was unaffected by RyR antagonists

To examine whether CmC-induced $[Ca^{2+}]_i$ rise in fura-2 ratio in BeWo and JEG-3 cells can be suppressed by RyR antagonists, tetracaine or ryanodine at inhibitory concentration (100 μM) were used. In BeWo cells, similar increases were found during CmC stimulation, regardless of the presence and absence of 100 μM ryanodine (Figure 4.4.A). Likewise, CmC-induced rise in fura-2 ratio was unaffected by the presence of tetracaine. In addition, pre-incubation with neither tetracaine nor 100 μM ryanodine were able to prevent the resultant lost of fluorescence detection that induced by CmC in these cells, as described previously in Section 4.1. These observations suggested that, in addition to activation of RyR-mediated Ca^{2+}-release, CmC also triggers other pathways that are independent of RyR activation, which caused the apparent rapid and massive rise $[Ca^{2+}]_i$ in BeWo cells.

In JEG-3 cells, 100 μM ryanodine pre-incubation did not affect the rise in fura-2 ratio induced by CmC, and the increase in ratio was similar to that without ryanodine (100 μM) (Figure 4.4.B). Pre-incubation with 100 μM tetracaine slightly enhanced the rise in fura-2 ratio. In addition, the response traces (data not shown) in the presence of either one of the antagonists, were apparently similar to ones with CmC alone. These observations suggest that CmC induced non-RyR-mediated Ca^{2+}-elevation in JEG-3 cells, as indicated by increases in fura-2 ratio; and these rises were unaffected by the addition of tetracaine or ryanodine.

In both BeWo and JEG-3 trophoblast-like cells, neither tetracaine nor ryanodine (100 μM) showed inhibitory effect upon CmC stimulation. In addition, the response traces and maximal increases in ratio were apparently similar, regardless of the presence or absence of RyR antagonists. These results indicate tha CmC induces other pathways that cause increases in $[Ca^{2+}]_i$. Since such rises in $[Ca^{2+}]_i$ were independent of RyR activation, CmC could not be used as an RyR-specific activator in BeWo or JEG-3 cells in this study.

Figure 4.4. Changes in fura-2 ratio in BeWo and JEG-3 cells in response to agonists and antagonists.

A. BeWo

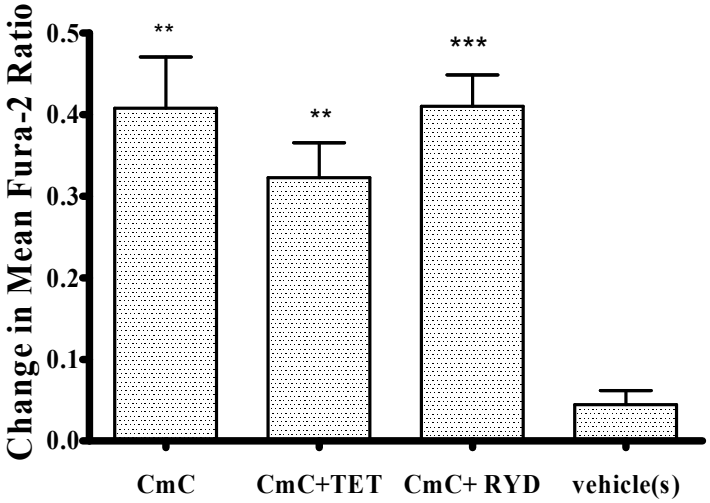

B. JEG-3

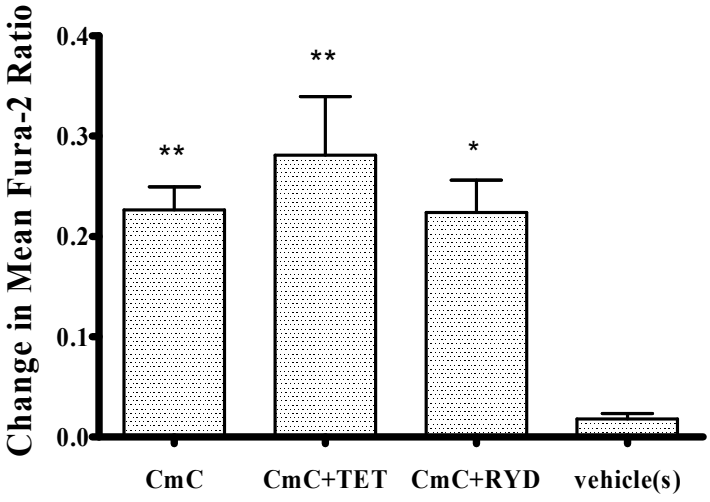

Figure 4.4 CmC induced changes in mean fura-2 ratios in BeWo and JEG-3 cells. Panel **A**. BeWo cells in response to 500 μM CmC in the absence and presence of antagonists (100 μM tetracaine, TET; 100 μM ryanodine, RYD). ** $P < 0.01$, CmC, CmC+TET vs vehicle (n = 8, 3 vs 3); *** $P < 0.001$, CmC+RYD vs vehicles (n = 3 vs 3); two-tailed unpaired t test. Panel **B**. JEG-3 cells response to 500 μM CmC in the absence and presence of antagonists (100 μM tetracaine, TET; 100 μM ryanodine, RYD). * $P < 0.05$, CmC+RYD vs vehicles (n = 8 vs 3); ** $P < 0.01$, CmC, CmC+TET vs vehicle (n = 16, 10 vs 3); two-tailed unpaired t test.

4.5 Physiologically relevant peptide hormones induce increases in $[Ca^{2+}]_i$ in BeWo cells

Angiotensin II (AGII), arginine vasopressin (AVP), and endothelin 1 (ET1) are peptides present in human placenta that are involved in various physiological functions (Punnonen *et al.*,1987; Ferré *et al.*,1993; Poisner,1998). AGII type 1 receptors (AT1) are expressed in human placenta and are responsible for hormonal secretion and vasoregulation (Li *et al.*,1998). AVP is a peptide hormone produced in the pituitary gland that plays important roles not only in the regulation of vasoconstriction and water re-absorption in the collecting ducts of the kidney, but also in the regulation of amniotic fluid (Punnonen *et al.*,1987). ET1 is the predominant isoform of endothelin peptide that stimulates cell differentiation, proliferation and cell invasion (Yohn *et al.*,1994; Cervar & Desoye,1998). To determine whether these endogenous peptides are involved in the regulation of $[Ca^{2+}]_i$ in trophoblast, AGII, AVP and ET1 were applied to both BeWo and JEG-3 cells. All three peptides used were dissolved and stored in ddH_2O. In the current study, there was no detectable change in mean fura-2 ratio observed in JEG-3 cells when selected endogenous peptides were applied. Therefore, experimental data obtained from BeWo cells are presented.

Figure 4.5.1.A, Figure 4.5.2.A and Figure 4.5.3.A show representative traces from BeWo cells stimulated by addition of endogenous peptide hormones. Increases in mean fura-2 ratios were measured as 0.37 ± 0.06, 0.16 ± 0.03 and 0.23 ± 0.04, during application of 200 nM AGII (n = 9) (Li *et al.*,1998), 200 nM AVP (n = 6) (Omura *et al.*,1999; Belkacemi *et al.*,2008) and 1 nM ET1 (n = 6) (Giulumian *et al.*,2000), respectively. These values for increases in mean fura-2 ratio are also equivalent to the rises in percentage over the basal ratio measurement of 74 ± 15 %, 33 ± 11 %, and 44 ± 9 %, for AGII, AVP and ET1 stimulation, respectively. All values are means ± SEM, $P < 0.05$ relative to cells stimulated with vehicle alone. Both AGII and ET1 stimulated a slow but steady increase of mean fura-2 ratio before reaching a plateau (Figure 4.5.1.A and Figure 4.5.3.A, respectively). In contrast, AVP stimulation of cells caused a transient increase in fura-2 ratio, followed by a return to the pre-stimulation level (Figure 4.5.2.A).

To determine which subtypes of GPCR that coupled to AGII, AVP or ET1, selective receptor antagonists were used. Since the AT1 receptor subtype mediates many of the known effects of AGII and this receptor is also predominantly expressed in BeWo cells (Ino *et al.*,2003; Ishimatsu *et al.*,2006), the AT1 seletive antagonist losartan (5 μM) was used. Figure 4.5.1.B shows a representative trace (n = 5) of the response to 200 nM AGII in BeWo cells in the presence of losartan. An inhibitory effect of this AT1 receptor antagonist was observed, as the change in mean fura-2 ratio was decreased to 0.06 ± 0.02 ($P > 0.05$, LOS+AGII vs vehicle, Figure 4.5.4.A). This result indicates that losartan significantly inhibited the AGII-induced rise in $[Ca^{2+}]_i$ in BeWo cells.

Expression of AVP receptors in trophoblast-like/ choriocarcinoma cells has not been extensively investigated to date. However, high levels of expression of both mRNA and protein for V1a AVP receptor subtype has been reported in the maternal stroma of ovine placenta (Koukoulas *et al.*,2003), as well as in equine conceptuses (Budik *et al.*,2012). In addition, the seletive V1a receptor antagonist SR49059 has been demonstrated to inhibit vasopressin binding to their myometrial and decicual receptors (Thibonnier *et al.*,1999). Therefore, SR49059 was used to investigate the role of V1a receptors in coupling AVP to rises in $[Ca^{2+}]_i$ in BeWo cells. As shown in Figure 4.5.2.B, the AVP-induced transient increase was abolished by the co-application of SR49059 (*$P < 0.05$, AVP vs SR+AVP). This observation indicates the significant inhibitory effect of SR49059 on AVP receptors coupled to $[Ca^{2+}]_i$ rises in BeWo cells. In addition, a representative trace (n = 4) of the response to 200 nM AVP in the presence of 100 nM SR49059 displayed no significant difference to trace in response to vehicle alone ($P > 0.05$, SR+AVP vs vehicle, Figure 4.5.4.B), which further indicates a full inhibition of AVP receptors coupled to Ca^{2+} signalling in BeWo cells.

Expression of slightly higher levels of ET_A receptors than ET_B receptors has been reported in BeWo cells (Mauschitz *et al.*,2000). Therefore, the ET_A receptor selective antagonist BQ123 was chosen to study the effect of ET1 in BeWo cells. Similar to the impact of AT1 antagonist, the ET_A receptor antagonist was also showed significant inhibitory effect on ET1-induced rise in $[Ca^{2+}]_i$ in BeWo cells (**$P < 0.01$, ET1 vs BQ+ET1; Figure 4.5.4.C). A representative trace (n = 4) in

Figure 4.5.3.B shows there was no further rise in mean fura-2 ratio by ET1 in the presence of 100 nM BQ123.

The increases in mean fura-2 ratios in experiments in which BeWo cells were stimulated by endogenously occurring peptide hormomes AGII, AVP and ET1, indicate all three peptides can stimulate rises in $[Ca^{2+}]_i$ in BeWo cells. The corresponding receptor antagonists losartan, SR49059 and BQ123 showed significant inhibitory effect on the increase in fura-2 ratio, suggesting that these hormone induced rises in BeWo $[Ca^{2+}]_i$ were mediated by the activation of AT1, V1a and ET_A receptors, respectively.

Figure 4.5.1. Increases in mean fura-2 ratio in BeWo cells stimulated by AGII in the absence or presence of losartan.

A.

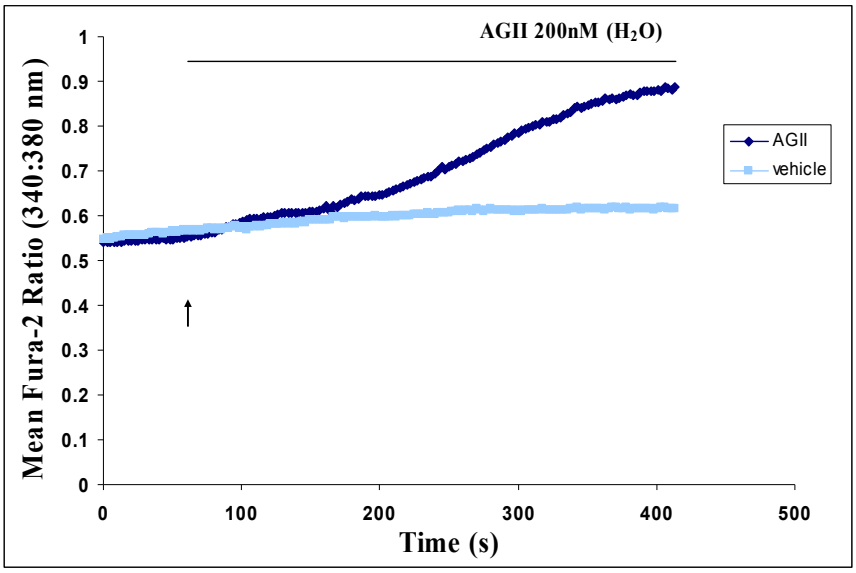

B.

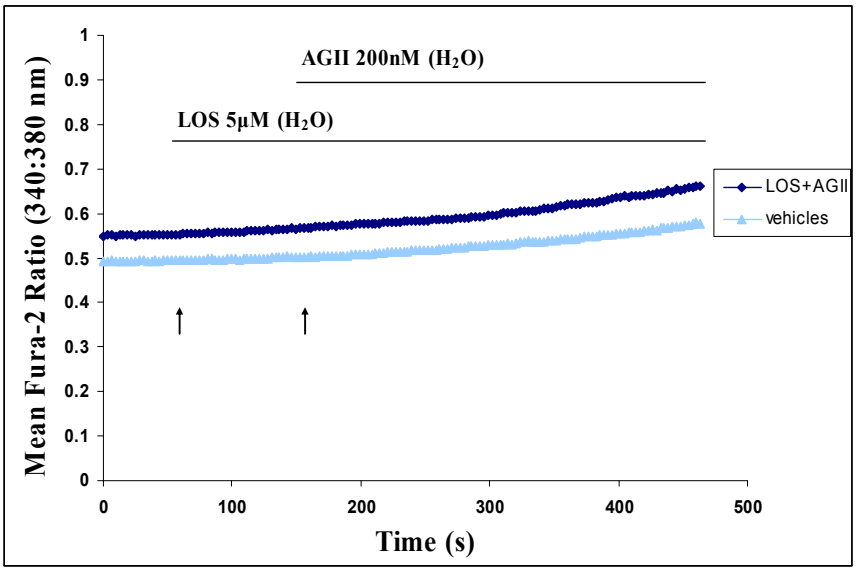

Figure 4.5.1. BeWo cell calcium responses to AGII in the presence or absence of losartan (LOS). Panel **A**. Representative trace (*dark blue*) of mean fura-2 ratio in cells stimulated by 200 nM AGII (n = 9). *light blue trace* represents fura-2 ratio during addition of 2.5 µl ddH_2O (vehicle). Panel **B**. Representative trace (*dark blue*) of mean fura-2 ratio in cells stimulated by 5 µM LOS and 200 nM AGII (n = 5). *light blue trace* represents fura-2 ratio during application of vehicle. In both panels, *black bars* at the top represent stimulation period in cells; arrows below traces represent time points when drugs/vehicle were added.

Figure 4.5.2. Increases in mean fura-2 ratio in BeWo cells stimulated by AVP in the absence or presence of SR49059.

A.

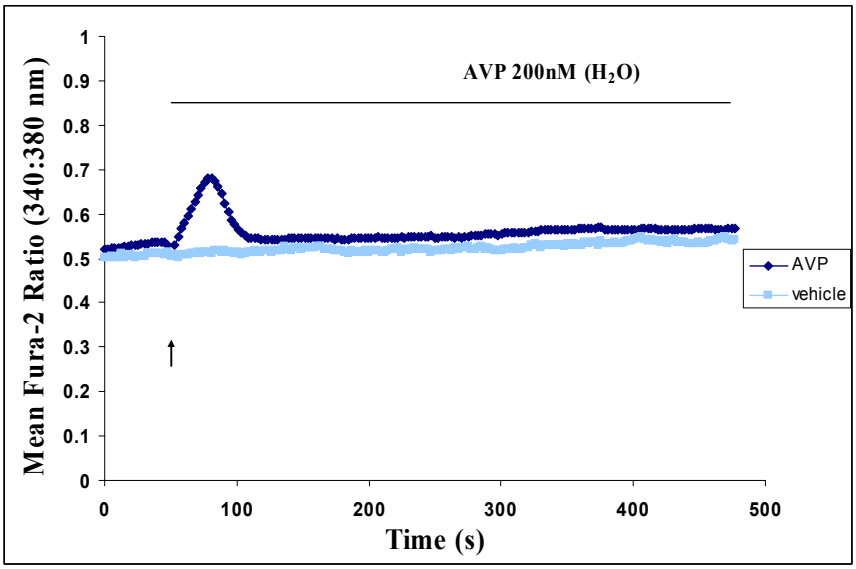

B.

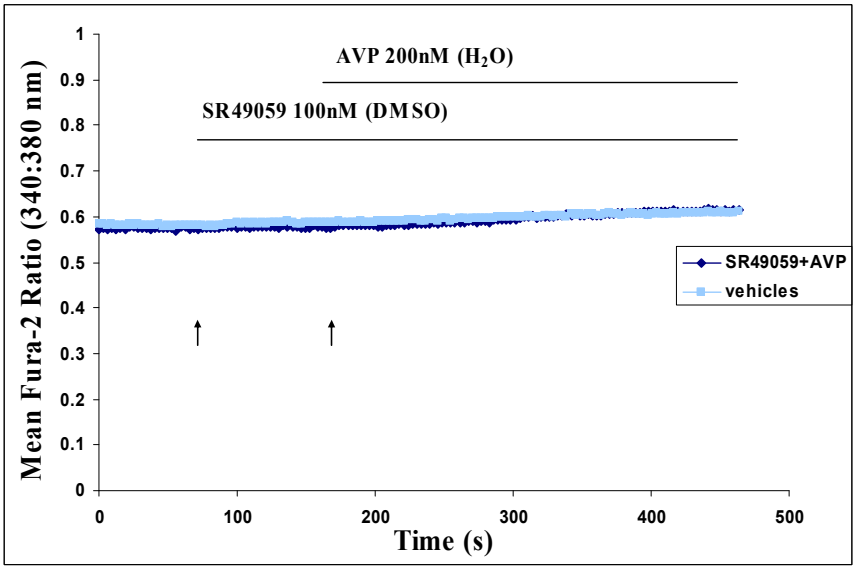

Figure 4.5.2. BeWo cell calcium responses to AVP in the presence or absence SR49059. Panel **A**. Representative trace (*dark blue*) of mean fura-2 ratio in cells stimulated by 200 nM AVP (n = 6). *light blue trace* represents fura-2 ratio during addition of 2.5 µl ddH_2O (vehicle). Panel **B**. Representative trace (*dark blue*) of mean fura-2 ratio in cells stimulated by 100 nM SR49059 and 200 nM AVP (n = 4). *light blue trace* represents fura-2 ratio during application of vehicle. In both panels, *black bars* at the top represent stimulation period; arrows below traces represent time points when drugs/vehicle were added.

Figure 4.5.3 Increase in mean fura-2 ratio in BeWo cells stimulated by ET1 in the absence or presence of BQ123.

A.

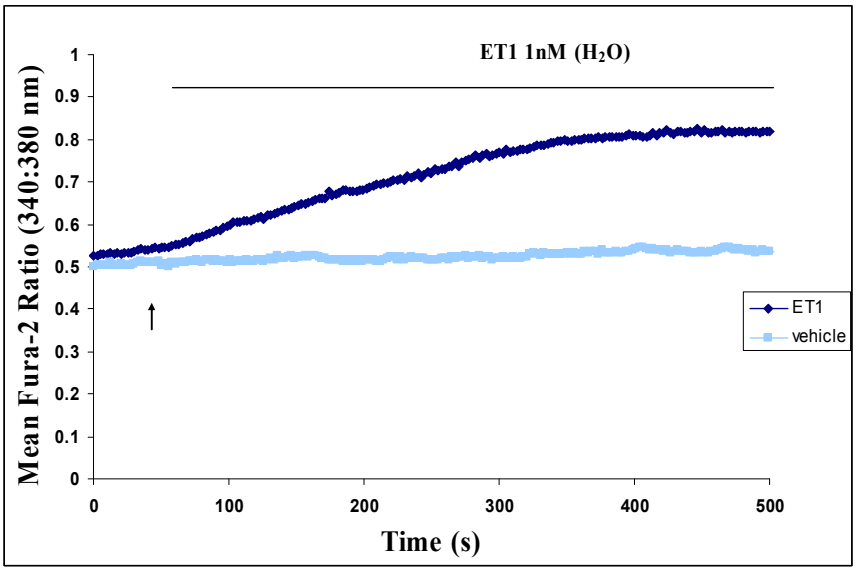

B.

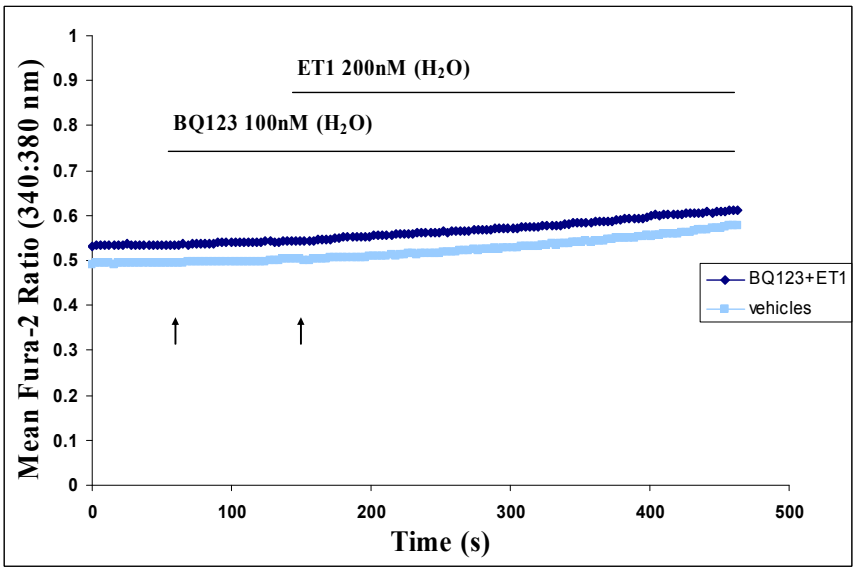

Figure 4.5.3. BeWo cell calcium responses to ET1 in the presence or absence of BQ123. Panel **A**. Representative trace (*dark blue*) of mean fura-2 ratio in cells stimulated by 1 nM ET1 (n = 6). *light blue trace* represents fura-2 ratio during addition of 2.5 µl ddH_2O (vehicle). Panel **B**. Representative trace (*dark blue*) of mean fura-2 ratio in cells stimulated by 100 nM BQ123 and 1 nM ET1 (n = 4). *light blue trace* represents change in fura-2 ratio during application of vehicle. In both panels, *black bars* at the top represent the stimulation period; arrows below traces represent time points when drugs/vehicle were added.

Figure 4.5.4. Change in mean fura-2 ratio in BeWo cells upon stimulation with peptide hormones and their antagonists.

A.

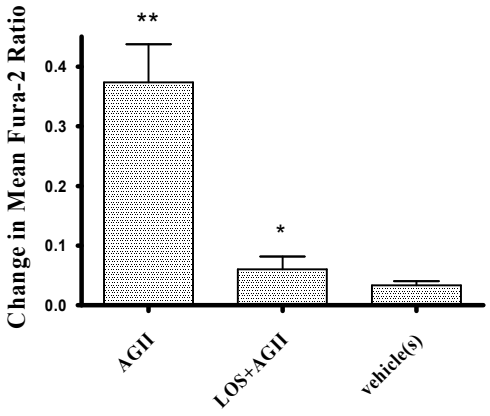

B.

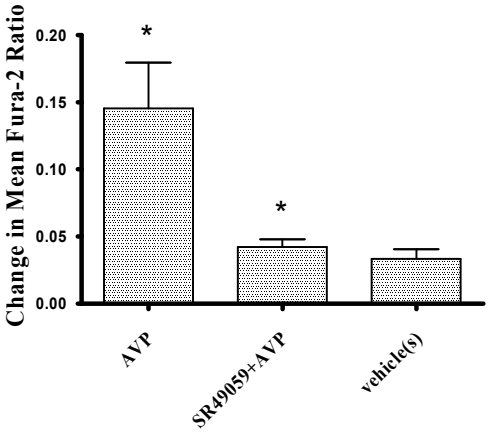

C.

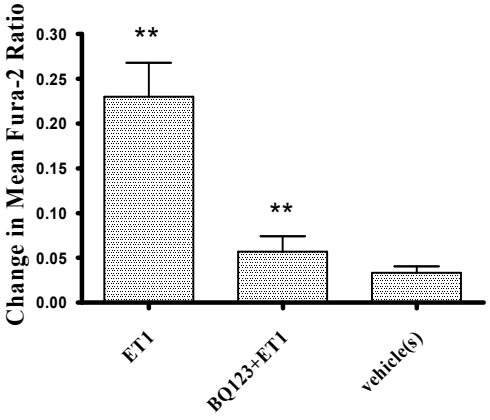

Figure 4.5.4. Changes in mean fura-2 ratio in BeWo cells in response to various hormones in the presence or absence of receptor antagonists. Panel **A**. AGII and AT1 antagonist: 200 nM AGII alone (AGII), with 5 μM losartan (LOS+AGII), * $P < 0.05$, AGII vs LOS+AGII, (n = 9 vs 3), ** $P < 0.01$, AGII vs vehicle (n = 9 vs 5); Panel **B**. AVP and V1a antagonist: 200 nM AVP alone (AVP), with 100 nM SR49059 (SR+AVP), * $P < 0.05$, AVP vs SR+AVP, vehicles (n = 6 vs 4, 5); Panel **C**. ET1 and ET_AR antagonist: 1 nM ET1 alone (ET1), with 100 nM BQ123 (BQ+ET1), ** $P < 0.01$, ET1 vs BQ+ET1, vehicles (n = 6 vs 4, 5); statistical difference in means determined using two-tailed unpaired t tests.

4.6 Role of RyRs in calcium responses to physiologically relevant peptide hormones

To determine whether RyR-mediated Ca^{2+} release of from internal stores contributed to hormone induced rise in $[Ca^{2+}]_i$ in BeWo cells, these trophoblasts were pre-incubated with the RyR antagonists tetracaine or ryanodine (100 μM), before the application of AGII, AVP or ET1. Figure 4.6.1.A, Figure 4.6.2.A and Figure 4.5.3.A show representative traces from BeWo cells treated with 100 μM tetracaine (TET) followed by addition of 200 nM AGII (n = 3), 200 nM AVP (n = 5) or 1 nM ET1 (n = 5), respectively. Tetracaine inhibited the rise in fura-2 ratio in response to AGII, AVP or ET1. Similarly, the presence of 100 μM ryanodine (RYD), significantly suppressed the AGII, AVP or ET1-induced rises in fura-2 ratio in BeWo cells (n = 7, 5, 4, respectively), as indicated in the response traces in Figure 4.6.1.B, Figure 4.6.2.B, and Figure 4.5.3.B. These observations indicated that RyR-mediated Ca^{2+} release makes a major contribution to the rise elevation of $[Ca^{2+}]_i$ in BeWo cells upon AGII, AVP or ET1 stimulation.

In addition, to determine whether the Ca^{2+} influx of cells via L-type Ca^{2+} channels from extracellular space contributed to the rise of $[Ca^{2+}]_i$ in response to the stimulation of these endogenous peptides, BeWo cells were pre-incubated with nifedipine, a dihydropyridine calcium channel blocker. Figure 4.6.5 shows a representative traces of BeWo cells in response to AGII (n = 10), AVP (n = 8) or ET1 (n = 10) in the presence of 100 nM nifedipine. Unexpectedly, addition of nifedipine resulted in rise of mean fura-2 ratio, implying that the presence of this dihydropyridine either triggered Ca^{2+} release from the internal store or Ca^{2+} influx of cell plasma membrane. The subsequent application of AGII or ET1 appeared to induce further small increase in mean fura-2 ratio (Figure 4.6.5, Panels A and C, respectively). However, it was not clear if such rises in ratio were due to peptide alone or due to the combined effect with nifedipine. Traces of responses to AVP in presence of nifedipine shows tendency of return to pre-stimulation level, which was similar as response to AVP alone. These observations indicated nifidepine was not sufficient to demonstrate the involvement of Ca^{2+} influx upon stimulation of AGII, AVP or ET1 in BeWo cells.

Figure 4.6.1. Traces of mean fura-2 ratio in BeWo cells stimulated with AGII and RyR antagonists

A.

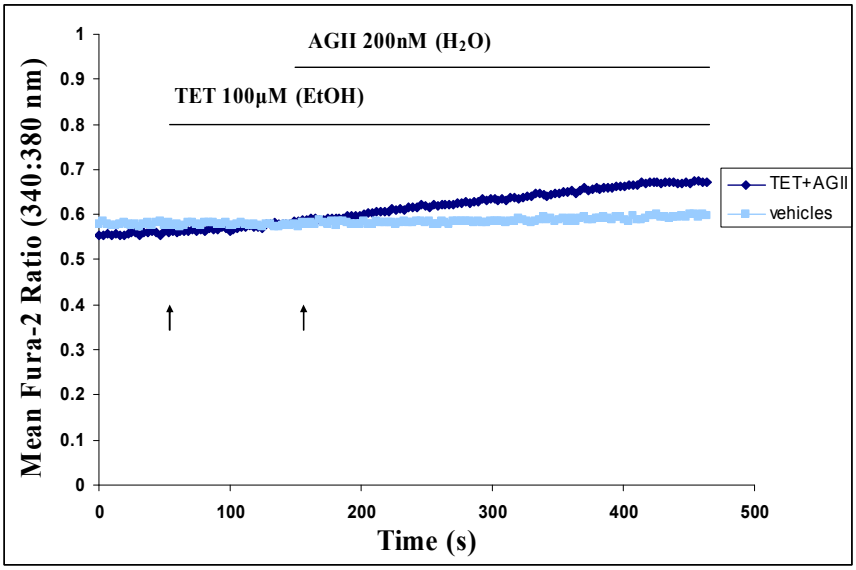

B.

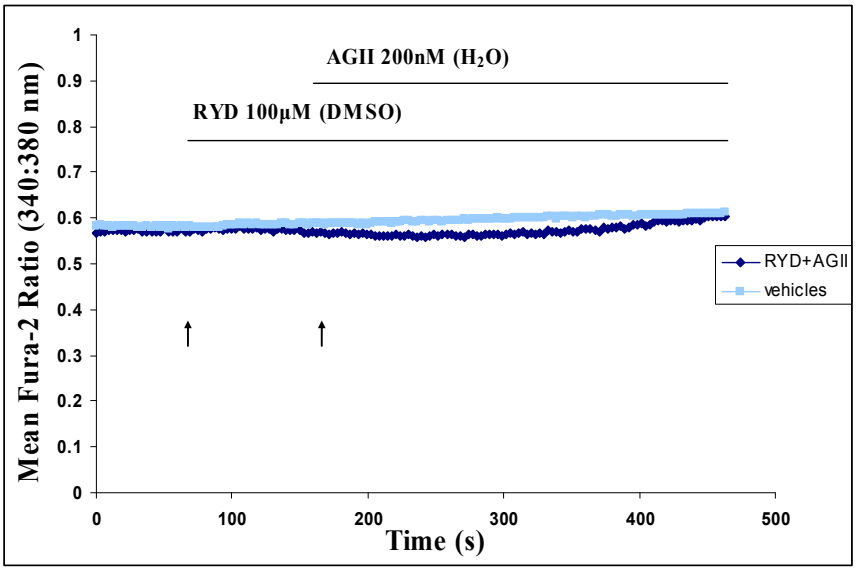

Figure 4.6.1. BeWo cell calcium responses to AGII in the presence and absence of RyR antagonists. Panel **A**. Representative trace (*dark blue*) of mean fura-2 ratio in cells stimulated with 100 µM TET and 200 nM AGII (n = 3). *light blue trace* represents change in fura-2 ratio during application of vehicle. Panel **B**. Representative trace (*dark blue*) of mean fura-2 ratio in cells stimulated with 100 µM RYD and 200 nM AGII (n = 7). *light blue trace* represents change in fura-2 ratio during application of vehicle. In both panels, *black bars* at the top represent stimulation period; arrows below traces represent time points when drugs/vehicle were added..

Figure 4.6.2 Traces of mean fura-2 ratio in BeWo cells stimulated with AVP and RyR antagonists

A.

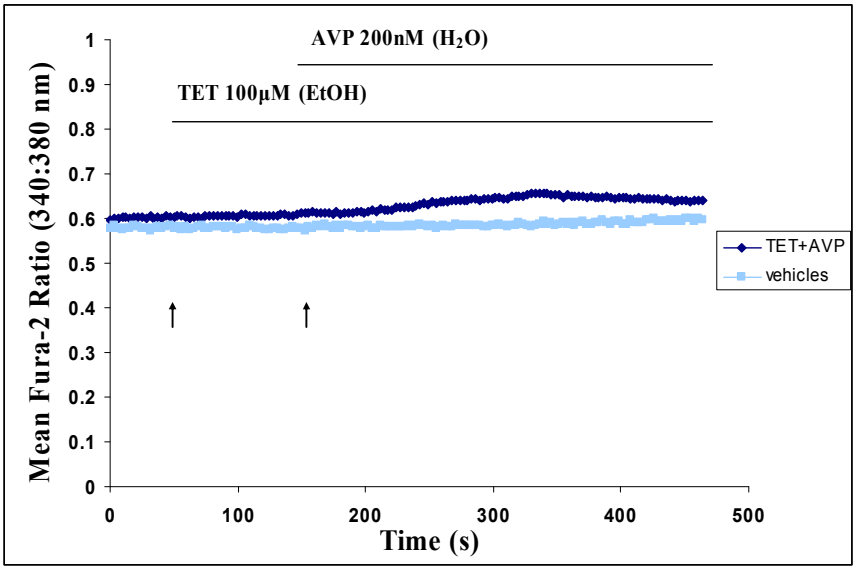

B.

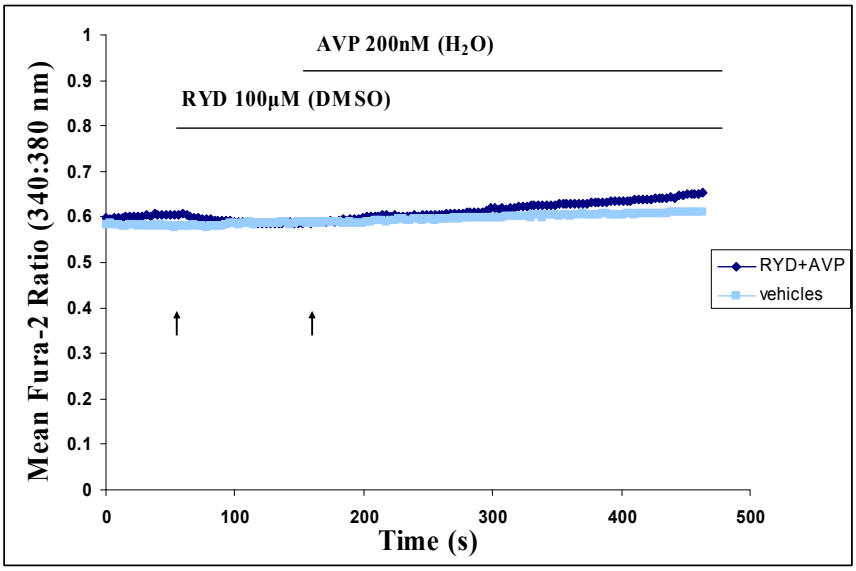

Figure 4.6.2. BeWo cell calcium responses to AVP in the presence or absence of RyR antagonists. Panel **A**. Representative trace (*dark blue*) of mean fura-2 ratio in cells stimulated with 100 µM TET and 200 nM AVP (n = 5). *light blue trace* represents change in fura-2 ratio during application of vehicle. Panel **B**. Representative trace (*dark blue*) of mean fura-2 ratio in cells stimulated with 100 µM RYD and 200 nM AVP (n = 5). *light blue trace* represents change in fura-2 ratio during application of vehicle. In both panels, *black bars* at the top represent stimulation period; arrows below traces represent time points when drugs/vehicle were added.

Figure 4.6.3. Traces of mean fura-2 ratio in BeWo cells stimulated with ET1 and RyR antagonists

A.

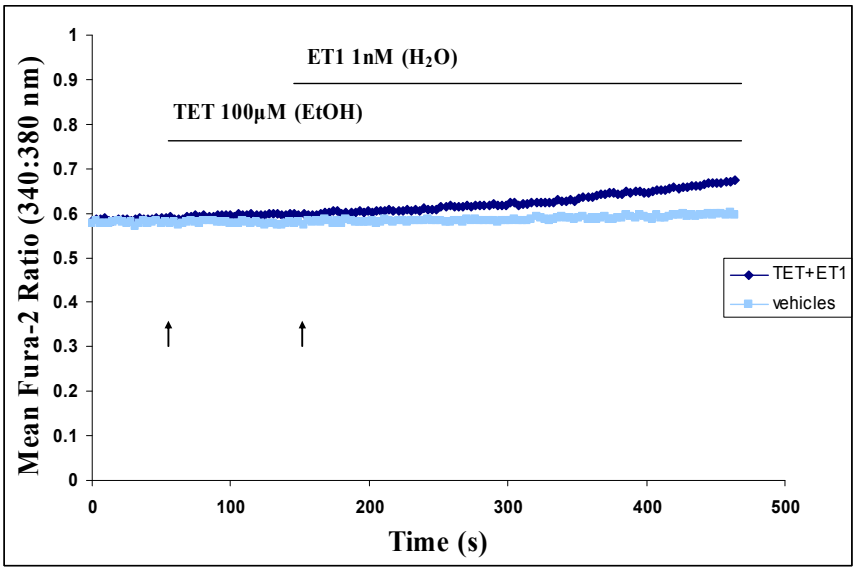

B.

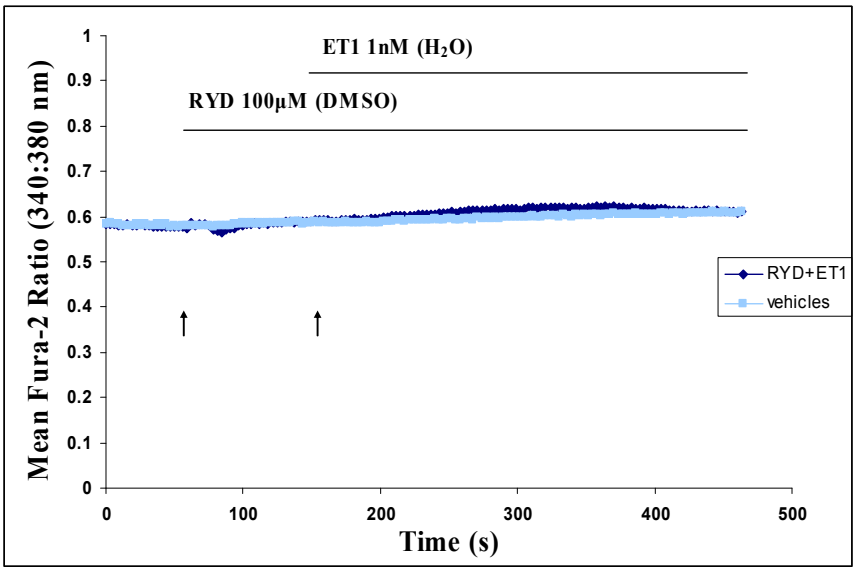

Figure 4.6.3. BeWo cell calcium response to ET1 and RyR antagonists. Panel **A**. Representative trace (*dark blue*) of mean fura-2 ratio in cells stimulated with 100 µM TET and 1 nM ET1 (n = 5). *light blue trace* represents change in fura-2 ratio during application of vehicle. Panel **B**. Representative trace (*dark blue*) of mean fura-2 ratio in cells stimulated with 100 µM RYD and 1 nM ET1 (n = 4). *light blue trace* represents change in fura-2 ratio during application of vehicle. In both panels, *black bars* at the top represent stimulation period; arrows below traces represent time points when drugs/vehicle were added.

Figure 4.6.4 Change in mean fura-2 ratio in BeWo cells upon stimulation with various hormones, their antagonists and RyR inhibitors

A.

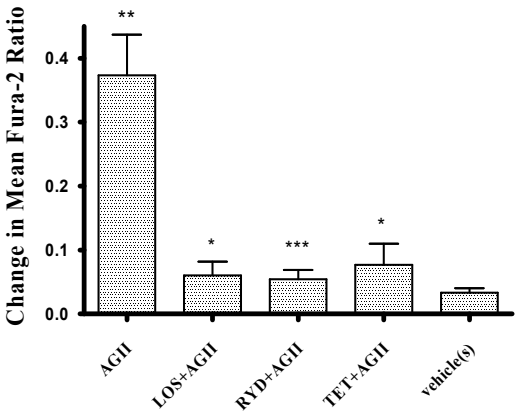

B.

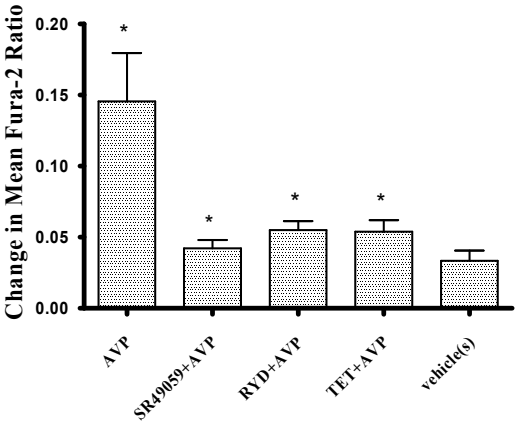

C.

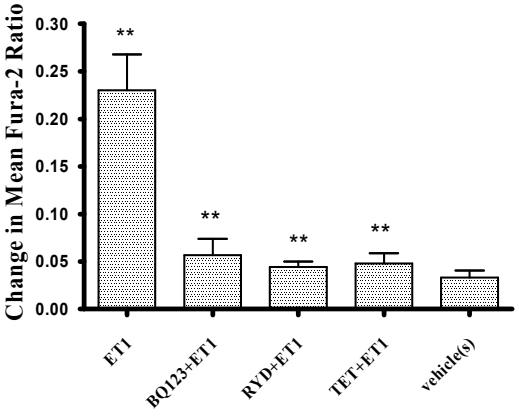

Figure 4.6.4 Changes in mean fura-2 ratio in BeWo cells in response to hormones in the presence or absence of RyR antagonists. Panel **A**. AGII group: cell calcium responses to 200 nM AGII alone (AGII), with 5 μM losartan pre-incubation (LOS+AGII), with 100 μM ryanodine pre-incubation (RYD+AGII), or with 100 μM tetracaine pre-incubation (TET+AGII). * $P < 0.05$, AGII vs LOS+AGII, TET+AGII (n = 9 vs 3, 3) ** $P < 0.01$, AGII vs vehicle (n = 9 vs 5); *** $P < 0.001$, AGII vs RYD+AGII (n = 9 vs 7); two-tailed unpaired t test. Panel **B**. AVP group: cells in response to 200 nM AVP alone (AVP), with 100 nM SR49059 pre-incubation (SR+AVP), with 100 μM ryanodine pre-incubation (RYD+AVP), and with 100 μM tetracaine pre-incubation (TET+AVP). * $P < 0.05$, AVP vs SR+AVP, RYD+AVP, TET+AVP, vehicle (n = 6 vs 4, 5, 5, 5); two-tailed unpaired t test. Panel **C**. ET1 group: cells in response to 1 nM ET1 alone (ET1), with 100 nM BQ123 pre-incubation (BQ+ET1), with 100 μM ryanodine pre-incubation (RYD+ET1), and with 100 μM tetracaine pre-incubation (TET+ET1). ** $P < 0.01$, ET1 vs BQ+ET1, RYD+ET1, TET+ET1, vehicle (n = 6 vs 4, 4, 5, 5); two-tailed unpaired t test.

Figure 4.6.5. Traces of mean fura-2 ratio in BeWo cells stimulated with peptide hormones and nifedipine

A.

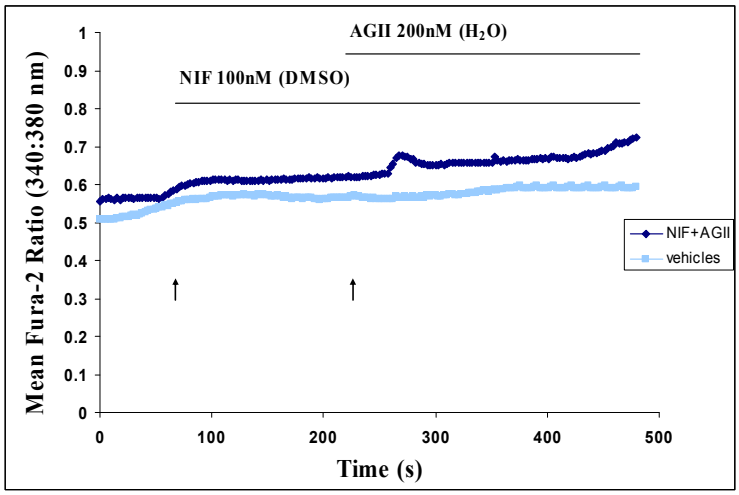

B.

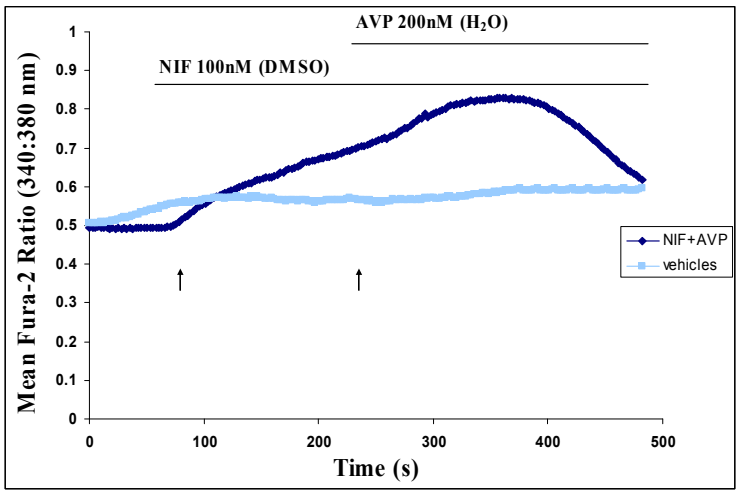

C.

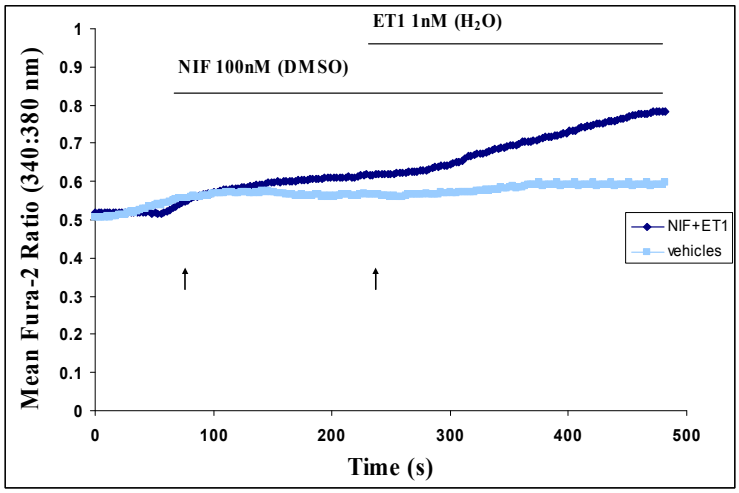

Figure 4.6.5 BeWo cells in response to AGII, AVP and ET1 in the presence of nifedipine (NIF). Panel **A**. Representative trace (*dark blue*) of mean fura-2 ratio in cells stimulated by 100 nM NIF and 200 nM AGII (n = 10). Panel **B**. Representative trace (*dark blue*) of mean fura-2 ratio in cells stimulated by 100 nM NIF and 200 nM AVP (n = 8). Panel **C**. Representative trace (*dark blue*) of mean fura-2 ratio in cells stimulated by 100 nM NIF and 1 nM ET1 (n = 10). The *light blue trace* of each panel represents fura-2 ratio during application of vehicle. In each panel, *black bars* at the top represent stimulation period; arrows below traces represent time points when drugs/vehicle were added.

4.7 Effect of CmC and ryanodine on trophoblast cell-line viability

To examine whether the changes in $[Ca^{2+}]_i$ observed during direct pharmacological activation of RyRs in BeWo and JEG-3 trophoblasts were linked to cell viability, cytotoxicity or changes in metabolic activity, cells were incubated with CmC, ryanodine or etoposide in various concentrations for 20 hours before being labelled with 3-(4,5-dimethylthiazol-2-yl)-2,5-diphenyltetrazolium-bromide (MTT), as described in Section 2.11. MTT assay is a colourimetric assay that reveals metabolic activity of viable cells. In this method, the tetrazolium salt MTT is used; and MTT can only be reduced to a coloured, water-insoluble formazan salt by viable cells; the formazan salt can be solubilised in a solubilisation solution and can be quantitated in a conventional ELISA plate reader. Therefore, the MTT assay is used to quantitate cell proliferation and cytotoxicity (Mosmann,1983). Etoposide is regarded as an anti-cancer agent that targets and stabilises on the DNA-topoisomerase II complex, and causes cell cycle arrest at G2 phase. The prevention of cell cycle progression leads to DNA strands breakage, and eventually results at apoptosis (Marks & Fox,1991). The use of etoposide in this study was to contribute a viability control group for drug-induced cell death.

The graphs in Figure 4.7.1 present the percentage of formazan formation over controls (non-stimulated) in BeWo cells. These values were plotted against various final concentration of drugs after a stimulation period of 20 hours (all values are means ± SEM, n = 3). Stimulation with CmC (500 μM) resulted in a decrease in formazan formation to 22 ± 17 % ($P < 0.05$, vs non-stimulated BeWo cells, one-way ANOVA with Tukey's multiple comparison test), as indicated in graph A of Figure 4.5.1. This rate was nearly half of the formazan production in cells treated with 100 μM etoposide (graph C, Figure 4.5.1), which was 42 ± 21 % ($P < 0.05$, vs non-stimulated BeWo cells, one-way ANOVA with Tukey's multiple comparison test). These values suggest the presence of CmC (500 μM) or etoposide (100 μM) significantly decrease the production of formazan from MTT in BeWo cells; in other words, both compounds affect BeWo cell viability.

In contrast, the rate of formazan production measured after 20 hours incubation with 1 μM ryanodine was 103 ± 41 %. This value suggests that 1 μM ryanodine neither suppress nor significantly enhances convertion of formazan from MTT, ie. ryanodine at this concentration has little effect on BeWo cell viability.

Formazan production by JEG-3 cells in response to these drugs was different from that in BeWo cells. Closer production rates were measured at the end treatment with 500 μM CmC and 1 μM ryanodine, which were 94 ± 13 % and 80 ± 18 %, respectively, as revealed in graph A and graph B of Figure 4.5.2 (all values are means ± SEM, n = 3). These values suggest treatment with 500 μM CmC or 1 μM ryanodine neither enhance nor significantly suppress the convertion of formazan salt from MTT, therefore, both drugs have little effect on JEG-3 cell viability. Graph C of Figure 4.5.2 displays JEG-3 cells that were incubated with etoposide for 20 hours. Treatment of 100 μM etoposide in JEG-3 cells resulted in a significant decrease in formazan production to 31 ± 15 % ($P < 0.05$, vs non-stimulated JEG-3 cells, one-way ANOVA with Tukey's multiple comparison test). This figure does not significantly differ from the measurement obtained in BeWo cells (42 ± 21 %).

Although these MTT assays were statistically insufficient, the preliminary data indicates that 1 μM ryanodine does not significantly affect the cell viability of either BeWo or JEG-3 cells; while 500 μM CmC has little effect on JEG-3 cells, it significantly suppressed formazan salt production, which implies the application of 500 μM CmC affects BeWo cell viability. Treatment of cells with 100 μM etoposide resulted in a significant decrease on formazan conversion. These results provide positive evidence supporting the cytotoxic effect of etoposide (Marks & Fox,1991).

Figure 4.5.1 CmC or ryanodine concentration dependent effects on BeWo cell viability

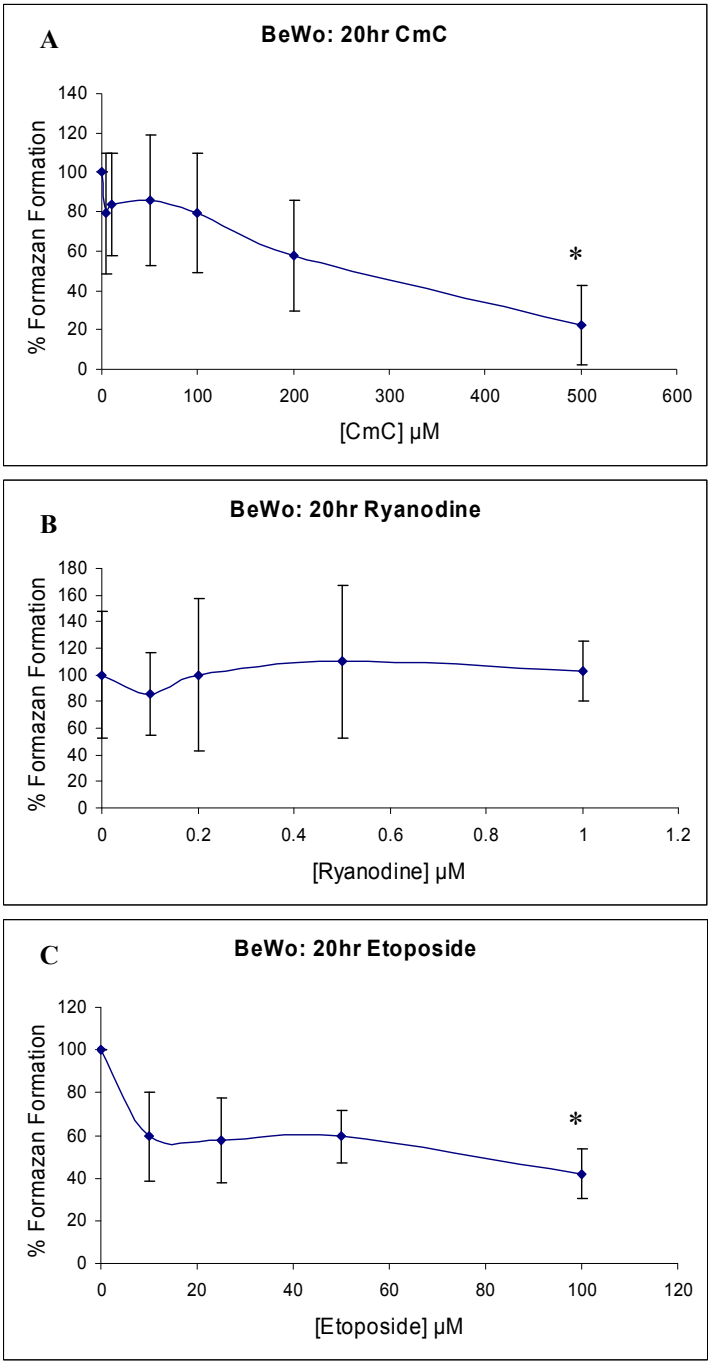

Figure 4.5.1. BeWo cell MTT reduction (n = 3) after 20 hour stimulation of CmC, ryanodine or etoposide at various concentrations. Panel A, BeWo cells were stimulated with CmC at various concentrations (0, 5, 10, 50, 100, 200, *500 µM); Panel B, BeWo cells were stimulated with ryanodine at various concentrations (0, 0.1, 0.2, 0.5, 1 µM); Panel C, BeWo cells were stimulated with etoposide at various concentrations (0, 10, 25, 50, *100 µM). * $P < 0.05$, vs non-stimulated BeWo cells, one-way ANOVA with Tukey's multiple comparison test.

Figure 4.5.2 CmC or ryanodine concentration dependent effects on BeWo cell viability

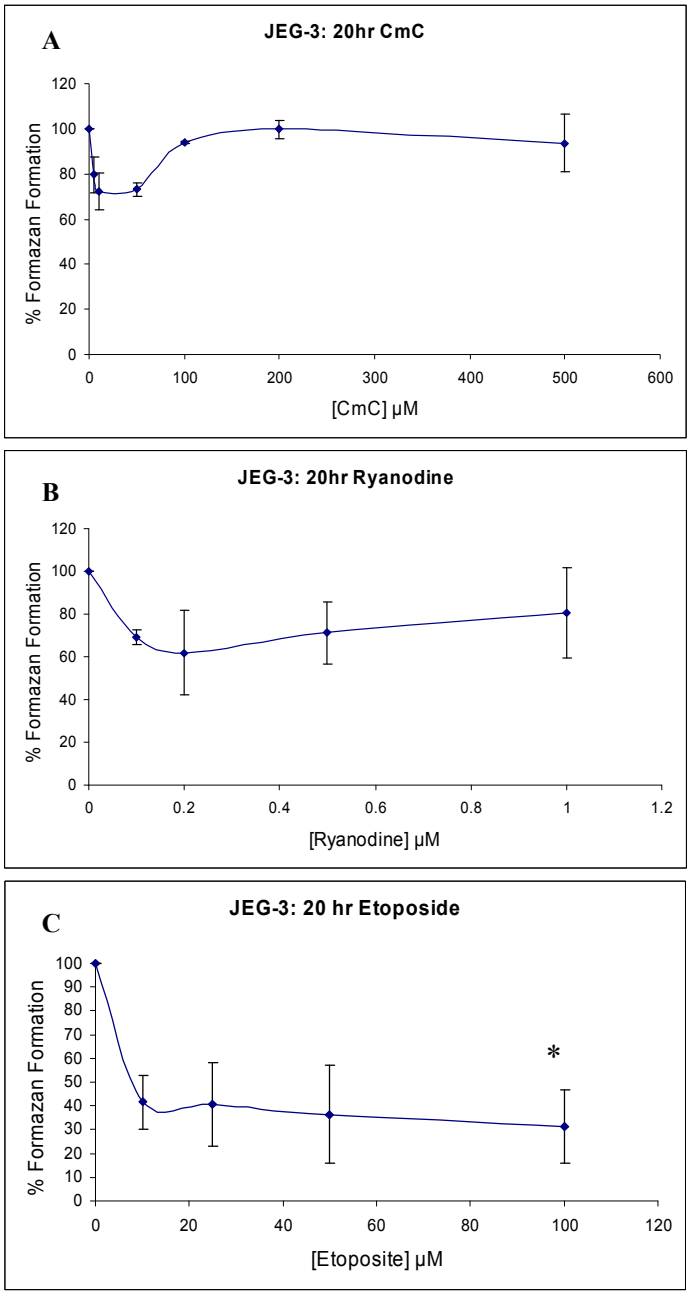

Figure 4.5.2. JEG-3 cell MTT reduction (n = 3) after 20 hour stimulation of CmC, ryanodine or etoposide at various concentrations. Panel A, JEG-3 cells were stimulated with CmC at various concentrations (0, 5, 10, 50, 100, 200, 500 µM); Panel B, JEG-3 cells were stimulated with ryanodine at various concentrations (0, 0.1, 0.2, 0.5, 1 µM); Panel C, JEG-3 cells were stimulated with etoposide at various concentrations (0, 10, 25, 50, *100 µM). * $P < 0.05$, vs non-stimulated BeWo cells, one-way ANOVA with Tukey's multiple comparison test.

Chapter V.

Discussion

Chapter V. Discussion

In present study, the expression of RyRs has been investigated in both human trophoblast-like cells and human placental villous samples. Results presented in Chapter III demonstrated that 1) RyR1 is expressed in both BeWo and JEG-3 trophoblastic cells (IF, RT-PCR and western blot); 2) RyR2 and RyR3 are co-expressed with RyR1 in BeWo and JEG-3 cells, respectively (IF and RT-PCR); 3) human first trimester placental villi express RyR1 (IHC and RT-PCR), plus either or both RyR2 (RT-PCR) and RyR3 (IHC); 4) human term placental villi express RyR3 (IHC and RT-PCR), plus either or both RyR1 (IHC) and RyR2 (RT-PCR); 5) both BeWo and JEG-3 cells express the RyR accessory proteins: CSQ and TRD (IF and western blot); 6) human first trimester placental villi express TRD (IHC and western blot), while CSQ was detected in human term placental villous tissue (western blot).

The preliminary functional investigation carried out in BeWo and JEG-3 cells. The results presented in Chapter IV indicate: 1) both CmC and ryanodine (1 μM) induced a rise in $[Ca^{2+}]_i$ in BeWo and JEG-3 cells; 2) application of 100 μM tetracaine suppressed ryanodine-induced $[Ca^{2+}]_i$ rise in BeWo and JEG-3 cells, but had little effect on CmC-induced $[Ca^{2+}]_i$ elevation, suggesting CmC also induces a non-RyR-mediated increase in $[Ca^{2+}]_i$ in these cells; 3) AGII, AVP and ET1 were demonstrated to induce $[Ca^{2+}]_i$ increases in BeWo cells, and such rise could be inhibited by losartan, SR49059 or BQ123, the corresponding antagonists of AGII, AVP and ET1; 4) both tetracaine and ryanodine (100 μM) inhibit AGII-, AVP- and ET1-induced rises in $[Ca^{2+}]_i$, suggesting RyR mediates peptide-stimulated signalling pathways in BeWo cells.

5.1 Differential Expression of RyRs in Human Trophoblast

Expression of RyRs and selected accessory proteins of RyRs was demonstrated and confirmed for the first time by using RT-PCR, western blotting and IIF/IHC microscopy in both human trophoblastic cell lines and human placental villous tissues, as summarised in Table 5.1. In the current study, RyR1 was shown to express in human first trimester villous tissue and in the BeWo trophoblastic cell line (Section 3.1 and 3.2), by all methods employed (RT-PCR, western blotting and IIF microscopy /IHC); while RyR1 expression in JEG-3 was demonstrated by western blotting and IIF microscopy; in addition, RyR2 and RyR3 proteins were also detected by IIF microscopy in BeWo and JEG-3 cells (Figure 3.5.1 A and Figure 3.5.1 B).

Table 5.1. RyR expression in trophoblast cell lines and human placental samples

Method of detection	BeWo	JAR	JEG-3	1st trimester samples	Term samples
RT-PCR	*RYR1*, *RYR2*	*RYR1*, *RYR2*	**N/A	*RYR1*, *RYR2*	**N/A
Western blot	RyR1	N/A	RyR1	+ve	+ve
IIF/IHC	RyR1, RyR2, RyR3	*RyR1, *RyR2, *RyR3	RyR1, RyR2, RyR3	RyR1, RyR3	RyR1, RyR3

* Data not shown;
** PCR product nucleotide sequence displayed less than 99% identity to target DNA templates (JEG-3 cells); or PCR products detected by electrophoresis but only partially sequenced (term samples).

In human placental villous samples, PCR products derived from *RYR1* (three out of four samples) and *RYR2* (four out of four samples) were amplified from RNA extract of first trimester placental tissue. Sequencing analysis of RyR1 and RyR2 PCR products by Eurofins (Eurofins MWG Operon, Germany) revealed 99% identity to both human RyR1 mRNA (NM_001042723.1; sequences 13997-14922; Appendix

XII) and RyR2 mRNA (NM_001035.2; sequences 13748-14703; Appendix XIII). Similarly, DNA sequencing indicated that the PCR products of *RYR1* and *RYR2* from BeWo and JAR cells displayed 99% to 100% identities to their corresponding *Homo sapiens* sequences. *RYR1* and *RYR2* from BeWo cells showed 99% identity to *Homo sapiens RYR1* (NM_001042723.1; sequences 13979-14831; Appendix I) and *Homo sapiens RYR2* (NM_001035.2; sequences 13750-14706; Appendix II), respectively; the product of *RYR1* from JAR cells showed 100% identity to *Homo sapiens RYR1* (NM_001042723.1; sequences 13933-14908; Appendix III), while product of *RYR2* from the same cell line displayed 99% identity to *Homo sapiens RYR2* (NM_001035.2; sequences 13784-14628; Appendix IV). The product of *RYR2* from human term placental villi displayed 100% identity to *Homo sapiens RYR2* (NM_001035.2; sequences 14239-14677; data not shown). Since less than half length (439 nucleotides) of expected PCR product was sequenced in current study, the presence of RyR2 mRNA in human term placental villous tissue was inconclusive.

Selective PCR products of *RYR3* of the expected size from JEG-3 and SGHPL-4 cells and human term placental villous samples (four out of five samples) were detected on agarose gels after electrophoresis (Figure 3.1.1.C and Figure 3.1.3.C). However, DNA sequencing indicated that none of these products displayed greater than 99% identity to *Homo sapiens RYR3* (NM_001036.3). Primer-BLAST (Ye *et al.*,2012) (available at: http://www.ncbi.nlm.nih.gov/tools/primer-blast/) results indicated that the primers used to target *Homo sapiens RYR3* in current study were not completely matched to template sequence. Specifically, two mismatched nucleotides were identified in the forward primer, and one mismatch was found in the reverse primer (Panel III, Appendix XI). These mismatched nucleotides increase the chance of attaching to a sequence beyond the target, which could result in an unrelated PCR product. In contrast, primers targeting *Homo sapiens RYR2* displayed completely matched alignment with the target sequence (Panel II, Appendix XI); whereas, one mismatched nucleotide was found in the common forward primer for *Homo sapiens RYR1* sequence (Panel I, Appendix XI). These results indicate that the primers used in current study that targeted on *Homo sapiens RYR2* and *RYR1* amplified products in expected size and sequence; whereas, PCR products produced

by primers targeted to *RYR3* required further verification experiments, possibly using new primers and then analysing by restriction digestion or DNA sequencing (Sei *et al.*,1999).

Western blot analyses demonstrated the protein expression of RyRs in trophoblast BeWo and JEG-3 cell lines and in human first and term placental villous tissue, as high molecular weight bands (>500 kDa) shown in Figure 3.2.1.A and Figure 3.2.2. Immunoblotting with isoform-specific antibodies for RyR1 further supported the presence of this receptor type in both BeWo and JEG-3 cells (Figure 3.2.1.B). Despite the use of protease inhibitors and preparation of samples at 4 ^{o}C, multiple lower molecular weight bands were still detected along with the high molecular weight RyR band. This observation suggests RyR protein degradation had occurred as seen in other reports (Meissner *et al.*,1989; Junankar & Dulhunty,1994; Fitzsimmons *et al.*,2000; Pedrozo *et al.*,2010; Pedrozo *et al.*,2013). Such degradation can be caused by endogenous proteases (Lai *et al.*,1988). The calcium-dependent cysteine proteases calpains for instance, are known to be ubiquitously expressed in many cells including trophoblasts (Nicola *et al.*,2005b; Gauster *et al.*,2010); these proteases have also been demonstrated as a potential contributors to RyR degradation (Pedrozo *et al.*,2010). Other possible degradation pathways that present in trophoblast such as ubiquitin-proteasome system (Trausch *et al.*,1993; Yehia *et al.*,2001; Fu *et al.*,2010) and autophagy complex (Oh *et al.*,2008; Curtis *et al.*,2013), also participated in cellular protein degradation (Pedrozo *et al.*,2010). In current study, bands at ~300 kDa and ~160 kDa were consistently detected on immunoblots probing for RyRs in skeletal muscle (Figure 3.2.1.A, Figure 3.2.1.B and Figure 3.2.2.B). These findings were in consistent with early studies, which suggested these proteolytic fragments were products of RyR degradation caused by endogenous proteases (Lai *et al.*,1988; Shoshan-Barmatz *et al.*,1994).

In addition to susceptibility of degradation of RyR protein, large molecular weight and low expression level of these receptors in cells and tissues of interest also contributes to the difficulty of protein transfer and detection by western blot, as low intensity RyR bands of on immunoblots have also been reported in other studies (Saldaña *et al.*,2009). RyRs are also subject to post-translational modifications, such as oxidation, glycation, isomerization, deamidation, racemization, and cross-linking

(Ferrington *et al.*,1998). These factors may also contribute to the differential turnover of proteins (Ferrington *et al.*,1998). The RyR is one of the largest ion channel complexes, which is functionally modulated by multiple accessory proteins via different interaction motifs, as mentioned in Section 1.6. Such natural complexity contributes to the challenge on the investigation of RyR in cells and tissue with low abundance.

Other antibody-dependent detection methods, such as IIF microscopy and IHC were used to support the limited detection of RyRs in trophoblasts by western blotting. Microscopy images indicated all isoforms of RyRs are expressed in both BeWo and JEG-3 trophoblast cell lines (Figure 3.5.1.A and Figure 3.5.1.B, respectively). In BeWo cells, the detection of RyR1 and RyR2 by IIF microscopy was consistent with RT-PCR assays, in which, *RYR1* and *RYR2* were amplified. The presence of *RYR3* in trophoblasts was not determined by RT-PCR, likely due to the lack of specificity of primers, as discussed previously. The same explanation may be extended to the discovery of RyR3 protein by IHC and failure to detect the corresponding mRNAs by RT-PCR in human first and term villous samples. Interestingly, the use of the same RyR3-specific antibody (AB9082) revealed expression of type 3 RyR by IIF microscopy/IHC, but not in western blotting. These results imply that this antibody is more sensitive for RyR3 detection in fixed cells or tissues. In other words, this antibody may be less sensitive in western blotting assays, where proteins might be denatured and display fewer conformational epitopes.

Another interesting finding was the detection of RyR1 and RyR3 by IHC in both human first trimester and term placental villous tissues, while staining of RyR2 remained negative (Figure 3.4.1 and Figure 3.4.2, respectively). However, in one sample of human first trimester decidua basalis, positive RyR2 expression was demonstrated in both stroma cells and trophoblasts (likely extravillous trophoblasts) by IHC (Figure 3.4.3.A). The RyR2-specific antibody (HPA016697) used in current study, has been approved for IHC application by manufacturer (antibody validation information available at: 'The Human Protein Atlas', http://www.proteinatlas.org/ENSG00000198626/antibody); the same antibody also recognized the cardiac RyRs in the rat heart by western blotting (Figure 3.2.1.C). These findings indicated the reliability of this anti-RyR2 antibody. The

demonstration of RyR2 positive staining in an IHC section of first trimester decidua basalis, therefore, suggests that RyR2 expression in trophoblastic cells is transient and highly regulated. This preliminary result was consistent with other reports. Particularly, transient upregulation *RYR2* mRNA level has been observed at day 4 and/or day 6 in trophoblast lineage of human embryonic stem cells that differentitated in culture; *RYR2* transient upregulation therefore, has been suggested to be associated with trophoblast differentiation and invasion (Marchand *et al.*,2011). The trophoblast phenotype possesses a sophisticated change from sessile to invasive during embryo implantation (Vićovac & Aplin,1996), followed by transformation back into non-invasive phenotypes and focus on nutritional and endocrinal functions of the mature placenta (Aplin,1991). Extravillous trophoblast in the decidua basalis, however, remains invasive in the mature placenta (Kaufmann & Castellucci,1997). In current study, both stroma cells and trophoblasts in decidua section were positive to RyR2 IHC detection, these stroma cells may contribute to the consistent detection of *RYR2* mRNA in first trimester placental villi trophoblast. It is also possible that RyR2 protein expression is associated with invasion process and may be transiently upregulated; gene expression of *RYR2* appeared to be down regulated or absent in trophoblast of term placenta, suggesting that RyR2 is involved in cell differentiation; protein expression of RyR1, RyR3 and TRD appeared to be constant in trophoblasts from first trimester and term placenta, suggesting that these proteins may be essential for trophoblastic cell function during pregnancy.

Using differential-display RT-PCR, it has been demonstrated that there are a high number of genes that are expressed differentially between first trimester and term placental trophoblastic cells (Huch *et al.*,1998). For example, β1-intergrin shows a much higher expression in first trimester trophoblast than in term placental trophoblasts at both mRNA and protein levels, correlating with invasiveness (Damsky *et al.*,1994; Huch *et al.*,1998). In addition, PBK1 gene (which is also known as ribosomal L1 domain containing 1 (RSL1D1)) was initially identified exclusively in first trimester by Huch and colleagues; high expression levels of PBK1 were also discovered in JAR cells by the same group, the authors proposed PBK1 is involved in the regulation of trophoblastic invasiveness (Huch *et al.*,1998). The current study demonstrated that *RYR2* mRNA is present in cytotrophoblast-like

cell lines of BeWo and JAR (in addition to *RYR1*), and in human first trimester villous trophoblasts (Figure 3.1.1 and Figure 3.1.2). These findings suggest that of RyR2 expression correlates with the sessile-invasive transformation of human trophoblast.

Phenotypically distinct trophoblastic cells distribute in different sites of the placenta. It has been demonstrated that the IHC staining intensities of EVT marker proteins CD9 and HLA-G were increased in where cells were found at near the maternal decidua, ie. trophoblastic cell column that differentiated into EVTs; in contrast, both SCTs and villous CTs of proximal CT cell columns (undifferentiated CTs) were negatively stained (Nagamatsu *et al.*,2004). In contrast, E-cadherin is down-regulated in EVTs as CT differentiates (Zhou *et al.*,1997). In the current study, IHC staining of RyR2 was positive in human decidua basalis of first trimester tissue sections. Similarly, IIF microscopy also shows RyR2 expression in both BeWo and JEG-3 cells. However, negative staining of E-cadherin is observed in malignant JEG-3 trophoblastic cells (Appendix 0), but positive in CT-like BeWo cells (Figure 3.5.1.A). These observations on human choriocarcinoma cell lines (BeWo and JEG-3 cells) suggest 1) variations exist between BeWo and JEG-3 cells; 2) variation exists between these trophoblastic-like cells and normal trophoblastic cells from primary culture. Therefore, BeWo or JEG-3 may not respond to regulatory agents in the same way as normal trophoblasts. As reviewed in Section 1.11, EVTs are invasive trophoblastic cells differentiated from CTs. Although samples from human decidua section were limited, these preliminary data further imply that RyR2 expression is correlated with invasiveness of trophoblastic cells. Based on this observation, *in vitro* demonstration of this hypothesis may be possible. Nagamatsu and colleagues have shown purified CTs from human first trimester can acquire EVT phenotype in a low [Ca^{2+}] culture medium (0.1 mM Ca^{2+}, dKSFM medium) within 96 hour without syncytialisation (Nagamatsu *et al.*,2004). The same method may be adapted and RyR2 expression could be examined when the EVT phenotype appears. Cytotrophoblast-like BeWo cells have been demonstrated to respond to forskolin and differentiate into SCTs (Wice *et al.*,1990). Therefore, differentiated BeWo cells may be used to demonstrate the loss of expression of RyR2. However, as mentioned earlier, variations do exist between 'trophoblastic-like' and normal trophoblastic

cells. Expression levels of RyR2 could be hard to predict in BeWo cells, even their apparent phenotype may be altered by corresponding regulatory agents (such as forskolin).

5.2 Impact of RyR Direct Pharmacological Stimulation on BeWo and JEG-3 Cells

The functional characterisation of RyRs in trophoblasts was carried in both BeWo and JEG-3 cells. The RyR agonist ryanodine modulates all types of RyRs by an allosteric mechanism, as reviewed in Introduction Section 1.4. The use of 1 μM final concentration of ryanodine should promote RyR channels opening, as reviewed by Zissimopoulos and Lai (Zissimopoulos & Lai,2007). Addition of ryanodine (1 μM) induced rise in $[Ca^{2+}]_i$ in both BeWo and JEG-3 cells (Figure 4.1.4). The ryanodine induced $[Ca^{2+}]_i$ increase in JEG-3 cells appeared to be transient, while a sustained increase was observed in BeWo cells. The addition of the RyR antagonist tetracaine completely abolished the ryanodine-induced $[Ca^{2+}]_i$ increase in JEG-3 cells (Figure 4.3.2), indicating that JEG-3 cells express functional RyRs, sensitive to both ryanodine and tetracaine. In BeWo cells, tetracaine appeared to only partially inhibit the ryanodine-induced $[Ca^{2+}]_i$ increase, as cell responses to ryanodine in the presence of tetracaine remained significant higher than to vehicle-alone (Figure 4.3.1.B). These observations suggest that teteracaine resulted in a delayed potentiation of spontaneous Ca^{2+} release in BeWo cells, as reported in an earlier studyon rat ventricular myocytes (Györke *et al.*,1997).

CmC has been demonstrated as an effective RyR activator that specifically targets on skeletal muscle RyR1 and cardiac muscle RyR2 (Zorzato *et al.*,1993; Herrmann-Frank *et al.*,1996), The final CmC concentration (500 μM) initially used in this study was above the estimated EC_{50} (about 100 μM) for skeletal muscle RyR (Herrmann-Frank *et al.*,1996), in order to achieve a maximum response. The addition of CmC was demonstrated to induce rise in $[Ca^{2+}]_i$ in both BeWo and JEG-3 cells. However, the presence of RyR antagonist (tetracaine or 100 μM ryanodine) did not inhibit this $[Ca^{2+}]_i$ rise (Figure 4.4). These observations indicated that CmC induced $[Ca^{2+}]_i$ increases in BeWo and JEG-3 cells via activation of other mechanisms,

independent of RyR gating. CmC not only induced rapid $[Ca^{2+}]_i$ increase in BeWo cells, but apparently also caused memebrane damage, as loss of fluorescence was observed (Figure 4.1.1.B) This unexpected outcome from CmC stimulation indicated that this molecule activated other rather than non-RyR-mediated pathways that cause $[Ca^{2+}]_i$ in BeWo cells, which leaded to membrane destruction. Such non-specific effect of CmC has also been reported to cause calcium flux and respiratory burst in human neutrophils (Hauser *et al.*,2005). Therefore, the use of CmC was not suitable for current study.

Another unexpected observation was that dantrolene enduced autofluorescence in fura-2-loaded BeWo and JEG-3 cells. Dantrolene was originally used to examine the involvement of RyR subtype activation in cells, as this molecule is known as an RyR channel blocker that directly targets RyR1 and RyR3 (Fruen *et al.*,1997). Decreases in fura-2 ratios were observed in both BeWo and JEG-3 cells upon application of dantrolene. Examination in the duo fluorescence intensities at excitation wavelength of 340 nm and 380 nm indicated that such decreases in fura-2 ratios were due to the rise in F_{380} unaccompanied by a change in F_{340} during dantrolene stimulation, rather than due to the decrease in the intracellular Ca^{2+} content of cells (Figure 4.2.3). The interference in cell caused fluorescence by dantrolene was further examined in fura-2-free cells. As Figure 4.2.4 shows, the rise of F_{380} was observed in both BeWo and JEG-3 cells, while F_{340} remained steady, during dantrolene stimulation. Despite increase in F_{380}, the ratios of fluorescence were relatively stable, by comparison to fura-2-loaded experiments. These obervations suggest that the cellular free Ca^{2+} indicator fura-2 and dantrolene co-ordinately enhance the F_{380} fluorescence and suppress the F_{340}/F_{380} ratio in BeWo and JEG-3 cells. Therefore, the use of dantrolene was not suitable as an RyR antagonist in fura-2 loaded BeWo and JEG-3 cells.

.

5.3 Impact of RyRs in BeWo Cell $[Ca^{2+}]_i$ Responses to Peptide Hormones

The channel activity of RyR can be regulated by various factors such as Ca^{2+} and CaM, as reviewed in Introduction Section 1.5 and 1.6. The channel activity and

the subsequent RyR-mediated Ca^{2+} mobilisation can also be modified by phosphorylation on specific serine/threonine domains of the channel subunit, as reviewed in Introduction Section 1.7. The release of Ca^{2+} mediated by phosphorylated RyR channels is one of the consequences of GPCR activation that transmits extracellular stimuli to intracellular events. In current study, BeWo and JEG-3 trophoblast-like cells were used for the first time to demonstrate changes in $[Ca^{2+}]_i$ in response to extracellular stimulation by endogenous peptides: AGII, AVP and ET1. In these experiments, JEG-3 cells displayed no overall change in fura-2 ratio upon addition of any of the peptides; whereas increased fura-2 ratios were observed in BeWo cells, which indicated a net change in $[Ca^{2+}]_i$ upon stimulation with these endogenously occuring peptides. As reported in Results Section 4.4, addition of AGII, AVP, or ET1 in BeWo cells, leads to a rise of over 30% in mean fura-2 ratio above the basal level. These hormonal peptide-induced rises in fura-2 ratios were inhibited by the presence of the corresponding GPCR blockers (losartan, SR49059 or BQ123), suggesting that AGII type 1 receptor (AT_1R), AVP V1a receptor, and ET_A receptor are the respective mediators of AGII, AVP and ET1 calcium signalling in BeWo cells. Such elevations in fura-2 ratio by AGII, AVP and ET1 were also abolished when BeWo cells were pre-incubated with tetracaine or ryanodine (100 μM). These experiments, therefore, demonstrated that functional RyRs in BeWo cells are involved in signal transduction initiated by AGII, AVP or ET1 via extracellular stimulation of GPCRs, ie. the activated RyRs are the mediators of subseqent Ca^{2+} mobilisation in BeWo cells in these events.

Studies using radioactive ligand binding assays have indicated that the AGII type 1 receptor (AT_1R) is the major AGII receptor of the placenta; whereas there is only 0 to 10% of AGII receptors were identified as the type 2 (AT_2R) subtype in the human placenta (Jiménez *et al.*,1996; Kalenga *et al.*,1996). Recently, expression of AT_4R, a specific receptor for angiotensin (3-8) (AngIV) has been identified in human placenta, along with AT_1R and AT_2R throughout both normal pregnancy and pre-eclampsia (Williams *et al.*,2010). Location of AT_1R in EVTs suggests the role of AGII in trophoblastic invasion and vaso-remodelling (Pringle *et al.*,2011). It has been demonstrated that BeWo choriocarcinoma cells express AT_1R that activates PKC-mediated ERK signalling pathways and phosphatidylinositol 3-kinase (PI3K)

pathways (Ino *et al.*,2003; Ishimatsu *et al.*,2006). The activation of RyRs by CaMKII phosphorylation therefore, is expected as a consequence of AT_1R activation by AGII via PKC-activation in BeWo cells, as illustrated in Figure 1.8. JEG-3 cells do not express the endogenous angiotensinogen mRNA (Brasier *et al.*,1989). However, the expression of angiotensin receptor protein is controversial in JEG-3 cells, as the presence of mRNA and protein of both AT_1R and AT_2R was demonstrated (Lanz *et al.*,2003). In current study, there was no increase in fura-2 ratio observed during AGII stimulation in JEG-3 cells. Such absence of response may due to absence of AT_1R-mediated signalling, or due to the activation of AT_2R in the membrane that inhibits cAMP-mediated pathways. The $G_{i/o}$-coupled GPCR AT_2R is distinct from that linked to AT_1R. The activation of AT_2R by AGII induces opposing actions of AT_1R, such as vasodilation, inhibition of cell proliferation and induction of programmed cell death (Horiuchi *et al.*,1999; de Gasparo *et al.*,2000). One consequence of such growth-inhibitory effects of AT_2R is the subsequent activation of a variety of phosphatases that protentially dephosphorylate RyRs and result in inhibition of Ca^{2+} release from the receptor channel, as reviewed in Introduction Section 1.8.

There are two subtypes of GPCRs that mediate the action of endothelins (ET1, ET2 and ET3). Of these, ET_AR has a higher affinity for ET1 than ET3, while ET_BR display similar binding affinity for both ET1 and ET3 (Sakurai *et al.*,1990). The effect of ET1 is primarily through the activation of ET_AR that subsequently triggers various subcellular events via different G protein-mediated signaling pathways, as reviewed by Bagnato and Rosanò (Bagnato & Rosanò,2008). Ligand binding studies using ^{125}I-labeled ET1 identified the expression of ET_AR and ET_BR in the microvillous membrane of early gestation placental microvilli, while only ET_BR was found in term placental microvilli (Rutherford *et al.*,1993; Mondon *et al.*,1998). In other words, the receptor ET_BR has been detected in trophoblastic cells throughout gestation (Kilpatrick *et al.*,1993), in contrast to the differential expression pattern of ET_AR during the developing placenta (Cervar *et al.*,2000). The expression of ET_AR and ET_BR has also been demonstrated in both BeWo and JEG-3 cells (Mauschitz *et al.*,2000), although the mRNA levels of both ET receptors in these chriocarcinoma cell lines were lower than in their nonmalignant tissue of origin (the trophoblast)

(Bilban *et al.*,2000). Moreover, both BeWo and JEG-3 cell lines secrete ET1 (Mauschitz *et al.*,2000). The presence of both ET receptors and ET1 secretion has been linked to the auto-/paracrine action and growth promotion effect of ET1 in human cancer cell lines (Shichiri *et al.*,1991; Bagnato *et al.*,1997).

Both AT_1R and ET_AR are GPCRs coupled to $G\alpha_q$; PLC is one of the effector proteins that mediate $G\alpha_q$-coupled GPCR responses (de Gasparo *et al.*,2000). Therefore, activation of AT_1R and ET_AR can lead to intracellular Ca^{2+} mobilisation and activation of PKC signaling cascade, as reviewed in Introduction Section 1.8. To investigate whether inhibition of PLC could also block $[Ca^{2+}]_i$ increase, the well known PLC inhibitor U73122 (1 μM) was initially used coupled to peptide stimulation. However, U73122 induced rise in fura-2 ratio in its own right, indicated by an increase in $[Ca^{2+}]_i$ (data not shown), as similarly seen in other reports (Klein *et al.*,2011). Therefore, the PLC-mediated downstream signaling cascade could not be examined by using U73122. Interestingly, AGII and ET1 stimulation in BeWo cells induced similar $[Ca^{2+}]_i$ responses, as slow and prolonged elevations in $[Ca^{2+}]_i$ took place when AGII and ET1 were added. These observations might suggest that common signaling pathways may be shared by different extracellular stimulating agents. According to the Ca^{2+} concentration gradients across membrane and cellular compartments (as reviewed in Introduction), it is possible that both intracellular stores and the extracellular space are sources for intracellular Ca^{2+} increases in response to these hormones. As illustrated in Figure 1.8, there are two pathways leading to Ca^{2+} mobilisation initiated by $G\alpha_q$-mediated GPCR activation: 1) Ca^{2+} influx via activation of either or both TRPC and L-type calcium channel (LTCC) on the plasma membrane; 2) Ca^{2+} release from internal stores via activation of either or both IP_3Rs and RyRs. To verify the source(s) of such Ca^{2+} increases, channel blockers were co-applied with stimulating agents. Blockade of LTCC-mediated Ca^{2+} influx with nifedipine pre-incubation caused little reduction on either AGII- or ET1-induced $[Ca^{2+}]_i$ elevation, suggesting that LTCC-mediated Ca^{2+} influx contributes little to the rise of $[Ca^{2+}]_i$ upon AGII or ET1 stimulation in BeWo cells. The commonly used IP_3R blocker 2-aminoethoxydiphenyl borate (2-APB) was initially used to examine the contribution of the IP_3R-mediated pathway in trophoblast peptide hormone induced calcium signals. However, an unexpected rise in $[Ca^{2+}]_i$

was observed in response to this molecule (data not shown), as reported by other groups (Bootman *et al.*,2002; Lefièvre *et al.*,2012). As both AGII- and ET1-induced $[Ca^{2+}]_i$ elevations were completely abolished in cells pre-incubated with tetracaine or ryanodine (100 μM), these results suggesting that RyR-mediated Ca^{2+} release makes a major contribution to Ca^{2+} rises in these cells. This finding is consistent with the cytofluorimetric analysis by Niger and colleagues, in which nifedipine (10^{-6} M) did not reduce ET1-induced Ca^{2+} entry in cultured human trophoblastic cells (Niger *et al.*,2004). Two mechanisms of RyR activation may be possible during the alteration of Ca^{2+} homeostasis following by GPCR activation: 1) CICR induced by the initial rise of $[Ca^{2+}]_i$ from the activation of IP_3R and/or Ca^{2+} entry via membrane Ca^{2+} channels; 2) phosphorylation of RyRs by activated CaMII, PKC and/or PKA (via AC activation via $G\alpha_s$-GPCR), as reviewed in Introduction Section 1.8. Collectively, these observations in BeWo cells upon AGII or ET1 stimulation suggest that RyRs contribute the cellular Ca^{2+} mobilisation; this Ca^{2+} release function of RyR may participate in the signal transduction of AGII and ET1, with an impact on trophoblastic invasion, vaso-remodeling, hormonal secretion and growth promotion (Cervar & Desoye,1998; Pringle *et al.*,2011).

Although Ca^{2+} release via RyR activation contribute to both AGII- and ET1-induced Ca^{2+} elevation, the possibility of Ca^{2+} entry via other mediators on the cell membrane cannot be excluded. Possible candidates that mediate the Ca^{2+} entry include the voltage-independent Ca^{2+} channels. For instance, both store-operated Ca^{2+} channel (SOCC, eg. TRPC) and non-seletive cation channel (NSCC) mediated Ca^{2+} entry may contribute the Ca^{2+} current, together with LTCC during AGII/ET1 stimulation, as both SOCC and NSCC have been demonstrated to mediate Ca^{2+} entry in human placental trophoblastic cells (Clarson *et al.*,2003; Niger *et al.*,2004). The current study did not investigate the connection between peptide hormone-evoked Ca^{2+} current and membrane Ca^{2+} entry pathways in trophoblast. To identify whether extracellular Ca^{2+} entry is involved in the rise of $[Ca^{2+}]_i$ in response to AGII or ET1 stimulation of BeWo cells, the Ca^{2+} chelator ethylene glycol tetraacetic acid (EGTA) may be applied to remove extracellular Ca^{2+}. Further investigation may also use of specific blockers/inhibitors of SOCC and NSCC.

AVP-evoked Ca^{2+} elevations displayed distinct profiles from those of AGII or ET1 in BeWo cells. Instead of a slow prolonged $[Ca^{2+}]_i$ increase, a transient $[Ca^{2+}]_i$ rise occurred upon AVP stimulation, as indicated by a transient increase in fura-2 signal before a return to resting levels (Figure 4.6.2.). Among AVP receptors, both V1a and V1b are GPCRs couple to $G\alpha_q$, whereas V2 is a $G\alpha_s$-coupled GPCR. In the current study, transient $[Ca^{2+}]_i$ elevation in response to AVP stimulation were observed in trophoblast-like cells, the BeWo cells. The absence of response in the presence of V1a blocker (SR49059) suggests that the V1a receptor mediates subsequent signalling. The co-application of AVP in the presence of the RyR antagonist (tetracaine or 100 μM ryanodine) abolished the fura-2 ratio. This observation implicates the involvement of RyR-mediated Ca^{2+} mobilisation in AVP-stimulated signaling events; this finding is also consistent with the study by Chou and colleagues. The authors reported that RyR-mediated Ca^{2+} cellular mobilization (together with CaM) is crucial for AVP-induced aquaporin 2 (AQP2)-contained vesicles trafficking in primary cultures of inner medullary collecting duct cells, as ryanodine at 100 μM concentration blocked the process (Chou *et al.*,2000). These authors have also demonstrated that neither IP_3R-mediated Ca^{2+} release nor extracellular Ca^{2+} are involved in the process of AVP-stimulated Ca^{2+} mobilization pathway in the renal collecting duct (Chou *et al.*,1998; Chou *et al.*,2000).

Although there are no detailed studies reporting the expression of AVP receptors in the human placenta, mRNAs encoding both V1a and V2 were detected in the developing ewe placenta (Koukoulas *et al.*,2003). In addition, an *in vitro* study demonstrated that expression of AQP1 gene in JEG-3 cells is up-regulated by AVP in a cAMP-dependent pathway, suggested that AVP regulated AQP1 expression is mediated by the activation of $G\alpha_s$-coupled GPCR (ie. via V2 receptor) in JEG-3 trophoblast-like cells (Belkacemi *et al.*,2008). Such a cAMP-dependent AQP expression pathway has also been demonstrated in the apical membrane of human SCT explants, where hCG enhances the expression and function of AQP9 via the cAMP pathways (Marino *et al.*,2010). These studies suggest that the cAMP-mediated cascades in trophoblast can be triggered by various stimulating agents via $G\alpha_s$-mediated GPCR. Such $G\alpha_s$-mediated GPCR processes lead to AC activation and cAMP elevation. Both PKA and EPAC are cAMP effector proteins that

independently conduct cAMP-sensitive downstream signaling cascades. In inner medullary collecting duct cells, the process of AQP2 exocytosis is EPAC-mediated, inducing Ca^{2+} mobilisation via RyR activation (Yip,2006). In cardiac myocytes, the EPAC-PLCξ-PKCξ-CaMKII cascade has been established as a cellular Ca^{2+} handling pathway that enhances RyR2 opening (Oestreich *et al.*,2007). This $G\alpha_s$-initiated EPAC-mediated signaling cascade has been demonstrated to result in phosphorylation of PLN, which subsequently relieves the inhibitory effect on SERCA, ie. enhances Ca^{2+} reuptake (Oestreich *et al.*,2007).

In the current study, there was no change in fura-2 ratio observed upon addition of AGII, ET1 or AVP in JEG-3 cells. These observation may reflect a dynamic balance of $[Ca^{2+}]_i$ in JEG-3 cells upon activation of different GPCRs. In other words, the signals lead to $[Ca^{2+}]_i$ increase via activations of $G\alpha_q$-PLC-PKC and $G\alpha_s$-cAMP-PKA pathways, might be compensated by signals that lead to $[Ca^{2+}]_i$ decrease via suppression of cAMP production. Particularly, as reviewed by Tanfin *et al*. (Tanfin *et al.*,2011), the activation of $G\alpha_{i/o}$-coupled ET_AR leads to the inhibition of cAMP production. During the stimulation of ET1 in JEG-3 cells, the possible activation of $G\alpha_{i/o}$-coupled to ET1-$ET_{A/B}R$ results in decrease of cAMP production that directly affects PKA-mediated signaling pathways acting on phosphorylation of RyR, CaMKII and LTCC. The signaling events initiated by AVP possibly involve activation of $G\alpha_s$-coupled GPCR, and the subsequent activation may involve phosphorylation of RyR, PLN and LTCC. All these downstream signaling pathways exert complex effects on global $[Ca^{2+}]_i$, hence, changes in fura-2 ratio. On the other hand, the intracellular buffering effect of fura-2 may also result in no detection of change in ratio. As fura-2 is a high-affinity Ca^{2+} indicator (Kd ≈ 224 nM), small changes in $[Ca^{2+}]$ in dye-loaded cells may be buffered (Hofer & Machen,1994). Moreover, other studies indicate that Ca^{2+}-buffering capacity of fura-2 at commonly used concentrations is 10-20% of the intrinsic buffering power of the cytosol in smooth muscle cells (Becker *et al.*,1988). Therefore, if the change in $[Ca^{2+}]_i$ is too small, too local and/or too transient in JEG-3 cells upon stimulation by endogenous peptides (AGII, AVP and ET1), Ca^{2+} indicator with lower affinity may be use in such conditions.

5.4 Other Possible Mechanism of RyR-mediated Ca^{2+} Mobilisation

The endogenous production of NO is involved in multiple functional regulation in the placenta, including vascular tone maintainance (Poston,1997; Lopez-Jaramillo *et al.*,2008), EVT invasion (Lyall *et al.*,1999); hormonal release (Ni *et al.*,1997; Rossmanith *et al.*,1999); and placental glucose uptake (Acevedo *et al.*,2005). Therefore, dysregulated NO-related signals are thought to be associated with pathlogical conditions in pregnancy, such as PE (Gilbert *et al.*,2008). NO-induced signals have been shown to couple to Ca^{2+} mobilisation, as stated in Introduction Section 1.9. Briefly, as summarised in Figure 1.9: NO initiates GC activation and cGMP production which activates PKG that in turn triggers the synthesis of two Ca^{2+} mobilising molecules NAADP and cADPR. Both NAADP and cADPR are potent Ca^{2+} mobilising inducers, and their subsequent actions can also indirectly result in RyR-mediated Ca^{2+} release from the ER (Figure 5.4, *cream zone*). Therefore, the potential contribution of both NAADP and cADPR to the modulation of global Ca^{2+} dynamics cannot be ignored. Particularly, synthesis of cADPR is favoured at physiological pH (Lee,1997).

The ADPR cyclase homolog CD38 is present on the surface of many human cells, including decidual granulated lymphocytes (Bulmer *et al.*,1988; Fernàndez *et al.*,1998). CD38 is a multi-functional enzyme that not only catalyses the production of cADPR but also serves as a permeating channel for cADPR, as reviewed by Lee (Lee,2000a). Therefore, cADPR could be available in placental trophoblast by either or both endogenous synthesis and transport via cADPR channels. In BeWo CT-like cells, self-production of NO has been described (Sooranna & Das,1995); inhibited Ca^{2+}/CaM-dependent NOS activity has been reported in the presence of L-arginine analog in these cells (Myat-Thanda *et al.*,1996). Collectively, these observations suggest NO-induced/cADPR-activated signals contribute to global Ca^{2+} mobilisation in BeWo cells.

Although the activation of the NO-induced cGMP-mediated pathway is independent to the GPCR-coupled pathways, such as the $G\alpha_q$-PLC-PKC and $G\alpha_s$-cAMP-PKA pathways mentioned in previous section; downstream signalling

regulation can be modified by cross-pathway interactions (Figure 5.4). For example, prostaglandin E2-induced angiogenesis involves activation of NO-cGMP pathway through PKA/PI3K/Akt (PKB)-dependent increase in eNOS activity (Namkoong *et al.*,2005; Hashimoto *et al.*,2006); in human umbilical vein endothelial cells, independent of the PI3K-Akt pathway, activation of 5'-AMP-activated protein kinase (AMPK) results in eNOS phosphorylation, hence activation of NO-cGMP pathway (Thors *et al.*,2004); these studies suggest that PKA signalling converges on the activation of eNOS and NO-induced cascade through the activation of other pathways (eg. Akt and AMPK), as reviewed by Bir *et al*. (Bir *et al.*,2012) (Figure 5.4, *pink zone*). It has been demonstrated that both PLC-β2 and PLC-β3 are directly phophorylated by PKG *in vitro* by purified proteins and *in vivo* with metabolic labelling; the phosphorylation of PLC by PKG therefore, blocks the activation of $G\alpha_q$-PLC-PKC pathway and results in inhibition of IP_3-dependent Ca^{2+} release (Xia *et al.*,2001). Although the cGMP-mediated pathway is in parallel to the cAMP-mediated pathway, the activation of either could trigger the ERK1/2 cascade (Figure 5.4, *cream zone* and *blue zone*, respectively). NO-induced cGMP-mediated signalling has been shown to stimulate the phosphorylation of ERK1/2 that results in cell migration in rat mammary tumours C3L5 cells and in human lung carcinoma A549 cells (Jadeski *et al.*,2003; Punathil & Katiyar,2009). Moreover, communication between downstream mediators that correspond to cAMP- or cGMP- mediated pathways has also been demonstrated. In cardiomyocytes, phosphodiesterases (PDEs) modulate crosstalk and feedback signalling through cAMP, cGMP and their associated protein kinases PKA and PKG, resepectively; these signalling mediators modify calcium transient and cardiac contractility by subsequent modulation of their downstream regulators including VGCC, RyR, SERCA and PLN, as reviewed by Rao and Xi (Rao & Xi,2009). Therefore, the experimental measurement of change in $[Ca^{2+}]_i$ reflect the end result of global Ca^{2+} mobilisation via independently activated but converging pathways.

In the current study, although there was no direct demonstration of activation of AVP-stimulated $G\alpha_s$-coupled pathway, changes in fura-2 ratio observed could result from the complexity of signalling crosstalk. A transient increase followed by the recovery to near initial fura-2 ratio was observed in during AVP stimulation. This

observation was different from that in AGII or ET1 stimulation in BeWo cells where no recovery of signal was observed. The initial rise of ratio may be due to the activation of $G\alpha_s$-cAMP-PKA pathway leading to the activation of RyR channel and release of ER Ca^{2+}; the drop of ratio may be due to the Ca^{2+} reuptake via subsequent PLN phosphoryaltion and SERCA activation (Figure 5.4, *pink zone*). Since BeWo cells are capable of NO production by eNOS (Kiss *et al.*,1998; Cha *et al.*,2001), signals converging on the activation of eNOS is possible in these cells (Figure 5.4 *cream zone*). The activation of PKG-mediated pathway results in subsequent inhibition of PLC-PKC pathway may also contribute to current observation (Figure 5.4 *blue zone*). Collectively, upon AVP stimulation in BeWo cells, activation of GPCRs could initially split into two pathways: 1) stimulation of V1a/b results activation of $G\alpha_q$-PLC-PKC pathway, in which, PLC results IP_3R-mediated Ca^{2+} release and possibly CICR via RyR; while PKC phosphorylates CaMKII resulting in RyR-mediated Ca^{2+} release; 2) PKC may also activate EPAC, results in PLN phosphorylation and Ca^{2+} reuptake via SERCA; while PKA activates CaMKII and promotes RyR-mediated Ca^{2+} release; it also activates eNOS and promotes NO-induced pathway via activation of PKG. The PKG-mediated pathway involves activation of cADPR-induced Ca^{2+} release via RyR and inhibition of PLC-PKC pathway that result in inhibitory IP_3R-mediated Ca^{2+} release. Therefore, further suppression of fura-2 ratio in AVP-treated dantrolene-preincubated BeWo cells suggesting that Ca^{2+} reuptake was promoted upon stimulation of GPCRs in these cells with RyRs blocked by dantrolene. The mechanism of enhancement of Ca^{2+} reuptake probably involves activation of the $G\alpha_s$-cAMP-PKA-EPAC-PKC-PLN pathway, while inhibitory mechanisn of Ca^{2+} release probably involves NO-induced PKG-meidated inhibition on PLC-PKC pathway, via PKA stimulated eNOS activation. Taken together, the observation of change in fura-2 ratio in BeWo cells upon AVP stimulation implicate a potential role of RyR in participation of gene expression and water homeostasis in trophoblast during gestation in response to AVP (Belkacemi *et al.*,2008).

Figure 5.4. Putative mechanisms triggering RyR-mediated Ca^{2+} mobilisation in trophoblasts.

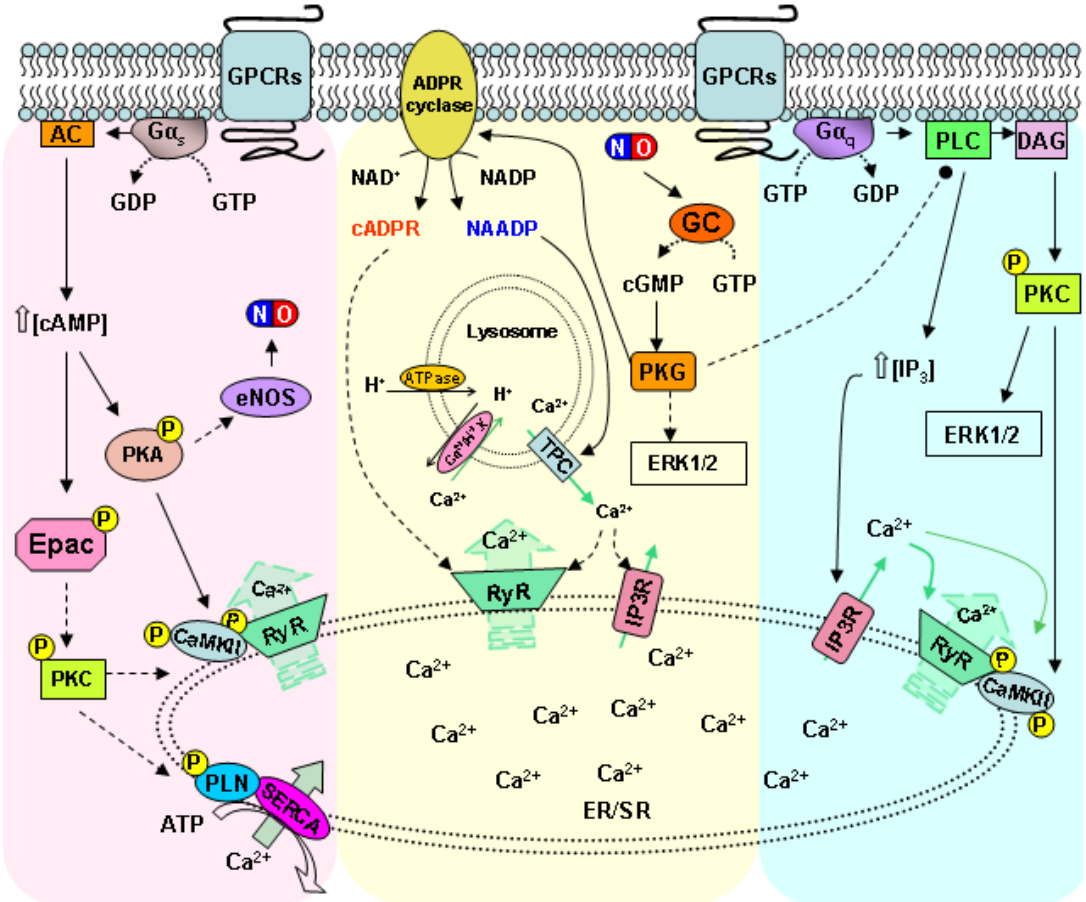

Figure 5.4. Possible Ca^{2+} mobilisation initiated by activation of GPCRs. Stimulation of $G\alpha_s$-coupled receptors, such as βAR and V2, leads to the activation of AC. The subsequent elevation of cAMP results in various cellular events via different signalling pathways (*left, pink zone*): 1) Augmentation of cAMP causes PKA phosphorylation; activated PKA leads to phosphorylation of RyRs and ER Ca^{2+} release; PKA can also converge on the activation of eNOS, as reviewed by Bir *et al*. (Bir *et al.*,2012); 2) Independent of PKA activation, cAMP also activates EPAC, mediates CICR from RyR via activation of PKC and CaMKII; another downstream effector of EPAC is PLN; phosphorylated PLN promotes SERCA activation and Ca^{2+} re-uptake. The nitric oxide (NO)-induced signalling pathways (*middle, cream zone*), catalysed by nitric oxide synthase (NOS) which is acitivated through the PKA pathway; NO activates soluble guanylate cyclase (GC) and produces intracellular cyclic guanosine monophosphate (cGMP) (Murad,1994). Elevated cGMP activates cGMP-dependent kinase (PKG); 1) PKG phosphorylates ADP-ribosyl cyclase (ADPR cyclase); activated ADPR cyclase in turn produces cyclic ADP-ribose (cADPR) and/or nicotinic acid adenine dinucleotide phosphate (NAADP) (Lee *et al.*,1989). NAADP targets on lysosmal two-pore channel (TPC) to release Ca^{2+}, which subsequently results in CICR possibly via endoplasmic RyR and/or IP_3R (Lee,1997). cADPR targets on the ER Ca^{2+} release channel RyR; 2) PKG also could trigger ERK1/2 cascade, and 3) mediate inhibition of PLC-PKC pathway. Signalling pathways initiated by activation of $G\alpha_q$-coupled receptors, such as αAR, AT_1R, ET_AR and V1, are mediated through PLC activation (*right, blue zone*): the activation of PLC leads to the production of DAG and IP_3. 1) IP_3 activates IP_3R channel and mediates Ca^{2+} mobilisation; Ca^{2+} can stimulate RyR channel directly through the CICR mechanism; 2) DAG activates PKC, leading to CaMKII activation, which subsequently phosphorylates RyR in the presence of Ca^{2+}; PKC also triggers ERK1/2 signalling cascade; the activation of both CaMKII and ERK1/2 leads to gene transcription.

Chapter VI.

Conclusion

Chapter VI. Conclusion

In summary, the major findings in present study are 1) BeWo and JEG-3 trophoblastic cells express functional RyRs that respond to several pharmacological agents; 2) in BeWo cells, the activation of RyRs was demonstrated to contribute to the rise of $[Ca^{2+}]_i$ induced by endogenously occuring peptides AGII, AVP and ET1; mechanisms contributing to the increase of $[Ca^{2+}]_i$ possibly involve GPCR-activated and NO-induced signaling cascades 3) both BeWo and JEG-3 cells express the RyR accessory proteins: CSQ and TRD; 4) human first trimester and term placental villi express RyR1 and RyR3, while RyR2 might be transiently expressed and highly associated with trophoblast differentiation; 5) human first trimester and term placental villous tissues were demonstrated to express TRD by IHC, while CSQ was detected in human term placental villi samples by western blotting.

Taken together, observations from the current study suggest that RyR are actively involved in human trophoblast Ca^{2+} mobilisation. Extracellular stimulating agents such as hCG, AGII, AVP, and ET1 are possible endogenous triggers of such RyR-mediated trophoblastic Ca^{2+} mobilisation.This is the first study provides direct evidence of RyR expression at both mRNA and protein levels in human trophoblast-like cells. The experimental results have shown that RyRs are capable of Ca^{2+} release upon direct pharmacological stimulation of the channel. The preliminary results also demonstrated RyR-mediated Ca^{2+} releasing in response to indirect stimulation via GPCR activation. However, the exact mechanism of interaction between RyR and GPCR is unknown; also, the possible participation of NO-induced cADPR-stimulated Ca^{2+} release via RyR has not been examined. Further investigation is required for the identification of downstream signaling mediators. For instance, cAMP-dependent $G\alpha_s$-mediated pathway splits into two sub-pathways: the PKA- and EPAC- dependent pathways; and the activation of PKA may also induce PKG-mediated cADPR-induced Ca^{2+} mobilisation and PKG-induced inhibition of PLC-PKC pathway. Therefore, specific inhibitors of PKA, EPAC, PKG and cADPR analogs may be induced to identify the exact cascade leads to RyR-sensitive Ca^{2+} releasing. In the current study, it has been demonstrated that LTCC is not involved in such process in BeWo cells; studies in cultured primary human trophoblastic cells also indicate that LTCC do not

participate in ET1-induced Ca^{2+} entry (Niger *et al.*,2004). As both voltage-independent Ca^{2+} channels such as SOCC and NSCC have been demonstrated to mediate Ca^{2+} entry in human placental trophoblastic cells (Clarson *et al.*,2003; Niger *et al.*,2004), the possible involvement of SOCC and NSCC in connection with GPCR-induced RyR-mediated Ca^{2+} release may be a worthy subject for further investigation to complete the Ca^{2+} trans-trophoblastic mobilisation theory. Furthermore, the mechanism of Ca^{2+} extrusion at the basal membrane in contact with fetal circulation has not been fully established. Although the involvement of PMCA and NCX has been proposed, and PMCA has been demonstrated to play a major role (Moreau *et al.*,2003a; Moreau *et al.*,2003b), the exact mechanism of how PMCA cooperate with Ca^{2+} binding proteins is unknown. In addition to the RyR-mediated Ca^{2+} mobilisation pathway as proposed in previous paragraph, evidence of co-localisation of RyRs and PMCA are essential to fulfill the proposal.

The predominant Ca^{2+} trans-trophoblastic transport theory is in favour of the Ca^{2+} binding and shuttling pathway, due to the high expression levels of different Ca^{2+} binding proteins in human trophoblast (Belkacemi *et al.*,2002), as reviewed by Belkacemi and colleagues (Belkacemi *et al.*,2005). The current study provided evidence of the possible involvement of RyR in an alternative pathway, ie. the RyR-mediated Ca^{2+} transport pathway, in additional to the 'binding and shuttling' pathway for Ca^{2+} trans-trophoblastic transport. The current study is still at preliminary stage of this proposal. However, the demonstration of RyR involvement in trophoblastic cell Ca^{2+} mobilisation suggests these calcium channels participate in maternal-fetal Ca^{2+} transport. Examination of RyRs and/or RyR accessory proteins in primary trophoblast cells may provide better understanding on IUGR, and/or other pregnancy-related diseases such as maternal diabetes that linked to fetal hypocalcaemia (Strid *et al.*,2003). The Ca^{2+} release channel RyR is regulated and targeted by multiple molecules. Therefore, RyR could be a multiple participant in the regulation of trophoblastic cell function. As discussed in previous section, RyR may be involved in trophoblastic invasion, hormonal secretion, gene expression and growth promotion. Such outcomes of RyR activation should also be considered in future studies and experimental design.

In conclusion, the current study demonstrated that functional RyRs are expressed in human trophoblast, and these Ca^{2+} release channels are sensitive to RyR agonists and antagonists in both BeWo and JEG-3 cells; RyR-mediated Ca^{2+}

mobilisation was also demonstrated in BeWo cells in response to endogenously occurring peptides (AGII, AVP and ET1), suggesting that RyRs contribute not only in trophoblastic cellular Ca^{2+} homeostasis, but also in cell function in connection with these hormonal induced events.

References

Aarhus R, Graeff R, Dickey D, Walseth T & Lee H (1995). ADP-ribosyl cyclase and CD38 catalyze the synthesis of a calcium-mobilizing metabolite from NADP. *J. Biol. Chem.* **270**: 30327–33.

Acevedo C, Márquez J, Rojas S & Bravo I (2005). Insulin and nitric oxide stimulates glucose transport in human placenta. *Life Sci.* **76**: 2643-53.

Ahern G, Junankar P & Dulhunty A (1997). Subconductance states in single-channel activity of skeletal muscle ryanodine receptors after removal of FKBP12. *Biophys J.* **72**: 146-62.

Al-Nasiry S, Spitz B, Hanssens M, Luyten C & Pijnenborg R (2006). Differential effects of inducers of syncytialization and apoptosis on BeWo and JEG-3 choriocarcinoma cells. *Hum Reprod.* **21**: 193-201.

Aplin J (1991). Implantation, trophoblast differentiation and haemochorial placentation: mechanistic evidence in vivo and in vitro. *J Cell Sci.* **99**: 681-92.

Aracena P, Tang W, Hamilton S & Hidalgo C (2005). Effects of S-glutathionylation and S-nitrosylation on calmodulin binding to triads and FKBP12 binding to type 1 calcium release channels. *Antioxid Redox Signal.* **7**: 870-81.

Ariel I, Hochberg A & Shochina M (1998). Endothelial nitric oxide synthase immunoreactivity in early gestation and in trophoblastic disease. *J Clin Pathol* **51**: 427–431.

Ashley RH & Williams AJ (1990). Divalent cation activation and inhibition of single calcium release channels from sheep cardiac sarcoplasmic reticulum. *J Gen Physiol* **95**: 981-1005.

Ayuk P, Sibley C, Donnai P, D'Souza S & Glazier J (2000). Development and polarization of cationic amino acid transporters and regulators in the human placenta. *Am J Physiol Cell Physiol.* **278**: C1162-71.

Babalola G, Coutifaris C, Soto E, Kliman H, Shuman H & Strauss Jr (1990). Aggregation of dispersed human cytotrophoblastic cells: lessons relevant to the morphogenesis of the placenta. *Dev Biol.* **137**: 100-8.

Baczyk D, Kingdom J & Uhlén P (2011). Calcium signaling in placenta. *Cell Calcium.* **49**: 350-6.

Bagnato A & Rosanò L (2008). The endothelin axis in cancer. *Int J Biochem Cell Biol.* **40**: 1443-51.

Bagnato A, Tecce R, Di Castro V & Catt K (1997). Activation of mitogenic signaling by endothelin 1 in ovarian carcinoma cells. *Cancer Res.* **57**: 1306-11.

Balschun D, Wolfer D, Bertocchini F, Barone V, Conti A, Zuschratter W, Missiaen L & Lipp H (1999). Deletion of the ryanodine receptor type 3 (RyR3) impairs forms of synaptic plasticity and spatial learning. *EMBO J.* **18**: 5264-73.

Bamberger A, Koglin M, Kempfert J, Löning T, Scholz H & Behrends S (2001). Expression and tissue localization of soluble guanylyl cyclase in the human placenta using novel antibodies directed against the alpha(2) subunit. *J Clin Endocrinol Metab.* **86**: 909-12.

Barg S, Copello JA & Fleischer S (1997). Different interactions of cardiac and skeletal muscle ryanodine receptors with FK-506 binding protein isoforms. *Am J Physiol.* **272**: C1726-33.

Baylis S, Strijbos P, Sandra A, Russell R, Rijhsinghani A, Charles I & Weiner C (1999). Temporal expression of inducible nitric oxide synthase in mouse and human placenta. *Mol Hum Reprod.* **5**: 277-86.

Becker PL, Walsh JV, Singer JJ & Fay FS (1988). Calcium buffering capacity, calcium currents, and [Ca2+] changes in voltage clamped, fura-2 loaded single smooth muscle cells. *Biophys. J.* **53**: 595a.

Belkacemi L, Beall M, Magee T, Pourtemour M & Ross M (2008). AQP1 gene expression is upregulated by arginine vasopressin and cyclic AMP agonists in trophoblast cells. *Life Sci.* **82**: 1272-80.

Belkacemi L, Bedard I, Simoneau L & Lafond J (2005). Calcium channels, transporters and exchangers in placenta: a review. *Cell Calcium.* **37**: 1-8.

Belkacemi L, Simoneau L & Lafond J (2002). Calcium-binding proteins: distribution and implication in mammalian placenta. *Endocrine.* **19**: 57-64.

Berridge M (1993). Inositol trisphosphate and calcium signalling. *Nature.* **361**: 315-25.

Berridge M, Lipp P & Bootman M (2000). The versatility and universality of calcium signalling. *Nat Rev Mol Cell Biol.* **1**: 11-21.

Berridge MJ (1997). Elementary and Global Aspects of Calcium Signalling. *J Physiol.* **499**: 291-306.

Berridge MJ, Bootman MD & Roderick HL (2003). Calcium signalling: dynamics, homeostasis and remodelling. *Nat. Rev. Mol. Cell. Biol.* **4**: 512-29.

Bers D (2002). Cardiac excitation-contraction coupling. *Nature.* **415**: 198-205.

Bers D & Stiffel V (1993). Ratio of ryanodine to dihydropyridine receptors in cardiac and skeletal muscle and implications for E-C coupling. *Am J Physiol.* **264**: C1587-93.

Bertocchini F, Ovitt C, Conti A, Barone V, Schöler H, Bottinelli R, Reggiani C & Sorrentino V (1997). Requirement for the ryanodine receptor type 3 for efficient contraction in neonatal skeletal muscles. *EMBO J.* **16**: 6956-63.

Beutner G, Sharma V, Giovannucci D, Yule D & Sheu S (2001). Identification of a ryanodine receptor in rat heart mitochondria. *J Biol Chem.* **276**: 21482-8.

Bhat MB, Zhao J, Hayek S, Freeman EC, Takeshima H & Ma J (1997). Deletion of amino acids 1641-2437 from the foot region of skeletal muscle ryanodine receptor alters the conduction properties of the Ca release channel. *Biophys J* **73**: 1320-8.

Bilban M, Barth S, Cervar M, Mauschitz R, Schaur R, Zivkovic F & Desoye G (2000). Differential regulation of endothelin secretion and endothelin receptor mRNA levels in JAR, JEG-3, and BeWo choriocarcinoma cell lines and in human trophoblasts, their nonmalignant counterpart. *Arch Biochem Biophys.* **382**: 245-52.

Bir S, Xiong Y, Kevil C & Luo J (2012). Emerging role of PKA/eNOS pathway in therapeutic angiogenesis for ischaemic tissue diseases. *Cardiovasc Res.* **95**: 7-18.

Bootman M, Collins T, Mackenzie L, Roderick H, Berridge M & Peppiatt C (2002). 2-aminoethoxydiphenyl borate (2-APB) is a reliable blocker of store-operated Ca2+ entry but an inconsistent inhibitor of InsP3-induced Ca2+ release. *FASEB J.* **16**: 1145-50.

Bourne H, Sanders D & McCormick F (1991). The GTPase superfamily: conserved structure and molecular mechanism. *Nature.* **349**: 117-27.

Boyd JD & Hamilton WJ (1970). THE HUMAN PLACENTA, Heffer, Cambridge.

Brasier A, Tate J, Ron D & Habener J (1989). Multiple cis-acting DNA regulatory elements mediate hepatic angiotensinogen gene expression. *Mol Endocrinol.* **3**: 1022-34.

Bruno A, Huang J, Bennett D, Marr R, Hastings M & Stutzmann G (2011). Altered ryanodine receptor expression in mild cognitive impairment and Alzheimer's disease. *Neurobiol Aging.* **33**: e1-6.

Buck E, Zimanyi I, Abramson J & Pessah I (1992). Ryanodine stabilizes multiple conformational states of the skeletal muscle calcium release channel. *J Biol Chem.* **267**: 23560-7.

Budik S, Palm F, Walter I, Helmreich M & Aurich C (2012). Increasing expression of oxytocin and vasopressin receptors in the equine conceptus between Days 10 and 16 of pregnancy. *Reprod Fertil Dev.* **24**: 641-8.

Bulmer J, Pace D & Ritson A (1988). Immunoregulatory cells in human decidua: morphology, immunohistochemistry and function. *Reprod Nutr Dev.* **28**: 1599-613.

Calcraft P, Ruas M, Pan Z, Cheng X, Arredouani A, Hao X, Tang J, Rietdorf K, Teboul L, Chuang K, Lin P, Xiao R, Wang C, Zhu Y, Lin Y, Wyatt C, Parrington J, Ma J, Evans A, Galione A & Zhu M (2009). NAADP mobilizes calcium from acidic organelles through two-pore channels. *Nature.* **459**: 596-600.

Camacho P & Lechleiter J (1995). Calreticulin inhibits repetitive intracellular Ca^{2+} waves. *Cell.* **82**: 765-71.

Carter S, Colyer J & Sitsapesan R (2006). Maximum phosphorylation of the cardiac ryanodine receptor at serine-2809 by protein kinase a produces unique modifications to channel gating and conductance not observed at lower levels of phosphorylation. *Circ Res.* **98**: 1506-13.

Cazorla O, Lucas A, Poirier F, Lacampagne A & Lezoualc'h F (2009). The cAMP binding protein Epac regulates cardiac myofilament function. *Proc Natl Acad Sci U S A.* **106**: 14144-9.

Cervar M & Desoye G (1998). The endothelin/ endothelin receptor system of human trophoblast in normal an pre-eclamptic pregnancies: A review. *Placenta* **19**: 341-357.

Cervar M, Huppertz B, Barth S, Hahn T, Weiss U, Kaufmann P & Desoye G (2000). Endothelin A and B receptors change their expression levels during development of human placental villi. *Placenta.* **21**: 536-46.

Cha M, Lee M, Je G & Kwak J (2001). Endogenous production of nitric oxide by vascular endothelial growth factor down-regulates proliferation of choriocarcinoma cells. *Biochem Biophys Res Commun.* **282**: 1061-6.

Chakraborty C, Barbin Y, Chakrabarti S, Chidiac P, Dixon S & Lala P (2003). Endothelin-1 promotes migration and induces elevation of [Ca2+]i and phosphorylation of MAP kinase of a human extravillous trophoblast cell line. *Mol Cell Endocrinol.* **201**: 63-73.

Chen S, Li X, Ebisawa K & Zhang L (1997). Functional characterization of the recombinant type 3 Ca^{2+} release channel (ryanodine receptor) expressed in HEK293 cells. *J Biol Chem.* **272**: 24234-46.

Chen S, Zhang L & MacLennan D (1994). Asymmetrical blockade of the Ca2+ release channel (ryanodine receptor) by 12-kDa FK506 binding protein. *Proc Natl Acad Sci U S A.* **91**: 11953-7.

Ching L, Williams A & Sitsapesan R (2000). Evidence for Ca(2+) activation and inactivation sites on the luminal side of the cardiac ryanodine receptor complex. *Circ Res.* **87**: 201-6.

Chou C, Rapko S & Knepper M (1998). Phosphoinositide signaling in rat inner medullary collecting duct. *Am J Physiol.* **274**: F564-72.

Chou C, Yip K, Michea L, Kador K, Ferraris J, Wade J & Knepper M (2000). Regulation of aquaporin-2 trafficking by vasopressin in the renal collecting duct. Roles of ryanodine-sensitive Ca^{2+} stores and calmodulin. *J Biol Chem.* **275**: 36839-46.

Choy M & Manyonda I (1998). The phagocytic activity of human first trimester extravillous trophoblast. *Hum Reprod.* **13**: 2941-9.

Chu A, Díaz-Muñoz M, Hawkes M, Brush K & Hamilton S (1990a). Ryanodine as a probe for the functional state of the skeletal muscle sarcoplasmic reticulum calcium release channel. *Mol Pharmacol.* **37**: 735-41.

Chu A, Sumbilla C, Inesi G, Jay S & KP. C (1990b). Specific association of calmodulin-dependent protein kinase and related substrates with the junctional sarcoplasmic reticulum of skeletal muscle. *Biochemistry.* **29**: 5899-905.

Churchill G, Okada Y, Thomas J, Genazzani A, Patel S & Galione A (2002). NAADP mobilizes Ca^{2+} from reserve granules, lysosome-related organelles, in sea urchin eggs. *Cell.* **111**: 703-8.

Clarson L, Roberts V, Hamark B, Elliott A & Powell T (2003). Store-operated Ca^{2+} entry in first trimester and term human placenta. *J Physiol.* **550**: 515-28.

Connelly L, Madhani M & Hobbs A (2005). Resistance to endotoxic shock in endothelial nitric-oxide synthase (eNOS) knock-out mice: a pro-inflammatory role for eNOS-derived NO *in vivo*. *J Biol Chem.* **280**: 10040-6.

Copello J, Barg S, Onoue H & Fleischer S (1997). Heterogeneity of Ca^{2+} gating of skeletal muscle and cardiac ryanodine receptors. *Biophys J.* **73**: 141-56.

Copello J, Barg S, Sonnleitner A, Porta M, Diaz-Sylvester P, Fill M, Schindler H & Fleischer S (2002). Differential activation by Ca^{2+}, ATP and caffeine of cardiac and skeletal muscle ryanodine receptors after block by Mg^{2+}. *J Membr Biol.* **187**: 54-64.

Coronado R, Morrissette J, Sukhareva M & Vaughan DM (1994). Structure and function of ryanodine receptors. *Am J Physiol.* **266**: C1485-504

Corrado D, Basso C & Thiene G (2000). Arrhythmogenic right ventricular cardiomyopathy: diagnosis, prognosis, and treatment. *Heart.* **83**: 588-95.

Coutifaris C, Kao L, Sehdev H, Chin U, Babalola G, Blaschuk O & Strauss Jr (1991). E-cadherin Expression During the Differentiation of Human Trophoblasts. *Development.* **113**: 767-77.

Csernoch L, Szentesi P, Sárközi S, Szegedi C, Jona I & Kovács L (1999). Effects of tetracaine on sarcoplasmic calcium release in mammalian skeletal muscle fibres. *J Physiol.* **515**: 843-57.

Curtis S, Jones C, Garrod A, Hulme C & Heazell A (2013). Identification of autophagic vacuoles and regulators of autophagy in villous trophoblast from normal

term pregnancies and in fetal growth restriction. *J Matern Fetal Neonatal Med.* **26**: 339-46.

Damsky C, Librach C, Lim K, Fitzgerald M, McMaster M, Janatpour M, Zhou Y, Logan S & Fisher S (1994). Integrin switching regulates normal trophoblast invasion. *Development.* **120**: 3657-66.

de Gasparo M, Catt K, Inagami T, Wright J & Unger T (2000). International union of pharmacology. XXIII. The angiotensin II receptors. *Pharmacol Rev.* **52**: 415-72.

Delidaki M, Gu M, Hein A, Vatish M & Grammatopoulos D (2011). Interplay of cAMP and MAPK pathways in hCG secretion and fusogenic gene expression in a trophoblast cell line. *Mol Cell Endocrinol.* **332**: 213-20.

DeWire S, Kim J, Whalen E, Ahn S, Chen M & Lefkowitz R (2008). Beta-arrestin-mediated signaling regulates protein synthesis. *J Biol Chem.* **283**: 10611–10620.

Doetschman T, Eistetter H, Katz M, Schmidt W & Kemler R (1985). The in vitro development of blastocyst-derived embryonic stem cell lines: formation of visceral yolk sac, blood islands and myocardium. *J Embryol Exp Morphol.* **87**: 27-45.

Don R, Cox P, Wainwright B, Baker K & Mattick J (1991). 'Touchdown' PCR to circumvent spurious priming during gene amplification. *Nucleic Acids Res.* **19**: 4008.

Dorn GI & Force T (2005). Protein kinase cascades in the regulation of cardiac hypertrophy. *J Clin Invest.* **115**: 527–537.

Doyle D, Morais Cabral J, Pfuetzner R, Kuo A, Gulbis J, Cohen S, Chait B & MacKinnon R (1998). The structure of the potassium channel: molecular basis of K+ conduction and selectivity. *Science.* **280**: 69-77.

Eis A, Brockman D, Pollock J & Myatt L (1995). Immunohistochemical localization of endothelial nitric oxide synthase in human villous and extravillous trophoblast populations and expression during syncytiotrophoblast formation in vitro. *Placenta.* **16**: 113-26.

Endo M, Tanaka M & Ogawa Y (1970). Calcium induced release of calcium from the sarcoplasmic reticulum of skinned skeletal muscle fibres. *Nature* **228**: 34-6.

Fehrenbacher K, Huckaba T, Yang HC, Boldogh I & Pon L (2003). Actin comet tails, endosomes and endosymbionts. . *J. Exp. Biol.* **206**: 1977-1984.

Fernàndez J, Deaglio S, Donati D, Beusan I, Corno F, Aranega A, Forni M, Falini B & Malavasi F (1998). Analysis of the distribution of human CD38 and of its ligand CD31 in normal tissues. *J Biol Regul Homeost Agents. Jul-Sep;(3):* **12**: 81-91.

Ferré F, Mondon F, Mignot T, Cronier L, Cavero I, Rostene W & Malassine A (1993). Endothelin-1 binding sites and immunoreactivity in the cultured human placental trophoblast: evidence for an autocrine and paracrine role for endothelin-1. *J Cardiovasc Pharmacol.* **22**: S214-8.

Ferreiro A, Monnier N, Romero N, Leroy J, Bönnemann C, Haenggeli C, Straub V, Voss W, Nivoche Y, Jungbluth H, Lemainque A, Voit T, Lunardi J, Fardeau M & Guicheney P (2002). A recessive form of central core disease, transiently presenting as multi-minicore disease, is associated with a homozygous mutation in the ryanodine receptor type 1 gene. *Ann Neurol.* **51**: 750-9.

Ferrington D, Krainev A & Bigelow D (1998). Altered turnover of calcium regulatory proteins of the sarcoplasmic reticulum in aged skeletal muscle. *J Biol Chem.* **273**: 5885-91.

Fessenden JD, Chen L, Wang Y, Paolini C, Franzini-Armstrong C, Allen PD & Pessah IN (2001). Ryanodine receptor point mutant E4032A reveals an allosteric interaction with ryanodine. *Proc Natl Acad Sci U S A* **98**: 2865-70.

Fill M & Copello JA (2002). Ryanodine Receptor Calcium Release Channels *Physiol. Rev.* **82**: 893-922.

Fitzsimmons T, Gukovsky I, McRoberts J, Rodriguez E, Lai F & Pandol S (2000). Multiple isoforms of the ryanodine receptor are expressed in rat pancreatic acinar cells. *Biochem J.* **351**: 265-71.

Fodor J, Gönczi M, Sztretye M, Dienes B, Oláh T, Szabó L, Csoma E, Szentesi P, Szigeti G, Marty I & Csernoch L (2008). Altered expression of triadin 95 causes parallel changes in localized Ca2+ release events and global Ca2+ signals in skeletal muscle cells in culture. *J Physiol.* **586**: 5803-18.

Forbes K, Westwood M, Baker P & Aplin J (2008). Insulin-like growth factor I and II regulate the life cycle of trophoblast in the developing human placenta. *Am J Physiol Cell Physiol* **294**: C1313–C1322.

Francis J, Sankar V, Nair V & Priori S (2005). Catecholaminergic polymorphic ventricular tachycardia. *Heart Rhythm.* **2**: 550-4.

Franzini-Armstrong C (1970). Studies of the triad: Istructure of the junction in frog twitch fibers. *J. Cell Biol.* **227**: 1124-31.

Franzini-Armstrong C (1999). The sarcoplasmic reticulum and the control of muscle contraction. *FASEB J.* **13**: S266–70.

Franzini-Armstrong C & Protasi F (1997). Ryanodine receptors of striated muscles: a complex channel capable of multiple interactions. *Physiol Rev.* **77**: 699-729.

Friedman S & Skehan P (1979). Morphological differentiation of human choriocarcinoma cells induced by methotrexate. *Cancer Res.* **39**: 1960-7.

Fruen B, Mickelson J & Louis C (1997). Dantrolene inhibition of sarcoplasmic reticulum Ca^{2+} release by direct and specific action at skeletal muscle ryanodine receptors. *J Biol Chem.* **272**: 26965-71.

Fruman D, Wood M, Gjertson C, Katz H, Burakoff S & Bierer B (1995). FK506 binding protein 12 mediates sensitivity to both FK506 and rapamycin in murine mast cells. *Eur J Immunol.* **25**: 563-71.

Fryer M & Stephenson D (1996). Total and sarcoplasmic reticulum calcium contents of skinned fibres from rat skeletal muscle. *J Physiol.* **493 .** 357-70.

Fu J, Lv X, Lin H, Wu L, Wang R, Zhou Z, Zhang B, Wang Y, Tsang B, Zhu C & Wang H (2010). Ubiquitin ligase cullin 7 induces epithelial-mesenchymal transition in human choriocarcinoma cells. *J Biol Chem.* **285**: 10870-9.

Furuichi T, Yoshikawa S, Miyawaki A, Wada K, Maeda N & Mikoshiba K (1989). Primary structure and functional expression of the inositol 1,4,5-trisphosphate-binding protein P400. *Nature.*
342: 32-8.

Galione A, Lee HC & Busa WB (1991). Ca^{2+}-induced Ca^{2+} release in sea urchin egg homogenates: modulation by cyclic ADP-ribose. *Science.* **253**: 1143–1146.

Gao L, Balshaw D, Xu L, Tripathy A, Xin C & Meissner G (2000). Evidence for a role of the lumenal M3-M4 loop in skeletal muscle Ca(2+) release channel (ryanodine receptor) activity and conductance. *Biophys J.* **79**: 828-40.

Garrington T & Johnson G (1999). Organization and regulation of mitogen-activated protein kinase signaling pathways. *Curr Opin Cell Biol.* **11**: 211–218.

Gauster M, Siwetz M, Orendi K, Moser G, Desoye G & Huppertz B (2010). Caspases rather than calpains mediate remodelling of the fodrin skeleton during human placental trophoblast fusion. *Cell Death Differ.* **17**: 336-45.

George C, Higgs G & Lai F (2003). Ryanodine receptor mutations associated with stress-induced ventricular tachycardia mediate increased calcium release in stimulated cardiomyocytes. *Circ Res.* **93**: 531-40.

Gether U (2000). Uncovering molecular mechanisms involved in activation of G protein-coupled receptors. *Endocr Rev.* **21**: 90-113.

Giannini G, Conti A, Mammarella S & Scrobogna M (1995). The ryanodine receptor/calcium channel genes are widely and differentially expressed in murine brain and peripheral tissues. *J. Cell Biol.* **128**: 893-904.

Gilbert JS, Ryan MJ, LaMarca BB, Sedeek M, Murphy SR & Granger JP (2008). Pathophysiology of hypertension during preeclampsia: linking placental ischemia with endothelial dysfunction. *Am J Physiol Heart Circ Physiol.* **294**: H541–H550.

Gilchrist JS, Wang KK, Katz S & Belcastro AN (1992). Calcium-activated neutral protease effects upon skeletal muscle sarcoplasmic reticulum protein structure and calcium release. *J. Biol. Chem.* **267**: 20857-65.

Gill D, Ghosh T & Mullaney J (1989). Calcium signalling mechanisms in endoplasmic reticulum activated by inositol 1,4,5-trisphosphate and GTP. *Cell Calcium.* **10**: 363-74.

Giulumian A, Meszaros L & Fuchs L (2000). Endothelin-1-induced contraction of mesenteric small arteries is mediated by ryanodine receptor Ca^{2+} channels and cyclic ADP-ribose. *J Cardiovasc Pharmacol.* **36**: 758-63.

Grümmer R, Hohn H, Mareel M & Denker H (1994). Adhesion and invasion of three human choriocarcinoma cell lines into human endometrium in a three-dimensional organ culture system. *Placenta.* **15**: 411-29.

Grümmer R, Hohn HP & Denker HW (1990). Choriocarcinoma cell spheroids: an *in vitro* model for the human trophoblast. *Trophoblast. Res.* **4**: 97-111.

Grunwald R & Meissner G (1995). Lumenal sites and C terminus accessibility of the skeletal muscle calcium release channel (ryanodine receptor) *J Biol Chem.* **270**: 11338-47.

Grynkiewicz G, Poenie M & Tsien R (1985). A new generation of Ca2+ indicators with greatly improved fluorescence properties. *J Biol Chem.* **260**: 3440-50.

Gude N, Roberts C, Kalionis B & King R (2004). Growth and function of the normal human placenta. *Thromb Res.* **114**: 397-407.

Guo W, Jorgensen AO, Jones LR & Campbell KP (1996). Biochemical characterization and molecular cloning of cardiac triadin. *J Biol Chem.* **271**: 458-65.

Györke I & Györke S (1998). Regulation of the cardiac ryanodine receptor channel by luminal Ca^{2+} involves luminal Ca^{2+} sensing sites. *Biophys J.* **75**: 2801-10.

Györke I, Hester N, Jones L & Györke S (2004). The role of calsequestrin, triadin, and junctin in conferring cardiac ryanodine receptor responsiveness to luminal calcium. *Biophys J.* **86**: 2121-8.

Györke S, Lukyanenko V & Györke I (1997). Dual effects of tetracaine on spontaneous calcium release in rat ventricular myocytes. *J Physiol.* **500**: 297-309.

Györke S, Vélez P, Suárez-Isla B & Fill M (1994). Activation of single cardiac and skeletal ryanodine receptor channels by flash photolysis of caged Ca^{2+}. *Biophys J.* **66**: 1879-86.

Haché S, Takser L, LeBellego F, Weiler H, Leduc L, Forest J, Giguère Y, Masse A, Barbeau B & Lafond J (2011). Alteration of calcium homeostasis in primary preeclamptic syncytiotrophoblasts: effect on calcium exchange in placenta. *J Cell Mol Med.* **15**: 654-67.

Haighn T, Chen C-P, Jones C & Aplin J (1999). Studies of mesenchymal cells from 1st trimester human placenta: expression of cytokeratin outside the trophoblast lineage. *Placenta* **20**: 615–25.

Hakamata Y, Nishimura S, Nakai J, Nakashima Y, Kita T & Imoto K (1994). Involvement of the brain type of ryanodine receptor in T-cell proliferation. *FEBS Lett.* **352**: 206-10.

Hallikas O, Aaltonen J, von Koskull H, Lindberg L, Valmu L, Kalkkinen N, Wahlström T, Kataoka H, Andersson L, Lindholm D & Schröder J (2006). Identification of antibodies against HAI-1 and integrin alpha6beta4 as immunohistochemical markers of human villous cytotrophoblast. *J Histochem Cytochem.* **54**: 745-52.

Hamilton S (2005). Ryanodine receptors. *Cell Calcium.* **38**: 253-60.

Hashimoto A, Miyakoda G, Hirose Y & Mori T (2006). Activation of endothelial nitric oxide synthase by cilostazol via a cAMP/protein kinase A- and phosphatidylinositol 3-kinase/Akt-dependent mechanism. *Atherosclerosis.* **189**: 350-7.

Hauser C, Kannan K, Deitch E & Itagaki K (2005). Non-specific effects of 4-chloro-m-cresol may cause calcium flux and respiratory burst in human neutrophils. *Biochem Biophys Res Commun.* **336**: 1087-95.

Herrmann-Frank A, Richter M, Sarközi S, Mohr U & Lehmann-Horn F (1996). 4-Chloro-m-cresol, a potent and specific activator of the skeletal muscle ryanodine receptor. *Biochim Biophys Acta.* **1289**: 31-40.

Hess P, Prod'Hom B & Pietrobon D (1989). Mechanisms of interaction of permeant ions and protons with dihydropyridine-sensitive calcium channels. *Ann N Y Acad Sci.* **560**: 80-93.

Hofer A & Machen T (1994). Direct measurement of free Ca in organelles of gastric epithelial cells. *Am J Physiol.* **267**: G442-51.

Hohenegger M & Suko J (1993). Phosphorylation of the purified cardiac ryanodine receptor by exogenous and endogenous protein kinases. *Biochem J.* **296**: 303-8.

Hoover CV (2004). Maternal, fetal, & neonatal physiology: a clinical perspective, 2nd edition. *Journal of Midwifery & Women's Health* **49**: 164-165.

Horiuchi M, Lehtonen J & Daviet L (1999). Signaling Mechanism of the AT2 Angiotensin II Receptor: Crosstalk between AT1 and AT2 Receptors in Cell Growth. *Trends Endocrinol Metab.* **10**: 391-396.

Hosoi E, Nishizaki C, Gallagher K, Wyre H, Matsuo Y & Sei Y (2001). Expression of the ryanodine receptor isoforms in immune cells. *J Immunol.* **167**: 4887-94.

Houle T, Ram M & Cala S (2004). Calsequestrin mutant D307H exhibits depressed binding to its protein targets and a depressed response to calcium. *Cardiovasc Res.* **64**: 227-33.

Huang F, Shan J, Reiken S, Wehrens X & Marks A (2006). Analysis of calstabin2 (FKBP12.6)-ryanodine receptor interactions: rescue of heart failure by calstabin2 in mice. *Proc Natl Acad Sci U S A.* **103**: 3456-61.

Huch G, Hohn H & Denker H (1998). Identification of differentially expressed genes in human trophoblast cells by differential-display RT-PCR. *Placenta.* **19**: 557-67.

Husain S & Mughal M (1992). Mineral transport across the placenta. *Arch Dis Child.* **67**: 874-8.

Icking A, Matt S, Opitz N, Wiesenthal A, Müller-Esterl W & Schilling K (2005). NOSTRIN functions as a homotrimeric adaptor protein facilitating internalization of eNOS. *J Cell Sci.* **118**: 5059-69.

Ikemoto N, Ronjat M, Mészáros L & Koshita M (1989). Postulated role of calsequestrin in the regulation of calcium release from sarcoplasmic reticulum. *Biochemistry.* **28**: 6764-71.

Ikemoto N & Yamamoto T (2002). Regulation of calcium release by interdomain interaction within ryanodine receptors. *Front Biosci.* **7**: d671-683.

Ino K, Uehara C, Kikkawa F, Kajiyama H, Shibata K, Suzuki T, Khin E, Ito M, Takeuchi M, Itakura A & Mizutani S (2003). Enhancement of aminopeptidase A expression during angiotensin II-induced choriocarcinoma cell proliferation through AT1 receptor involving protein kinase C- and mitogen-activated protein kinase-dependent signaling pathway. *J Clin Endocrinol Metab.* **88**: 3973-82.

Ishibashi K, Suzuki M & Imai M (2000). Molecular cloning of a novel form (two-repeat) protein related to voltage-gated sodium and calcium channels. *Biochem. Biophys. Res. Commun.* **270**: 370–376.

Ishimatsu S, Itakura A, Okada M, Kotani T, Iwase A, Kajiyama H, Ino K & Kikkawa F (2006). Angiotensin II augmented migration and invasion of choriocarcinoma cells involves PI3K activation through the AT1 receptor. *Placenta.* **27**: 587-91.

Jadeski L, Chakraborty C & Lala P (2003). Nitric oxide-mediated promotion of mammary tumour cell migration requires sequential activation of nitric oxide synthase, guanylate cyclase and mitogen-activated protein kinase. *Int J Cancer.* **106**: 496-504.

Jayaraman T, Brillantes A, Timerman A, Fleischer S, Erdjument-Bromage H, Tempst P & Marks A (1992). FK506 binding protein associated with the calcium release channel (ryanodine receptor). *J. Biol. Chem.* **267**: 9474-77.

Jeyakumar L, Copello J, O'Malley A, Wu G, Grassucci R, Wagenknecht T & Fleischer S (1998). Purification and characterization of ryanodine receptor 3 from mammalian tissue. *J Biol Chem.* **273**: 16011-20.

Jiménez E, Muñoz M, Pavia J & Montiel M (1996). Angiotensin II receptor in human placental syncytiotrophoblast plasma membranes. *Life Sci.* **58**: 877-82.

Jin D, Liu H, Hirai H, Torashima T, Nagai T, Lopatina O, Shnayder N, Yamada K, Noda M, Seike T, Fujita K, Takasawa S, Yokoyama S, Koizumi K, Shiraishi Y, Tanaka S, Hashii M, Yoshihara T, Higashida K, Islam M, Yamada N, Hayashi K, Noguchi N, Kato I, Okamoto H, Matsushima A, Salmina A, Munesue T, Shimizu N, Mochida S, Asano M & Higashida H (2007). CD38 is critical for social behaviour by regulating oxytocin secretion. *Nature.* **446**: 41-5.

Jones J, Reynolds D, Lai F & Blayney L (2005). Ryanodine receptor binding to FKBP12 is modulated by channel activation state. *J Cell Sci.* **118**: 4613-9.

Jones P, Meng X, Xiao B, Cai S, Bolstad J, Wagenknecht T, Liu Z & Chen S (2008). Localization of PKA phosphorylation site, Ser(2030), in the three-dimensional structure of cardiac ryanodine receptor. *Biochem J.* **410**: 261-70.

Junankar P & Dulhunty A (1994). Monoclonal antibody to skeletal muscle ryanodine receptor detects a polypeptide in rat brain: comparison of immunogenic fragments after limited proteolysis. *Biochem Mol Biol Int.* **32**: 29-37.

Jurkat-Rott K, McCarthy T & Lehmann-Horn F (2000). Genetics and pathogenesis of malignant hyperthermia. *Muscle Nerve.* **23**: 4-17.

Kalenga M, de Gasparo M, Thomas K & de Hertogh R (1996). Angiotensin II and its different receptor subtypes in placenta and fetal membranes. *Placenta.* **17**: 103-110.

Kamath S & Smith C (1994). Na^{+}/Ca^{2+} exchange, Ca^{2+} binding, and electrogenic Ca^{2+} transport in plasma membranes of human placental syncytiotrophoblast. *Pediatr Res.* **36**: 461-7.

Kannankeril P, Mitchell B, Goonasekera S, Chelu M, Zhang W, Sood S, Kearney D, Danila C, De Biasi M, Wehrens X, Pautler R, Roden D, Taffet G, Dirksen R, Anderson M & Hamilton S (2006). Mice with the R176Q cardiac ryanodine receptor mutation exhibit catecholamine-induced ventricular tachycardia and cardiomyopathy. *Proc Natl Acad Sci U S A.* **103**: 12179-84.

Kaufmann P & Castellucci M (1997). Extravillous trophoblast in the human placenta: A review. *Placenta* **18**: 21-65.

Kelliher M, Fastbom J, Cowburn R, Bonkale W, Ohm T, Ravid R, Sorrentino V & O'Neill C (1999). Alterations in the ryanodine receptor calcium release channel correlate with Alzheimer's disease neurofibrillary and beta-amyloid pathologies. *Neuroscience.* **92**: 499-513.

Kermode H, Williams A & Sitsapesan R (1998). The interactions of ATP, ADP, and inorganic phosphate with the sheep cardiac ryanodine receptor. *Biophys J.* **74**: 1296-304.

Kilpatrick S, Roberts J, Lykins D & Taylor R (1993). Characterization and ontogeny of endothelin receptors in human placenta. *Am J Physiol.* **264**: E367-72.

Kinnear N, Boittin F, Thomas J, Galione A & Evans A (2004). Lysosome-sarcoplasmic reticulum junctions: A trigger zone for calcium signaling by nicotinic acid adenine dinucleotide phosphate and endothelin-1. *J. Biol. Chem.* **279**: 54319–54326.

Kiss H, Schneeberger C, Tschugguel W, Lass H, Huber J, Husslein P & Knöfler M (1998). Expression of endothelial (type III) nitric oxide synthase in cytotrophoblastic cell lines: regulation by hypoxia and inflammatory cytokines. *Placenta.* **19**: 603-11.

Klein R, Bourdon D, Costales C, Wagner C, White W, Williams J, Hicks S, Sondek J & Thakker D (2011). Direct activation of human phospholipase C by its well known inhibitor u73122. *J Biol Chem.* **286**: 12407-16.

Knobil E & Neill JD, Eds. (1998). Encyclopedia of Reproduction. From Trophoblast to Human Placenta ACADEMIC PRESS.

Kobayashi S, Bannister M, Gangopadhyay J, Hamada T, Parness J & Ikemoto N (2005). Dantrolene stabilizes domain interactions within the ryanodine receptor. *J Biol Chem.* **280**: 6580-7.

Kobayashi Y, Alseikhan B & Jones L (2000). Localization and characterization of the calsequestrin-binding domain of triadin 1. Evidence for a charged beta-strand in mediating the protein-protein interaction. *J Biol Chem.* **275**: 17639-46.

Kontula K, Laitinen P, Lehtonen A, Toivonen L, Viitasalo M & Swan H (2005). Catecholaminergic polymorphic ventricular tachycardia: recent mechanistic insights. *Cardiovasc Res.* **67**: 379-87.

Koukoulas I, Risvanis J, Douglas-Denton R, Burrell L, Moritz K & Wintour E (2003). Vasopressin receptor expression in the placenta. *Biol Reprod.* **69**: 679-86.

Krause B, Hanson M & Casanello P (2011). Role of nitric oxide in placental vascular development and function. *Placenta.* **32**: 797-805.

Kristiansen K (2004). Molecular mechanisms of ligand binding, signaling, and regulation within the superfamily of G-protein-coupled receptors: molecular modeling and mutagenesis approaches to receptor structure and function. *Pharmacol Ther.* **103**: 21-80.

Kuemmerle J & Murthy K (2001). Coupling of the insulin-like growth factor-I receptor tyrosine kinase to Gi2 in human intestinal smooth muscle: Gbetagamma -dependent mitogen-activated protein kinase activation and growth. *J Biol Chem.* **276**: 7187-94.

Kushnir A & Marks A (2010). The ryanodine receptor in cardiac physiology and disease. *Adv Pharmacol.* **59**: 1-30.

Kushnir A, Shan J, Betzenhauser M, Reiken S & Marks A (2010). Role of CaMKIIdelta phosphorylation of the cardiac ryanodine receptor in the force frequency relationship and heart failure. *Proc Natl Acad Sci U S A.* **107**: 10274-9.

Lafond J, Goyer-O'Reilly I, Laramée M & Simoneau L (2001). Hormonal regulation and implication of cell signaling in calcium transfer by placenta. *Endocrine.* **14**: 285-94.

Lai F, Erickson H, Rousseau E, Liu Q & Meissner G (1988). Purification and reconstitution of the calcium release channel from skeletal muscle. *Nature.* **331**: 315-9.

Lanner J, Georgiou D, Joshi A & Hamilton S (2010). Ryanodine receptors: structure, expression, molecular details, and function in calcium release. *Cold Spring Harb Perspect Biol.* **2**: a003996.

Lanz B, Kadereit B, Ernst S, Shojaati K, Causevic M, Frey B, Frey F & Mohaupt M (2003). Angiotensin II regulates 11beta-hydroxysteroid dehydrogenase type 2 via AT2 receptors. *Kidney Int.* **64**: 970-7.

Laver D, O'Neill E & Lamb G (2004). Luminal Ca2+-regulated Mg2+ inhibition of skeletal RyRs reconstituted as isolated channels or coupled clusters. *J Gen Physiol.* **124**: 741-58.

Lee E, Rho S, Kwon S, Eom S, Allen P & Kim dH (2004). N-terminal region of FKBP12 is essential for binding to the skeletal ryanodine receptor. *J Biol Chem.* **2004**: 26481-8.

Lee H (1997). Mechanisms of calcium signaling by cyclic ADP-ribose and NAADP. *Physiol. Rev.* **77**: 1133–64.

Lee H (2000a). Enzymatic functions and structures of CD38 and homologs. *Chem Immunol.* **75**: 39–59.

Lee H (2000b). NAADP: An emerging calcium signaling molecule. . *J. Memb. Biol.* **173**: 1–8.

Lee H (2011). Cyclic ADP-ribose and NAADP: fraternal twin messengers for calcium signaling. *Sci China Life Sci* **54**: 699–711.

Lee H, Walseth T, Bratt G, Hayes R & Clapper D (1989). Structural determination of a cyclic metabolite of NAD^+ with intracellular Ca^{2+}-mobilizing activity. *J Biol Chem.* **264**: 1608-15.

Lee M & Severson D (1994). Signal transduction in vascular smooth muscle: diacylglycerol second messengers and PKC action. *Am J Physiol.* **267**: C659-78.

Lefièvre L, Nash K, Mansell S, Costello S, Punt E, Correia J, Morris J, Kirkman-Brown J, Wilson S, Barratt C & Publicover S (2012). 2-APB-potentiated channels amplify CatSper-induced Ca^{2+} signals in human sperm. *Biochem J.* **448**: 189-200.

Li P & Chen SR (2001). Molecular basis of Ca2+ activation of the mouse cardiac Ca2+ release channel (ryanodine receptor). *J Gen Physiol* **118**: 33-44.

Li X, Shams M, Zhu J, Khalig A, Wilkes M, Whittle M, Barnes N & Ahmed A (1998). Cellular localization of AT1 receptor mRNA and protein in normal placenta and its reduced expression in intrauterine growth restriction. Angiotensin II stimulates the release of vasorelaxants. *J Clin Invest.* **101**: 442-54.

Liang W, Buluc M, van Breemen C & Wang X (2004). Vectorial Ca^{2+} release via ryanodine receptors contributes to Ca^{2+} extrusion from freshly isolated rabbit aortic endothelial cells. *Cell Calcium.* **36**: 431-43.

Lindsay A, Manning S & Williams A (1991). Monovalent cation conductance in the ryanodine receptor-channel of sheep cardiac muscle sarcoplasmic reticulum. *J Physiol.* **439**: 463-80.

Lloyd-Evans E, Morgan AJ, He X, Smith DA, Elliot-Smith E, Sillence DJ, Churchill GC, Schuchman EH, Galione A & Platt FM (2008). Niemann-Pick disease type C1 is a sphingosine storage disease that causes deregulation of lysosomal calcium. . *Nat. Med.* **14**: 1247–1255.

Lopez-Jaramillo P, Arenas WD, Garcia RG, Rincon MY & Lopez M (2008). The role of the L-arginine-nitric oxide pathway in preeclampsia. *Ther Adv Cardiovasc Dis.* **2**: 261–275.

López J, Cordovez G, Linares N & Allen P (2000). Cyclic ADP-ribose induces a larger than normal calcium release in malignant hyperthermia-susceptible skeletal muscle fibers. *Pflugers Arch.* **440**: 236-42.

Lorenzon P, Grohovaz F & F. R (2000). Voltage- and Ligand-gated Ryanodine Receptors are Functionally Separated in Developing C2C12 Mouse Myotubes. *J Physiol.* **525**: 499-507.

Lukyanenko V, Györke I & Györke S (1996). Regulation of calcium release by calcium inside the sarcoplasmic reticulum in ventricular myocytes. *Pflugers Arch.* **432**: 1047-54.

Lunghi L, Ferretti M, Medici S, Biondi C & Vesce F (2007). Control of human trophoblast function. *Reprod Biol Endocrinol.* **5**(6).

Lyall F, Bulmer J, Kelly H, Duffie E & Robson S (1999). Human trophoblast invasion and spiral artery transformation: the role of nitric oxide. *Am J Pathol.* **154**: 1105-14.

Lyall F, Jablonka-Shariff A, Johnson R, Olson L & Nelson D (1998). Gene expression of nitric oxide synthase in cultured human term placental trophoblast during in vitro differentiation. *Placenta.* **19**: 253-60.

Ma J (1993). Block by ruthenium red of the ryanodine-activated calcium release channel of skeletal muscle. *J Gen Physiol.* **102**: 1031-56.

Ma J, Hayek S & Bhat M (2004). Membrane topology and membrane retention of the ryanodine receptor calcium release channel. *Cell Biochem Biophys.* **40**: 207-24.

Mackrill J (1999). Protein-protein interactions in intracellular Ca^{2+}-release channel function. *Biochem J.* **337**: 345-61.

Mackrill JJ, Challiss RA, O'Connell DA, Lai FA & Nahorski SR (1997). Differential expression and regulation of ryanodine receptor and myoinositol 1,4,5-trisphosphate receptor Ca^{2+} release channels in mammalian tissues and cell lines. *Biochem J.* **327**: 251-8.

MacLennan D, Duff C, Zorzato F, Fujii J, Phillips M, Korneluk R, Frodis W, Britt B & Worton R (1990). Ryanodine receptor gene is a candidate for predisposition to malignant hyperthermia. *Nature.* **343**: 559-61.

MacNicol M, JeffersonA B & Schulman H (1990). Ca^{2+}/calmodulin kinase is activated by the phosphatidylinositol signaling pathway and becomes Ca^{2+}-independent in PC12 cells. *J Biol Chem.* **265**: 18055-8.

Manunta M, Rossi D, Simeoni I, Butelli E, Romanin C, Sorrentino V & Schindler H (2000). ATP-induced activation of expressed RyR3 at low free calcium. *FEBS Lett.* **471**: 256-60.

Marchand M, Horcajadas J, Esteban F, McElroy S, Fisher S & Giudice L (2011). Transcriptomic signature of trophoblast differentiation in a human embryonic stem cell model. *Biol Reprod.* **84**: 1258-71.

Marengo J, Hidalgo C & Bull R (1998). Sulfhydryl oxidation modifies the calcium dependence of ryanodine-sensitive calcium channels of excitable cells. *Biophys J.* **74**: 1263-77.

Marino G, Castro-Parodi M, Dietrich V & Damiano A (2010). High levels of human chorionic gonadotropin (hCG) correlate with increased aquaporin-9 (AQP9) expression in explants from human preeclamptic placenta. *Reprod Sci.* **17**: 444-53.

Marks D & Fox R (1991). DNA damage, poly (ADP-ribosyl)ation and apoptotic cell death as a potential common pathway of cytotoxic drug action. *Biochem Pharmacol.* **42**: 1859-67.

Marty I, Villaz M, Arlaud G, Bally I & Ronjat M (1994). Transmembrane orientation of the N-terminal and C-terminal ends of the ryanodine receptor in the sarcoplasmic reticulum of rabbit skeletal muscle. *Biochem J.* **298**: 743-9.

Marx S, Reiken S, Hisamatsu Y, Gaburjakova M, Gaburjakova J, Yang Y, Rosemblit N & AR. M (2001). Phosphorylation-dependent regulation of ryanodine receptors: a novel role for leucine/isoleucine zippers. *J Cell Biol.* **153**: 699-708.

Marx S, Reiken S, Hisamatsu Y, Jayaraman T, Burkhoff D, Rosemblit N & Marks A (2000). PKA phosphorylation dissociates FKBP12.6 from the calcium release channel (ryanodine receptor): defective regulation in failing hearts. *Cell.* **101**: 365-76.

Matthews R, Guthrie C, Wailes L, Zhao X, Means A & McKnight G (1994). Calcium/calmodulin-dependent protein kinase types II and IV differentially regulate CREB-dependent gene expression. *Mol Cell Biol.* **14**: 6107-16.

Matyash M, Matyash V, Nolte C, Sorrentino V & Kettenmann H (2002). Requirement of functional ryanodine receptor type 3 for astrocyte migration. *FASEB J.* **16**: 84-6.

Mauschitz R, Cervar M, Hahn T, Pürstner P & Desoye G (2000). Self-regulation of the endothelin receptor system in choriocarcinoma cells. *Biochim Biophys Acta.* **1502**: 224-34.

Mayr B & Montminy M (2001). Transcriptional regulation by the phosphorylation-dependent factor CREB. *Nat Rev Mol Cell Biol.* **2**: 599-609.

Mayrleitner M, Timerman A, Wiederrecht G & Fleischer S (1994). The calcium release channel of sarcoplasmic reticulum is modulated by FK-506 binding protein: effect of FKBP-12 on single channel activity of the skeletal muscle ryanodine receptor. *Cell Calcium.* **15**: 99-108.

McCarthy T & Mackrill J (2004). Unravelling calcium-release channel gating: clues from a 'hot' disease. *Biochem J.* **380**: e1-3.

McPherson P & Campbell K (1993). The ryanodine receptor/Ca2+ release channel. *J Biol Chem.* **268**: 13765-8.

Meissner G (1984). Adenine nucleotide stimulation of Ca^{2+}-induced Ca^{2+} release in sarcoplasmic reticulum. *J Biol Chem.* **259**: 2365-74.

Meissner G & Henderson J (1987). Rapid calcium release from cardiac sarcoplasmic reticulum vesicles is dependent on Ca^{2+} and is modulated by Mg^{2+}, adenine nucleotide, and calmodulin. *J Biol Chem.* **262**: 3065-73.

Meissner G, Rios E, Tripathy A & Pasek D (1997). Regulation of skeletal muscle Ca^{2+} release channel (ryanodine receptor) by Ca^{2+} and monovalent cations and anions. *J Biol Chem.* **272**: 1628-38.

Meissner G, Rousseau E & Lai F (1989). Structural and functional correlation of the trypsin-digested Ca^{2+} release channel of skeletal muscle sarcoplasmic reticulum. *J Biol Chem.* **264**: 1715-22.

Meldolesi J, Krause K & Michalak M (1996). Calreticulin: how many functions in how many cellular compartments? . *Cell Calcium.* **20**: 83-6.

Michalak M & Milner R (1991). Calreticulin: A Functional Analogue of Calsequestrin? *European Journal of Translational Myology: Basic Applied Myology* **1**: 121-8.

Mickelson J & Louis C (1996). Malignant hyperthermia: excitation-contraction coupling, Ca2+ release channel, and cell Ca2+ regulation defects. *Physiol Rev.* **76**: 537-92.

Misra RP, Bonni A, Miranti CK, Rivera VM, Sheng M & Greenberg ME (1994). L-type voltage-sensitive calcium channel activation stimulates gene expression by a serum response factor-dependent pathway. *J. Biol. Chem.* **269**: 25483–25493.

Mondon F, Anouar A & Ferré F (1998). Endothelin receptor subtypes in the microvillous trophoblastic membrane of early gestation and term human placentas. *Eur J Endocrinol.* **139**: 231-7.

Moore C, Rodney G, Zhang J, Santacruz-Toloza L, Strasburg G & Hamilton S (1999). Apocalmodulin and Ca^{2+} calmodulin bind to the same region on the skeletal muscle Ca^{2+} release channel. *Biochemistry.* **38**: 8532-7.

Moreau R, Daoud G, Masse A, Simoneau L & Lafond J (2003a). Expression and role of calcium-ATPase pump and sodium-calcium exchanger in differentiated trophoblasts from human term placenta. *Mol Reprod Dev.* **65**: 283-8.

Moreau R, Simoneau L & Lafond J (2003b). Calcium fluxes in human trophoblast (BeWo) cells: calcium channels, calcium-ATPase, and sodium-calcium exchanger expression. *Mol. Reprod. Dev.* **64**: 189-98.

Mosmann T (1983). Rapid colorimetric assay for cellular growth and survival: application to proliferation and cytotoxicity assays. *J Immunol Methods.* **65**: 55-63.

Murad F (1994). The nitric oxide-cyclic GMP signal transduction system for intracellular and intercellular communication. *Recent Prog Horm Res.* **49**: 239-48.

Murayama T, Oba T, Katayama E, Oyamada H, Oguchi K, Kobayashi M, Otsuka K & Ogawa Y (1999). Further characterization of the type 3 ryanodine receptor (RyR3) purified from rabbit diaphragm. *J Biol Chem.* **1999**(274): 17297-308.

Myat-Thanda, Hitsumoto Y, Saheki S, Kitagawa H, Yano J & Matsuura S (1996). Attenuation of human chorionic gonadotropin release by nitric oxide in choriocarcinoma cell lines. *J Endocrinol.* **150**: 243-53.

Myatt L (2010). Review: reactive oxygen and nitrogen species and functional adaptation of the placenta. *Placenta* **31**: S66–S69.

Nagamatsu T, Fujii T, Ishikawa T, Kanai T, Hyodo H, Yamashita T, Osuga Y, Momoeda M, Kozuma S & Taketani Y (2004). A primary cell culture system for human cytotrophoblasts of proximal cytotrophoblast cell columns enabling in vitro acquisition of the extra-villous phenotype. *Placenta.* **25**: 153-65.

Namkoong S, Lee S, Kim C, Kim Y, Chung H, Lee H, Han J, Ha K, Kwon Y & Kim Y (2005). Prostaglandin E2 stimulates angiogenesis by activating the nitric oxide/cGMP pathway in human umbilical vein endothelial cells. *Exp Mol Med.* **37**: 588-600.

Nelson M, Cheng H, Rubart M, Santana L, Bonev A, Knot H & Lederer W (1995). Relaxation of arterial smooth muscle by calcium sparks. *Science.* **270**: 633-7.

Ni X, Chan E, Fitter J & Smith R (1997). Nitric oxide inhibits corticotropin-releasing hormone exocytosis but not synthesis by cultured human trophoblasts. *J Clin Endocrinol Metab.* **82**: 4171-5.

Nicola C, Timoshenko A, Dixon S, Lala P & Chakraborty C (2005a). EP1 receptor-mediated migration of the first trimester human extravillous trophoblast: the role of intracellular calcium and calpain. *J Clin Endocrinol Metab.* **90**: 4736-46.

Nicola C, Timoshenko A, Dixon S, Lala P & Chakraborty C (2005b). EP1 receptor-mediated migration of the first trimester human extravillous trophoblast: the role of intracellular calcium and calpain.

J Clin Endocrinol Metab. Aug;90(8):4736-46. Epub 2005 May 10.

Niger C, Malassiné A & Cronier L (2004). Calcium channels activated by endothelin-1 in human trophoblast. *J Physiol.* **561**: 449-58.

Nohmi M, Kuba K & Hua S (1991). Ultraviolet light activates blocking actions of dantrolene on intracellular Ca2+ release in bullfrog sympathetic neurones. *J Biol Chem.* **266**: 22254-9.

Oda T, Yano M, Yamamoto T, Tokuhisa T, Okuda S, Doi M, Ohkusa T, Ikeda Y, Kobayashi S, Ikemoto N & Matsuzaki M (2005). Defective regulation of interdomain interactions within the ryanodine receptor plays a key role in the pathogenesis of heart failure. *Circulation.* **111**: 3400-10.

Oestreich E, Wang H, Malik S, Kaproth-Joslin K, Blaxall B, Kelley G, Dirksen R & Smrcka A (2007). EPAC-mediated activation of phospholipase Cepsilon plays a critical role in beta-adrenergic receptor dependent enhancement of Ca^{2+} mobilization in cardiac myocytes.
. *J Biol Chem.* **282**: 5488–5495.

Oh S, Choi S, Kim K, Cho E, Kim J & Roh C (2008). Autophagy-related proteins, LC3 and Beclin-1, in placentas from pregnancies complicated by preeclampsia. *Reprod Sci.* **15**: 912-20.

Okada T, Inoue R, Yamazaki K, Maeda A, Kurosaki T, Yamakuni T, Tanaka I, Shimizu S, Ikenaka K, Imoto K & Mori Y (1999). Molecular and functional characterization of a novel mouse transient receptor potential protein homologue TRP7. Ca^{2+}-permeable cation channel that is constitutively activated and enhanced by stimulation of G protein-coupled receptor. *J Biol Chem.* **274**: 27359-70.

Omura T, Nabekura J & Akaike N (1999). Intracellular pathways of V(1) and V(2) receptors activated by arginine vasopressin in rat hippocampal neurons. *J Biol Chem.* **274**: 32762-70.

Partida-Sánchez S, Cockayne D, Monard S, Jacobson E, Oppenheimer N, Garvy B, Kusser K, Goodrich S, Howard M, Harmsen A, Randall T & Lund F (2001). Cyclic ADP-ribose production by CD38 regulates intracellular calcium release, extracellular calcium influx and chemotaxis in neutrophils and is required for bacterial clearance *in vivo*. *Nat Med.* **7**: 1209-16.

Pattillo R & Gey G (1968). The establishment of a cell line of human hormone-synthesizing trophoblastic cells in vitro. *Cancer Res.* **28**: 1231-6.

Pattillo R, Gey G, Delfs E, Huang W, Hause L, Garancis D, Knoth M, Amatruda J, Bertino J, Friesen H & Mattingly R (1971). The hormone-synthesizing trophoblastic cell in vitro: a model for cancer research and placental hormone synthesis. *Ann N Y Acad Sci.* **172**: 288-98.

Pedrozo Z, Sánchez G, Torrealba N, Valenzuela R, Fernández C, Hidalgo C, Lavandero S & Donoso P (2010). Calpains and proteasomes mediate degradation of ryanodine receptors in a model of cardiac ischemic reperfusion. *Biochim Biophys Acta.* **1802**: 356-62.

Pedrozo Z, Torrealba N, Fernández C, Gatica D, Toro B, Quiroga C, Rodriguez A, Sanchez G, Gillette T, Hill J, Donoso P & Lavandero S (2013). Cardiomyocyte ryanodine receptor degradation by chaperone-mediated autophagy. *Cardiovasc Res.* .

Pereira L, Métrich M, Fernández-Velasco M, Lucas A, Leroy J, Perrier R, Morel E, Fischmeister R, Richard S, Bénitah J, Lezoualc'h F & Gómez A (2007). The cAMP binding protein Epac modulates Ca^{2+} sparks by a Ca^{2+}/calmodulin kinase signalling pathway in rat cardiac myocytes. *J Physiol.* **583**: 685-94.

Pessah I, Stambuk R & Casida J (1987). Ca^{2+}-activated ryanodine binding: mechanisms of sensitivity and intensity modulation by Mg^{2+}, caffeine, and adenine nucleotides. *Mol Pharmacol.* **31**: 232-8.

Pessah I & Zimanyi I (1991). Characterization of multiple [3H]ryanodine binding sites on the Ca^{2+} release channel of sarcoplasmic reticulum from skeletal and cardiac muscle: evidence for a sequential mechanism in ryanodine action. *Mol Pharmacol.* **39**: 679-89.

Pessah IN, Waterhouse AL & Casida JE (1985). The calcium-ryanodine receptor complex of skeletal and cardiac muscle. *Biochem. Biophys. Res. Comm.* **67**: 1834-50.

Pitt S, Funnell T, Sitsapesan M, Venturi E, Rietdorf K, Ruas M, Ganesan A, Gosain R, Churchill G, Zhu M, Parrington J, Galione A & Sitsapesan R (2010). TPC2 is a novel NAADP-sensitive Ca^{2+} release channel, operating as a dual sensor of luminal pH and Ca^{2+}. *J Biol Chem.* **285**: 35039-46.

Poisner A (1998). The human placental renin-angiotensin system. *Front Neuroendocrinol.* **19**: 232-52.

Pospechova K, Rozehnal V, Stejskalova L, Vrzal R, Pospisilova N, Jamborova G, May K, Siegmund W, Dvorak Z, Nachtigal P, Semecky V & Pavek P (2009).

Expression and activity of vitamin D receptor in the human placenta and in choriocarcinoma BeWo and JEG-3 cell lines. *Mol Cell Endocrinol.* **299**: 178-87.

Poston L (1997). The control of blood flow to the placenta. *Exp Physiol.* **82**: 377-87.

Pringle K, Tadros M, Callister R & Lumbers E (2011). The expression and localization of the human placental prorenin/renin-angiotensin system throughout pregnancy: roles in trophoblast invasion and angiogenesis? *Placenta.* **32**: 956-62.

Punathil T & Katiyar S (2009). Inhibition of non-small cell lung cancer cell migration by grape seed proanthocyanidins is mediated through the inhibition of nitric oxide, guanylate cyclase, and ERK1/2. *Mol Carcinog.* **48**: 232-42.

Punnonen R, Tuimala R & Viinamäki O (1987). Fetal vasopressin in late pregnancy. Levels in amniotic fluid and in fetal urine. *Ann Chir Gynaecol Suppl.* **202**: 17-9.

Quinlivan RM, Muller CR, Davis M, Laing NG, Evans GA & Dwyer J (2003). Central core disease: clinical, pathological, and genetic features *Archives of Disease in Childhood* **88**: 1051-5.

Ramirez M, Zhao X, Schulman H & Brown J (1997). The nuclear deltaB isoform of Ca^{2+}/calmodulin-dependent protein kinase II regulates atrial natriuretic factor gene expression in ventricular myocytes. *J Biol Chem.*(272): 31203-8.

Rao Y & Xi L (2009). Pivotal effects of phosphodiesterase inhibitors on myocyte contractility and viability in normal and ischemic hearts. *Acta Pharmacol Sin.* **30**: 1-24.

Ratto G, Payne R, Owen W & Tsien R (1988). The concentration of cytosolic free calcium in vertebrate rod outer segments measured with fura-2. *J Neurosci.* **8**: 3240-6.

Regnault T, Galan H, Parker T & Anthony R (2002). Placental development in normal and compromised pregnancies-- a review. *Placenta.* **23**: S119-29.

Rodney G & Schneider M (2003). Calmodulin modulates initiation but not termination of spontaneous Ca^{2+} sparks in frog skeletal muscle. *Biophys J.* **85**: 921-32.

Rodney G, Williams B, Strasburg G, Beckingham K & Hamilton S (2000). Regulation of RYR1 activity by Ca^{2+} and calmodulin. *Biochemistry.* **39**: 7807-12.

Rodriguez P, Bhogal M & Colyer J (2003). Stoichiometric phosphorylation of cardiac ryanodine receptor on serine 2809 by calmodulin-dependent kinase II and protein kinase A. *J Biol Chem.* **278**: 38593-600.

Rossi D & Sorrentino V (2002). Molecular genetics of ryanodine receptors Ca^{2+}-release channels. *Cell Calcium.* **32**: 307-19.

Rossmanith W, Hoffmeister U, Wolfahrt S, Kleine B, McLean M, Jacobs R & Grossman A (1999). Expression and functional analysis of endothelial nitric oxide synthase (eNOS) in human placenta. *Mol Hum Reprod.* **5**: 487–494.

Ruas M, Rietdorf K, Arredouani A, Davis L, Lloyd-Evans E, Koegel H, Funnell T, Morgan A, Ward J, Watanabe K, Cheng X, Churchill G, Zhu M, Platt F, Wessel G, Parrington J & Galione A (2010). Purified TPC isoforms form NAADP receptors with distinct roles for Ca(2+) signaling and endolysosomal trafficking. *Curr Biol.* **20**: 703-9.

Rutherford R, Wharton J, McCarthy A, Gordon L, Sullivan M, Elder M & Polak J (1993). Differential localization of endothelin ETA and ETB binding sites in human placenta. *Br J Pharmacol.* **109**: 544-52.

Sadler TW (2006a). First week of development: ovulation to implantation. Langman's Medical Embryology, Lippincott Williams & Wilkins**:** 31-49.

Sadler TW (2006b). Second week of development: bilaminar germ disc. Langman's Medical Embryology, Lippincott Williams & Wilkins**:** 51-63.

Sadler TW (2006c). Third week of development: trilaminar germ disc. Langman's Medical Embryology, Lippincott Williams & Wilkins**:** 65-86.

Sakurai T, Yanagisawa M, Takuwa Y, Miyazaki H, Kimura S, Goto K & Masaki T (1990). Cloning of a cDNA encoding a non-isopeptide-selective subtype of the endothelin receptor. *Nature.* **348**: 732-5.

Salamonsen L, Dimitriadis E, Jones R & Nie G (2003). Complex regulation of decidualization: a role for cytokines and proteases--a review. *Placenta* **24**: 76-85.

Saldaña C, Díaz-Muñoz M, Antaramián A, González-Gallardo A, García-Solís P & Morales-Tlalpan V (2009). MCF-7 breast carcinoma cells express ryanodine receptor type 1: functional characterization and subcellular localization. *Mol Cell Biochem.* **323**: 39-47.

Salle B, Senterre J, Glorieux F, Delvin E & Putet G (1987). Vitamin D metabolism in preterm infants. *Biol Neonate.* **52** 119-30.

Scarfì S, Ferraris C, Fruscione F, Fresia C, Guida L, Bruzzone S, Usai C, Parodi A, Millo E, Salis A, Burastero G, De Flora A & Zocchi E (2008). Cyclic ADP-ribose-mediated expansion and stimulation of human mesenchymal stem cells by the plant hormone abscisic acid. *Stem Cells.* **26**: 2855-64.

Schauberger C & Pitkin R (1979). Maternal-perinatal calcium relationships. *Obstet Gynecol.* **53**: 74-6.

Schieder M, Rötzer K, Brüggemann A, Biel M & Wahl-Schott C (2010). Characterization of two-pore channel 2 (TPCN2)-mediated Ca^{2+} currents in isolated lysosomes. *J Biol Chem.* **285**: 21219-22.

Schiefer A, Meissner G & Isenberg G (1995). Ca^{2+} activation and Ca^{2+} inactivation of canine reconstituted cardiac sarcoplasmic reticulum Ca(2+)-release channels. *J Physiol.* **489**: 337-48.

Schiessl B, Mylonas I, Hantschmann P, Kuhn C, Schulze S, Kunze S, Friese K & Jeschke U (2005). Expression of endothelial NO synthase, inducible NO synthase, and estrogen receptors alpha and beta in placental tissue of normal, preeclamptic, and intrauterine growth-restricted pregnancies. *J Histochem Cytochem.* **53**: 1441-9.

Sei Y, Gallagher K & Basile A (1999). Skeletal Muscle Type Ryanodine Receptor Is Involved in Calcium Signaling in Human B Lymphocytes. *J Biol Chem.* **274**: 5995-6002.

Senior P, Heath D & Beck F (1991). Expression of parathyroid hormone-related protein mRNA in the rat before birth: demonstration by hybridization histochemistry. *J Mol Endocrinol.* **6**: 281-90.

Sharma MR, Jeyakumar LH, Fleischer S & Wagenknecht T (2000). Three-dimensional Structure of Ryanodine Receptor Isoform Three in Two Conformational States as Visualized by Cryo-electron Microscopy. *J Biol Chem.* **275**: 9485-91.

Shichiri M, Hirata Y, Nakajima T, Ando K, Imai T, Yanagisawa M, Masaki T & Marumo F (1991). Endothelin-1 is an autocrine/paracrine growth factor for human cancer cell lines. *J Clin Invest.* **87**: 1867-71.

Shin D, Ma J & Kim D (2000). The asp-rich region at the carboxyl-terminus of calsequestrin binds to Ca^{2+} and interacts with triadin. *FEBS Lett.* **486**: 178-82.

Shin D, Pan Z, Kim E, Lee J, Bhat M, Parness J, Kim D & J. M (2003). A retrograde signal from calsequestrin for the regulation of store-operated Ca2+ entry in skeletal muscle. *J Biol Chem.* **278**: 3286-92.

Shobe J (2002). The role of PKA, CaMKII, and PKC in avoidance conditioning: permissive or instructive? *Neurobiol Learn Mem.* **77**: 291-312.

Shoshan-Barmatz V, Weil S, Meyer H, Varsanyi M & Heilmeyer L (1994). Endogenous, Ca^{2+}-dependent cysteine-protease cleaves specifically the ryanodine receptor/Ca2+ release channel in skeletal muscle. *J Membr Biol.* **142**: 281-8.

Sitsapesan R, McGarry S & Williams A (1994). Cyclic ADP-ribose competes with ATP for the adenine nucleotide binding site on the cardiac ryanodine receptor Ca^{2+}-release channel. . *Circ Res.* **75**: 596–600.

Sitsapesan R & Williams A (1994). Regulation of the gating of the sheep cardiac sarcoplasmic reticulum Ca^{2+}-release channel by luminal Ca^{2+}. *J Membr Biol.* **137**: 215-26.

Sitsapesan R & Williams A (1995). The gating of the sheep skeletal sarcoplasmic reticulum Ca^{2+}-release channel is regulated by luminal Ca^{2+}. *J Membr Biol.* **146**: 133-44.

Smith I, Hitt B, Green K, Oddo S & LaFerla F (2005). Enhanced caffeine-induced Ca2+ release in the 3xTg-AD mouse model of Alzheimer's disease. *J Neurochem.* **94**: 1711-8.

Smith J, Coronado R & Meissner G (1985). Sarcoplasmic reticulum contains adenine nucleotide-activated calcium channels. *Nature* **316**: 446–449.

Smith JS, Coronado R & Meissner G (1986). Single channel measurements of the calcium release channel from skeletal muscle sarcoplasmic reticulum. Activation by Ca2+ and ATP and modulation by Mg2+. *J Gen Physiol* **88**: 573-88.

Sooranna S & Das I (1995). The inter-relationship between polyamines and the L-arginine nitric oxide pathway in the human placenta. *Biochem Biophys Res Commun.* **212**: 229-34.

Sorrentino V & Volpe P (1993). Ryanodine receptors: how many, where and why? *Trends Pharmacol Sci* **14**: 98-103.

Strid H, Bucht E, Jansson T, Wennergren M & Powell T (2003). ATP dependent Ca^{2+} transport across basal membrane of human syncytiotrophoblast in pregnancies complicated by intrauterine growth restriction or diabetes. *Placenta.* **24**: 445-52.

Stutzmann G, Smith I, Caccamo A, Oddo S, Parker I & Laferla F (2007). Enhanced ryanodine-mediated calcium release in mutant PS1-expressing Alzheimer's mouse models. *Ann N Y Acad Sci.* **1097**: 265-77.

Suko J, Maurer-Fogy I, Plank B, Bertel O, Wyskovsky W, Hohenegger M & Hellmann G (1993). Phosphorylation of serine 2843 in ryanodine receptor-calcium release channel of skeletal muscle by cAMP-, cGMP- and CaM-dependent protein kinase. *Biochim Biophys Acta.* **1175**: 193-206.

Supnet C, Grant J, Kong H, Westaway D & Mayne M (2006). Amyloid-beta-(1-42) increases ryanodine receptor-3 expression and function in neurons of TgCRND8 mice. *J Biol Chem.* **281**: 38440-7.

Supnet C, Noonan C, Richard K, Bradley J & Mayne M (2010). Up-regulation of the type 3 ryanodine receptor is neuroprotective in the TgCRND8 mouse model of Alzheimer's disease. *J Neurochem.* **112**: 356-65.

Sutko J & Airey J (1996). Ryanodine receptor Ca2+ release channels: does diversity in form equal diversity in function? *Physiol Rev.* **76**: 1027-71.

Sydorenko V, Shuba Y, Thebault S, Roudbaraki M, Lepage G, Prevarskaya N & Skryma R (2003). Receptor-coupled, DAG-gated Ca2+-permeable cationic channels in LNCaP human prostate cancer epithelial cells. *J Physiol.* **548**: 823-36.

Takasago T, Imagawa T & Shigekawa M (1989). Phosphorylation of the cardiac ryanodine receptor by cAMP-dependent protein kinase. *J Biochem.* **106**: 872-7.

Takeshima H (1993). Primary structure and expression from cDNAs of the ryanodine receptor. *Ann N Y Acad Sci.* **707**: 165-77.

Takeshima H, Iino M, Takekura H, Nishi M, Kuno J, Minowa O, Takano H & Noda T (1994). Excitation-contraction uncoupling and muscular degeneration in mice lacking functional skeletal muscle ryanodine-receptor gene. *Nature.* **369**: 556-9.

Takeshima H, Ikemoto T, Nishi M, Nishiyama N, Shimuta M & Sugitani Y (1996). Generation and characterization of mutant mice lacking ryanodine receptor type 3. *J Biol Chem.* **271**: 19649-52.

Takeshima H, Komazaki S, Hirose K, Nishi M, Noda T & Iino M (1998). Embryonic lethality and abnormal cardiac myocytes in mice lacking ryanodine receptor type 2. *EMBO J.* **17**: 3309-16.

Takeshima H, Nishimura S, Matsumoto T, Ishida H & Kangawa K (1989). Primary structure and expression from complementary DNA of skeletal muscle ryanodine receptor. *Nature* **339**: 439-45.

Tanfin Z, Leiber D, Robin P, Oyeniran C & Breuiller-Fouché M (2011). Endothelin-1: physiological and pathological roles in myometrium. *Int J Biochem Cell Biol.* **43**: 299-302.

Tao R, Sun H, Lau C, Tse H, Lee H & Li G (2011). Cyclic ADP ribose is a novel regulator of intracellular Ca^{2+} oscillations in human bone marrow mesenchymal stem cells. *J Cell Mol Med.* **15**: 2684-96.

Terentyev D, Nori A, Santoro M, Viatchenko-Karpinski S, Kubalova Z, Gyorke I, Terentyeva R, Vedamoorthyrao S, Blom N, Valle G, Napolitano C, Williams S, Volpe P, Priori S & Gyorke S (2006). Abnormal interactions of calsequestrin with the ryanodine receptor calcium release channel complex linked to exercise-induced sudden cardiac death. *Circ Res.* **98**: 1151-8.

Terentyev D, Viatchenko-Karpinski S, Gyorke I, Terentyeva R & Gyorke S (2003). Protein phosphatases decrease sarcoplasmic reticulum calcium content by stimulating calcium release in cardiac myocytes. *J Physiol.* **552**: 109-18.

Thibonnier M, Kilani A, Rahman M, DiBlasi T, Warner K, Smith M, Leenhardt A & Brouard R (1999). Effects of the nonpeptide V(1) vasopressin receptor antagonist SR49059 in hypertensive patients. *Hypertension.* **34**: 1293-300.

Thomas AP & Delaville F (1991). The Use of Fluorescent Indicators for Measurements of Cytosolic-free Calcium Concentration in Cell Populations and Single Cells. Cellular Calcium: A Practical Approach. J. G. McCormack and P. H. Cobbold. Oxford, Oxford University Press**:** 27.

Thors B, Halldórsson H & Thorgeirsson G (2004). Thrombin and histamine stimulate endothelial nitric-oxide synthase phosphorylation at Ser1177 via an AMPK mediated pathway independent of PI3K-Akt. *FEBS Lett.* **573**: 175-80.

Tilgen N, Zorzato F, Halliger-Keller B, Muntoni F, Sewry C, Palmucci L, Schneider C, Hauser E, Lehmann-Horn F, Müller C & Treves S (2001). Identification of four novel mutations in the C-terminal membrane spanning domain of the ryanodine receptor 1: association with central core disease and alteration of calcium homeostasis. *Hum Mol Genet.* **10**: 2879-87.

Timerman A, Wiederrecht G, Marcy A & Fleischer S (1995). Characterization of an exchange reaction between soluble FKBP-12 and the FKBP.ryanodine receptor complex. Modulation by FKBP mutants deficient in peptidyl-prolyl isomerase activity. *J Biol Chem.* **270**: 2451-9.

Timerman AP, Ogunbumni E, Freund E, Wiederrecht G, Marks AR & Fleischer S (1993). The calcium release channel of sarcoplasmic reticulum is modulated by FK-506-binding protein. Dissociation and reconstitution of FKBP-12 to the calcium release channel of skeletal muscle sarcoplasmic reticulum. *J Biol Chem.* **268**: 22992-9.

Timerman AP, Onoue H, Xin HB, Barg S, Copello JA, Wiederrecht G & Fleischer S (1996). Selective binding of FKBP12.6 by the cardiac ryanodine receptor. *J Biol Chem.* **271**: 20385-91.

Tinker A & Williams A (1992). Divalent cation conduction in the ryanodine receptor channel of sheep cardiac muscle sarcoplasmic reticulum. *J Gen Physiol.* **100**: 479-93.

Tinker A & Williams AJ (1995). Measuring the length of the pore of the sheep cardiac sarcoplasmic reticulum calcium-release channel using related trimethylammonium ions as molecular calipers. *Biophys J.* **68**: 111-20.

Togashi K, Hara Y, Tominaga T, Higashi T, Konishi Y, Mori Y & Tominaga M (2006). TRPM2 activation by cyclic ADP-ribose at body temperature is involved in insulin secretion. *EMBO J.* **25**: 1804-15.

Tohgo A, Pierce K, Choy E, Lefkowitz R & Luttrell L (2002). beta-Arrestin scaffolding of the ERK cascade enhances cytosolic ERK activity but inhibits ERK-mediated transcription following angiotensin AT1a receptor stimulation. *J Biol Chem.* **277**: 9429–9436.

Trausch J, Grenfell S, Handley-Gearhart P, Ciechanover A & Schwartz A (1993). Immunofluorescent localization of the ubiquitin-activating enzyme, E1, to the nucleus and cytoskeleton. *Am J Physiol.* **264**: C93-102.

Treves S, Larini F, Menegazzi P, Steinberg T, Koval M, Vilsen B, Andersen J & Zorzato F (1994). Alteration of intracellular Ca2+ transients in COS-7 cells transfected with the cDNA encoding skeletal-muscle ryanodine receptor carrying a mutation associated with malignant hyperthermia. *Biochem J.* **301**: 661-5.

Tunwell R, Wickenden C, Bertrand B, Shevchenko V, Walsh M, Allen P & Lai F (1996). The human cardiac muscle ryanodine receptor-calcium release channel: identification, primary structure and topological analysis. *Biochem J.* **318**: 477-87.

Vassilopoulos S, Thevenon D, Rezgui S, Brocard J, Chapel A, Lacampagne A, Lunardi J, Dewaard M & Marty I (2005). Triadins are not triad-specific proteins: two new skeletal muscle triadins possibly involved in the architecture of sarcoplasmic reticulum. *J Biol Chem.* **280**: 28601-9.

Venkatachalam K, Ma H, Ford D & Gill D (2001). Expression of functional receptor-coupled TRPC3 channels in DT40 triple receptor InsP3 knockout cells. *J Biol Chem.* **276**: 33980-5.

Venturi E, Pitt S, Galfré E & Sitsapesan R (2012). From eggs to hearts: what is the link between cyclic ADP-ribose and ryanodine receptors? *Cardiovasc Ther.* **30**: 109-16.

Viatchenko-Karpinski S, Terentyev D, Györke I, Terentyeva R, Volpe P, Priori S, Napolitano C, Nori A, Williams S & Györke S (2004). Abnormal calcium signaling and sudden cardiac death associated with mutation of calsequestrin. *Circ Res.* **94**: 471-7.

Vićovac L & Aplin J (1996). Epithelial-mesenchymal transition during trophoblast differentiation. *Acta Anat (Basel).* **156**: 202-16.

Vukcevic M, Broman M, Islander G, Bodelsson M, Ranklev-Twetman E, Müller C & Treves S (2010). Functional properties of RYR1 mutations identified in Swedish patients with malignant hyperthermia and central core disease. *Anesth Analg.* **111**: 185-90.

Wagenknecht T & Radermacher M (1997). Ryanodine receptors: structure and macromolecular interactions. *Curr Opin Struct Biol.* **7**: 958-265.

Wang J, Needleman D & Hamilton S (1993). Relationship of low affinity [3]ryanodine binding sites to high affinity sites on the skeletal muscle Ca^{2+} release channel. *J Biol Chem.* **268**: 20974-82.

Wang S, Trumble W, Liao H, Wesson C, Dunker A & Kang C (1998). Crystal structure of calsequestrin from rabbit skeletal muscle sarcoplasmic reticulum. *Nat Struct Biol.* **5**: 476-83.

Wang X, Reznick S, Li P, Liang W & van Breemen C (2002). Ca^{2+} removal mechanisms in freshly isolated rabbit aortic endothelial cells. *Cell Calcium.* **31**: 265-77.

Wang Y, Li X, Duan H, Fulton T, Eu J & Meissne G (2009). Altered stored calcium release in skeletal myotubes deficient of triadin and junctin. *Cell Calcium.* **45**: 29-37.

Wegner M, Cao Z & Rosenfeld MG (1992). Calcium-Regulated Phosphorylation Within the Leucine Zipper of C/EBPβ. *Science.* **256**: 370–373.

Wehrens X, Lehnart S, Huang F, Vest J, Reiken S, Mohler P, Sun J, Guatimosim S, Song L, Rosemblit N, D'Armiento J, Napolitano C, Memmi M, Priori S, Lederer W & Marks A (2003). FKBP12.6 deficiency and defective calcium release channel

(ryanodine receptor) function linked to exercise-induced sudden cardiac death. *Cell.* **113**: 829-40.

Wehrens X, Lehnart S, Reiken S & Marks A (2004). Ca^{2+}/calmodulin-dependent protein kinase II phosphorylation regulates the cardiac ryanodine receptor. *Circ Res.* **94**: e61-70.

Wehrens X, Lehnart S, Reiken S, Vest J, Wronska A & AR. M (2006). Ryanodine receptor/calcium release channel PKA phosphorylation: a critical mediator of heart failure progression. *Proc Natl Acad Sci U S A.* **103**: 511-8.

Wice B, Menton D, Geuze H & Schwartz A (1990). Modulators of cyclic AMP metabolism induce syncytiotrophoblast formation *in vitro*. *Exp Cell Res.* **186**: 306-16.

Williams P, Mistry H, Innes B, Bulmer J & Pipkin F (2010). Expression of AT1R, AT2R and AT4R and their roles in extravillous trophoblast invasion in the human. *Placenta.* **31**: 448-55.

Witcher D, Kovacs R, Schulman H, Cefali D & Jones L (1991). Unique phosphorylation site on the cardiac ryanodine receptor regulates calcium channel activity. *J Biol Chem.* **266**: 11144-52.

Xia C, Bao Z, Yue C, Sanborn B & Liu M (2001). Phosphorylation and regulation of G-protein-activated phospholipase C-beta 3 by cGMP-dependent protein kinases. *J Biol Chem.* **276**: 19770-7.

Xiao B, Sutherland C, Walsh M & Chen S (2004). Protein kinase A phosphorylation at serine-2808 of the cardiac Ca2+-release channel (ryanodine receptor) does not dissociate 12.6-kDa FK506-binding protein (FKBP12.6). *Circ Res.* **94**: 487-95.

Xu L & Meissner G (2004). Mechanism of calmodulin inhibition of cardiac sarcoplasmic reticulum Ca^{2+} release channel (ryanodine receptor). *Biophys J.* **86**: 797-804.

Xue H, Zhao D, Suda T, Uchida C, Oda T, Chida K, Ichiyama A & Nakamura H (2000). Store depletion by caffeine/ryanodine activates capacitative Ca^{2+} entry in nonexcitable A549 cells. *J Biochem.* **128**: 329-36.

Yamaguchi N, Xu L, Pasek D, Evans K, Chen S & Meissner G (2005). Calmodulin regulation and identification of calmodulin binding region of type-3 ryanodine receptor calcium release channel. *Biochemistry.* **44**: 15074-81.

Yamaguchi N, Xu L, Pasek D, Evans K & Meissner G (2003). Molecular basis of calmodulin binding to cardiac muscle Ca^{2+} release channel (ryanodine receptor). *J Biol Chem.* **278**: 23480-6.

Yamasaki M, Masgrau R, Morgan A, Churchill G, Patel S, Ashcroft S & Galione A (2004). Organelle selection determines agonist-specific Ca^{2+} signals in pancreatic acinar and beta cells. *J Biol Chem.* **279**: 7234-40.

Yano M, Ono K, Ohkusa T, Suetsugu M, Kohno M, Hisaoka T, Kobayashi S, Hisamatsu Y, Yamamoto T, Kohno M, Noguchi N, Takasawa S, Okamoto H & Matsuzaki M (2000). Altered stoichiometry of FKBP12.6 versus ryanodine receptor as a cause of abnormal Ca^{2+} leak through ryanodine receptor in heart failure. *Circulation.* **102**: 2131-6.

Ye J, Coulouris G, Zaretskaya I, Cutcutache I, Rozen S & Madden T (2012). Primer-BLAST: a tool to design target-specific primers for polymerase chain reaction. *BMC Bioinformatics.* **13**: 134.

Yehia G, Schlotter F, Razavi R, Alessandrini A & Molina C (2001). Mitogen-activated protein kinase phosphorylates and targets inducible cAMP early repressor to ubiquitin-mediated destruction. *J Biol Chem.* **276**: 35272-9.

Yip K (2006). Epac-mediated Ca^{2+} mobilization and exocytosis in inner medullary collecting duct. *Am J Physiol Renal Physiol.* **291**: F882-90.

Yohn JJ, Smith C, Stevens T, Hoffman TA, Morelli JG, Hurt DL, Yanagisawa M, Kane MA & Zamora MR (1994). Human melanoma cells express functional endothelin-1 receptors. *Biochem Biophys Res Commun.* **201**: 449-57.

Zaidi M, Shankar V, Tunwell R, Adebanjo O, Mackrill J, Pazianas M, O'Connell D, Simon B, Rifkin B, Venkitaraman A & al. e (1995). A ryanodine receptor-like molecule expressed in the osteoclast plasma membrane functions in extracellular Ca^{2+} sensing. *J Clin Invest.* **96**: 1582-90.

Zalk R, Lehnart SE & Marks AR (2007). Modulation of the Ryanodine Receptor and Intracellular Calcium. *Annu Rev Biochem.* **76**: 367-85.

Zhang L, Kelley J, Schmeisser G, Kobayashi Y & Jones L (1997). Complex formation between junctin, triadin, calsequestrin, and the ryanodine receptor. Proteins of the cardiac junctional sarcoplasmic reticulum membrane. *J Biol Chem.* **272**: 23389-97.

Zhang Y, Chen H, Khanna V, De Leon S, Phillips M, Schappert K, Britt B, Browell A & MacLennan D (1993). A mutation in the human ryanodine receptor gene associated with central core disease. *Nat Genet.* **5**: 46-50.

Zhao F, Li P, Chen S, Louis C & Fruen B (2001). Dantrolene inhibition of ryanodine receptor Ca^{2+} release channels. Molecular mechanism and isoform selectivity. *J Biol Chem.* **276**: 13810-6.

Zhao M, Li P, Li X, Zhang L, Winkfein R & Chen S (1999). Molecular identification of the ryanodine receptor pore-forming segment. *J Biol Chem.* **274**: 25971-4.

Zhou H, Lillis S, Loy RE, Ghassemi F, Rose M, Norwood F, Mills K, Al-Sarraj S, Lane R, Feng L, Matthews E, Sewry C, Abbs S, Buk S, Hanna M, Treves S, Dirksen R, Meissner G, Muntoni F & Jungbluth H (2010). Multi-minicore disease and atypical periodic paralysis associated with novel mutations in the skeletal muscle ryanodine receptor (RYR1) gene. *Neuromuscul Disord.* **20**: 166-73.

Zhou Y, Fisher S, Janatpour M, Genbacev O, Dejana E, Wheelock M & Damsky C (1997). Human cytotrophoblasts adopt a vascular phenotype as they differentiate. A strategy for successful endovascular invasion? *J Clin Invest.* **99**: 2139-51.

Zimányi I, Buck E, Abramson J, Mack M & Pessah I (1992). Ryanodine induces persistent inactivation of the Ca2+ release channel from skeletal muscle sarcoplasmic reticulum. *Mol Pharmacol.* **42**: 1049-57.

Zissimopoulos S, Docrat N & Lai F (2007). Redox sensitivity of the ryanodine receptor interaction with FK506-binding protein. *J Biol Chem.* **282**: 6976-83.

Zissimopoulos S & Lai FA (2007). Ryanodine receptor structure, function and pathophysiology. Calcium : A Matter of Life or Death. J. Krebs and M. Michalak. **41:** 287-342.

Zorzato F, Fujii J, Otsu K, Phillips M, Green N, Lai F, Meissner G & MacLennan D (1990). Molecular cloning of cDNA encoding human and rabbit forms of the Ca2+ release channel (ryanodine receptor) of skeletal muscle sarcoplasmic reticulum. *J Biol Chem.* **265**: 2244-56.

Zorzato F, Scutari E, Tegazzin V, Clementi E & Treves S (1993). Chlorocresol: an activator of ryanodine receptor-mediated Ca^{2+} release. *Mol Pharmacol.* **44**: 1192-201.

Appendix 0. IF Microscopy in JEG-3 Cells

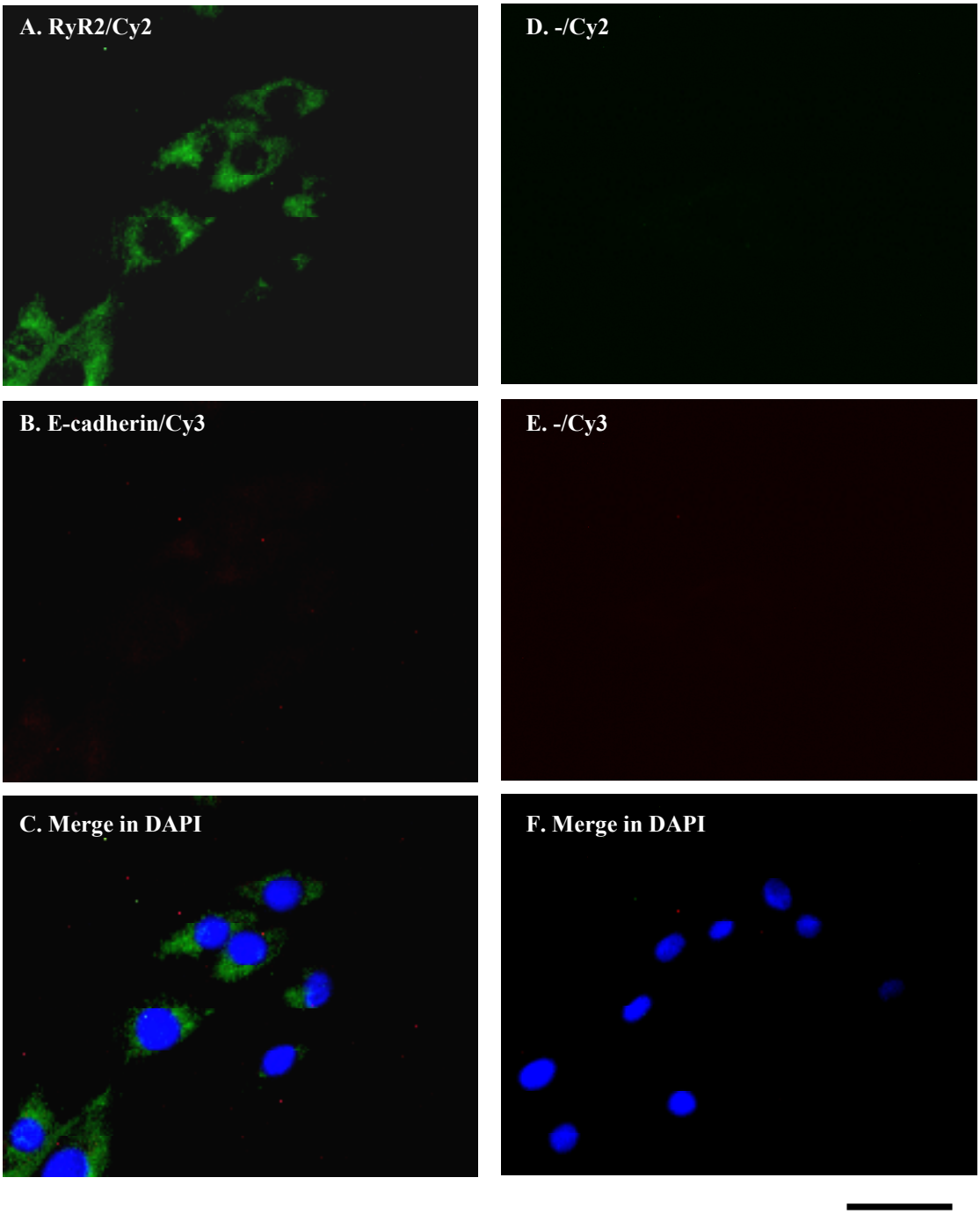

Appendix 0.. The IF microscopy in JEG-cells. Panel A, cells were stained with anti-RyR2 antiserum (AB9080) as primary antibody; Panel B, cells were stained with anti-E-cadherin (ab1416) as primary antibody; Panel D and E, negative controls: no primary antibodies used; Panel C and F, merge images. Scale bar: 10 µm.

Appendix I.

Sequences alignment of human skeletal *RYR1* (NM_001042723) and PCR product obtained from BeWo cell RNA (query). The PCR product of *RYR1* was amplified by using downstream primer (5′-dCAGATGAAGCATTTGGTCTCCAT-3′) pairs to the upstream primers JBR1 (5′-dGACATGGAAGGCTCAGCTGCT-3′).

>ref|NM_001042723.1| Homo sapiens ryanodine receptor 1 (skeletal) (RYR1), transcript variant 2, mRNA
Length=15376

GENE ID: 6261 RYR1 | ryanodine receptor 1 (skeletal) [Homo sapiens]
(Over 100 PubMed links)

Score = 1570 bits (850), Expect = 0.0
Identities = 852/853 (99%), Gaps = 0/853 (0%)
Strand=Plus/Plus

```
Query  2      GGCGATGAGGATGAGAACATGGTGTACTACTTCCTGGAGGAAAGCACAGGCTACATGGAA  61
              ||||||||||||||||||||||||||||||||||||||||||||||||||||||||||||
Sbjct  13979  GGCGATGAGGATGAGAACATGGTGTACTACTTCCTGGAGGAAAGCACAGGCTACATGGAA  14038

Query  62     CCCGCCCTGCGGTGTCTGAGCCTCCTGCATACACTGGTGGCCTTTCTCTGCATCATTGGC  121
              ||||||||||||||||||||||||||||||||||||||||||||||||||||||||||||
Sbjct  14039  CCCGCCCTGCGGTGTCTGAGCCTCCTGCATACACTGGTGGCCTTTCTCTGCATCATTGGC  14098

Query  122    TATAATTGTCTCAAGGTGCCCCTGGTAATCTTTAAGCGGGAGAAGGAGCTGGCCCGGAAG  181
              ||||||||||||||||||||||||||||||||||||||||||||||||||||||||||||
Sbjct  14099  TATAATTGTCTCAAGGTGCCCCTGGTAATCTTTAAGCGGGAGAAGGAGCTGGCCCGGAAG  14158

Query  182    CTGGAGTTTGATGGCCTGTACATCACGGAGCAGCCTGAGGACGATGACGTGAAGGGGCAG  241
              ||||||||||||||||||||||||||||||||||||||||||||||||||||||||||||
Sbjct  14159  CTGGAGTTTGATGGCCTGTACATCACGGAGCAGCCTGAGGACGATGACGTGAAGGGGCAG  14218

Query  242    TGGGACCGACTGGTGCTCAACACGCCGTCTTTCCCTAGCAACTACTGGGACAAGTTTGTC  301
              ||||||||||||||||||||||||||||||||||||||||||||||||||||||||||||
Sbjct  14219  TGGGACCGACTGGTGCTCAACACGCCGTCTTTCCCTAGCAACTACTGGGACAAGTTTGTC  14278

Query  302    AAGCGCAAGGTCCTGGACAAACATGGGGACATCTACGGGCGGGAGCGGATTGCTGAGCTA  361
              ||||||||||||||||||||||||||||||||||||||||||||||||||||||||||||
Sbjct  14279  AAGCGCAAGGTCCTGGACAAACATGGGGACATCTACGGGCGGGAGCGGATTGCTGAGCTA  14338

Query  362    CTGGGCATGGACCTGGCCACACTAGAGATCACCGCCCACAATGAGCGCAAGCCCAACCCG  421
              ||||||||||||||||||||||||||||||| ||||||||||||||||||||||||||||
Sbjct  14339  CTGGGCATGGACCTGGCCACACTAGAGATCACAGCCCACAATGAGCGCAAGCCCAACCCG  14398

Query  422    CCGCCAGGGCTGCTGACCTGGCTCATGTCCATCGATGTCAAGTACCAGATCTGGAAGTTC  481
              ||||||||||||||||||||||||||||||||||||||||||||||||||||||||||||
Sbjct  14399  CCGCCAGGGCTGCTGACCTGGCTCATGTCCATCGATGTCAAGTACCAGATCTGGAAGTTC  14458

Query  482    GGGGTCATCTTCACAGACAACTCCTTCCTGTACCTGGGCTGGTATATGGTGATGTCCCTC  541
              ||||||||||||||||||||||||||||||||||||||||||||||||||||||||||||
Sbjct  14459  GGGGTCATCTTCACAGACAACTCCTTCCTGTACCTGGGCTGGTATATGGTGATGTCCCTC  14518

Query  542    TTGGGACACTACAACAACTTCTTCTTTGCTGCCCATCTCCTGGACATCGCCATGGGGGTC  601
              ||||||||||||||||||||||||||||||||||||||||||||||||||||||||||||
Sbjct  14519  TTGGGACACTACAACAACTTCTTCTTTGCTGCCCATCTCCTGGACATCGCCATGGGGGTC  14578

Query  602    AAGACGCTGCGCACCATCCTGTCCTCTGTCACCCACAATGGGAAACAGCTGGTGATGACC  661
              ||||||||||||||||||||||||||||||||||||||||||||||||||||||||||||
Sbjct  14579  AAGACGCTGCGCACCATCCTGTCCTCTGTCACCCACAATGGGAAACAGCTGGTGATGACC  14638

Query  662    GTGGGCCTTCTGGCGGTGGTCGTCTACCTGTACACCGTGGTGGCCTTCAACTTCTTCCGC  721
              ||||||||||||||||||||||||||||||||||||||||||||||||||||||||||||
Sbjct  14639  GTGGGCCTTCTGGCGGTGGTCGTCTACCTGTACACCGTGGTGGCCTTCAACTTCTTCCGC  14698

Query  722    AAGTTCTACAACAAGAGCGAGGATGAGGATGAACCTGACATGAAGTGTGATGACATGATG  781
              ||||||||||||||||||||||||||||||||||||||||||||||||||||||||||||
Sbjct  14699  AAGTTCTACAACAAGAGCGAGGATGAGGATGAACCTGACATGAAGTGTGATGACATGATG  14758

Query  782    ACGTGTTACCTGTTTCACATGTACGTGGGTGTCCGGGCTGGCGGAGGCATTGGGGACGAG  841
              ||||||||||||||||||||||||||||||||||||||||||||||||||||||||||||
Sbjct  14759  ACGTGTTACCTGTTTCACATGTACGTGGGTGTCCGGGCTGGCGGAGGCATTGGGGACGAG  14818

Query  842    ATCGAGGACCCCG  854
              |||||||||||||
Sbjct  14819  ATCGAGGACCCCG  14831
```

Appendix II.

Sequences alignment of human cardiac *RYR2* (NM_001035.2) and PCR product obtained from BeWo cell RNA (query). The PCR product of *RYR2* was amplified by using downstream primer (5′-dCAGATGAAGCATTTGGTCTCCAT-3′) pairs to the upstream primers JBR2 (5′-dAAGGAGCTCCCCACGAGAAGT-3′).

>ref|NM_001035.2| Homo sapiens ryanodine receptor 2 (cardiac) (RYR2), mRNA
Length=16365

GENE ID: 6262 RYR2 | ryanodine receptor 2 (cardiac) [Homo sapiens]
(Over 100 PubMed links)

Score = 1760 bits (953), Expect = 0.0
Identities = 956/957 (99%), Gaps = 1/957 (0%)
Strand=Plus/Plus

```
Query  1      GTGAC-AGCCTGGACAGCAGCTCCCATAGAATCATCGCAGTTCACTATGTACTAGAGGAG  59
              ||||| ||||||||||||||||||||||||||||||||||||||||||||||||||||||
Sbjct  13750  GTGACAAGCCTGGACAGCAGCTCCCATAGAATCATCGCAGTTCACTATGTACTAGAGGAG  13809

Query  60     AGCAGCGGCTACATGGAGCCCACGTTGCGTATCTTAGCTATTCTGCACACGGTCATTTCT  119
              ||||||||||||||||||||||||||||||||||||||||||||||||||||||||||||
Sbjct  13810  AGCAGCGGCTACATGGAGCCCACGTTGCGTATCTTAGCTATTCTGCACACGGTCATTTCT  13869

Query  120    TTCTTCTGCATCATTGGATACTACTGCTTGAAAGTCCCATTGGTTATTTTTAAGCGAGAA  179
              ||||||||||||||||||||||||||||||||||||||||||||||||||||||||||||
Sbjct  13870  TTCTTCTGCATCATTGGATACTACTGCTTGAAAGTCCCATTGGTTATTTTTAAGCGAGAA  13929

Query  180    AAGGAAGTGGCACGGAAATTGGAATTTGATGGGCTTTATATTACAGAACAGCCTTCAGAA  239
              ||||||||||||||||||||||||||||||||||||||||||||||||||||||||||||
Sbjct  13930  AAGGAAGTGGCACGGAAATTGGAATTTGATGGGCTTTATATTACAGAACAGCCTTCAGAA  13989

Query  240    GATGATATTAAAGGCCAGTGGGATAGACTCGTAATCAACACACAGTCATTTCCCAACAAC  299
              ||||||||||||||||||||||||||||||||||||||||||||||||||||||||||||
Sbjct  13990  GATGATATTAAAGGCCAGTGGGATAGACTCGTAATCAACACACAGTCATTTCCCAACAAC  14049

Query  300    TACTGGGACAAATTTGTTAAAAGAAAGGTTATGGATAAATATGGAGAGTTCTACGGCCGA  359
              ||||||||||||||||||||||||||||||||||||||||||||||||||||||||||||
Sbjct  14050  TACTGGGACAAATTTGTTAAAAGAAAGGTTATGGATAAATATGGAGAGTTCTACGGCCGA  14109

Query  360    GACAGAATCAGTGAATTACTTGGCATGGACAAGGCAGCTCTGGACTTCAGTGATGCCAGA  419
              ||||||||||||||||||||||||||||||||||||||||||||||||||||||||||||
Sbjct  14110  GACAGAATCAGTGAATTACTTGGCATGGACAAGGCAGCTCTGGACTTCAGTGATGCCAGA  14169

Query  420    GAAAAGAAGAAGCCAAAGAAAGACAGCTCCTTATCAGCTGTACTGAACTCCATTGATGTG  479
              ||||||||||||||||||||||||||||||||||||||||||||||||||||||||||||
Sbjct  14170  GAAAAGAAGAAGCCAAAGAAAGACAGCTCCTTATCAGCTGTACTGAACTCCATTGATGTG  14229

Query  480    AAGTATCAGATGTGGAAACTAGGAGTCGTTTTCACTGACAACTCCTTCCTCTACCTAGCC  539
              ||||||||||||||||||||||||||||||||||||||||||||||||||||||||||||
Sbjct  14230  AAGTATCAGATGTGGAAACTAGGAGTCGTTTTCACTGACAACTCCTTCCTCTACCTAGCC  14289

Query  540    TGGTATATGACTATGTCTGTTCTTGGACACTATAACAACtttttttttGCCGCTCACCTT  599
              ||||||||||||||||||||||||||||||||||||||||||||||||||||||||||||
Sbjct  14290  TGGTATATGACTATGTCTGTTCTTGGACACTATAACAACTTTTTTTTTGCCGCTCACCTT  14349

Query  600    CTCGACATTGCTATGGGATTCAAGACATTAAGAACCATCTTGTCCTCAGTAACTCACAAT  659
              ||||||||||||||||||||||||||||||||||||||||||||||||||||||||||||
Sbjct  14350  CTCGACATTGCTATGGGATTCAAGACATTAAGAACCATCTTGTCCTCAGTAACTCACAAT  14409

Query  660    GGCAAACAGCTCGTATTAACCGTTGGCTTATTAGCTGTTGTTGTATACCTATACACTGTG  719
              ||||||||||||||||||||||||||||||||||||||||||||||||||||||||||||
Sbjct  14410  GGCAAACAGCTCGTATTAACCGTTGGCTTATTAGCTGTTGTTGTATACCTATACACTGTG  14469

Query  720    GTGGCATTCAATTTTTTCCGAAAATTCTACAATAAAAGTGAAGATGGTGATACACCAGAT  779
              ||||||||||||||||||||||||||||||||||||||||||||||||||||||||||||
Sbjct  14470  GTGGCATTCAATTTTTTCCGAAAATTCTACAATAAAAGTGAAGATGGTGATACACCAGAT  14529

Query  780    ATGAAATGTGACGATATGCTAACATGCTATATGTTCCACATGTATGTTGGAGTTCGTGCT  839
              ||||||||||||||||||||||||||||||||||||||||||||||||||||||||||||
Sbjct  14530  ATGAAATGTGACGATATGCTAACATGCTATATGTTCCACATGTATGTTGGAGTTCGTGCT  14589

Query  840    GGAGGAGGGATCGGGGATGAAATCGAAGACCCAGCAGGAGATGAATATGAGATCTATCGA  899
              ||||||||||||||||||||||||||||||||||||||||||||||||||||||||||||
Sbjct  14590  GGAGGAGGGATCGGGGATGAAATCGAAGACCCAGCAGGAGATGAATATGAGATCTATCGA  14649

Query  900    ATCATCTTTGACATCACTTTCTTCTTCTTTGTTATTGTCATTCTCTTGGCCATAATA  956
              ||||||||||||||||||||||||||||||||||||||||||||||||||||||||||
Sbjct  14650  ATCATCTTTGACATCACTTTCTTCTTCTTTGTTATTGTCATTCTCTTGGCCATAATA  14706
```

Appendix III.

Sequences alignment of human skeletal *RYR1* (NM_001042723) and PCR product obtained from JAR cell RNA (query). The PCR product of *RYR1* was amplified by using downstream primer (5′-dCAGATGAAGCATTTGGTCTCCAT-3′) pairs to the upstream primers JBR1 (5′-dGACATGGAAGGCTCAGCTGCT-3′).

>ref|NM_001042723.1| Homo sapiens ryanodine receptor 1 (skeletal) (RYR1), transcript variant 2, mRNA
Length=15376

GENE ID: 6261 RYR1 | ryanodine receptor 1 (skeletal) [Homo sapiens]
(Over 100 PubMed links)

Score = 1803 bits (976), Expect = 0.0
Identities = 976/976 (100%), Gaps = 0/976 (0%)
Strand=Plus/Plus

```
Query  1      TGGTGGCAGCTCTGGCTGGGGCTTGGGGGCCCGGAGAGGAGGCACAGGGCGATGAGGATGA  60
              ||||||||||||||||||||||||||||||||||||||||||||||||||||||||||||||
Sbjct  13933  TGGTGGCAGCTCTGGCTGGGGCTTGGGGGCCCGGAGAGGAGGCAGAGGGCGATGAGGATGA  13992

Query  61     GAACATGGTGTACTACTTCCTGGAGGAAAGCACAGGCTACATGGAACCCGCCCTGCGGTG  120
              ||||||||||||||||||||||||||||||||||||||||||||||||||||||||||||||
Sbjct  13993  GAACATGGTGTACTACTTCCTGGAGGAAAGCACAGGCTACATGGAACCCGCCCTGCGGTG  14052

Query  121    TCTGAGCCTCCTGCATACACTGGTGGCCTTTCTCTGCATCATTGGCTATAATTGTCTCAA  180
              ||||||||||||||||||||||||||||||||||||||||||||||||||||||||||||||
Sbjct  14053  TCTGAGCCTCCTGCATACACTGGTGGCCTTTCTCTGCATCATTGGCTATAATTGTCTCAA  14112

Query  181    GGTGCCCCTGGTAATCTTTAAGCGGGAGAAGGAGCTGGCCCGGAAGCTGGAGTTTGATGG  240
              ||||||||||||||||||||||||||||||||||||||||||||||||||||||||||||||
Sbjct  14113  GGTGCCCCTGGTAATCTTTAAGCGGGAGAAGGAGCTGGCCCGGAAGCTGGAGTTTGATGG  14172

Query  241    CCTGTACATCACGGAGCAGCCTGAGGACGATGACGTGAAGGGGCAGTGGGACCGACTGGT  300
              ||||||||||||||||||||||||||||||||||||||||||||||||||||||||||||||
Sbjct  14173  CCTGTACATCACGGAGCAGCCTGAGGACGATGACGTGAAGGGGCAGTGGGACCGACTGGT  14232

Query  301    GCTCAACACGCCGTCTTTCCCTAGCAACTACTGGGACAAGTTTGTCAAGCGCAAGGTCCT  360
              ||||||||||||||||||||||||||||||||||||||||||||||||||||||||||||||
Sbjct  14233  GCTCAACACGCCGTCTTTCCCTAGCAACTACTGGGACAAGTTTGTCAAGCGCAAGGTCCT  14292

Query  361    GGACAAACATGGGGACATCTACGGGCGGGAGCGGATTGCTGAGCTACTGGGCATGGACCT  420
              ||||||||||||||||||||||||||||||||||||||||||||||||||||||||||||||
Sbjct  14293  GGACAAACATGGGGACATCTACGGGCGGGAGCGGATTGCTGAGCTACTGGGCATGGACCT  14352

Query  421    GGCCACACTAGAGATCACAGCCCACAATGAGCGCAAGCCCAACCCGCCGCCAGGGCTGCT  480
              ||||||||||||||||||||||||||||||||||||||||||||||||||||||||||||||
Sbjct  14353  GGCCACACTAGAGATCACAGCCCACAATGAGCGCAAGCCCAACCCGCCGCCAGGGCTGCT  14412

Query  481    GACCTGGCTCATGTCCATCGATGTCAAGTACCAGATCTGGAAGTTCGGGGTCATCTTCAC  540
              ||||||||||||||||||||||||||||||||||||||||||||||||||||||||||||||
Sbjct  14413  GACCTGGCTCATGTCCATCGATGTCAAGTACCAGATCTGGAAGTTCGGGGTCATCTTCAC  14472

Query  541    AGACAACTCCTTCCTGTACCTGGGCTGGTATATGGTGATGTCCCTCTTGGGACACTACAA  600
              ||||||||||||||||||||||||||||||||||||||||||||||||||||||||||||||
Sbjct  14473  AGACAACTCCTTCCTGTACCTGGGCTGGTATATGGTGATGTCCCTCTTGGGACACTACAA  14532

Query  601    CAACTTCTTCTTTGCTGCCCATCTCCTGGACATCGCCATGGGGGTCAAGACGCTGCGCAC  660
              ||||||||||||||||||||||||||||||||||||||||||||||||||||||||||||||
Sbjct  14533  CAACTTCTTCTTTGCTGCCCATCTCCTGGACATCGCCATGGGGGTCAAGACGCTGCGCAC  14592

Query  661    CATCCTGTCCTCTGTCACCCACAATGGGAAACAGCTGGTGATGACCGTGGGCCTTCTGGC  720
              ||||||||||||||||||||||||||||||||||||||||||||||||||||||||||||||
Sbjct  14593  CATCCTGTCCTCTGTCACCCACAATGGGAAACAGCTGGTGATGACCGTGGGCCTTCTGGC  14652

Query  721    GGTGGTCGTCTACCTGTACACCGTGGTGGCCTTCAACTTCTTCCGCAAGTTCTACAACAA  780
              ||||||||||||||||||||||||||||||||||||||||||||||||||||||||||||||
Sbjct  14653  GGTGGTCGTCTACCTGTACACCGTGGTGGCCTTCAACTTCTTCCGCAAGTTCTACAACAA  14712

Query  781    GAGCGAGGATGAGGATGAACCTGACATGAAGTGTGATGACATGATGACGTGTTACCTGTT  840
              ||||||||||||||||||||||||||||||||||||||||||||||||||||||||||||||
Sbjct  14713  GAGCGAGGATGAGGATGAACCTGACATGAAGTGTGATGACATGATGACGTGTTACCTGTT  14772

Query  841    TCACATGTACGTGGGTGTCCGGGCTGGCGGAGGCATTGGGGACGAGATCGAGGACCCCGC  900
              ||||||||||||||||||||||||||||||||||||||||||||||||||||||||||||||
Sbjct  14773  TCACATGTACGTGGGTGTCCGGGCTGGCGGAGGCATTGGGGACGAGATCGAGGACCCCGC  14832

Query  901    GGGTGACGAATACGAGCTCTACAGGGTGGTCTTCGACATCACCTTCTTCTTCTTCGTCAT  960
              ||||||||||||||||||||||||||||||||||||||||||||||||||||||||||||||
Sbjct  14833  GGGTGACGAATACGAGCTCTACAGGGTGGTCTTCGACATCACCTTCTTCTTCTTCGTCAT  14892

Query  961    CGTCATCCTGTTGGCC  976
              ||||||||||||||||
Sbjct  14893  CGTCATCCTGTTGGCC  14908
```

Appendix IV.

Sequences alignment of human cardiac *RYR2* (NM_001035.2) and PCR product obtained from JAR cell RNA (query). The PCR product of *RYR2* was amplified by using downstream primer (5′-dCAGATGAAGCATTTGGTCTCCAT-3′) pairs to the upstream primers JBR2 (5′-dAAGGAGCTCCCCACGAGAAGT-3′).

>ref|NM_001035.2| Homo sapiens ryanodine receptor 2 (cardiac) (RYR2), mRNA
Length=16365

GENE ID: 6262 RYR2 | ryanodine receptor 2 (cardiac) [Homo sapiens]
(Over 100 PubMed links)

Score = 1555 bits (842), Expect = 0.0
Identities = 844/845 (99%), Gaps = 0/845 (0%)
Strand=Plus/Plus

```
Query  1      TCGCAATTCACTATGTACTAGAGGAGAGCAGCGGCTACATGGAGCCCACGTTGCGTATCT  60
              ||||| ||||||||||||||||||||||||||||||||||||||||||||||||||||||
Sbjct  13784  TCGCAGTTCACTATGTACTAGAGGAGAGCAGCGGCTACATGGAGCCCACGTTGCGTATCT  13843

Query  61     TAGCTATTCTGCACACGGTCATTTCTTTCTTCTGCATCATTGGATACTACTGCTTGAAAG  120
              ||||||||||||||||||||||||||||||||||||||||||||||||||||||||||||
Sbjct  13844  TAGCTATTCTGCACACGGTCATTTCTTTCTTCTGCATCATTGGATACTACTGCTTGAAAG  13903

Query  121    TCCCATTGGTTATTTTTAAGCGAGAAAAGGAAGTGGCACGGAAATTGGAATTTGATGGGC  180
              ||||||||||||||||||||||||||||||||||||||||||||||||||||||||||||
Sbjct  13904  TCCCATTGGTTATTTTTAAGCGAGAAAAGGAAGTGGCACGGAAATTGGAATTTGATGGGC  13963

Query  181    TTTATATTACAGAACAGCCTTCAGAAGATGATATTAAAGGCCAGTGGGATAGACTCGTAA  240
              ||||||||||||||||||||||||||||||||||||||||||||||||||||||||||||
Sbjct  13964  TTTATATTACAGAACAGCCTTCAGAAGATGATATTAAAGGCCAGTGGGATAGACTCGTAA  14023

Query  241    TCAACACACAGTCATTTCCCAACAACTACTGGGACAAATTTGTTAAAAGAAAGGTTATGG  300
              ||||||||||||||||||||||||||||||||||||||||||||||||||||||||||||
Sbjct  14024  TCAACACACAGTCATTTCCCAACAACTACTGGGACAAATTTGTTAAAAGAAAGGTTATGG  14083

Query  301    ATAAATATGGAGAGTTCTACGGCCGAGACAGAATCAGTGAATTACTTGGCATGGACAAGG  360
              ||||||||||||||||||||||||||||||||||||||||||||||||||||||||||||
Sbjct  14084  ATAAATATGGAGAGTTCTACGGCCGAGACAGAATCAGTGAATTACTTGGCATGGACAAGG  14143

Query  361    CAGCTCTGGACTTCAGTGATGCCAGAGAAAAGAAGAAGCCAAAGAAAGACAGCTCCTTAT  420
              ||||||||||||||||||||||||||||||||||||||||||||||||||||||||||||
Sbjct  14144  CAGCTCTGGACTTCAGTGATGCCAGAGAAAAGAAGAAGCCAAAGAAAGACAGCTCCTTAT  14203

Query  421    CAGCTGTACTGAACTCCATTGATGTGAAGTATCAGATGTGGAAACTAGGAGTCGTTTTCA  480
              ||||||||||||||||||||||||||||||||||||||||||||||||||||||||||||
Sbjct  14204  CAGCTGTACTGAACTCCATTGATGTGAAGTATCAGATGTGGAAACTAGGAGTCGTTTTCA  14263

Query  481    CTGACAACTCCTTCCTCTACCTAGCCTGGTATATGACTATGTCTGTTCTTGGACACTATA  540
              ||||||||||||||||||||||||||||||||||||||||||||||||||||||||||||
Sbjct  14264  CTGACAACTCCTTCCTCTACCTAGCCTGGTATATGACTATGTCTGTTCTTGGACACTATA  14323

Query  541    ACAACttttttttttGCCGCTCACCTTCTCGACATTGCTATGGGATTCAAGACATTAAGAA  600
              ||||||||||||||||||||||||||||||||||||||||||||||||||||||||||||
Sbjct  14324  ACAACTTTTTTTTTGCCGCTCACCTTCTCGACATTGCTATGGGATTCAAGACATTAAGAA  14383

Query  601    CCATCTTGTCCTCAGTAACTCACAATGGCAAACAGCTCGTATTAACCGTTGGCTTATTAG  660
              ||||||||||||||||||||||||||||||||||||||||||||||||||||||||||||
Sbjct  14384  CCATCTTGTCCTCAGTAACTCACAATGGCAAACAGCTCGTATTAACCGTTGGCTTATTAG  14443

Query  661    CTGTTGTTGTATACCTATACACTGTGGTGGCATTCAATTTTTTCCGAAAATTCTACAATA  720
              ||||||||||||||||||||||||||||||||||||||||||||||||||||||||||||
Sbjct  14444  CTGTTGTTGTATACCTATACACTGTGGTGGCATTCAATTTTTTCCGAAAATTCTACAATA  14503

Query  721    AAAGTGAAGATGGTGATACACCAGATATGAAATGTGACGATATGCTAACATGCTATATGT  780
              ||||||||||||||||||||||||||||||||||||||||||||||||||||||||||||
Sbjct  14504  AAAGTGAAGATGGTGATACACCAGATATGAAATGTGACGATATGCTAACATGCTATATGT  14563

Query  781    TCCACATGTATGTTGGAGTTCGTGCTGGAGGAGGGATCGGGGATGAAATCGAAGACCCAG  840
              ||||||||||||||||||||||||||||||||||||||||||||||||||||||||||||
Sbjct  14564  TCCACATGTATGTTGGAGTTCGTGCTGGAGGAGGGATCGGGGATGAAATCGAAGACCCAG  14623

Query  841    CAGGA  845
              |||||
Sbjct  14624  CAGGA  14628
```

Appendix V.

Sequences alignment between *RYR1* PCR products obtained from RNA extract of BeWo (query) and JAR cells. Both PCR products obtained from BeWo and JAR cells were amplified by using downstream primer (5′-dCAGATGAAGCATTTGGTCTCCAT-3′) pairs to the upstream primers JBR1 (5′-dGACATGGAAGGCTCAGCTGCT-3′).

```
>lcl|31171
Length=976

 Score = 1570 bits (850),  Expect = 0.0
 Identities = 852/853 (99%), Gaps = 0/853 (0%)
 Strand=Plus/Plus

Query  2    GGCGATGAGGATGAGAACATGGTGTACTACTTCCTGGAGGAAAGCACAGGCTACATGGAA  61
            ||||||||||||||||||||||||||||||||||||||||||||||||||||||||||||
Sbjct  47   GGCGATGAGGATGAGAACATGGTGTACTACTTCCTGGAGGAAAGCACAGGCTACATGGAA  106

Query  62   CCCGCCCTGCGGTGTCTGAGCCTCCTGCATACACTGGTGGCCTTTCTCTGCATCATTGGC  121
            ||||||||||||||||||||||||||||||||||||||||||||||||||||||||||||
Sbjct  107  CCCGCCCTGCGGTGTCTGAGCCTCCTGCATACACTGGTGGCCTTTCTCTGCATCATTGGC  166

Query  122  TATAATTGTCTCAAGGTGCCCCTGGTAATCTTTAAGCGGGAGAAGGAGCTGGCCCGGAAG  181
            ||||||||||||||||||||||||||||||||||||||||||||||||||||||||||||
Sbjct  167  TATAATTGTCTCAAGGTGCCCCTGGTAATCTTTAAGCGGGAGAAGGAGCTGGCCCGGAAG  226

Query  182  CTGGAGTTTGATGGCCTGTACATCACGGAGCAGCCTGAGGACGATGACGTGAAGGGGCAG  241
            ||||||||||||||||||||||||||||||||||||||||||||||||||||||||||||
Sbjct  227  CTGGAGTTTGATGGCCTGTACATCACGGAGCAGCCTGAGGACGATGACGTGAAGGGGCAG  286

Query  242  TGGGACCGACTGGTGCTCAACACGCCGTCTTTCCCTAGCAACTACTGGGACAAGTTTGTC  301
            ||||||||||||||||||||||||||||||||||||||||||||||||||||||||||||
Sbjct  287  TGGGACCGACTGGTGCTCAACACGCCGTCTTTCCCTAGCAACTACTGGGACAAGTTTGTC  346

Query  302  AAGCGCAAGGTCCTGGACAAACATGGGGACATCTACGGGCGGGAGCGGATTGCTGAGCTA  361
            ||||||||||||||||||||||||||||||||||||||||||||||||||||||||||||
Sbjct  347  AAGCGCAAGGTCCTGGACAAACATGGGGACATCTACGGGCGGGAGCGGATTGCTGAGCTA  406

Query  362  CTGGGCATGGACCTGGCCACACTAGAGATCACCGCCCACAATGAGCGCAAGCCCAACCCG  421
            |||||||||||||||||||||||||||||||| ||||||||||||||||||||||||||||
Sbjct  407  CTGGGCATGGACCTGGCCACACTAGAGATCACAGCCCACAATGAGCGCAAGCCCAACCCG  466

Query  422  CCGCCAGGGCTGCTGACCTGGCTCATGTCCATCGATGTCAAGTACCAGATCTGGAAGTTC  481
            ||||||||||||||||||||||||||||||||||||||||||||||||||||||||||||
Sbjct  467  CCGCCAGGGCTGCTGACCTGGCTCATGTCCATCGATGTCAAGTACCAGATCTGGAAGTTC  526

Query  482  GGGGTCATCTTCACAGACAACTCCTTCCTGTACCTGGGCTGGTATATGGTGATGTCCCTC  541
            ||||||||||||||||||||||||||||||||||||||||||||||||||||||||||||
Sbjct  527  GGGGTCATCTTCACAGACAACTCCTTCCTGTACCTGGGCTGGTATATGGTGATGTCCCTC  586

Query  542  TTGGGACACTACAACAACTTCTTCTTTGCTGCCCATCTCCTGGACATCGCCATGGGGGTC  601
            ||||||||||||||||||||||||||||||||||||||||||||||||||||||||||||
Sbjct  587  TTGGGACACTACAACAACTTCTTCTTTGCTGCCCATCTCCTGGACATCGCCATGGGGGTC  646

Query  602  AAGACGCTGCGCACCATCCTGTCCTCTGTCACCCACAATGGGAAACAGCTGGTGATGACC  661
            ||||||||||||||||||||||||||||||||||||||||||||||||||||||||||||
Sbjct  647  AAGACGCTGCGCACCATCCTGTCCTCTGTCACCCACAATGGGAAACAGCTGGTGATGACC  706

Query  662  GTGGGCCTTCTGGCGGTGGTCGTCTACCTGTACACCGTGGTGGCCTTCAACTTCTTCCGC  721
            ||||||||||||||||||||||||||||||||||||||||||||||||||||||||||||
Sbjct  707  GTGGGCCTTCTGGCGGTGGTCGTCTACCTGTACACCGTGGTGGCCTTCAACTTCTTCCGC  766

Query  722  AAGTTCTACAACAAGAGCGAGGATGAGGATGAACCTGACATGAAGTGTGATGACATGATG  781
            ||||||||||||||||||||||||||||||||||||||||||||||||||||||||||||
Sbjct  767  AAGTTCTACAACAAGAGCGAGGATGAGGATGAACCTGACATGAAGTGTGATGACATGATG  826

Query  782  ACGTGTTACCTGTTTCACATGTACGTGGGTGTCCGGGCTGGCGGAGGCATTGGGGACGAG  841
            ||||||||||||||||||||||||||||||||||||||||||||||||||||||||||||
Sbjct  827  ACGTGTTACCTGTTTCACATGTACGTGGGTGTCCGGGCTGGCGGAGGCATTGGGGACGAG  886

Query  842  ATCGAGGACCCCG  854
            |||||||||||||
Sbjct  887  ATCGAGGACCCCG  899
```

Appendix VI.

Sequences alignment between *RYR2* PCR products obtained from RNA extract of BeWo (query) and JAR cells. Both PCR products obtained from BeWo and JAR cells were amplified by using downstream primer (5′-dCAGATGAAGCATTTGGTCTCCAT-3′) pairs to the upstream primers JBR2 (5′-dAAGGAGCTCCCCACGAGAAGT-3′).

```
>lcl|63703
Length=845

 Score = 1555 bits (842),  Expect = 0.0
 Identities = 844/845 (99%), Gaps = 0/845 (0%)
 Strand=Plus/Plus

Query  34   TCGCAGTTCACTATGTACTAGAGGAGAGCAGCGGCTACATGGAGCCCACGTTGCGTATCT  93
            ||||| ||||||||||||||||||||||||||||||||||||||||||||||||||||||
Sbjct  1    TCGCAATTCACTATGTACTAGAGGAGAGCAGCGGCTACATGGAGCCCACGTTGCGTATCT  60

Query  94   TAGCTATTCTGCACACGGTCATTTCTTTCTTCTGCATCATTGGATACTACTGCTTGAAAG  153
            ||||||||||||||||||||||||||||||||||||||||||||||||||||||||||||
Sbjct  61   TAGCTATTCTGCACACGGTCATTTCTTTCTTCTGCATCATTGGATACTACTGCTTGAAAG  120

Query  154  TCCCATTGGTTATTTTTAAGCGAGAAAAGGAAGTGGCACGGAAATTGGAATTTGATGGGC  213
            ||||||||||||||||||||||||||||||||||||||||||||||||||||||||||||
Sbjct  121  TCCCATTGGTTATTTTTAAGCGAGAAAAGGAAGTGGCACGGAAATTGGAATTTGATGGGC  180

Query  214  TTTATATTACAGAACAGCCTTCAGAAGATGATATTAAAGGCCAGTGGGATAGACTCGTAA  273
            ||||||||||||||||||||||||||||||||||||||||||||||||||||||||||||
Sbjct  181  TTTATATTACAGAACAGCCTTCAGAAGATGATATTAAAGGCCAGTGGGATAGACTCGTAA  240

Query  274  TCAACACACAGTCATTTCCCAACAACTACTGGGACAAATTTGTTAAAAGAAAGGTTATGG  333
            ||||||||||||||||||||||||||||||||||||||||||||||||||||||||||||
Sbjct  241  TCAACACACAGTCATTTCCCAACAACTACTGGGACAAATTTGTTAAAAGAAAGGTTATGG  300

Query  334  ATAAATATGGAGAGTTCTACGGCCGAGACAGAATCAGTGAATTACTTGGCATGGACAAGG  393
            ||||||||||||||||||||||||||||||||||||||||||||||||||||||||||||
Sbjct  301  ATAAATATGGAGAGTTCTACGGCCGAGACAGAATCAGTGAATTACTTGGCATGGACAAGG  360

Query  394  CAGCTCTGGACTTCAGTGATGCCAGAGAAAAGAAGAAGCCAAAGAAAGACAGCTCCTTAT  453
            ||||||||||||||||||||||||||||||||||||||||||||||||||||||||||||
Sbjct  361  CAGCTCTGGACTTCAGTGATGCCAGAGAAAAGAAGAAGCCAAAGAAAGACAGCTCCTTAT  420

Query  454  CAGCTGTACTGAACTCCATTGATGTGAAGTATCAGATGTGGAAACTAGGAGTCGTTTTCA  513
            ||||||||||||||||||||||||||||||||||||||||||||||||||||||||||||
Sbjct  421  CAGCTGTACTGAACTCCATTGATGTGAAGTATCAGATGTGGAAACTAGGAGTCGTTTTCA  480

Query  514  CTGACAACTCCTTCCTCTACCTAGCCTGGTATATGACTATGTCTGTTCTTGGACACTATA  573
            ||||||||||||||||||||||||||||||||||||||||||||||||||||||||||||
Sbjct  481  CTGACAACTCCTTCCTCTACCTAGCCTGGTATATGACTATGTCTGTTCTTGGACACTATA  540

Query  574  ACAACttttttttttGCCGCTCACCTTCTCGACATTGCTATGGGATTCAAGACATTAAGAA  633
            ||||||||||||||||||||||||||||||||||||||||||||||||||||||||||||
Sbjct  541  ACAACTTTTTTTTTGCCGCTCACCTTCTCGACATTGCTATGGGATTCAAGACATTAAGAA  600

Query  634  CCATCTTGTCCTCAGTAACTCACAATGGCAAACAGCTCGTATTAACCGTTGGCTTATTAG  693
            ||||||||||||||||||||||||||||||||||||||||||||||||||||||||||||
Sbjct  601  CCATCTTGTCCTCAGTAACTCACAATGGCAAACAGCTCGTATTAACCGTTGGCTTATTAG  660

Query  694  CTGTTGTTGTATACCTATACACTGTGGTGGCATTCAATTTTTTCCGAAAATTCTACAATA  753
            ||||||||||||||||||||||||||||||||||||||||||||||||||||||||||||
Sbjct  661  CTGTTGTTGTATACCTATACACTGTGGTGGCATTCAATTTTTTCCGAAAATTCTACAATA  720

Query  754  AAAGTGAAGATGGTGATACACCAGATATGAAATGTGACGATATGCTAACATGCTATATGT  813
            ||||||||||||||||||||||||||||||||||||||||||||||||||||||||||||
Sbjct  721  AAAGTGAAGATGGTGATACACCAGATATGAAATGTGACGATATGCTAACATGCTATATGT  780

Query  814  TCCACATGTATGTTGGAGTTCGTGCTGGAGGAGGGATCGGGGATGAAATCGAAGACCCAG  873
            ||||||||||||||||||||||||||||||||||||||||||||||||||||||||||||
Sbjct  781  TCCACATGTATGTTGGAGTTCGTGCTGGAGGAGGGATCGGGGATGAAATCGAAGACCCAG  840

Query  874  CAGGA  878
            |||||
Sbjct  841  CAGGA  845
```

Appendix VII.

Sequences alignment of human skeletal *RYR1* (NM_001042723) and PCR product obtained from RNA extract of human first trimester villi sample (E66) (query). The PCR product of *RYR1* was amplified by using downstream primer (5′-dCAGATGAAGCATTTGGTCTCCAT-3′) pairs to the upstream primers JBR1 (5′-dGACATGGAAGGCTCAGCTGCT-3′).

>ref|NM_001042723.1| UEGMD Homo sapiens ryanodine receptor 1 (skeletal) (RYR1), transcript variant 2, mRNA
Length=15376

GENE ID: 6261 RYR1 | ryanodine receptor 1 (skeletal) [Homo sapiens]
(Over 100 PubMed links)

Score = 1681 bits (910), Expect = 0.0
Identities = 921/926 (99%), Gaps = 2/926 (0%)
Strand=Plus/Plus

```
Query  1      ATGGTGGACTACTTCCTGGAGGAAAGCACAGGCTACATGGAACCCGCCCTGCGGTGTCTG  60
              ||||||| ||||||||||||||||||||||||||||||||||||||||||||||||||||
Sbjct  13997  ATGGTGTACTACTTCCTGGAGGAAAGCACAGGCTACATGGAACCCGCCCTGCGGTGTCTG  14056

Query  61     AGCCTCCTGCATACACTGGTGGCCTTTCTCTGCATCATTGGCTATAATTGTCTCAAGGTG  120
              ||||||||||||||||||||||||||||||||||||||||||||||||||||||||||||
Sbjct  14057  AGCCTCCTGCATACACTGGTGGCCTTTCTCTGCATCATTGGCTATAATTGTCTCAAGGTG  14116

Query  121    CCCCTGGTAATCTTTAAGCGGGAGAAGGAGCTGGCCCGGAAGCTGGAGTTTGATGGCCTG  180
              ||||||||||||||||||||||||||||||||||||||||||||||||||||||||||||
Sbjct  14117  CCCCTGGTAATCTTTAAGCGGGAGAAGGAGCTGGCCCGGAAGCTGGAGTTTGATGGCCTG  14176

Query  181    TACATCACGGAGCAGCCTGAGGACGATGACGTGAAGGGGCAGTGGGACCGACTGGTGCTC  240
              ||||||||||||||||||||||||||||||||||||||||||||||||||||||||||||
Sbjct  14177  TACATCACGGAGCAGCCTGAGGACGATGACGTGAAGGGGCAGTGGGACCGACTGGTGCTC  14236

Query  241    AACACGCCGTCTTTCCCTAGCAACTACTGGGACAAGTTTGTCAAGCGCAAGGTCCTGGAC  300
              ||||||||||||||||||||||||||||||||||||||||||||||||||||||||||||
Sbjct  14237  AACACGCCGTCTTTCCCTAGCAACTACTGGGACAAGTTTGTCAAGCGCAAGGTCCTGGAC  14296

Query  301    AAACATGGGGACATCTACGGGCGGGAGCGGATTGCTGAGCTACTGGGCATGGACCTGGCC  360
              ||||||||||||||||||||||||||||||||||||||||||||||||||||||||||||
Sbjct  14297  AAACATGGGGACATCTACGGGCGGGAGCGGATTGCTGAGCTACTGGGCATGGACCTGGCC  14356

Query  361    ACACTAGAGATCACCGCCCACAATGAGCGCAAGCCCAACCCGCCGCCAGGGCTGCTGACC  420
              ||||||||||||||| ||||||||||||||||||||||||||||||||||||||||||||
Sbjct  14357  ACACTAGAGATCACAGCCCACAATGAGCGCAAGCCCAACCCGCCGCCAGGGCTGCTGACC  14416

Query  421    TGGCTCATGTCCATCGATGTCAAGTACCAGATCTGGAAGTTCGGGGTCATCTTCACAGAC  480
              ||||||||||||||||||||||||||||||||||||||||||||||||||||||||||||
Sbjct  14417  TGGCTCATGTCCATCGATGTCAAGTACCAGATCTGGAAGTTCGGGGTCATCTTCACAGAC  14476

Query  481    AACTCCTTCCTGTACCTGGGCTGGTATATGGTGATGTCCCTCTTGGGACACTACAACAAC  540
              ||||||||||||||||||||||||||||||||||||||||||||||||||||||||||||
Sbjct  14477  AACTCCTTCCTGTACCTGGGCTGGTATATGGTGATGTCCCTCTTGGGACACTACAACAAC  14536

Query  541    TTCTTCTTTGCTGCCCATCTCCTGGACATCGCCATGGGGGTCAAGACGCTGCGCACCATC  600
              ||||||||||||||||||||||||||||||||||||||||||||||||||||||||||||
Sbjct  14537  TTCTTCTTTGCTGCCCATCTCCTGGACATCGCCATGGGGGTCAAGACGCTGCGCACCATC  14596

Query  601    CTGTCCTCTGTCACCCACAATGGGAAACAGCTGGTGATGACCGTGGGCCTTCTGGCGGTG  660
              ||||||||||||||||||||||||||||||||||||||||||||||||||||||||||||
Sbjct  14597  CTGTCCTCTGTCACCCACAATGGGAAACAGCTGGTGATGACCGTGGGCCTTCTGGCGGTG  14656

Query  661    GTCGTCTACCTGTACACCGTGGTGGCCTTCAACTTCTTCCGCAAGTTCTACAACAAGAGC  720
              ||||||||||||||||||||||||||||||||||||||||||||||||||||||||||||
Sbjct  14657  GTCGTCTACCTGTACACCGTGGTGGCCTTCAACTTCTTCCGCAAGTTCTACAACAAGAGC  14716

Query  721    GAGGATGAGGATGAACCTGACATGAAGTGTGATGACATGATGACGTGTTACCTGTTTCAC  780
              ||||||||||||||||||||||||||||||||||||||||||||||||||||||||||||
Sbjct  14717  GAGGATGAGGATGAACCTGACATGAAGTGTGATGACATGATGACGTGTTACCTGTTTCAC  14776

Query  781    ATGTACGTGGGTGTCCGGGCTGGCGGAGGCATTGGGGACGAGATCGAGGACCCCGCGGGT  840
              ||||||||||||||||||||||||||||||||||||||||||||||||||||||||||||
Sbjct  14777  ATGTACGTGGGTGTCCGGGCTGGCGGAGGCATTGGGGACGAGATCGAGGACCCCGCGGGT  14836

Query  841    GACGAATACGAGCTCTACAGGGTGGTCTTCGACATCACCTTCTTCTTCTTCGTCATCGTC  900
              ||||||||||||||||||||||||||||||||||||||||||||||||||||||||||||
Sbjct  14837  GACGAATACGAGCTCTACAGGGTGGTCTTCGACATCACCTTCTTCTTCTTCGTCATCGTC  14896

Query  901    ATCCTGT-GGTCATCATCCAGG-TCT  924
              ||||||| || |||||||||| ||| 
Sbjct  14897  ATCCTGTTGGCCATCATCCAGGGTCT  14922
```

Appendix VIII.

Sequences alignment of human cardiac *RYR2* (NM_001035.2) and PCR product obtained from RNA extract of human first trimester villi sample (E66) (query). The PCR product of *RYR2* was amplified by using downstream primer (5′-dCAGATGAAGCATTTGGTCTCCAT-3′) pairs to the upstream primers JBR2 (5′-dAAGGAGCTCCCCACGAGAAGT-3′).

>ref|NM_001035.2| Homo sapiens ryanodine receptor 2 (cardiac) (RYR2), mRNA
Length=16365

GENE ID: 6262 RYR2 | ryanodine receptor 2 (cardiac) [Homo sapiens]
(Over 100 PubMed links)

Score = 1759 bits (952), Expect = 0.0
Identities = 955/956 (99%), Gaps = 1/956 (0%)
Strand=Plus/Plus

```
Query  1      AAGTGAC-AGCCTGGACAGCAGCTCCCATAGAATCATCGCAGTTCACTATGTACTAGAGG  59
              ||||||| ||||||||||||||||||||||||||||||||||||||||||||||||||||
Sbjct  13748  AAGTGACAAGCCTGGACAGCAGCTCCCATAGAATCATCGCAGTTCACTATGTACTAGAGG  13807

Query  60     AGAGCAGCGGCTACATGGAGCCCACGTTGCGTATCTTAGCTATTCTGCACACGGTCATTT  119
              ||||||||||||||||||||||||||||||||||||||||||||||||||||||||||||
Sbjct  13808  AGAGCAGCGGCTACATGGAGCCCACGTTGCGTATCTTAGCTATTCTGCACACGGTCATTT  13867

Query  120    CTTTCTTCTGCATCATTGGATACTACTGCTTGAAAGTCCCATTGGTTATTTTTAAGCGAG  179
              ||||||||||||||||||||||||||||||||||||||||||||||||||||||||||||
Sbjct  13868  CTTTCTTCTGCATCATTGGATACTACTGCTTGAAAGTCCCATTGGTTATTTTTAAGCGAG  13927

Query  180    AAAAGGAAGTGGCACGGAAATTGGAATTTGATGGGCTTTATATTACAGAACAGCCTTCAG  239
              ||||||||||||||||||||||||||||||||||||||||||||||||||||||||||||
Sbjct  13928  AAAAGGAAGTGGCACGGAAATTGGAATTTGATGGGCTTTATATTACAGAACAGCCTTCAG  13987

Query  240    AAGATGATATTAAAGGCCAGTGGGATAGACTCGTAATCAACACACAGTCATTTCCCAACA  299
              ||||||||||||||||||||||||||||||||||||||||||||||||||||||||||||
Sbjct  13988  AAGATGATATTAAAGGCCAGTGGGATAGACTCGTAATCAACACACAGTCATTTCCCAACA  14047

Query  300    ACTACTGGGACAAATTTGTTAAAAGAAAGGTTATGGATAAATATGGAGAGTTCTACGGCC  359
              ||||||||||||||||||||||||||||||||||||||||||||||||||||||||||||
Sbjct  14048  ACTACTGGGACAAATTTGTTAAAAGAAAGGTTATGGATAAATATGGAGAGTTCTACGGCC  14107

Query  360    GAGACAGAATCAGTGAATTACTTGGCATGGACAAGGCAGCTCTGGACTTCAGTGATGCCA  419
              ||||||||||||||||||||||||||||||||||||||||||||||||||||||||||||
Sbjct  14108  GAGACAGAATCAGTGAATTACTTGGCATGGACAAGGCAGCTCTGGACTTCAGTGATGCCA  14167

Query  420    GAGAAAAGAAGAAGCCAAAGAAAGACAGCTCCTTATCAGCTGTACTGAACTCCATTGATG  479
              ||||||||||||||||||||||||||||||||||||||||||||||||||||||||||||
Sbjct  14168  GAGAAAAGAAGAAGCCAAAGAAAGACAGCTCCTTATCAGCTGTACTGAACTCCATTGATG  14227

Query  480    TGAAGTATCAGATGTGGAAACTAGGAGTCGTTTTCACTGACAACTCCTTCCTCTACCTAG  539
              ||||||||||||||||||||||||||||||||||||||||||||||||||||||||||||
Sbjct  14228  TGAAGTATCAGATGTGGAAACTAGGAGTCGTTTTCACTGACAACTCCTTCCTCTACCTAG  14287

Query  540    CCTGGTATATGACTATGTCTGTTCTTGGACACTATAACAACttttttttttGCCGCTCACC  599
              ||||||||||||||||||||||||||||||||||||||||||||||||||||||||||||
Sbjct  14288  CCTGGTATATGACTATGTCTGTTCTTGGACACTATAACAACTTTTTTTTTTGCCGCTCACC  14347

Query  600    TTCTCGACATTGCTATGGGATTCAAGACATTAAGAACCATCTTGTCCTCAGTAACTCACA  659
              ||||||||||||||||||||||||||||||||||||||||||||||||||||||||||||
Sbjct  14348  TTCTCGACATTGCTATGGGATTCAAGACATTAAGAACCATCTTGTCCTCAGTAACTCACA  14407

Query  660    ATGGCAAACAGCTCGTATTAACCGTTGGCTTATTAGCTGTTGTTGTATACCTATACACTG  719
              ||||||||||||||||||||||||||||||||||||||||||||||||||||||||||||
Sbjct  14408  ATGGCAAACAGCTCGTATTAACCGTTGGCTTATTAGCTGTTGTTGTATACCTATACACTG  14467

Query  720    TGGTGGCATTCAATTTTTTCCGAAAATTCTACAATAAAAGTGAAGATGGTGATACACCAG  779
              ||||||||||||||||||||||||||||||||||||||||||||||||||||||||||||
Sbjct  14468  TGGTGGCATTCAATTTTTTCCGAAAATTCTACAATAAAAGTGAAGATGGTGATACACCAG  14527

Query  780    ATATGAAATGTGACGATATGCTAACATGCTATATGTTCCACATGTATGTTGGAGTTCGTG  839
              ||||||||||||||||||||||||||||||||||||||||||||||||||||||||||||
Sbjct  14528  ATATGAAATGTGACGATATGCTAACATGCTATATGTTCCACATGTATGTTGGAGTTCGTG  14587

Query  840    CTGGAGGAGGGATCGGGGATGAAATCGAAGACCCAGCAGGAGATGAATATGAGATCTATC  899
              ||||||||||||||||||||||||||||||||||||||||||||||||||||||||||||
Sbjct  14588  CTGGAGGAGGGATCGGGGATGAAATCGAAGACCCAGCAGGAGATGAATATGAGATCTATC  14647

Query  900    GAATCATCTTTGACATCACTTTCTTCTTCTTTGTTATTGTCATTCTCTTGGCCATA  955
              |||||||||||||||||||||||||||||||||||||||||||||||||||||||
Sbjct  14648  GAATCATCTTTGACATCACTTTCTTCTTCTTTGTTATTGTCATTCTCTTGGCCATA  14703
```

Appendix IX.

Sequences alignment between *RYR1* PCR products obtained from RNA extract of BeWo (query) and human first trimester villi sample (E66). Both PCR products obtained from BeWo and sample E66 were amplified by using downstream primer (5′-dCAGATGAAGCATTTGGTCTCCAT-3′) pairs to the upstream primers JBR1 (5′-dGACATGGAAGGCTCAGCTGCT-3′).

```
>lcl|20009
Length=924

 Score = 1537 bits (832),  Expect = 0.0
 Identities = 834/835 (99%), Gaps = 0/835 (0%)
 Strand=Plus/Plus

Query  20   ATGGTGTACTACTTCCTGGAGGAAAGCACAGGCTACATGGAACCCGCCCTGCGGTGTCTG  79
            ||||||||||||||||||||||||||||||||||||||||||||||||||||||||||||
Sbjct  1    ATGGTGGACTACTTCCTGGAGGAAAGCACAGGCTACATGGAACCCGCCCTGCGGTGTCTG  60

Query  80   AGCCTCCTGCATACACTGGTGGCCTTTCTCTGCATCATTGGCTATAATTGTCTCAAGGTG  139
            ||||||||||||||||||||||||||||||||||||||||||||||||||||||||||||
Sbjct  61   AGCCTCCTGCATACACTGGTGGCCTTTCTCTGCATCATTGGCTATAATTGTCTCAAGGTG  120

Query  140  CCCCTGGTAATCTTTAAGCGGGAGAAGGAGCTGGCCCGGAAGCTGGAGTTTGATGGCCTG  199
            ||||||||||||||||||||||||||||||||||||||||||||||||||||||||||||
Sbjct  121  CCCCTGGTAATCTTTAAGCGGGAGAAGGAGCTGGCCCGGAAGCTGGAGTTTGATGGCCTG  180

Query  200  TACATCACGGAGCAGCCTGAGGACGATGACGTGAAGGGGCAGTGGGACCGACTGGTGCTC  259
            ||||||||||||||||||||||||||||||||||||||||||||||||||||||||||||
Sbjct  181  TACATCACGGAGCAGCCTGAGGACGATGACGTGAAGGGGCAGTGGGACCGACTGGTGCTC  240

Query  260  AACACGCCGTCTTTCCCTAGCAACTACTGGGACAAGTTTGTCAAGCGCAAGGTCCTGGAC  319
            ||||||||||||||||||||||||||||||||||||||||||||||||||||||||||||
Sbjct  241  AACACGCCGTCTTTCCCTAGCAACTACTGGGACAAGTTTGTCAAGCGCAAGGTCCTGGAC  300

Query  320  AAACATGGGGACATCTACGGGCGGGAGCGGATTGCTGAGCTACTGGGCATGGACCTGGCC  379
            ||||||||||||||||||||||||||||||||||||||||||||||||||||||||||||
Sbjct  301  AAACATGGGGACATCTACGGGCGGGAGCGGATTGCTGAGCTACTGGGCATGGACCTGGCC  360

Query  380  ACACTAGAGATCACCGCCCACAATGAGCGCAAGCCCAACCCGCCGCCAGGGCTGCTGACC  439
            ||||||||||||||||||||||||||||||||||||||||||||||||||||||||||||
Sbjct  361  ACACTAGAGATCACCGCCCACAATGAGCGCAAGCCCAACCCGCCGCCAGGGCTGCTGACC  420

Query  440  TGGCTCATGTCCATCGATGTCAAGTACCAGATCTGGAAGTTCGGGGTCATCTTCACAGAC  499
            ||||||||||||||||||||||||||||||||||||||||||||||||||||||||||||
Sbjct  421  TGGCTCATGTCCATCGATGTCAAGTACCAGATCTGGAAGTTCGGGGTCATCTTCACAGAC  480

Query  500  AACTCCTTCCTGTACCTGGGCTGGTATATGGTGATGTCCCTCTTGGGACACTACAACAAC  559
            ||||||||||||||||||||||||||||||||||||||||||||||||||||||||||||
Sbjct  481  AACTCCTTCCTGTACCTGGGCTGGTATATGGTGATGTCCCTCTTGGGACACTACAACAAC  540

Query  560  TTCTTCTTTGCTGCCCATCTCCTGGACATCGCCATGGGGGTCAAGACGCTGCGCACCATC  619
            ||||||||||||||||||||||||||||||||||||||||||||||||||||||||||||
Sbjct  541  TTCTTCTTTGCTGCCCATCTCCTGGACATCGCCATGGGGGTCAAGACGCTGCGCACCATC  600

Query  620  CTGTCCTCTGTCACCCACAATGGGAAACAGCTGGTGATGACCGTGGGCCTTCTGGCGGTG  679
            ||||||||||||||||||||||||||||||||||||||||||||||||||||||||||||
Sbjct  601  CTGTCCTCTGTCACCCACAATGGGAAACAGCTGGTGATGACCGTGGGCCTTCTGGCGGTG  660

Query  680  GTCGTCTACCTGTACACCGTGGTGGCCTTCAACTTCTTCCGCAAGTTCTACAACAAGAGC  739
            ||||||||||||||||||||||||||||||||||||||||||||||||||||||||||||
Sbjct  661  GTCGTCTACCTGTACACCGTGGTGGCCTTCAACTTCTTCCGCAAGTTCTACAACAAGAGC  720

Query  740  GAGGATGAGGATGAACCTGACATGAAGTGTGATGACATGATGACGTGTTACCTGTTTCAC  799
            ||||||||||||||||||||||||||||||||||||||||||||||||||||||||||||
Sbjct  721  GAGGATGAGGATGAACCTGACATGAAGTGTGATGACATGATGACGTGTTACCTGTTTCAC  780

Query  800  ATGTACGTGGGTGTCCGGGCTGGCGGAGGCATTGGGGACGAGATCGAGGACCCCG  854
            |||||||||||||||||||||||||||||||||||||||||||||||||||||||
Sbjct  781  ATGTACGTGGGTGTCCGGGCTGGCGGAGGCATTGGGGACGAGATCGAGGACCCCG  835
```

Appendix X.

Sequences alignment between *RYR2* PCR products obtained from RNA extract of BeWo (query) and human first trimester villi sample (E66). Both PCR products obtained from BeWo and sample E66 were amplified by using downstream primer (5′-dCAGATGAAGCATTTGGTCTCCAT-3′) pairs to the upstream primers JBR2 (5′-dAAGGAGCTCCCCACGAGAAGT-3′).

```
>lcl|9273
Length=955

 Score = 1760 bits (953),  Expect = 0.0
 Identities = 953/953 (100%), Gaps = 0/953 (0%)
 Strand=Plus/Plus

Query  1    GTGACAGCCTGGACAGCAGCTCCCATAGAATCATCGCAGTTCACTATGTACTAGAGGAGA  60
            ||||||||||||||||||||||||||||||||||||||||||||||||||||||||||||
Sbjct  3    GTGACAGCCTGGACAGCAGCTCCCATAGAATCATCGCAGTTCACTATGTACTAGAGGAGA  62

Query  61   GCAGCGGCTACATGGAGCCCACGTTGCGTATCTTAGCTATTCTGCACACGGTCATTTCTT  120
            ||||||||||||||||||||||||||||||||||||||||||||||||||||||||||||
Sbjct  63   GCAGCGGCTACATGGAGCCCACGTTGCGTATCTTAGCTATTCTGCACACGGTCATTTCTT  122

Query  121  TCTTCTGCATCATTGGATACTACTGCTTGAAAGTCCCATTGGTTATTTTTAAGCGAGAAA  180
            ||||||||||||||||||||||||||||||||||||||||||||||||||||||||||||
Sbjct  123  TCTTCTGCATCATTGGATACTACTGCTTGAAAGTCCCATTGGTTATTTTTAAGCGAGAAA  182

Query  181  AGGAAGTGGCACGGAAATTGGAATTTGATGGGCTTTATATTACAGAACAGCCTTCAGAAG  240
            ||||||||||||||||||||||||||||||||||||||||||||||||||||||||||||
Sbjct  183  AGGAAGTGGCACGGAAATTGGAATTTGATGGGCTTTATATTACAGAACAGCCTTCAGAAG  242

Query  241  ATGATATTAAAGGCCAGTGGGATAGACTCGTAATCAACACACAGTCATTTCCCAACAACT  300
            ||||||||||||||||||||||||||||||||||||||||||||||||||||||||||||
Sbjct  243  ATGATATTAAAGGCCAGTGGGATAGACTCGTAATCAACACACAGTCATTTCCCAACAACT  302

Query  301  ACTGGGACAAATTTGTTAAAAGAAAGGTTATGGATAAATATGGAGAGTTCTACGGCCGAG  360
            ||||||||||||||||||||||||||||||||||||||||||||||||||||||||||||
Sbjct  303  ACTGGGACAAATTTGTTAAAAGAAAGGTTATGGATAAATATGGAGAGTTCTACGGCCGAG  362

Query  361  ACAGAATCAGTGAATTACTTGGCATGGACAAGGCAGCTCTGGACTTCAGTGATGCCAGAG  420
            ||||||||||||||||||||||||||||||||||||||||||||||||||||||||||||
Sbjct  363  ACAGAATCAGTGAATTACTTGGCATGGACAAGGCAGCTCTGGACTTCAGTGATGCCAGAG  422

Query  421  AAAAGAAGAAGCCAAAGAAAGACAGCTCCTTATCAGCTGTACTGAACTCCATTGATGTGA  480
            ||||||||||||||||||||||||||||||||||||||||||||||||||||||||||||
Sbjct  423  AAAAGAAGAAGCCAAAGAAAGACAGCTCCTTATCAGCTGTACTGAACTCCATTGATGTGA  482

Query  481  AGTATCAGATGTGGAAACTAGGAGTCGTTTTCACTGACAACTCCTTCCTCTACCTAGCCT  540
            ||||||||||||||||||||||||||||||||||||||||||||||||||||||||||||
Sbjct  483  AGTATCAGATGTGGAAACTAGGAGTCGTTTTCACTGACAACTCCTTCCTCTACCTAGCCT  542

Query  541  GGTATATGACTATGTCTGTTCTTGGACACTATAACAACttttttttGCCGCTCACCTTC  600
            ||||||||||||||||||||||||||||||||||||||||||||||||||||||||||||
Sbjct  543  GGTATATGACTATGTCTGTTCTTGGACACTATAACAACTTTTTTTTTGCCGCTCACCTTC  602

Query  601  TCGACATTGCTATGGGATTCAAGACATTAAGAACCATCTTGTCCTCAGTAACTCACAATG  660
            ||||||||||||||||||||||||||||||||||||||||||||||||||||||||||||
Sbjct  603  TCGACATTGCTATGGGATTCAAGACATTAAGAACCATCTTGTCCTCAGTAACTCACAATG  662

Query  661  GCAAACAGCTCGTATTAACCGTTGGCTTATTAGCTGTTGTTGTATACCTATACACTGTGG  720
            ||||||||||||||||||||||||||||||||||||||||||||||||||||||||||||
Sbjct  663  GCAAACAGCTCGTATTAACCGTTGGCTTATTAGCTGTTGTTGTATACCTATACACTGTGG  722

Query  721  TGGCATTCAATTTTTTCCGAAAATTCTACAATAAAAGTGAAGATGGTGATACACCAGATA  780
            ||||||||||||||||||||||||||||||||||||||||||||||||||||||||||||
Sbjct  723  TGGCATTCAATTTTTTCCGAAAATTCTACAATAAAAGTGAAGATGGTGATACACCAGATA  782

Query  781  TGAAATGTGACGATATGCTAACATGCTATATGTTCCACATGTATGTTGGAGTTCGTGCTG  840
            ||||||||||||||||||||||||||||||||||||||||||||||||||||||||||||
Sbjct  783  TGAAATGTGACGATATGCTAACATGCTATATGTTCCACATGTATGTTGGAGTTCGTGCTG  842

Query  841  GAGGAGGGATCGGGGATGAAATCGAAGACCCAGCAGGAGATGAATATGAGATCTATCGAA  900
            ||||||||||||||||||||||||||||||||||||||||||||||||||||||||||||
Sbjct  843  GAGGAGGGATCGGGGATGAAATCGAAGACCCAGCAGGAGATGAATATGAGATCTATCGAA  902

Query  901  TCATCTTTGACATCACTTTCTTCTTCTTTGTTATTGTCATTCTCTTGGCCATA  953
            |||||||||||||||||||||||||||||||||||||||||||||||||||
Sbjct  903  TCATCTTTGACATCACTTTCTTCTTCTTTGTTATTGTCATTCTCTTGGCCATA  955
```

Appendix XI.

Sequences alignment between primers and human RyR1, RyR2 and RyR3 mRNA by Primer-BLAST The PCR product of *RYR1, RYR2* and *RYR3* was amplified by using the same forward primer (5′-dCAGATGAAGCATTTGGTCTCCAT-3′) pairs to the corresponding reverse primers: Panel **I**. JBR1 (5'-GACATGGAAGGCTCAGCTGCT-3'), Panel **II**. JBR2 (5'-dAAGGAGCTCCCCACGAGAAGT-3') and Panel **III**. JBR3 (5′-dGAGGAAGAAGCGATGGTGTT-3′).

I.

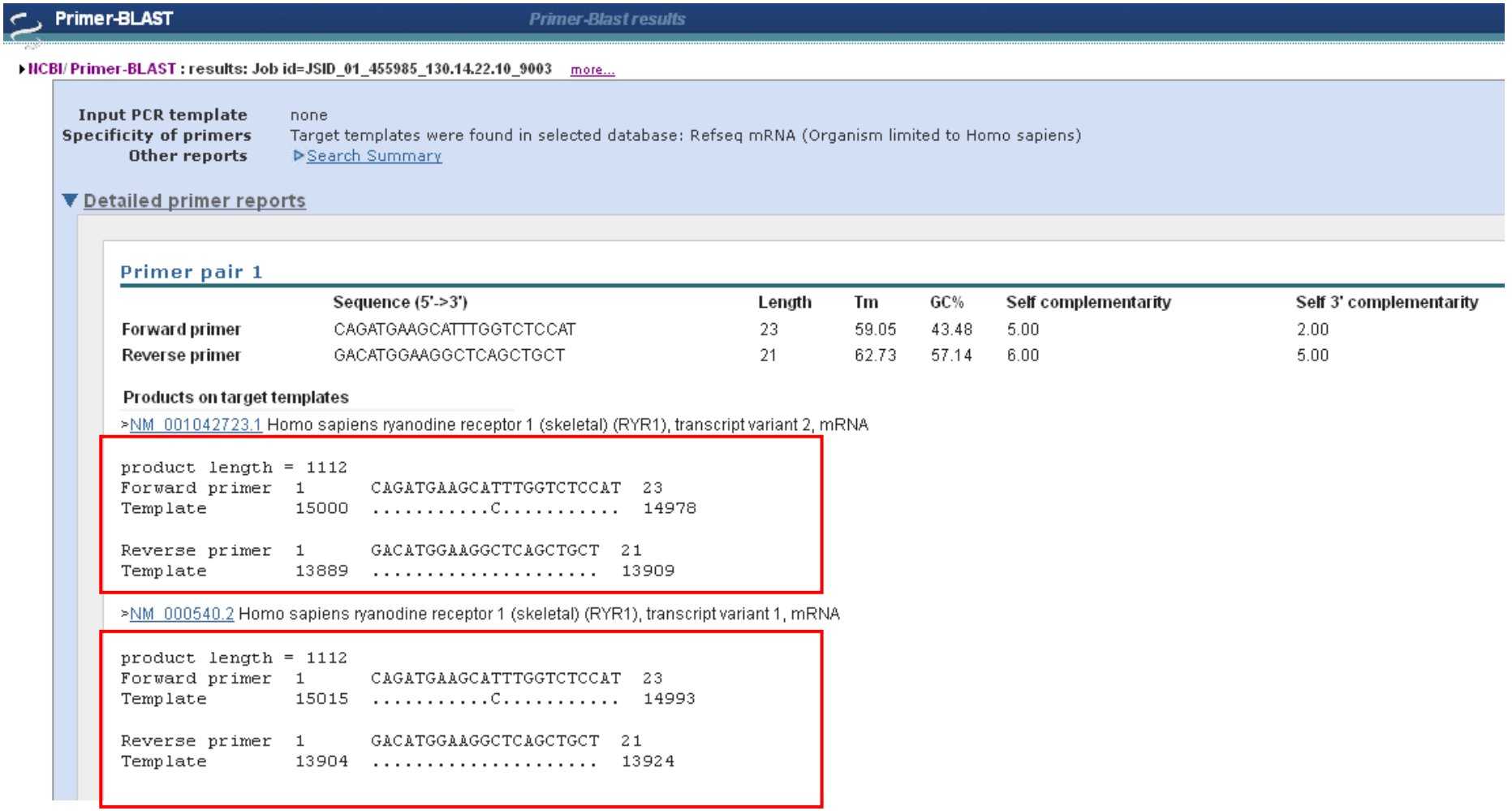

Primer-BLAST — Primer-Blast results

NCBI/ Primer-BLAST : results: Job id=JSID_01_455985_130.14.22.10_9003 more...

Input PCR template	none
Specificity of primers	Target templates were found in selected database: Refseq mRNA (Organism limited to Homo sapiens)
Other reports	▷Search Summary

▼ Detailed primer reports

Primer pair 1

	Sequence (5'->3')	Length	Tm	GC%	Self complementarity	Self 3' complementarity
Forward primer	CAGATGAAGCATTTGGTCTCCAT	23	59.05	43.48	5.00	2.00
Reverse primer	GACATGGAAGGCTCAGCTGCT	21	62.73	57.14	6.00	5.00

Products on target templates

>NM_001042723.1 Homo sapiens ryanodine receptor 1 (skeletal) (RYR1), transcript variant 2, mRNA

```
product length = 1112
Forward primer  1      CAGATGAAGCATTTGGTCTCCAT  23
Template        15000  ..........C...........  14978

Reverse primer  1      GACATGGAAGGCTCAGCTGCT  21
Template        13889  ......................  13909
```

>NM_000540.2 Homo sapiens ryanodine receptor 1 (skeletal) (RYR1), transcript variant 1, mRNA

```
product length = 1112
Forward primer  1      CAGATGAAGCATTTGGTCTCCAT  23
Template        15015  ..........C...........  14993

Reverse primer  1      GACATGGAAGGCTCAGCTGCT  21
Template        13904  ......................  13924
```

II.

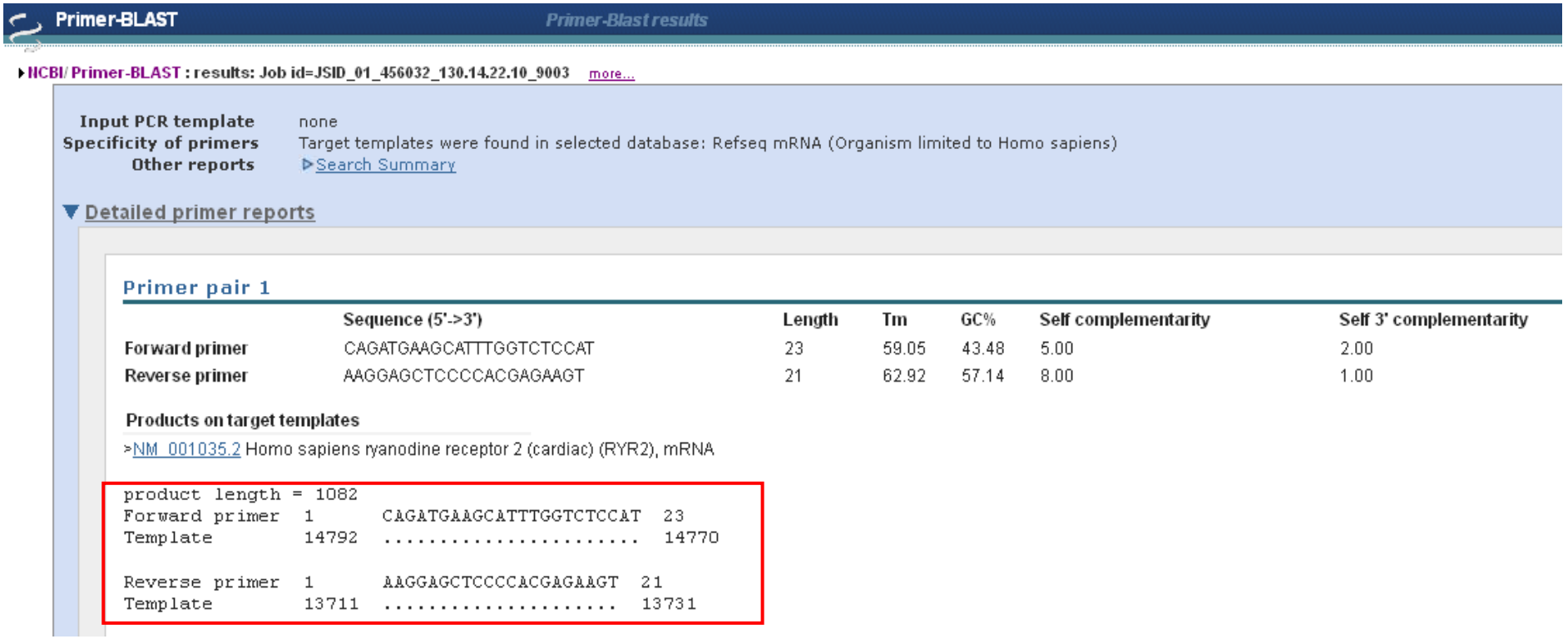
Primer-BLAST
Primer-Blast results
NCBI/ Primer-BLAST : results: Job id=JSID_01_456032_130.14.22.10_9003 more...
Input PCR template none
Specificity of primers Target templates were found in selected database: Refseq mRNA (Organism limited to Homo sapiens)
Other reports Search Summary
Detailed primer reports
Primer pair 1
Sequence (5'->3') Length Tm GC% Self complementarity Self 3' complementarity
Forward primer CAGATGAAGCATTTGGTCTCCAT 23 59.05 43.48 5.00 2.00
Reverse primer AAGGAGCTCCCCACGAGAAGT 21 62.92 57.14 8.00 1.00
Products on target templates
>NM_001035.2 Homo sapiens ryanodine receptor 2 (cardiac) (RYR2), mRNA
product length = 1082
Forward primer 1 CAGATGAAGCATTTGGTCTCCAT 23
Template 14792 14770
Reverse primer 1 AAGGAGCTCCCCACGAGAAGT 21
Template 13711 13731

III.

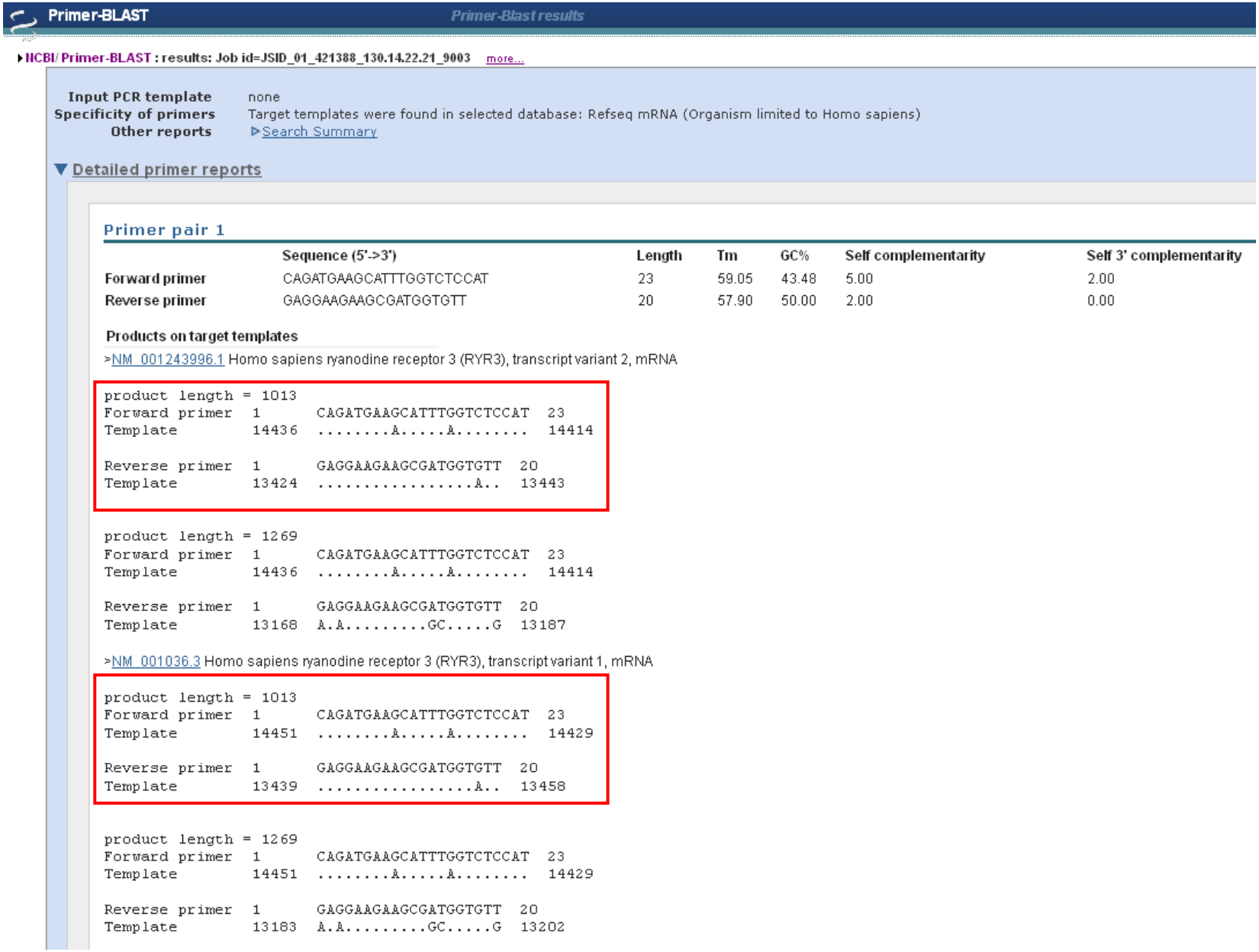
Primer-BLAST
Primer-Blast results
NCBI/ Primer-BLAST : results: Job id=JSID_01_421388_130.14.22.21_9003 more...
Input PCR template none
Specificity of primers Target templates were found in selected database: Refseq mRNA (Organism limited to Homo sapiens)
Other reports Search Summary
Detailed primer reports
Primer pair 1
Sequence (5'->3') Length Tm GC% Self complementarity Self 3' complementarity
Forward primer CAGATGAAGCATTTGGTCTCCAT 23 59.05 43.48 5.00 2.00
Reverse primer GAGGAAGAAGCGATGGTGTT 20 57.90 50.00 2.00 0.00
Products on target templates
>NM_001243996.1 Homo sapiens ryanodine receptor 3 (RYR3), transcript variant 2, mRNA
product length = 1013
Forward primer 1 CAGATGAAGCATTTGGTCTCCAT 23
Template 14436 ........A.....A........ 14414
Reverse primer 1 GAGGAAGAAGCGATGGTGTT 20
Template 13424 ....A.. 13443
product length = 1269
Forward primer 1 CAGATGAAGCATTTGGTCTCCAT 23
Template 14436 ........A.....A........ 14414
Reverse primer 1 GAGGAAGAAGCGATGGTGTT 20
Template 13168 A.A.........GC.....G 13187
>NM_001036.3 Homo sapiens ryanodine receptor 3 (RYR3), transcript variant 1, mRNA
product length = 1013
Forward primer 1 CAGATGAAGCATTTGGTCTCCAT 23
Template 14451 ........A.....A........ 14429
Reverse primer 1 GAGGAAGAAGCGATGGTGTT 20
Template 13439 ....A.. 13458
product length = 1269
Forward primer 1 CAGATGAAGCATTTGGTCTCCAT 23
Template 14451 ........A.....A........ 14429
Reverse primer 1 GAGGAAGAAGCGATGGTGTT 20
Template 13183 A.A.........GC.....G 13202